CHARLES UNIVERSITY IN PRAGUE
2ND FACULTY OF MEDICINE

and

ACADEMY OF SCIENCES OF THE CZECH REPUBLIC
INSTITUTE OF EXPERIMENTAL MEDICINE





Mgr. Dávid Džamba

Physiological and pathological potential of astroglial NMDA receptors

PhD thesis

Supervisor: Ing. Miroslava Anděrová, CSc.

Prague 2016

Prohlášení:

Prohlašuji, že jsem závěrečnou práci zpracoval samostatně a že jsem řádně uvedl a citoval všechny použité prameny a literaturu. Současně prohlašuji, že práce nebyla využita k získání jiného nebo stejného titulu.

Souhlasím s trvalým uložením elektronické verze mé práce v databázi systému meziuniverzitního projektu Theses.cz za účelem soustavné kontroly podobnosti kvalifikačních prací.

V Praze 14.2.2016

Dávid Džamba

DŽAMBA, Dávid. *Fyziologické a patologické vlastnosti NMDA receptorů astrocytů. [Physiological and pathological potential of astroglial NMDA receptors]*. Praha, 2016. 104 stran, 3 přílohy. Disertační práce (Ph.D.). Univerzita Karlova v Praze, 2. lékařská fakulta. Vedoucí práce Ing. Miroslava Anděrová, CSc.

Abstrakt*:*

Kortikální gliové buňky obsahují jak ionotropní, tak i metabotropní glutamátové receptory. Přes veškeré úsilí komplexní analýza celé rodiny glutamátových receptorů a jejich podjednotek přítomných v gliových buňkách stále chybí. V této práci poskytujeme celkový obraz genové exprese ionotropních (AMPA, kainát, NMDA) a hlavních metabotropních glutamátových receptorů u kortikálních gliových buněk izolovaných z GFAP/EGFP myší v průběhu stárnutí a před a po fokální cerebrální ischemii. Použitím jednobuněčné RT-qPCR metody jsme zjistili expresi genů kódujících podjednotky glutamátových receptorů u kortikálních GFAP/EGFP pozitivních (GFAP/EGFP$^+$) gliových buněk. Většina z analyzovaných buněk exprimovala mRNA kódující podjednotky glutamátových receptorů a ve většině případů byla tato exprese po ischemickém poškození zvýšená. Analýza dat ukázala několik skupin GFAP/EGFP$^+$ gliových buněk s ohledem na glutamátové receptory, a také na to, jakým způsobem jejich exprese koreluje s expresí gliových markerů před a po ischemii. Dále jsme zkoumali proteinovou expresi a funkční význam NMDA receptorů u gliových buněk. Imunohistochemická analýza všech sedmi podjednotek NMDA receptorů ukázala, že GluN3A podjednotka je přítomna v GFAP/EGFP$^+$ gliových buňkách, a že se tato exprese po ischemii zvyšuje. Sledování změn vnitrobuněčné koncentrace Ca^{2+} in situ a in vitro prokázala, že Ca^{2+} odpovědi vyvolané aplikací NMDA byly u GFAP/EGFP$^+$ gliových buněk po ischemii sníženy. Naše práce poskytuje komplexní popis glutamátových receptorů u kortikálních GFAP/EGFP$^+$ gliových buněk a může tak sloužit jako základ pro další výzkum gliových buněk za fyziologických a patofyziologických podmínek.

Abstract:

Cortical glial cells contain both ionotropic and metabotropic glutamate receptors. Despite several efforts, a comprehensive analysis of the entire family of glutamate receptors and their subunits present in glial cells is still missing. Here, we provide an overall picture of the gene expression of ionotropic (AMPA, kainate, NMDA) and the main metabotropic glutamate receptors in cortical glial cells isolated from GFAP/EGFP mice during ageing as well as before and after focal cerebral ischemia. Employing single-cell RT-qPCR, we detected the expression of genes encoding subunits of glutamate receptors in cortical GFAP/EGFP-positive (GFAP/EGFP$^+$) glial cells. Most of the analyzed cells expressed mRNA for glutamate receptor subunits, the expression of which, in most cases, even increased after ischemic injury. Data analyses disclosed several classes of GFAP/EGFP$^+$ glial cells with respect to glutamate receptors and revealed in what manner their expression correlates with the expression of glial markers prior to and after ischemia. Furthermore, we also examined the protein expression and functional significance of NMDA receptors in glial cells. Immunohistochemical analyses of all seven NMDA receptor subunits provided direct evidence that the GluN3A subunit is present in GFAP/EGFP$^+$ glial cells and that its expression is increased after ischemia. In situ and in vitro Ca^{2+} imaging revealed that Ca^{2+} elevations evoked by the application of NMDA were diminished in GFAP/EGFP$^+$ glial cells following ischemia. Our work provides a comprehensive description of glutamate receptors in cortical GFAP/EGFP$^+$ glial cells and may serve as a basis for further research on glial cell physiology and pathophysiology.

Klíčová slova: astrocyty, NG2 glie, glutamátové receptory, NMDA receptory, MCAO

Keywords: astrocytes, NG2 glia, glutamate receptors, NMDA receptors, MCAO

Acknowledgements

I would like to express my special thanks to my supervisor, Dr. Miroslava Anděrová, for initiating me into the mysteries of neuroscience, patiently guiding me on the journey. Secondly, I would also like to thank to my colleagues and technicians who helped me with the experiments.

Author's publications

Publications related to the thesis and contributions of individual co-authors:

1. **David Dzamba**, Pavel Honsa, Martin Valny, Jan Kriska, Lukas Valihrach, Vendula Novosadova, Mikael Kubista, Miroslava Anderova (2015), Quantitative analysis of glutamate receptors in glial cells from the cortex of GFAP/EGFP mice following ischemic injury – focus on NMDA receptors, Cellular and Molecular Neurobiology 35(8):1187-202, IF 2.201

   CONTRIBUTIONS:
   Animal surgery: Dzamba D., Honsa P.
   Cell isolation: Dzamba D., Honsa P., Kriska J.
   RT-qPCR: Novosadova V., Valihrach L.
   Immunohistochemical analysis: Honsa P.
   Calcium imaging experiments: Dzamba D., Valny M.
   Data analysis: Dzamba D., Kubista M., Anderova M.

2. **David Dzamba**, Pavel Honsa, Miroslava Anderova (2013), NMDA Receptors in Glial Cells: Pending Questions, Current Neuropharmacology 11, 250-262, IF 2.347

   CONTRIBUTIONS:
   Astrocytes: Dzamba D.
   Polydendrocytes: Honsa P.
   Oligodendrocytes: Anderova M.

3. Vendula Rusnakova, Pavel Honsa, **David Dzamba**, Anders Ståhlberg, Mikael Kubista, Miroslava Anderova (2013), Heterogeneity of Astrocytes: From Development to Injury–Single Cell Gene Expression, PloS one 8 (8), IF 3.730

   CONTRIBUTIONS:
   Animal surgery: Honsa P.
   Cell isolation: Dzamba D., Honsa P.
   RT-qPCR: Rusnakova V.
   Data analysis: Dzamba D., Stahlberg A., Kubista M., Anderova M.

Other author's publications:

1. **David Dzamba**, Lenka Harantova, Olena Butenko, Miroslava Anderova (2016), Glial cells – the key elements of Alzheimer's disease, Current Alzheimer Research, Epub ahead of print, IF 3.889

2. Miroslava Anderova, Jana Benesova, Michaela Mikesova, **David Dzamba**, Pavel Honsa, Jan Kriska, Olena Butenko, Vendula Novosadova, Lukas Valihrach, Mikael Kubista, Lesia Dmytrenko, Michal Cicanic, Lydia Vargova (2014), Altered Astrocytic Swelling in the Cortex of α-Syntrophin-Negative GFAP/EGFP Mice, PloS one 9 (11), IF 3.534

3. Pavel Honsa, Helena Pivonkova, Lenka Harantova, Olena Butenko, Jan Kriska, **David Dzamba**, Vendula Rusnakova, Lukas Valihrach, Mikael Kubista, Miroslava Anderova (2014) Increased expression of hyperpolarization-activated cyclic nucleotide-gated (HCN) channels in reactive astrocytes following ischemia. Glia. 2014 Jul 14. doi: 10.1002/glia.22721, IF 5.466

4. Olena Butenko, **David Dzamba**, Jana Benesova, Pavel Honsa, Valentina Benfenati, Vendula Rusnakova, Stefano Ferroni, Miroslava Anderova (2012), The increased activity of TRPV4 channel in the astrocytes of the adult rat hippocampus after cerebral hypoxia/ischemia, PloS One 7 (6), IF 3.730

5. Pavel Honsa, Helena Pivonkova, **David Dzamba**, Marcela Filipova, Miroslava Anderova (2012), Polydendrocytes display large lineage plasticity following focal cerebral ischemia, PloS One 7(5), IF 3.730

6. Jana Benesova, Vendula Rusnakova, Pavel Honsa, Helena Pivonkova, **David Dzamba**, Mikael Kubista, Miroslava Anderova (2012), Distinct expression/function of potassium and chloride channels contributes to the diverse volume regulation in cortical astrocytes of GFAP/EGFP mice, PloS One 7(1), IF 3.730

Table of contents

Acknowledgements 1

Author's publications 2

Table of contents 4

List of abbreviations 7

1. INTRODUCTION 11

1.1 Astrocytes 12

1.1.1 Glial cell types 12

1.1.2 Characteristics of astrocytes 15

1.1.3 Astrocytic functions under physiological conditions 17

1.1.4 Membrane properties of astrocytes 19

1.2 NMDA receptors 21

1.2.1 Glutamate receptors 21

1.2.2 Structure of NMDA receptors 23

1.2.3 Function of NMDA receptors 24

1.3 Cerebral ischemia 26

1.3.1 Focal cerebral ischemia 26

1.3.2 Mouse models of focal cerebral ischemia 28

1.3.3 Astrocytes in cerebral ischemia 29

1.4 NMDA receptors in astrocytes 31

1.4.1 Expression of genes coding NMDA receptor subunits in astrocytes 31

1.4.2 Detection of astrocytic NMDA receptors on the protein level 32

1.4.3 Functional studies of NMDA receptors in astrocytes 33

2. AIMS OF THE STUDY: 37

3. MATERIALS AND METHODS: 39

3.1 Transgenic mice 39
3.2 MCAO induction 39
3.3 Preparation of cell suspensions from the cortex of GFAP/EGFP mice 40
3.4 Collection of single GFAP/EGFP$^+$ cells by flow cytometry 41
3.5 Complementary DNA (cDNA) synthesis 41
3.6 qPCR 42
3.7 Preamplification and qPCR 44
3.8 High throughput qPCR 44
3.9 Data pre-processing 45
3.10 Analysis of data obtained from the reverse transcription quantitative polymerase chain reaction (RT-qPCR) 45
3.11 Immunohistochemistry 46
3.12 Preparation of primary cultures 47
3.13 Calcium imaging measurements 48
3.14 Statistics 49
4. RESULTS: 50
4.1 Detection and quantification of mRNA expression in individual GFAP/EGFP$^+$ glial cells 50
4.1.1 Validation of experimental procedure 50
4.1.2 Gene expression profile of GFAP/EGFP$^+$ glial cells changes during development and following ischemic injury 53
4.1.3 Glutamate receptors in GFAP/EGFP$^+$ glial cells 58
4.2 Immunohistochemical protein detection of NMDA receptor subunits 67
4.3 Functional properties of NMDA receptors under physiological conditions and following ischemia 72
4.3.1 Calcium imaging measurements in tissue slices (*in situ*) 72
4.3.2 Calcium imaging measurements in cell cultures (*in vitro*) 78
5. DISCUSSION: 82

5.1 Analysis of gene expression..... 82
5.1.1 Relationship between RT-qPCR data obtained from single cells and bulk samples 82
5.1.2 Identification of GFAP/EGFP^{+} glial cells..... 83
5.1.3 Expression of glutamate receptors in GFAP/EGFP^{+} glial cells 84
5.1.4 Correlation between genes coding glutamate receptors and glial cell markers changes following ischemia..... 87
5.2 Immunohistochemical analysis revealed presence of NMDA receptor subunits in GFAP/EGFP^{+} glial cells 88
5.3 Functional NMDA receptors in GFAP/EGFP^{+} glial cells 89
6. CONCLUSIONS:..... 92
7. REFERENCES: 94
8. ATTACHEMENTS:..... 104

List of abbreviations

20-HETE	20-hydroxyeicosatetraenoic acid
AA	arachidonic acid
ACA	anterior cerebral artery
aCSF	artificial cerebrospinal fluid
Aldh1l1/ALDH1L1	aldehyde dehydrogenase 1 family gene/protein
AMPA	α-amino-3-hydroxy-5-methyl-4-isoxazolepropionic acid
Aqp4/AQP4	aquaporin 1 gene/protein
ATP	adenosine triphosphate
BA	basilar artery
BBB	blood-brain barrier
cDNA	complementary DNA
CNQX	6-cyano-7- nitroquinoxaline-2,3-dione
Controls	uninjured mice
Cq	quantification cycle
CNS	central nervous system
CSF	cerebrospinal fluid
Cspg4/CSPG4	chondroitin sulphate proteoglycan gene/protein
Cx	connexin
D-APV	D-2-amino-5-phosphonovaleric acid
D3-14	3-14 days after MCAO
DL-APV	DL-2-amino-5-phosphonovaleric acid

DXM	dextromethorphan
ECS	extracellular space
EET	epoxyeicosatrienoic acid
EGFP	enhanced green fluorescent protein
F	fluorescence intensity
FACS	fluorescence-activated cell sorting
Fb	background fluorescence intensity
GABA	gamma-aminobutyric acid
GFAP	glial fibrillary acidic protein
GFAP/EGFP$^+$	GFAP/EGFP-positive
GLAST	glutamate aspartate transporter
GLT-1	glial high affinity glutamate transporter
Glul	gene coding glutamine synthetase
GluR	glutamate receptors
GluT	glutamate transporters
GS	glutamine synthetase
HCN	hyperpolarization-activated cyclic nucleotide-gated
ICA	internal carotid artery
I_{Na}	fast-activating tetrodotoxin-sensitive Na^+ current
i.p.	intraperitoneal
IP_3	inositol 1,4,5-triphosphate
K_A	A-type potassium current
kDa	kilodalton

K_{DR}	delayed outwardly rectifying potassium current
K_{IR}	inwardly rectifying potassium current
LTD	long-term depression
LTP	long-term potentiation
MCA	middle cerebral artery
MCAO	middle cerebral artery occlusion
MK-801	dizocilpine
NBQX	2,3-dihydroxy-6-nitro-7-sulfamoyl-benzo[f]quinoxaline-2,3-dione
NG2	neural/glial antigen 2
NMDA	N-methyl-D-aspartate
NO	nitrous oxide
OGB-1 AM	Oregon Green 488 BAPTA-1, AM, cell permeant
P10-600	postnatal day 10-600
PCA	principal component analysis
PcerA	posterior cerebral artery
PCP	phencyclidine
PDC	L-trans-pyrollidine-2,4-dicarboxylic acid
Pdgfra/PDGFαR	platelet-derived growth factor receptor alpha gene/protein
PFA	paraformaldehyde
PGE2	prostaglandin E2
PPADS	pyridoxalphosphate-6-azophenyl-2',4'-disulfonic acid
PTB	pentobarbital
ROS	reactive oxygen species

RT-PCR	reverse transcription polymerase chain reaction
RT-qPCR	reverse transcription quantitative polymerase chain reaction
SCA	superior cerebellar artery
SD	standard deviation
Slc1a2	gene coding glial high affinity glutamate transporter GLT-1
Slc1a3	gene coding glutamate aspartate transporter GLAST
SOM	self-organizing map
TNFα	tumor necrosis factor-alpha
TRP	transient receptor potential
TTC	2,3,5-Triphenyltetrazolium chloride
TTX	tetrodotoxin
UBP141	(2R*,3S*)-1-(Phenanthrenyl-3-carbonyl)piperazine-2,3-dicarboxylic acid

1. INTRODUCTION

Glutamate is the principal excitatory neurotransmitter in the brain. Glutamatergic synaptic transmission was discovered over a period of two decades starting in the 1950s (Watkins and Jane 2006). The synthesis of N-methyl-D-aspartate (NMDA) enabled discovery of the NMDA receptor, which represents a distinct subtype of glutamate receptors. Since then, NMDA receptors were shown to play a key role in synaptic transmission, synaptic plasticity, neural development, as well as learning, memory and cognition (Van Dongen 2009).

For a long time, NMDA receptors were considered to reside only on neurons; however, discoveries of the last 25 years indicate their presence in glial cells. Sensitivity of glial cells to glutamate was discovered by Bowman, Kimelberg, Kettenmann and colleagues who demonstrated that application of glutamate depolarized cultured astrocytes and oligodendrocytes (Bowman and Kimelberg 1984; Kettenmann et al. 1984a; Kettenmann et al. 1984b). The following experiments identified α-amino-3-hydroxy-5-methyl-4-isoxazolepropionic acid (AMPA) receptors as dominant type of ionotropic glutamate receptors in glia (Verkhratsky and Kirchhoff 2007a). Probably the first evidence of functional expression of NMDA receptors in glia was provided in 1992 by Evans and colleagues, who found that NMDA receptors mediate changes in the membrane potential of Schwann cells (Evans et al. 1992). In the next years, NMDA receptors were also observed in other glial cell types by studying different cell parameters like specific gene expression or functional properties of these receptors (Žiak et al. 1998; Gallo and Ghiani 2000; Verkhratsky and Kirchhoff 2007b; Dzamba et al. 2013). This PhD thesis focuses on the astrocytic NMDA receptors, since astrocytes are the most widespread glial cell type in the brain with primary influence on many physiological and pathological processes.

Despite the number of studies in the field, there are still many unresolved questions concerning the role of NMDA receptors in astrocytes. What is the composition of NMDA receptors in astrocytes? How do they differ from neuronal NMDA receptors? What is their subcellular localization? How do they change after ischemic injury? What do astrocytes actually need them for? The main objective of this thesis was to give answers to these questions even though we knew that by answering them, many more will come.

1.1 Astrocytes

1.1.1 Glial cell types

The cells in the brain, also called neural cells, are divided into two main classes – neurons and glial cells. In contrast to neurons, glial cells are not able to generate action potentials as they represent non-excitable neural cells. The concept of glia first appeared in 1858 in the commentary of Rudolf Ludwig Karl Virchow to his earlier published paper (Virchow 1858). Initially, glia was defined as a connective substance, devoid of any cellular elements, in which nervous system elements were embedded. Heinrich Müller obtained the first image of a neuroglial cell in the retina, and these cells are now known as retinal Müller cells. In the 1860s, Otto Deiters and later also Jakob Henle described stellate cells closely resembling cells which we today know as astrocytes.

In the brain, glial cells outnumber neurons and the glia-neuron ratio differs in particular brain regions (Verkhratsky and Butt 2007). Glial cells are not only very populous but also heterogeneous. In central nervous system (CNS), they are divided according to their origin to microglia (mesodermal origin) and macroglia (ectodermal origin). Microglia are the resident macrophages of the CNS and ensure its immune defense. As for the macroglia, there are four main cell types – astrocytes, oligodendrocytes, NG2 glia (the name is derived from neural/glial antigen 2, also known as polydendrocytes) and ependymal cells, and they are further divided according to their function and location in the brain (**Fig. 1**, for detailed classification of glial cells see **Table 1**). The main function of oligodendrocytes is to insulate neuronal axons in the CNS by myelin. NG2 glia function as precursors of oligodendrocytes and serve as multipotent adult neural stem cells. The role of ependymal cells is to form separating layer between the cerebrospinal fluid (CSF) and CNS cellular compartments. Astrocytes represent the largest group of glial cells, having numerous functions in CNS, such as maintaining ionic-, neurotransmitter-, water- and pH homeostasis and controlling cerebral blood flow (Kimelberg 2007).

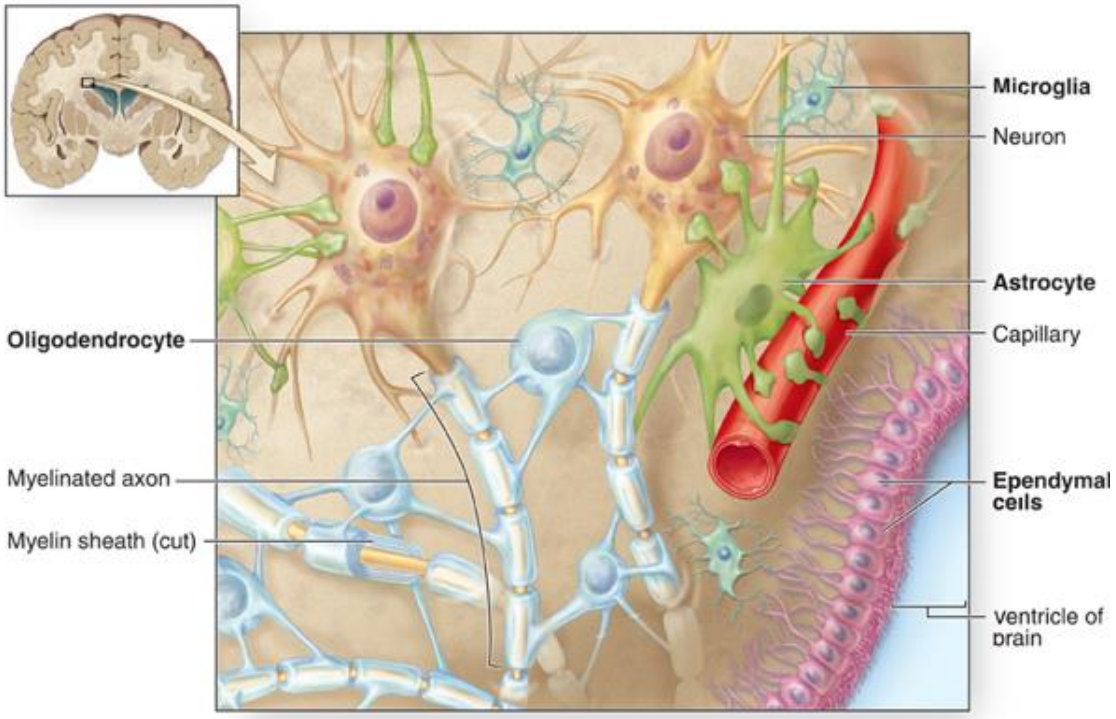


Figure 1. The main glial cell types (McKinley and O'Loughlin 2005).

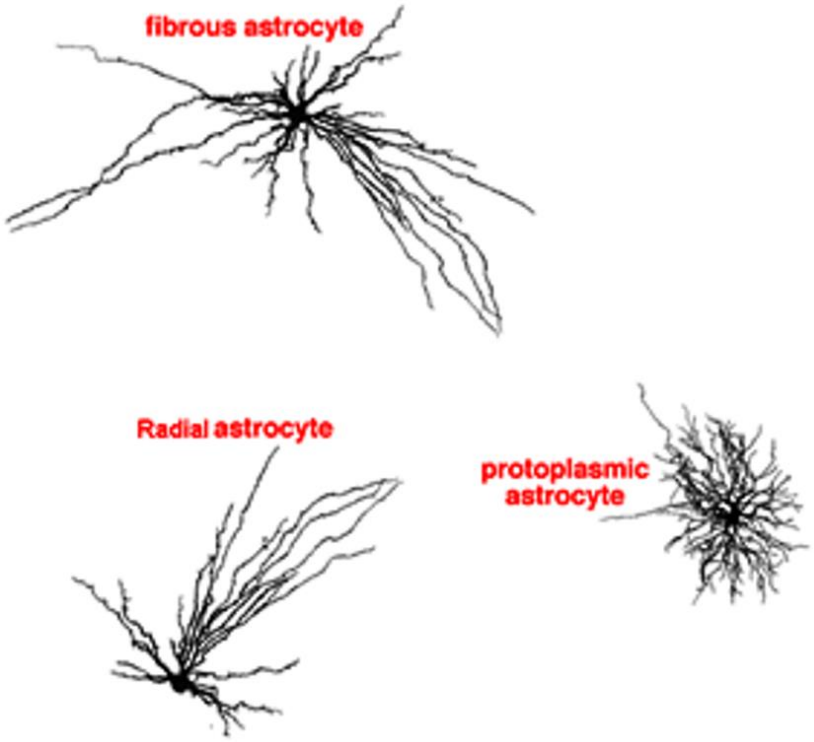


Figure 2. Basic morphology of three main types of astrocytes – radial glia (radial astrocyte), fibrous and protoplasmic astrocytes (Kalash 2013).

Glial cells in central nervous system	Mircoglia (10%) - mesodermal origin		Resting		have small somas and are present in normal non-injured brain
			Activated		originate from resting microglia when brain injury is sensed
			Phagocytic		originate further from activated microglia to provide active brain defence system
	Macroglia (90%) - ectodermal origin	Astrocytes	Protoplasmic (grey matter)		endowed with many fine processes (cca 50um long) which are extremely complex
					their processes contact blood vessels, forming so called 'perivascular' endfeet
					cover practically all neuronal membranes within their reach
					surface area of their processes is up to 80000 μm^2
					density in the cortex is 10000-30000 per mm^3
			Fibrous (white matter)		contain long (up to 30 µm) processes
					their processes send extensions contact axons at nodes of Ranvier
					density is 200000 per mm^3
			Radial glia		send out processes to form the pia-glial membrane
					play a role in neuron migration
					mostly present during development (except for Müller and Bergmann glia)
				Müller glia (retina)	density is 20000-25000 per mm^3 of retinal surface
				Bergmann glia (cerebellum)	relatively small cell bodies (15 µm in diameter)
					3-6 processes extend from the Purkinje cell layer to the pia
					each cell provides coverage for up to 8000 synapses formed by parallel fibres on Purkinje neurons
			Location-specific astrocytes	Velate (cerebellum)	form a seath surrounding granule neurones - each cell enwraps a single granule neuron
				Interlaminar (primate cortex)	contain very long processes (up to 1 mm)
					specific to cerebral cortex of higher primates with unknown function
				Tanycytes (periventricular organs, the hypophysis and the raphe part of the spinal cord)	in the periventricular organs form blood-brain barrier
					form tight junctions with capillaries
				Pituicytes (neurohypophysis)	their processes surround neuro-secretory axons and axonal endings
				Perivascular and Marginal	localized very close to the pia where they form numerous endfeet with blood vessels
					do not form contacts with neurons
					their main function is in forming the pial and perivascular glia limitans barrier
				Ependymocytes, choroid plexus cells and retinal pigment epithelial cells	line the ventricles or the subretinal space
		Oligodendrocytes	Myelinating	Type I (forebrain, cerebellum, spinal cord) and type II (white matter - corpus callosum, optic nerve, cerebellal white matter etc.)	small rounded cell body
					produce 4-6 primary processes which branch and myelinate 10-30 thin axons
					each secondary process forms a single internodal myelin segment 100-200 µm long
				Type III (cerebral and cerebellar peduncles, medulla oblongata and spinal cord)	much larger cell body with several thick primary processes
					myelinate up to 5 thick axons and produce internodal myelin seaths 200-500 µm long
				Type IV (entrances of the nerve roots into the CNS)	do not have processes
					form a single long myelin seath (1 mm internodal length)
			Non-myelinating	Satellite oligodendrocytes (grey matter)	applied to neuronal perikaria
					unknown function
		NG2 glia			have small somata and extending numerous thin, radially oriented processes
					serve as multipotent adult neural stem cell
					in the grey matter they form contacts with neurons and receive neuronal afferents
					do not form contacts with each other
		Ependymal cells			involved in production and movement of cerebrospinal fluid
					form separating layer between the cerebrospinal fluid and cellular compartments of CNS

Table 1: Division of glial cells (Verkhratsky and Butt 2007).

1.1.2 Characteristics of astrocytes

The term “astrocyte” is derived from their star-shaped bodies; however, their morphology differs depending on particular type of astrocytes. We distinguish three main types - radial glia, fibrous astrocytes and protoplasmic astrocytes **(Fig. 2)** (Kalash 2013). Radial glia are bipolar cells usually with two main processes, one of which forms endfeet at the ventricular wall and the other at the pial surface. They are mostly present during brain development, with the exception of Müller cells in retina and Bergmann glia cells in cerebellar cortex, which persist also in adulthood. Fibrous astrocytes are situated in the white matter and their long processes establish several perivascular or subpial endfeet. Protoplasmic astrocytes are found only in grey matter and are the most prevalent astrocytic type. They have bushy like morphology characterized by many fine processes, which enwrap neuronal synapses and contact blood vessels forming perivascular endfeet (Verkhratsky and Butt 2007).

One of the main characteristics of astrocytes is their mutual interconnection via gap junctions into large syncytium. The gap junction is formed by two hemichannels (also called connexons), one from each of the two connected cells. Each hemichannel consists of six connexins (Cx) which can be either of the same type (homomeric hemichannels) or of different types (heteromeric hemichannels). There are two main types of connexins, which are specific for astrocytes, Cx43 and Cx30 (Giaume et al. 2010). Gap junctions allow bidirectional flow of ions and signaling molecules with molecular weight up to 1-2 kilodaltons (kDa), such as inositol 1,4,5-triphosphate (IP_3) or adenosine triphosphate (ATP). The syncytium formed by connected astrocytes enables spatial communication and has strong impact on astrocytic functions (**Fig. 3**). Another interesting feature of astrocytes is that they establish distinct, almost non-overlaping microdomains. Each astrocyte has a region in the brain in which it is situated and these regions are separated from each other. At the borders of these microdomains there are gap junctions which enable interconnection of neighboring astrocytes (**Fig. 3**). Moreover, astrocytes also form higher anatomical domains within which they are interconnected, but the connection between these domains is very low (Houades et al. 2008).

Identification of astrocytes is commonly performed via presence of astrocytic markers. Some of the markers are connected with specific functions of astrocytes in the brain. For example, excitatory amino-acid transporters 1 and 2, also known as GLAST (glutamate

aspartate transporter) and GLT-1 (glial high affinity glutamate transporter) coded by *Slc1a3* and *Slc1a2* genes respectively, provide uptake of glutamate in astrocytes. Another example of astrocytic markers is aquaporin 4 (coded by *Aqp4* gene) or glutamine synthetase (GS) coded by *Glul* gene. Aquaporin 4 conducts water in the brain specifically through the astrocytic membrane contributing to the water homeostasis in the CNS. GS is an enzyme that plays essential role in the glutamate-glutamine shuttle between astrocytes and neurons. Among other astrocytic markers, glial fibrillary acidic protein (GFAP) is one of the most commonly used and aldehyde dehydrogenase 1 family (ALDH1L1), coded by *Aldh1l1* gene, is currently considered to be one of the most astrocyte-specific (Cahoy et al. 2008).

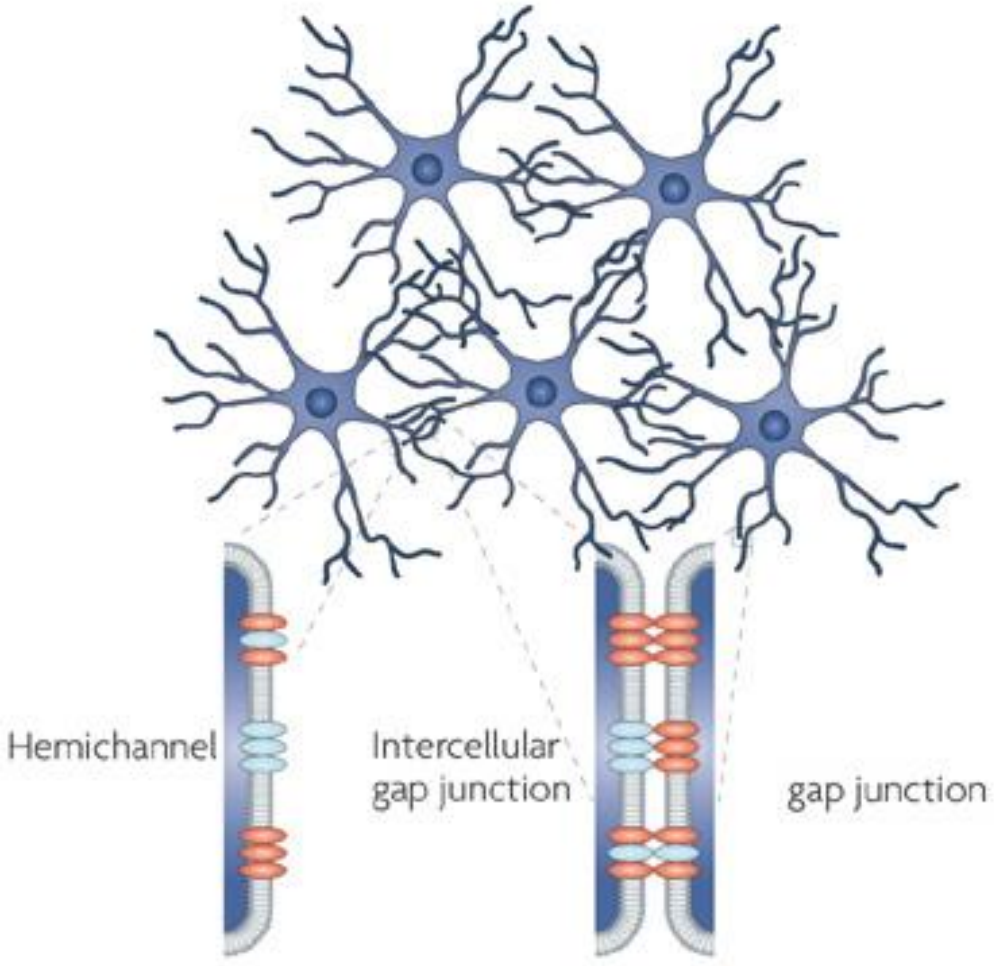


Figure 3. Localization and structure of connexin (Cx) channels in astrocytes. Domains that are occupied by neighboring astrocytes do not overlap, and intercellular gap junction channels are located at contact points between neighboring astrocytes. Connexins can also operate as hemichannels at the surface of the cell membrane to exchange information with the extracellular space. Astrocytes express mainly two connexins, Cx43 (blue) and Cx30 (red), and they function in several possible combinations (Giaume et al. 2010).

1.1.3 Astrocytic functions under physiological conditions

The large quantity and diversity of astrocytes is also connected with a number of functions they fulfill under physiological and pathological conditions. Originally were astrocytes considered to be passive elements of the brain, serving as a structural scaffold for neurons and insulators preventing undesirable spread of neuronal excitation. It was known that their processes are in a tight contact with blood vessels and neurons, so neuronal nourishment was considered as their main function. However, over the last decades, research of astrocytes brought evidences about new important functions of these cells.

One of the best characterized astrocytic functions is their maintenance of ionic homeostasis in the CNS. Astrocytes possess large K^+ conductance so they can detect even very small changes in the extracellular concentration of K^+ produced for instance by neuronal excitations. Astrocytes react to these changes by subtle shift in their membrane potential, intake of K^+ ions at sites of high neuronal activity and their subsequent redistribution within the astrocytic syncytium to the compartments with low extracellular K^+ concentrations, where they are extruded. This process is known as K^+ spatial buffering and serves as a regulator of extracellular K^+ concentration in CNS (Orkand et al. 1966; Kuffler 1967). Similar mechanism of extracellular K^+ concentration regulation, called K^+ siphoning, was described in retinal Müller glia. K^+ siphoning occurs only within one Müller cell, in which K^+ is taken up via Kir2.1 channels in the proximity of neuronal synapses, redistributed within the cell and extruded by Kir4.1 channels near blood vessels (Kofuji and Newman 2004).

Another important function of astrocytes is glutamate clearance from the neuronal synaptic cleft, which prevents undesired prolongation of glutamate activity on postsynaptic neurons and glutamate excitotoxicity. The glutamate clearance is performed via astrocytic glutamate transporters GLAST and GLT-1, acting as the primary sink for the glutamate in the CNS (Schousboe and Waagepetersen 2005). Within the astrocytic intracellular space, glutamate is processed in the glutamate-glutamine cycle, also called glutamate-glutamine shuttle. First, it is converted to glutamine by glutamine synthetase and glutamine is then transported back to the extracellular space (ECS), since it does not function as a neurotransmitter. Glutamine is further taken up by glutamine transporters on presynaptic neurons and hydrolysed by phosphate-dependent glutaminase to glutamate (Daikhin and Yudkoff 2000).

Another function of astrocytes, which was proposed already in 19th century based on observation that astrocytes are in contact with both neurons and blood vessels, is providing of energetic substrate, such as glucose, to neurons. Glucose is either taken up from blood vessels or converted from glycogen stored in astrocytic vesicles by glycogenolysis, which occurs mainly in the absence of glucose in the blood. Gap junction proteins Cx43 and Cx30 were shown to allow intracellular trafficking of glucose and its metabolites in the astrocytic syncytium (Rouach et al. 2008). Glucose in astrocytes can be converted to pyruvate and further to lactate which is then transported to neurons via the neuronal-glial lactate shuttle and serves as one of the energy sources, especially in immature brain (Pellerin 2003). Apart from glucose, astrocytes produce and provide neurons with glutathione, which scavenges reactive oxygen species and functions as endogenous antioxidant (Chen et al. 2001). A recent study reports that NMDA receptors in astrocytes play an important role in the neuronal antioxidant defense (Jimenez-Blasco et al. 2015).

The tight contact of astrocytes and blood vessels is connected with another function of astrocytes. Astrocytic endfeet enwrap the endothelial cells of blood vessels and participate thus in the formation of blood-brain barrier (BBB), a highly selective permeability structure separating the intracerebral blood vessels from the brain parenchyma interstitial fluid. BBB fulfils a protective function, as it prevents CNS from bacterial infections or an entrance of neurotoxins such as botulinum which could cause a serious fatal damage to the brain. Furthermore, the contact of astrocytic endfeet with blood vessels enables astrocytes to regulate microcirculation of blood in the brain. In the case of higher energy demands, e.g. during increased neuronal activity, the capillary vasodilation increases blood supply in the region, and astrocytes play a key role in this process. The regulation of blood microcirculation is achieved in neuro-glio-vascular units, in which astrocytes regulate both constriction and dilation of blood vessels depending on their intracellular Ca^{2+} concentration, which results from neuronal activity in the astrocytic vicinity. Astrocytes contain Ca^{2+}-sensitive phospholipase A2 which produces arachidonic acid (AA), which can be further converted either to 20-hydroxyeicosatetraenoic acid (20-HETE) and cause vasoconstriction, or prostaglandin E2 (PGE2) and epoxyeicosatrienoic acid (EET) leading to dilation. Moreover, the effect of astrocytes on microcirculation can be achieved also by modifying vascular tone by the hyperpolarization and relaxation of smooth muscle cells (Gordon et al. 2007).

Astrocytes have been considered to be passive, non-excitable cells for a long time. However, results of experiments in the last 3 decades showed that astrocytes are able to respond to neuronal activity by Ca^{2+} oscillations and these oscillations can propagate within astrocytic syncytium and serve for a long-distance signal transmission in the CNS. In response to oscillating elevations of Ca^{2+} concentration in astrocytes, they are able to release gliotransmitters, such as glutamate, ATP or D-serine by exocytosis (Hamilton and Attwell 2010). Astrocytes thus participate in an interneuronal communication, since release of gliotransmitters near the neuronal synapses can modulate synaptic activity. These findings led to discovery of tripartite synapse concept, in which presynaptic and postsynaptic neurons, together with astrocytic endfeet enwrapping the synapse, participate in signal transduction (Araque et al. 1999). From this perspective, astrocytes can be seen as cells able to generate, receive and propagate signals by means of Ca^{2+} waves (Fiacco and McCarthy 2006).

Astrocytes mostly fulfil regulatory functions. Besides already mentioned functions, astrocytes also play a role in CNS development, in which they regulate neurogenesis and gliogenesis (Ganat et al. 2006). They are responsible for the regulation of pH in CNS via the Na^+/H^+ exchanger and the Na^+/HCO_3^- cotransporter (Deitmer and Rose 1996). Furthermore, astrocytes are equipped by aquaporins AQP1 and AQP4, which ensure water homeostasis in the brain by regulating water movement between blood and CNS (Gao et al. 2006).

1.1.4 Membrane properties of astrocytes

Invention of patch-clamp technique started a revolution in studying cell membrane properties (Hamill et al. 1981). The first experiments aimed to characterize the membrane properties of glia were performed on glial cell cultures in the 1980s, followed by studies in brain slices in 1990s. The results from these studies showed that glial cells express a number of voltage-gated ion channels and neurotransmitters (Sontheimer 1994) and initiated a debate about their possible functions. Moreover, patch-clamp studies of glial cells in hippocampal slices revealed that glial cells differ in their membrane properties (Steinhauser et al. 1992; Tse et al. 1992; Steinhäuser et al. 1994). Some of the glial cells were characterized by passive current profile, which was defined by time- and voltage-independent K^+ conductance, while the other were characterized by complex current profile represented by passive K^+ conductance with delayed outwardly rectifying K^+ current (K_{DR}), fast activating and inactivating A-type K^+ current (K_A), inwardly rectifying K^+ current (K_{IR}) and tetrodotoxin (TTX)-sensitive Na^+ current (I_{Na}).

Later studies aiming specifically at astrocytes in the transgenic mice expressing enhanced green fluorescent protein (EGFP) under the control of the human promotor for GFAP discovered that cells with bright EGFP fluorescence have a passive current profiles and express glutamate transporters (GluT), whereas weakly fluorescent cells have a complex current profile and express glutamate receptors (GluR) (Matthias et al. 2003). The division of GFAP/EGFP-positive (GFAP/EGFP$^+$) glial cells was further supported by the fact that in contrast to the GluR cells, the GluT cells were reported to be extensively dye coupled. It was later shown that the GluR cells are positive to NG2 chondroitin sulphate proteoglycan (CSPG4) and belong thus to a distinct NG2 glial cell population (Wallraff et al. 2004). Currently, we can distinguish cell types according to their current pattern; outwardly rectifying current pattern is a hallmark of glial precursors, complex current pattern belongs to NG2 glia and cells with passive current profile are considered to be mature astrocytes (**Fig. 4**). Distinct current patterns are thus very helpful in cell identification in the electrophysiological experiments.

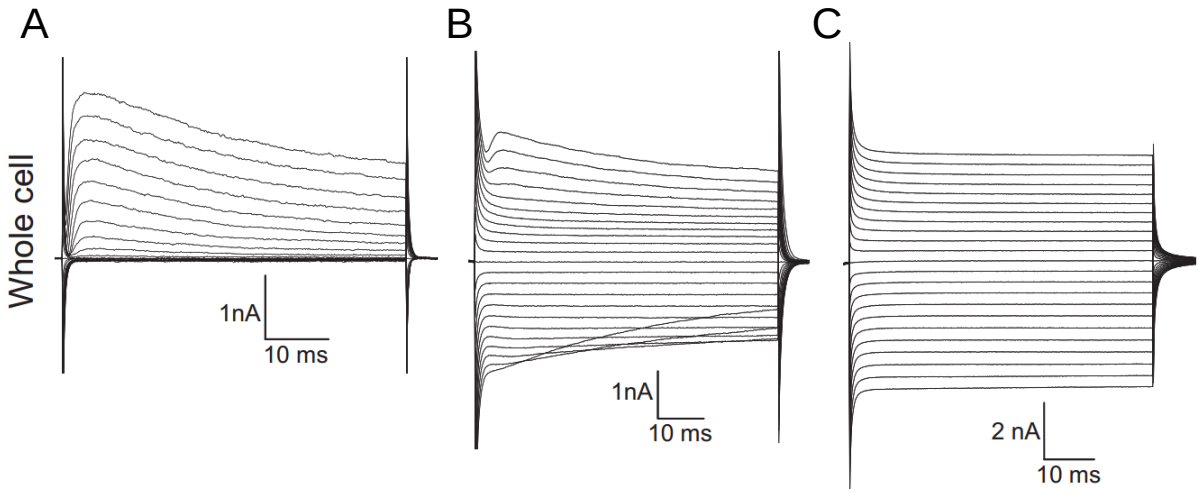


Figure 4. Distinct electrophysiological current profiles of glial cells obtained from the whole cell voltage-clamp. (**A**) Outwardly rectifying current profile indicating glial precursors, (**B**) complex current profile indicating NG2 glia and (**C**) passive current profile indicating mature astrocytes (Schools et al. 2006).

The presence of constitutive K^+ conductance (passive current profile) of astrocytes is crucial for astrocytic functions such as K^+ spatial buffering. Originally, it was suggested to be carried by weakly inwardly rectifying Kir4.1 channels, which are typically expressed in

astrocytes, and partially also by currents flowing through gap junctions formed by connexins Cx30 and Cx43 (Wallraff et al. 2006; Adermark and Lovinger 2008). Discoveries of Seifert and Zhou with colleagues, however, showed that the passive K^+ conductance of astrocytes is a result of combination of Kir4.1 channels and two-pore domain K^+ channels, such as inward rectifying TWIK-1 and outward rectifying TREK-1 channels (Seifert et al. 2009; Zhou et al. 2009).

The membrane properties of astrocytes are also influenced by voltage-gated Ca^{2+} and Na^+ channels. Their expression in astrocytes is regulated during development and they are mostly expressed in glial precursors and immature glial cells (Kressin et al. 1995). Furthermore, astrocytes express multiple membrane proteins, such as transient receptor potential (TRP) channels (Butenko et al. 2012; Scimemi 2013), hyperpolarization-activated cyclic nucleotide-gated (HCN) channels (Honsa et al. 2014), purinergic receptors (Abbracchio and Ceruti 2006) or gamma-aminobutyric acid (GABA) receptors (Fraser et al. 1994; Lee et al. 2011), which function as cellular sensors and enable flux of specific ions across the cell membrane. Glutamate receptors, including NMDA receptors, are also part of this palette; however, their role and function in astrocytes is still to be discovered.

1.2 NMDA receptors

1.2.1 Glutamate receptors

Glutamate receptors are either ionotropic, which form an ion channel pore, or metabotropic, which are coupled via heterotrimeric G proteins to effector channels or enzymes. Ionotropic receptors are divided into three classes according to their specific agonist, namely NMDA (GluN1, GluN2A-D and GluN3A-B subunits), AMPA (GluA1-4 subunits) and kainate receptors (GluK1-5 subunits). There are 8 metabotropic glutamate receptors (mGluR1-8) divided into three groups according to their structure and physiological activity. Schematic representation of glutamate receptors is depicted in **Fig. 5** and their classification is in **Fig. 6**. Glutamate receptors have a wide range of their functional properties; they differ in their sensitivity to glutamate, requirement of a co-agonist, permeability for particular ions, deactivation time, and their specific agonists and antagonists.

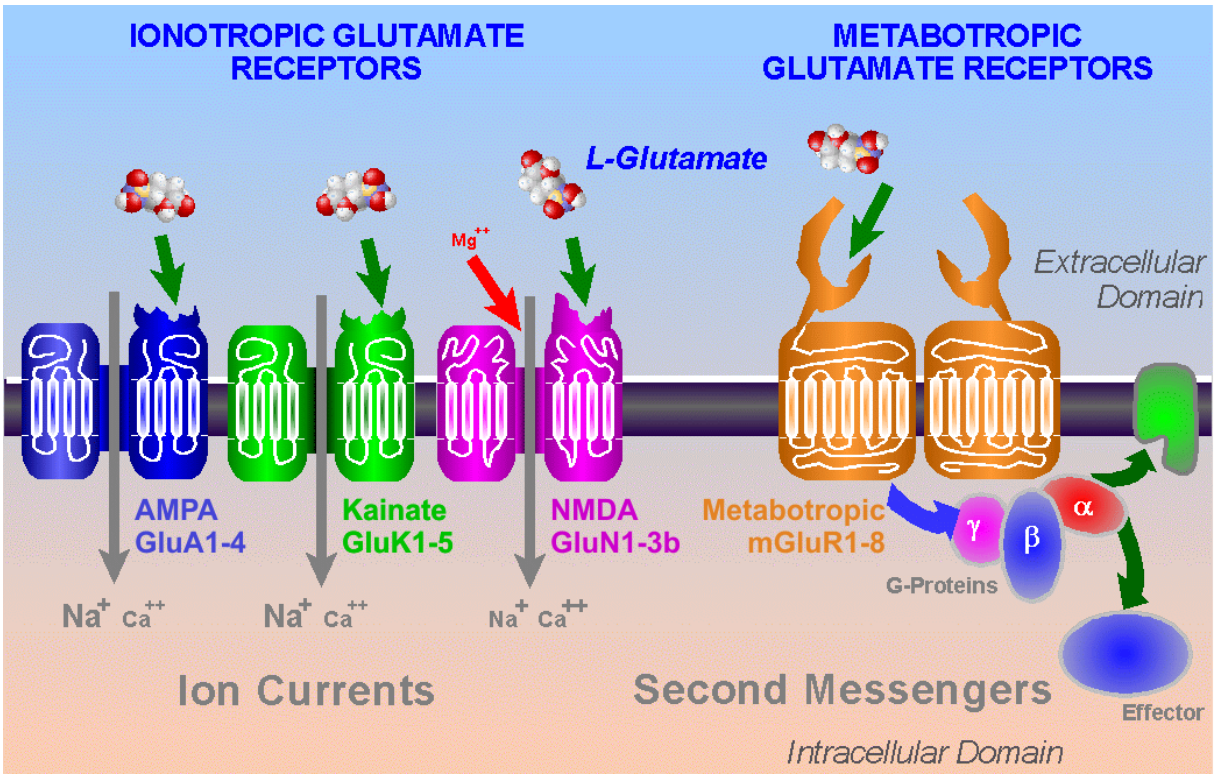


Figure 5. Schematic representation of glutamate receptors family - AMPA, kainate, NMDA and metabotropic glutamate receptors (with modifications from (Salt 2012)).

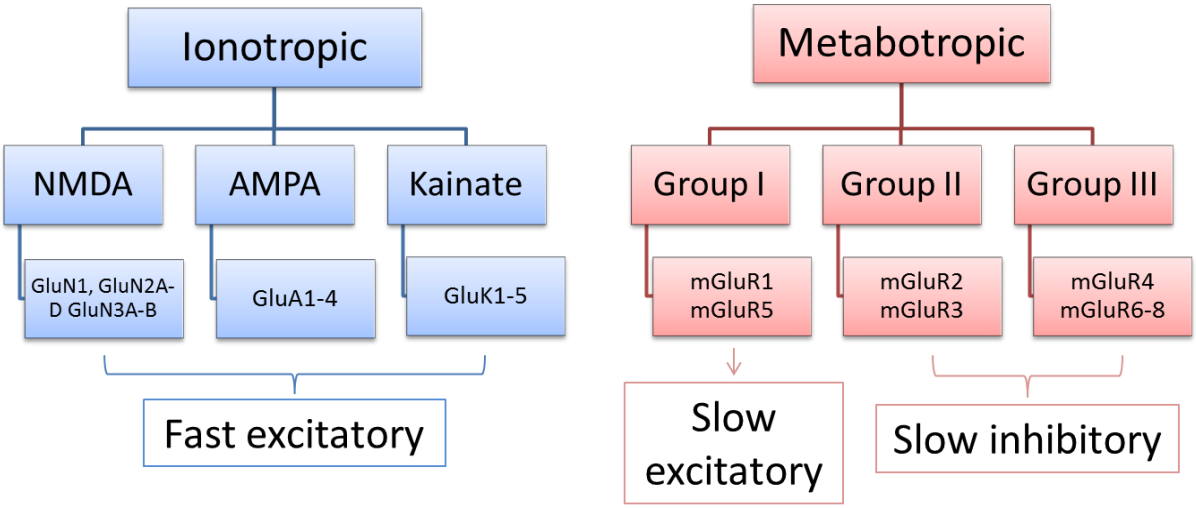


Figure 6. Classification of glutamate receptors (Blackshaw et al. 2011).

1.2.2 Structure of NMDA receptors

NMDA receptors (**Fig. 7**) can form subtypes with distinct properties, depending on their subunit composition, as they form heterotetramers comprising a combination of GluN1, GluN2A-D and GluN3A-B subunits (Hollmann and Heinmann 1994). Splice variants have been reported for most of the subunits (Rafiki et al. 2000; Eriksson et al. 2002), but the best studied is the GluN1 subunit with 8 different isoforms (Petralia and Wenthold 2008). The main agonists are glutamate and NMDA, which both bind to GluN2A-D subunits, while the binding site for the co-agonists D-serine and glycine is at GluN1 and GluN3A-B subunits (Johnson and Ascher 1987). The most common combination of subunits in functional NMDA receptors is two GluN1 and two GluN2 subunits, or two GluN1, one GluN2 and one GluN3 subunit. Combination of GluN1 and GluN3 subunits is also functional, but these receptors lack the glutamate binding site (Smothers and Woodward 2007). Moreover, there are indications that NMDA receptors can be co-assembled without the GluN1 subunit, but their functional properties are debatable (Perez-Otano et al. 2001; Matsuda et al. 2003).

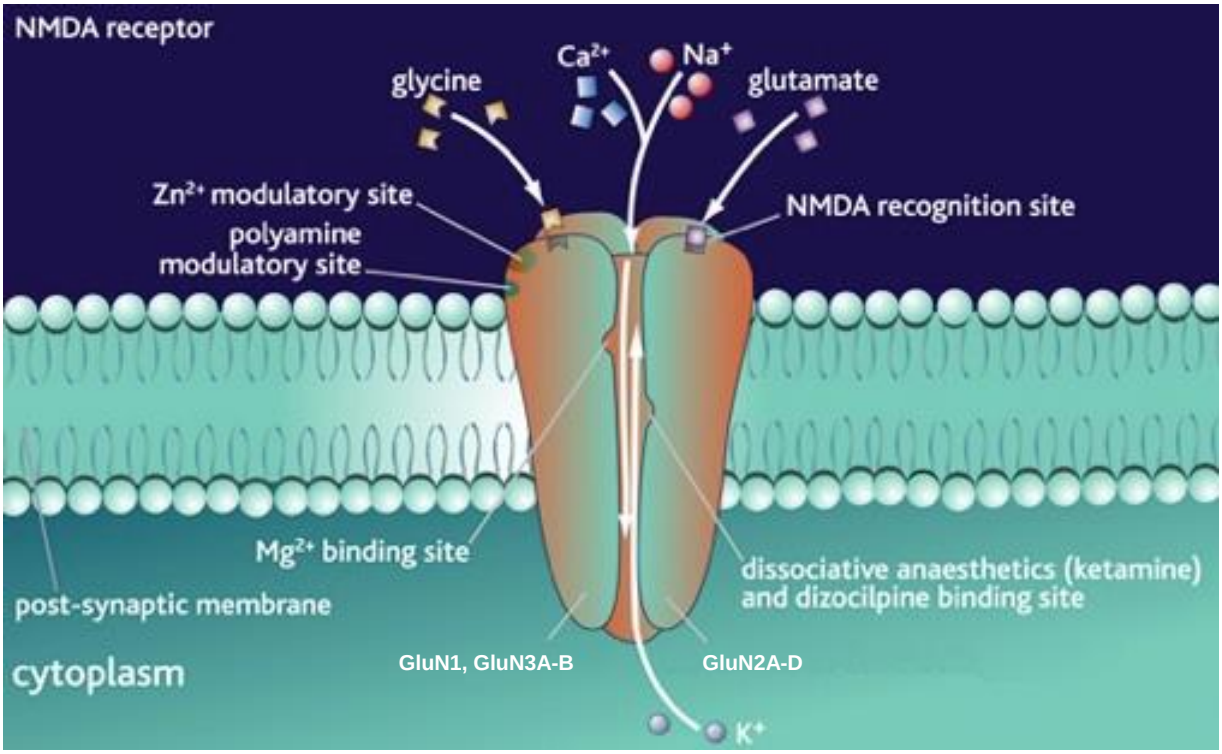


Figure 7. Schematic representation of NMDA receptor. Glycine and glutamate binding sites are in the extracellular parts of GluN1,3A-B and GluN2A-D subunits, respectively. Binding sites for Mg^{2+} and dissociative anesthetics (such as ketamine) with dizocilpine binding sites are inside the NMDA receptor (Baraldo 2002).

The large variety in composition of NMDA receptors leads to a large variation in their functional properties, such as deactivation time, specificity in ionic conductivity, sensitivity to Mg^{2+} block and antagonist specificity. The composition of NMDA receptors is brain region specific and depends also on a developmental stage (Akazawa et al. 1994). Activated NMDA receptors are permeable to Ca^{2+}, Na^{+} and K^{+} ions, but this permeability strongly varies with receptor subunits composition. For example, inclusion of the GluN3 subunit in the NMDA receptor co-assembly leads to insensitivity to Mg^{2+} block, decreased permeability for Ca^{2+} as well as reduced overall current (Cavara and Hollmann 2008). Recently, x-ray crystal structure of GluN1/GluN2B NMDA receptor was published, which had a profound impact on elucidation of its structure and pore architecture (Lee et al. 2014).

1.2.3 Function of NMDA receptors

The function of NMDA receptors was initially described in neurons. It was shown that they mediate signal transduction in neuronal networks and participate in long-term potentiation (LTP) and long-term depression (LTD). NMDA receptors are thus a target of several drugs with antagonistic effect used for anesthesia, such as ketamine or nitrous oxide (N_2O), which is used especially in dentistry, as well as recreational drugs, such as dizocilpine (known also as MK-801), phencyclidine (PCP) or dextromethorphan (DXM). In general, antagonists of NMDA receptors can be divided according to the mechanism of action into three groups. Competitive antagonists, which compete with glutamate and glycine at their binding sites; channel blockers, which are uncompetitive and act at the ion channel pore; and negative allosteric modulators, also called non-competitive antagonists, which act at the amino terminal domain of the receptor subunit. On the other hand, there are also positive allosteric modulators, which potentiate agonists' effect. Each of these NMDA receptor modulators shows subunit specificity which can be utilized in modulation of NMDA receptors subtypes. The history of discovery of these NMDA receptor ligands is depicted in a timeline in **Fig. 8** (Ogden and Traynelis 2011).

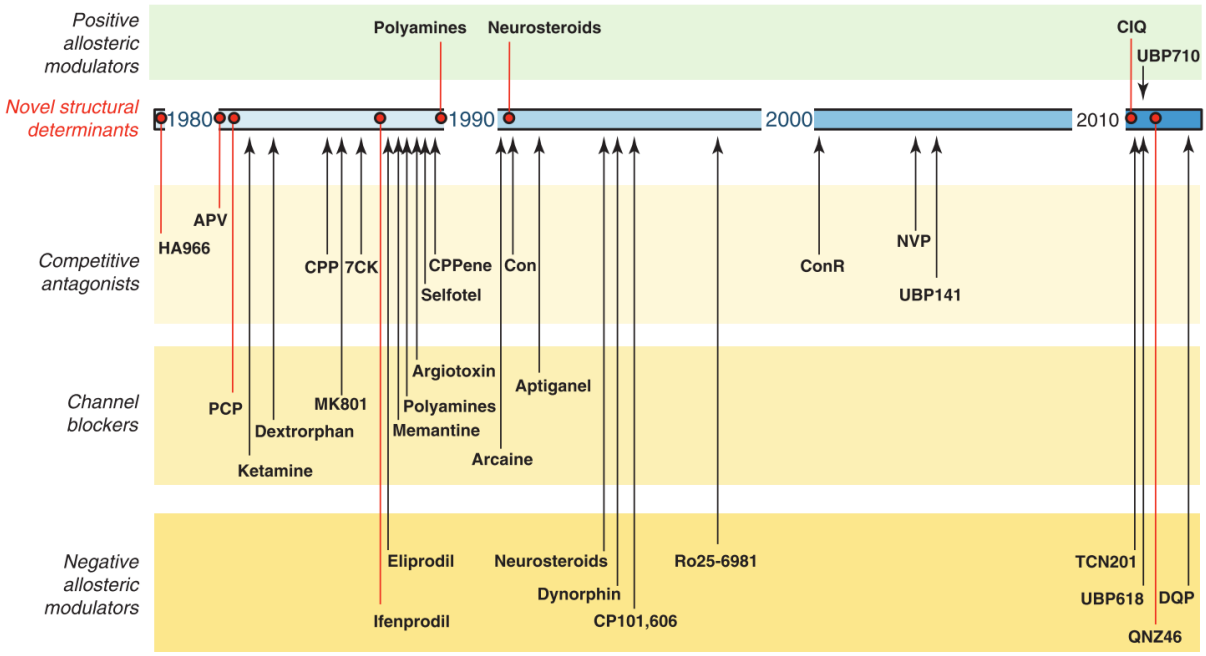


Figure 8. Examples of competitive antagonists, channel blockers and negative/positive allosteric modulators of NMDA receptors. Red circles within the timeline correspond to identification of a new site of action in NMDA receptors (Ogden and Traynelis 2011).

An appreciation of the functional importance of NMDA receptors led to a number of clinical trials, in which NMDA receptor antagonists were tested in the treatment of brain pathologies, such as stroke, traumatic brain injury, epilepsy and Alzheimer's disease. The rationale for the treatment is that excessive glutamate present during these pathologic situations is excitotoxic and leads to neuronal death by necrotic or apoptotic mechanisms. NMDA receptor antagonists are thus supposed to serve as neuroprotective agents. However, these trials revealed unacceptable psychotomimetic side effects of the drugs, resulting from the fact that NMDA receptor activity is also required for normal neuronal function, so the first clinical studies were unsuccessful. The interest was, therefore, gradually shifted to low-affinity, uncompetitive open-channel blockers, such as memantine. The uncompetitive antagonism and relatively fast off-rate enables memantine to block excessive NMDA receptor activation with sparing low levels of NMDA receptor activity needed for normal physiological processes like neurotransmission, which ensures clinical tolerability as well as neuroprotection and is currently used for the treatment of moderate-to-severe Alzheimer's disease (Muir 2006; Chen and Lipton 2006). Since NMDA receptors were documented also in glial cells, the future clinical trials should also consider effect on these receptors. Better understanding of differences between neuronal and glial NMDA receptors could thus contribute to the treatments in which only neuronal NMDA receptors would be affected.

1.3 Cerebral ischemia

Cerebral ischemia is a condition that occurs when there is insufficient supply of blood in the brain. We distinguish two types of cerebral ischemia – focal ischemia, which is confined to a specific region of the brain; and global ischemia, which encompasses the whole brain tissue.

1.3.1 Focal cerebral ischemia

Focal cerebral ischemia occurs when a cerebral vessel is blocked by a blood clot caused by thrombosis or embolism and reduces thus blood flow to the particular brain region. The brain cells in the affected region cannot perform aerobic metabolism due to the loss of oxygen supply and since they are not able to switch to anaerobic metabolism, their levels of ATP drop rapidly within few minutes. With energy depletion, cells in the affected region fail to maintain ionic gradients and lose their ability to maintain membrane potential. Consequently, voltage-dependent Ca^{2+} channels become activated, excitatory neurotransmitters are released into the ECS and their reuptake is impeded due low cellular ATP levels, which leads to excitotoxicity. Glutamate accumulated in the ECS activates glutamate receptors, which further contribute to Ca^{2+} overload, initiating a series of cytoplasmic and nuclear processes, such as activation of proteolytic enzymes that degrade cytoskeletal proteins, mitochondrial damage, production of reactive oxygen species (ROS) and finally leading to cell death. As a result of glutamate-mediated overactivation, Na^{+} and Cl^{-} influx occurs and causes cellular swelling resulting in a brain edema, which has further negative effect on the cell survival. This process is accompanied by efflux of K^{+}, which together with excess of glutamate causes peri-infarct depolarization (Dirnagl et al. 1999). The basic overview of pathophysiological mechanisms in the focal cerebral ischemia is depicted in **Fig. 9**. In contrast to the global cerebral ischemia, focal cerebral ischemia occurs only regionally, so the blood flow in the rest of the brain is intact. The brain damage is therefore the most severe in the ischemic core, which is surrounded by an area called penumbra, in which intermediate blood perfusion prevails and despite repeated transient depolarization and associated ion shifts (Rossi et al. 2007), the cells in this region are able to survive (**Fig. 10**). In the ischemic core, vast majority of cells undergo necrosis; however, in the penumbra region, part of the cells undergoes apoptosis and part survives.

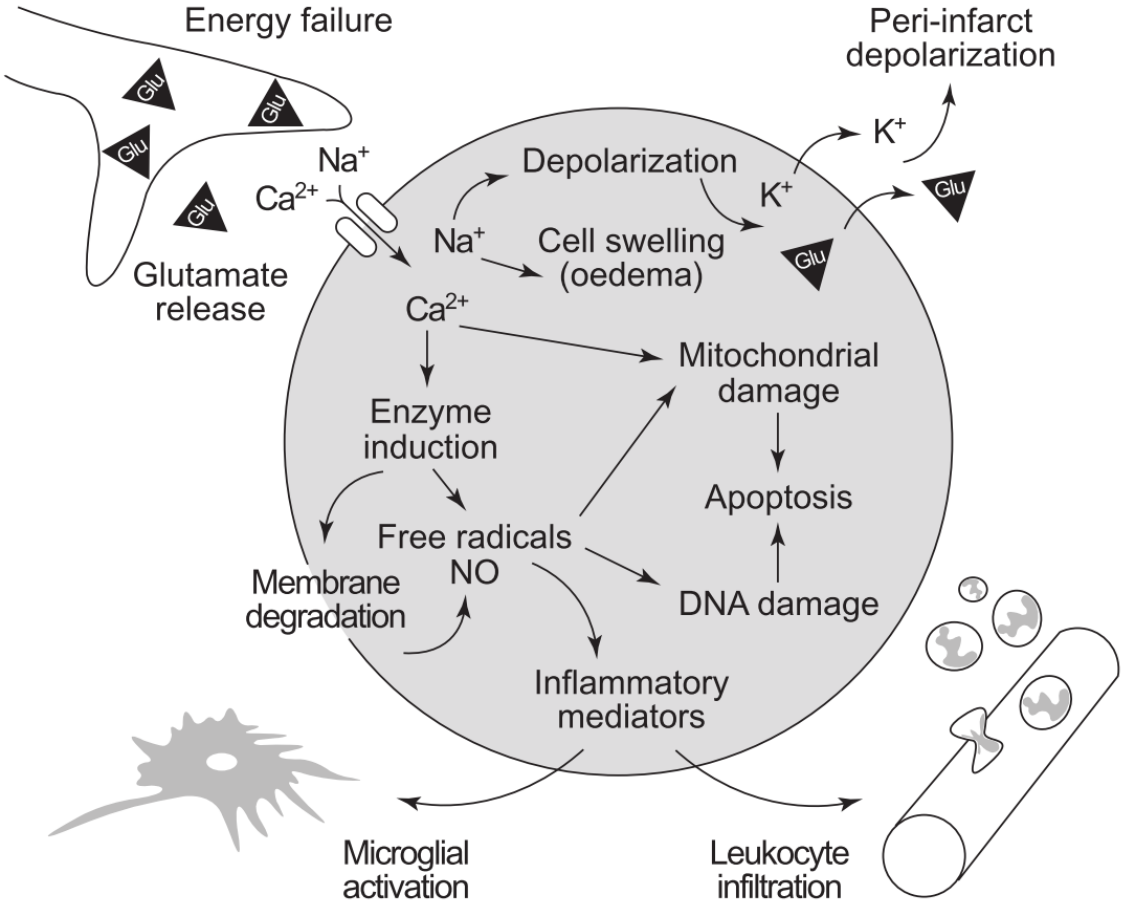


Figure 9. Focal cerebral ischemia - simplified overview of pathophysiological mechanisms. Energy failure causes neuron depolarization and activation of glutamate receptors, which increases intracellular levels of Ca^{2+}, Na^{+} and Cl^{-} while K^{+} is released into the extracellular space. Extracellular glutamate and high concentration of K^{+} cause peri-infarct depolarization. The increased level of intracellular concentration of Ca^{2+} activates enzyme systems inducing membrane degradation and free radicals formation, which are further responsible for the formation of inflammatory mediators leading to the activation of microglia and leukocyte infiltration. Moreover, mitochondrial damage takes place, which together with DNA damage leads to cell apoptosis (Dirnagl et al. 1999).

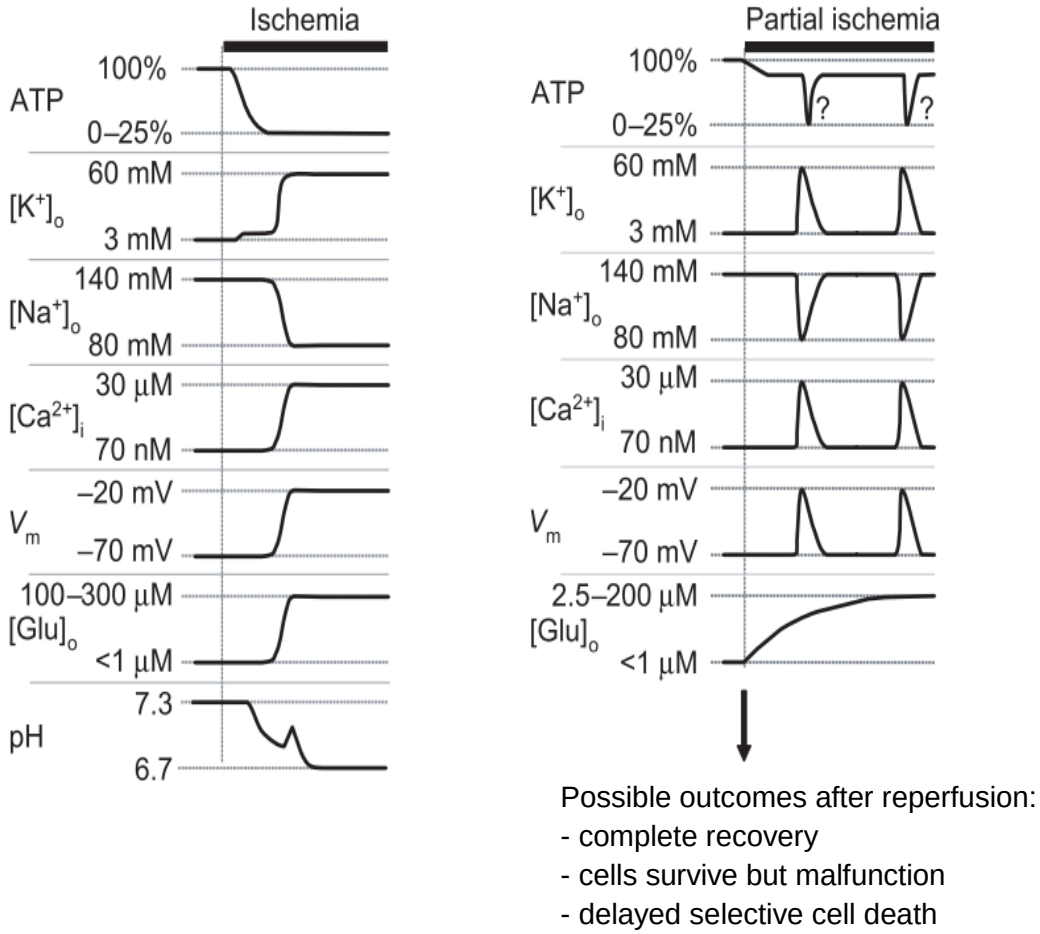


Figure 10. Schematic illustration of events occurring in focal cerebral ischemia. In the ischemic core (left), the interruption of ATP production causes inhibition of the Na^+/K^+ ATPase, which leads to distortion of ionic gradients, cell depolarization and release of glutamate into the extracellular space (ECS). In the penumbra region of focal ischemia (partial ischemia, right), the initial drop of ATP is less severe, so it triggers only transient oscillations in ionic gradients and membrane potential. However, concentration of glutamate in ECS gradually rises. If the reperfusion occurs early after ischemia, complete or partial recovery may occur, otherwise the cells undergo delayed cell death (Rossi et al. 2007).

1.3.2 Mouse models of focal cerebral ischemia

To study focal cerebral ischemia in mice, several different models exist (Traystman 2003). Most of them use occlusion of the middle cerebral artery (MCA) (**Fig. 11**) mimicking human thromboembolic stroke. The middle cerebral artery occlusion (MCAO) is either permanent or temporary and the occlusion of MCA can be either at proximal or at distal part of the vessel. The permanent MCAO is achieved by electrocoagulation of MCA through a craniotomy and the reproducibility of this model is relatively high. The temporary MCAO is usually achieved by intraluminal filament, which is inserted into the internal carotid and the

cerebral blood flow is monitored by a laser Doppler flow probe. The temporary MCAO model enables to study brain injury associated also with reperfusion after the occlusion. Apart from MCAO models of focal cerebral ischemia, there are also models utilizing homologous blood clot fragments injected directly into the common carotid artery or photochemical lesion evoked by means of photo-activation of a previously injected light-sensitive dye (Labat-gest and Tomasi 2013).

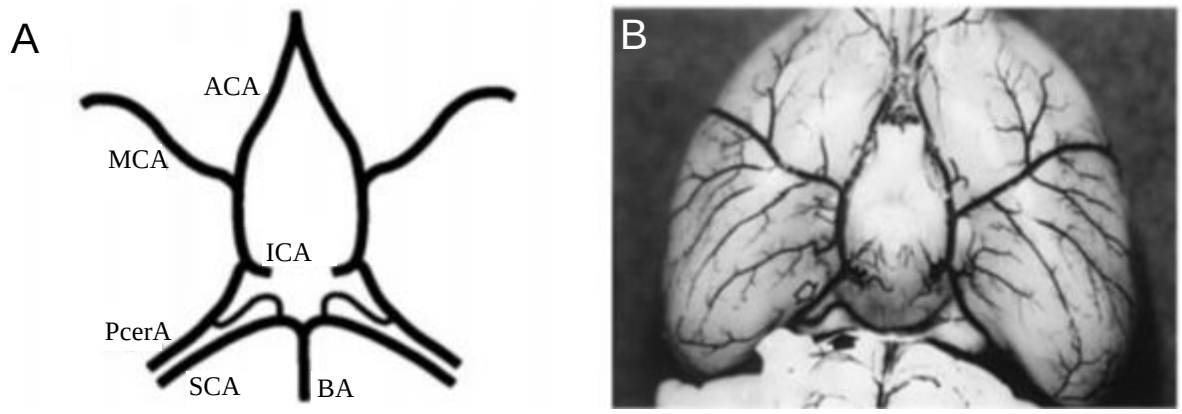


Figure 11. Major blood vessels in the mouse brain. (**A**) The scheme showing positions of anterior cerebral artery (ACA), middle cerebral artery (MCA), internal carotid artery (ICA), posterior cerebral artery (PcerA), superior cerebellar artery (SCA), and basilar artery (BA). (**B**) Photomicrograph showing major blood vessels (Murakami et al. 1998).

1.3.3 Astrocytes in cerebral ischemia

The animal models of cerebral ischemia were used in a series of studies focused on elucidation of the role of astrocytes in this pathology. Cerebral ischemia induces large morphological and functional changes in astrocytes. The protective astrocytic functions, such as K^+ buffering, glutamate uptake, or elimination of free radicals, are in ischemia compromised due to the impairment of their metabolism (Nedergaard and Dirnagl 2005; Pekny et al. 2014).

In focal cerebral ischemia, ischemic core is formed in which severe reduction of blood flow reduces cell survival. Nonetheless, in peripheral areas of focal ischemia, on the boundary between the ischemic core and penumbra, the malfunctioning astrocytes cause neuronal death, so this border of the ischemic infarct region is occupied mostly by astrocytes. The astrocytes in this region become reactive, enlarge their processes and increase synthesis of GFAP. They begin to produce more supportive structures and extend pseudopodia, which

eventually leads to formation of a dense web that fills the space generated by dead neurons. This process is called astrogliosis and is accompanied by secretion of molecules, such as laminin, fibronectin or proteoglycans, which modify the extracellular matrix surrounding the damaged region. Reactive astrocytes in this region also modulate tissue inflammatory response by releasing cytokines, such as tumor necrosis factor-alpha (TNFα) or interleukins. Astrogliosis results in the formation of glial scar separating the necrotic tissue from the healthy brain, which is important in protecting and healing of the nervous system. Furthermore, glial scar also prevents the propagation of seizure activity from injured to healthy tissue. The positive effect of glial scar formation was confirmed in the study, in which ablation of scar-forming reactive astrocytes was performed. Absence of glial scar led to the spreading of inflammation into a larger brain area and a longer inflammatory response. The ablation of reactive astrocytes further resulted in a significant secondary tissue degeneration connected with neuronal and oligodendrocyte cell death, demyelination and massive edema (Bush et al. 1999). The formation of glial scar was studied also by Pekny and colleagues, who discovered that mice lacking GFAP or vimentin are still able to form glial scar after injury. Nonetheless, in mice lacking both, GFAP and vimentin, the formation of glial scar was markedly impaired (Pekny et al. 1999).

Under pathophysiological conditions, not all of the astrocytic functions are positive. For example, already mentioned astrogliosis, prevents cell migration to the site of injury and limits ingrowth and regeneration of axons in injured CNS, which is problematic particularly in spinal cord injuries. Another negative outcome of astrocytes under pathophysiological conditions is their swelling which may lead to cytotoxic and vasogenic edema. The astrocytic swelling further causes changes in the extrasynaptic transmission as a result of shrinkage of the ECS (Vargová and Syková 2008). Spreading depression, which is a propagating wave of high K^+ concentration expanding from the necrotic region, or Ca^{2+} waves, also propagating in severe brain injuries, are both mediated by astrocytes and cause further harm in already injured brain tissue. The role of astrocytes in injuries, especially those of a large scope, is therefore both, beneficial and detrimental.

The functions of reactive astrocytes result from activity of their ion channels, which undergo marked changes after ischemic insult leading to altered astrocytic membrane properties. First of all, the insult leads to decrease in the number of glial cells with passive current profile specific for mature astrocytes, when compared to glial cells with complex current profile (Schröder et al. 1999; Wang and Bordey 2008). Moreover, most of the studies

report a decrease of K_{IR} currents, which was observed after MCAO (Köller et al. 2000), cortical stab wound (Perillán et al. 1999) or also after a fluid percussion injury (Stewart et al. 2010). Observed decrease in K_{IR} currents was shown to be associated with astrocytic proliferation which is accompanied by an increase in outwardly rectifying K^+ currents (MacFarlane and Sontheimer 2000; Bordey et al. 2001). Downregulation of K_{IR} currents in passive and complex glial cells and upregulation of K_{DR} currents in proliferating astrocytes after a cortical stab wound injury in rats was described by Anderova and colleagues (Anderova et al. 2004). Apart from K^+ channels, there are reports that astrocytes after injury undergo dramatic changes also in other types of membrane proteins. For example, there are reports of increased expression of HCN channels (Honsa et al. 2014), increased activity of TRPV4 channels, which results in elevated Ca^{2+} influx (Butenko et al. 2012) or upregulation of L-type Ca^{2+} channels (Westenbroek et al. 1998). There are indications that the changes in Ca^{2+} influx in astrocytes after ischemic insult might be regulated also by glutamate receptors, especially NMDA receptors (Krebs et al. 2003). Nonetheless, the response of astrocytes to the injury with respect to NMDA receptors is still not fully understood and is a subject of current research.

Reactive astrocytes are characterized by a profound change in their phenotype and their properties are studied in order to better understand their new roles, which can eventually be helpful in improving post-ischemic therapy. NMDA glutamate receptor antagonists were also considered as an option in the treatment of cerebral ischemia, since they diminish neurotoxicity and were thought to increase survival of neurons after ischemia; however all of the clinical trials failed, which is supposed to be a consequence of NMDA receptor block, which is impeding post-ischemic neuronal repair (Ikonomidou and Turski 2002). Nonetheless, astrocytic NMDA receptors were not considered in the suggested NMDA-oriented treatment of ischemia, which is due to the fact that the role of astrocytic NMDA receptors, especially after ischemia, is still not fully elucidated.

1.4 NMDA receptors in astrocytes

1.4.1 Expression of genes coding NMDA receptor subunits in astrocytes

In the last two decades there have been several attempts to detect subunits of NMDA receptors in astrocytes. In one of the first studies, Conti and colleagues used *in situ* hybridization together with immunocytochemistry to detect a marker of astrocytes, GFAP, and showed that in adult rat cortical slices virtually no astrocytes contained mRNA

transcripts of the GluN1 subunit (Conti et al. 1994). Other *in situ* hybridization studies in adult rat cerebellar Bergmann glial cells confirmed the presence of GluN2B and GluN2C mRNA transcripts (Akazawa et al. 1994; Luque and Richards 1995) which; however, cannot form functional NMDA receptors without the GluN1 subunit. The absence of GluN1 transcripts in cultivated as well as acutely isolated astrocytes from 1-17-day-old mice was also confirmed by Affymetrix GeneChip Arrays (Cahoy et al. 2008). Nevertheless, in mature acutely isolated cortical astrocytes, Cahoy and co-authors confirmed the presence of GluN2C transcripts, which were statistically highly enriched when compared to their numbers in neurons or oligodendrocytes. It is very interesting that in all astrocytes tested, a high level of GluN3A subunit transcripts was detected. In the study of Cahoy, both genes coding GluN2C and GluN3A subunits were statistically augmented in acutely isolated astrocytes when compared to cultured ones. In contrast to these findings, there are also studies showing the presence of the crucial GluN1 mRNA in astrocytes. In the first of these, reverse transcription polymerase chain reaction (RT-PCR) analysis of fluorescence-activated cell sorted astrocytes acutely isolated from the cortices of 2-week-old GFAP/EGFP transgenic mice revealed the presence of GluN1, GluN2B and GluN2C and the absence of GluN2A, GluN2D and GluN3 mRNA transcripts (Schipke et al. 2001). In another work studying astrocytes in primary cultures prepared from newborn mice, the authors showed the presence of GluN1 mRNA transcripts in these cells, which was significantly down-regulated after 2 weeks of cultivation (Zhou et al. 2010). On the other hand, the mRNA levels of GluN2A and GluN2B significantly increased with cultivation time for up to 4 weeks. A very interesting result, especially with respect to human medicine, was obtained using end-point PCR results and showed that cultivated astrocytes isolated from both adult humans and human fetuses express mRNA of all known NMDA receptor subunits, GluN1, GluN2A-D and GluN3A-B (Lee et al. 2010).

1.4.2 Detection of astrocytic NMDA receptors on the protein level

The first attempt to detect NMDA receptors in astrocytes on the protein level was performed in the rat visual cortex. GluN1 immunoreactivity in the astrocytic processes was detected by electron microscopy, especially in the deeper cortical layers starting at postnatal day 14. By postnatal day 30, the GluN1 immunoreactive profile in these layers became predominantly astroglial (Aoki et al. 1994). GluN1 and GluN2A/B immunoreactivity in adult rat cortical astrocytes was also confirmed by Conti and colleagues and was detected primarily in the astrocytic processes and occasionally in the cell bodies (Conti et al. 1996). In astrocytic

primary cultures prepared from the cortex of newborn mice, only a few astrocytes were GluN1- or GluN2B-positive, while the majority of them was negative (Zhou et al. 2010). The presence of NMDA receptor subunits seems to be brain region-specific, since in the CA1 region of the adult rat hippocampus, no GluN1 or GluN2A/B immunostaining was detected in astrocytes under physiological conditions (Gottlieb and Matute 1997; Krebs et al. 2003). In contrast to the hippocampus, the GluN1 protein was detected in adult rat astrocytes in the basolateral amygdala and the bed nucleus of the stria terminalis (Gracy and Pickel 1995), the lateral and basal nuclei of the amygdala (Farb et al. 1995) and the nucleus locus coeruleus (Bockstaele and Colago 1996). The results obtained in rat astrocytes are in accord with those reported from studies on human astrocytes. Conti et al. showed that the processes of human cortical astrocytes are immunopositive for GluN1, GluN2A and/or GluN2B subunits (Conti et al. 1999). The study of Lee and colleagues confirmed the presence of all NMDA receptor subunits located on the membrane of cultivated astrocytes isolated from 16-19-week-old fetuses (Lee et al. 2010). GluN1-positive cells were also found in cultured Müller glial cells isolated from the adult human retina, as confirmed by Western blots (Puro et al. 1996).

1.4.3 Functional studies of NMDA receptors in astrocytes

There are numerous functional studies providing insight into the astrocytic NMDA receptors enigma and clearly showing that astrocytic NMDA receptors are brain region-specific. In the cerebral cortex, the first attempts to detect NMDA receptors in astrocytes were performed on cultures prepared from neonatal mice. Even though glutamate, aspartate, kainate and several other neurotransmitters evoked electrophysiological responses, in none of these studies were detected responses after NMDA application (Bowman and Kimelberg 1984; Kettenmann and Schachner 1985; Sontheimer et al. 1988; Backus et al. 1989). Similar results were obtained in Ca^{2+} imaging experiments on cultured cerebral astrocytes (Jensen and Chiu 1990; Holzwarth et al. 1994; Kato et al. 2006). The only exception was the study of Zhang and colleagues, in which the NMDA receptor antagonist D-2-amino-5-phosphonovaleric acid (D-APV) diminished the Ca^{2+} response to glutamate (Zhang et al. 2003). Completely different results were obtained when cortical astrocytes were studied in slices from juvenile and adult mice. The application of NMDA triggered inward currents in most astrocytes, which were partially reduced by Cd^{2+} and almost completely and irreversibly blocked by the NMDA receptor antagonist MK-801 (Schipke et al. 2001). Since a cocktail containing TTX, L-trans- pyrollidine-2,4-dicarboxylic acid (PDC), Cd^{2+} and the competitive AMPA/kainite receptor antagonist 6-cyano-7- nitroquinoxaline-2,3-dione (CNQX) reduced

NMDA-evoked responses by ~45%, Shipke and colleagues suggested that most of the NMDA-induced currents are due to an indirect effect via neuronal glutamate release and glial glutamate uptake, but there is still a component indicating the presence of intrinsic NMDA receptors in astrocytes. Calcium imaging experiments showing NMDA-evoked Ca^{2+} elevations, especially in distal astrocytic processes, in the presence of the above-mentioned cocktail of inhibitors, leads to the same conclusion. The application of 4 mM Mg^{2+} abolished the NMDA-induced current, and this blockage could be overcome only by depolarizing the cell membrane. Recently, two studies proved the presence of NMDA receptors on astrocytes by measuring the glial synaptic currents evoked by stimulating neurons. These currents were blocked or partially blocked by the NMDA antagonists MK-801, D-APV, 2R*,3S*-1-(Phenanthrenyl-3-carbonyl)piperazine-2,3-dicarboxylic acid (UBP141) and memantine, but not by ifenprodil (Lalo et al. 2006; Palygin et al. 2011) and they were maximal at 6 months of age and decreased with increasing age (Lalo et al. 2011). These results were also verified by Ca^{2+} imaging measurements that showed Ca^{2+} elevations after NMDA application, with maximum amplitude reached between 3 and 6 months of age (Palygin et al. 2010; Lalo et al. 2011). Similarly, NMDA-evoked currents were detected in cerebral astrocytes (Oliveira et al. 2011), however without blocking neuronal activity by TTX. The only work that cast doubt on the presence of NMDA receptors in cortical astrocytes *in situ* was published in 1997 by Pasti and co-authors (Pasti et al. 1997), who reported that Ca^{2+} elevations were delayed by 20-30 s following NMDA application, in contrast to the immediate neuronal responses reported by other authors. This might be due to the fact that Pasti and colleagues carried out their experiments on relatively young, 5-day-old mice. The ultimate proof of the presence of functional NMDA receptors on cerebral astrocytes was provided in astrocytes acutely isolated using a vibrating ball technique. In these studies, astrocytes isolated from the possible influence of other surrounding cells, showed NMDA-induced inward currents, which were potentiated by the addition of glycine. The responses were blocked by MK-801 or partially blocked by UBP141, while ifenprodil had no influence (Palygin et al. 2010; Palygin et al. 2011). In contrast to the data of Shipke and colleagues, these astrocytes were insensitive to blockage by Mg^{2+}. The NMDA receptor-mediated currents were maximal at 6 months, followed by a decline with increasing age (Lalo et al. 2011). NMDA application also induced Ca^{2+} responses in these acutely isolated cerebral astrocytes with lower amplitudes than those evoked by glutamate, and they were D-APV sensitive (Palygin et al. 2010; Palygin et al. 2011). As for the NMDA receptor subunit composition, the lack of Mg^{2+} block together with lower Ca^{2+} permeability strongly suggest the presence of GluN3 subunits. Pharmacological

studies suggest the incorporation of GluN2C/D subunits in astrocytic NMDA receptors. Therefore, the most probable composition of the NMDA receptors in cortical astrocytes under physiological conditions is tri-heteromeric, containing GluN1, GluN2C or GluN2D and GluN3 subunits (Palygin et al. 2011).

For an overall summary of NMDA receptor subunits in astrocytes on mRNA, protein and functional level, see **Table 2**. The most probable composition of NMDA receptors in cortical and hippocampal astrocytes under physiological and pathological conditions are depicted in **Fig. 12.** The composition of NMDA receptors in cortical astrocytes after ischemia (depicted by a question mark in **Fig. 12**) was until now not elucidated. Therefore, the main objective of this PhD thesis was to examine NMDA receptors of cortical astrocytes after focal cerebral ischemia.

level	brain area	NMDA receptor subunits							reference
		GluN1	GluN2A	GluN2B	GluN2C	GluN2D	GluN3A	GluN3B	
mRNA	cortex	✗							Conti et al., 1994
		✓		✓	✓				Schipke et al., 2001
		✗			✓		✓		Cahoy et al., 2008
	cerebellum				✓				Akazawa et al., 1994
				✓					Luque et al., 1995
protein	cortex	✓							Aoki et al., 1994
		✓	✓	✓					Conti et al., 1996
	hippocampus	✗	✗	✗					Gottlieb et al., 1997
		✗		✗					Krebs et al., 2003
	amygdala	✓							Gracy et al., 1995
		✓							Farb et al., 1995
	nucleus locus coeruleus	✓							Bockstaele et al., 1996
function	cortex	✓			✓	✓	✓	✓	Palygin et al., 2010, 2011

Table 2. NMDA receptor subunits in murine astrocytes under physiological conditions. The data were obtained from studies performed *in situ* and on freshly isolated glial cells, while those obtained *in vitro* were not included due to the possible influence of the cultivation process.

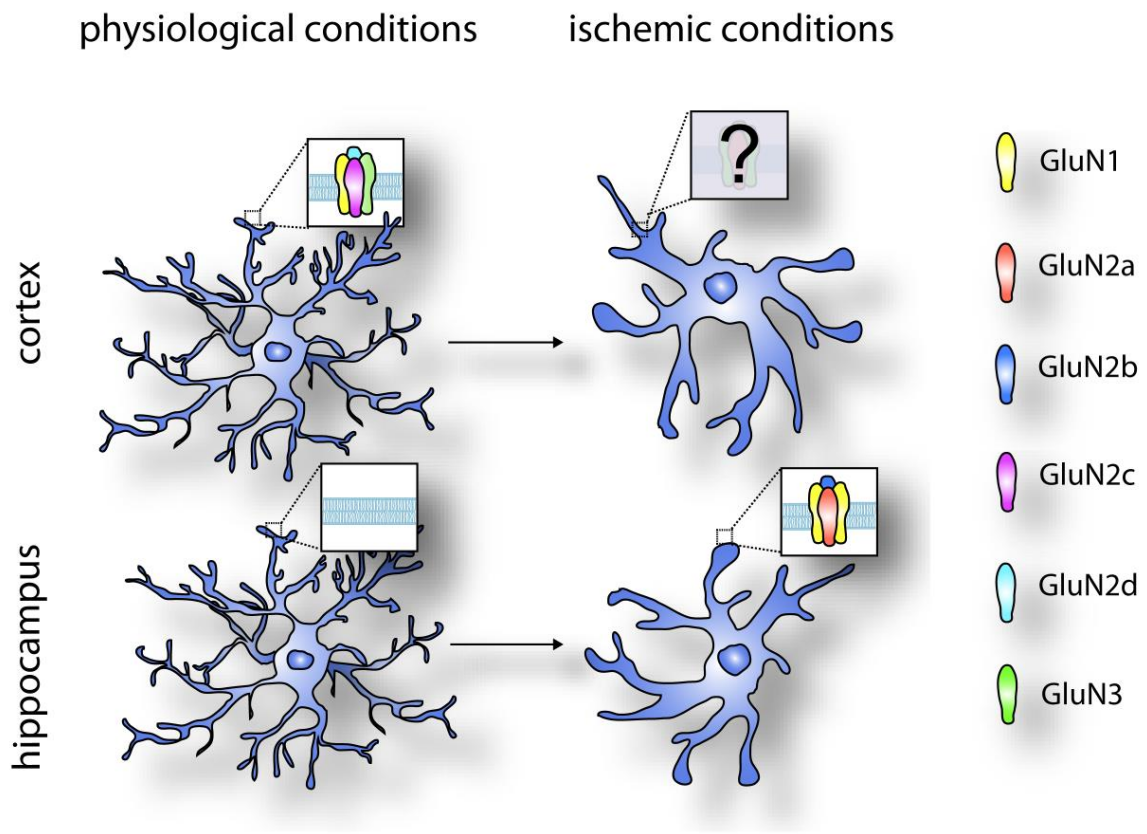


Figure 12. The most probable composition of NMDA receptors in cortical and hippocampal astrocytes under physiological and pathological conditions. The compositions are based on published data predominantly from functional studies. Question mark indicates unknown NMDA receptor composition. Note the presumed absence of NMDA receptors in hippocampal astrocytes under physiological conditions.

2. AIMS OF THE STUDY:

Hypothesis 1: Cortical astrocytes were shown to express ionotropic and metabotropic glutamate receptors. Most of the studies were, however, performed only under physiological conditions, in young mice or were focused on some particular subunits of glutamate receptors. We were interested in an overall picture of gene expression of all currently known subunits of ionotropic glutamate receptors and the main metabotropic receptors. We hypothesize that detailed analysis will reveal changes in their expression during development, in ageing and especially after MCAO.

Aim 1: To reveal the changes in the expression of mRNA coding AMPA, kainate, NMDA and metabotropic glutamate receptors in cortical astrocytes during development, ageing and following MCAO model of focal cerebral ischemia employing single cell RT-qPCR.

Hypothesis 2: There are several studies which aimed to find NMDA receptors in astrocytes on the protein level; however, their results were often inconclusive (Dzamba et al. 2013). Moreover, most of these studies were performed only under physiological conditions and did not study the most currently discovered GluN3A-B subunits. Therefore, our goal was to show the presence of all 7 currently known NMDA receptor subunits in cortical astrocytes on the protein level using immunohistochemistry. Furthermore, we hypothesize that composition of NMDA receptor subunits might change following focal cerebral ischemia.

Aim 2: To identify NMDA receptor subunits in cortical astrocytes under physiological conditions and following MCAO, utilizing immunohistochemistry.

Hypothesis 3: Functional properties of astrocytic NMDA receptors are still matter of debate, especially due to the fact, that astrocytes do not depolarize their membrane to release Mg^{2+} block which is required for NMDA receptors functioning in neurons. Nonetheless, discoveries of the last decade indicated that astrocytic NMDA receptors contain GluN3A subunit, which changes their properties so that they lack Mg^{2+} block (Palygin et al. 2010; Palygin et al. 2011). We aimed to verify this observation by Ca^{2+} imaging experiments *in situ* and we hypothesized that functional properties of astrocytic NMDA receptors will be altered in reactive astrocytes after MCAO.

Aim 3: To investigate functional properties of astrocytic NMDA receptors in cortical tissue slices and to identify possible changes in their function following MCAO using Ca^{2+} imaging *in situ*.

Hypothesis 4: Since *in situ* experiments are performed in brain slices containing also other cell types, such as neurons, which might influence results of measurements, we performed also *in vitro* experiments (cultured adult astrocytes isolated from cortices of healthy mice and those after MCAO) without influence of other cell types in order to verify the *in situ* results. Our hypothesis was that we will observe similar results as in *in situ* experiments, even though small differences might be detected as a result of the cultivation process.

Aim 4: To verify results obtained from *in situ* functional study (Ca^{2+} imaging) by *in vitro* experiments without possible influence of other cellular elements.

3. MATERIALS AND METHODS:

3.1 Transgenic mice

For identification of astrocytes in the experiments, we utilized GFAP/EGFP transgenic mice [line designation TgN(GFAP-EGFP)], in which the expression of EGFP is controlled by the human GFAP promoter (Nolte et al. 2001). In these mice, astrocytes and a subpopulation of NG2 glia are fluorescently labeled with EGFP. All procedures involving the use of laboratory animals were performed in accordance with the European Communities Council Directive 24 November 1986 (86/609/EEC) and animal care guidelines approved by the Institute of Experimental Medicine ASCR Animal Care Committee on April 17, 2009.

3.2 MCAO induction

For the focal cerebral ischemia we used a permanent transcranial MCAO model. Before the induction of MCAO, mice were anesthetized with 1.5% isoflurane (Abbot, IL, USA) and maintained in 1% isoflurane using a vaporizer (Tec-3, Cyprane Ltd., UK). A skin incision between the orbit and the external auditory meatus was made, and a hole (1-2 mm in diameter) was drilled through the frontal bone 1 mm rostral to the fusion of the zygoma and the squamosal bone and about 3.5 mm ventral to the dorsal surface of the brain. The dura was opened, gently removed and the exposed middle cerebral artery was occluded by a short coagulation with bipolar tweezers (SMT, Czech Republic) at a proximal location, followed by transection of the vessel to ensure permanent occlusion. During the surgery, heating pad was used to maintain the mouse's body temperature at 37 ± 1°C (Honsa et al. 2012). For visualization of ischemic region we used 2% 2,3,5-Triphenyltetrazolium chloride (TTC) at 37°C for 20 minutes (**Fig. 13**). The MCAO model has relatively high survival ratio (~95%) with good reproducibility and results in an infarct localized only in the cortical region.

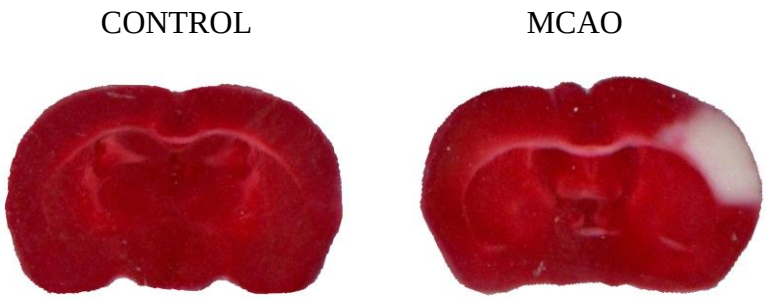


Figure 13. Visualization of ischemic region after induction of middle cerebral artery occlusion (MCAO) in comparison with uninjured mouse brain (CONTROL). The staining was performed with 2,3,5-Triphenyltetrazolium chloride (TTC) and the white area represents an infarct tissue after MCAO.

3.3 Preparation of cell suspensions from the cortex of GFAP/EGFP mice

Before the collection of GFAP/EGFP^{+} single cells utilizing flow cytometry, the cortical tissue was dissociated using papain treatment. In the experiments, the total amount of 1432 single cells was collected from 27 mice, which were either uninjured mice (controls; 10-668-day-old) or mice 3, 7 and 14 days after MCAO (D3, D7 and D14; 50-64-day-old). The mice were deeply anesthetized with intraperitoneal (i.p.) administration of pentobarbital (PTB, 100 mg/kg; Sigma-Aldrich, MO, USA) and perfused transcardially with cold (4–8°C) isolation buffer containing (in mM): NaCl 136.0, KCl 5.4, HEPES 10.0, glucose 5.5, osmolality 290 ± 3 mOsm/kg. To isolate the cerebral cortex, a part of the brain (+2 mm to -2 mm rostro-caudally from bregma) was sliced into 400 µm coronal sections using an HM650V vibrating microtome (MICROM International GmbH, Germany), and the dorsal cerebral cortex was carefully dissected out from the ventral white matter tracks. In mice after MCAO, the ischemic core with its surrounding tissue (cca ½ of the injured hemisphere) was used. The tissue was incubated with continuous shaking at 37°C for 45-60 minutes in 5 ml of a papain solution (20 U/ml) and 0.2 ml DNase (both from Worthington, NJ, USA) prepared in isolation buffer. After papain treatment, the tissue was mechanically dissociated by gentle trituration using a 1 ml pipette. According to the manufacturer's instructions, the dissociated cells were layered on top of 5 ml of ovomucoid inhibitor solution and harvested by centrifugation (140 x g for 6 minutes). Cell aggregates were removed by filtering with a 30 µm cell strainer (Becton Dickinson, NJ, USA), and the cells were kept on ice until sorting. This method routinely yielded ~2 x 10^6 dissociated cells per mouse brain (**Fig. 14**).

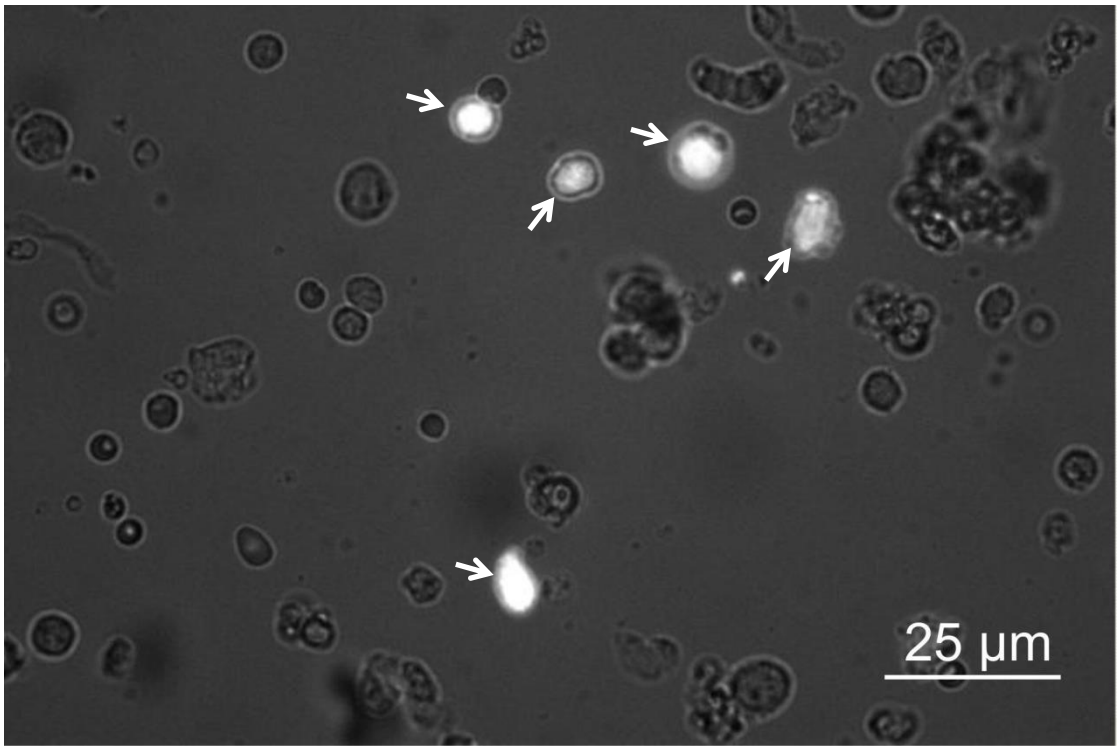


Figure 14. Cell suspensions from the cortex of GFAP/EGFP mice prepared for fluorescence-activated cell sorting (FACS). The cell suspension was prepared using papain treatment. The picture is a combination of bright-field and fluorescence imaging with excitation wavelength 488 nm, so that both morphology and EGFP-positivity is visualized. The bright cells marked by arrows are GFAP/EGFP-positive cells.

3.4 Collection of single GFAP/EGFP$^+$ cells by flow cytometry

The collection of single cells was performed using flow cytometer (BD Influx, CA, USA), which was manually calibrated to deposit single cells in the center of each well of 96-well plates (Life Technologies, CA, USA) that were placed on a pre-cooled rack. Only viable and GFAP/EGFP$^+$ cells were collected. The viability of the cells was checked using Hoechst 33258 (Life Technologies). Single cells were collected into 5 µl nuclease-free water with bovine serum albumin (1 mg/ml; Fermentas, IL, USA), which was in some experiments supplemented by RNaseOut (20 U; Life Technologies). Collected cells in 96-well plates were stored at -80°C immediately after sorting.

3.5 Complementary DNA (cDNA) synthesis

cDNA synthesis was performed with SuperScript III RT (Life Technologies). Lysed single cells in 5 ml water containing 0.5 µM dNTP (Promega), 1.0 µM oligo (dT15) (Invitrogen) and 1.0 µM random hexamers (Eastport) were incubated at 70°C for 5 min. 50

mM Tris–HCl, 75 mM KCl, 3 mM $MgCl_2$, 5 mM dithiothreitol, 20 U RNaseOut and 100 U SuperScript III (all Life Technologies) were added to a final volume of 10 µl. Reverse transcription was performed at 25°C for 5 min, then at 50°C for 60 min, followed by 55°C for 15 min and finally terminated by heating at 70°C for 15 min. Four µl from each sample was diluted 4 times and used for pre-testing. Five µl of cDNA was used for preamplification.

3.6 qPCR

Primers were designed using BeaconDesigner (version 7.91, Premier Biosoft International) as previously described (Benesova et al. 2012). Primer sequences are provided in **Table 3**. All single cells were pre-tested for the expression of genes coding GLAST (*Slc1a3*), glutamine synthetase (*Glul*), both markers of astrocytes, chondroitin sulfate proteoglycan (*Cspg4*) and platelet-derived growth factor α receptor (*Pdgfra*), both markers of NG2 glia, to select samples for further gene expression profiling using assays for 47 genes. CFX384 (Biorad) was used for all qPCR measurements. To each reaction (10 µl) containing iQ SYBR Green Supermix (BioRad) and 400 nM of each primer (EastPort), we added 3 µl of diluted cDNA. The temperature profile was 95°C for 3 min followed by 50 cycles of amplification (95°C for 15 s, 60°C for 15 s and 72°C for 20 s). All samples were subjected to melting curve analysis. The same experimental setup was used to test preamplification.

Gene	Protein	Forward primer	Reverse primer
Aldh1l1	ALDH1L1	CTGGAAGATGGCAAGATGATG	TTCTACCTCTGGGACATTGG
Aqp1	AQP1	CTGGCTGCGGTATCAACC	GGATGAAGTCATAGATGAGCACTG
Aqp4	AQP4	CGGCATCCTCTACCTGGTCACA	GCCAGCGGTGAGGTTTCCAT
Aqp9	AQP9	GAAGGATGGAGTGGTTCAAGTTC	TGGCACGGATACAAATGGTTT
Clcn2	CLC2	TGCCAATGTCTTCCTTACTCTG	ATTCGGTAGGTGCTGCTATC
Cspg4	CSPG4/NG2	TGATGGAAGTGAGACACAGACAGA	GGAAGGATGGTGATCGTGAAGG
Gfap	GFAP	GAACAACCTGGCTGCGTATAG	GCGATTCAACCTTTCTCTCCAA
Gfap (splice δ)	GFAP δ	ATGTGTCTCAGTTGTGAAGGTCTA	TGGAAGGATGGTTGTGGATTCT
Glul	Glutamine synthetase	CGCAAAGACCCCAACAAG	ATTCCTGCTCCATTCCAAAC
Gria1	GluA1	ACTCAAGCGTCCAGAATAGAAC	AATCTCAAGTCGGTAGGAATAGC

Gria2	GluA2	CAGATTGTAGACTACGACGACTC	TCATCACTTGGACAGCATCATAA
Gria3	GluA3	GGTCATTCTCACGGAGGATTC	GGTGTTCTGGTTGGTGTTGTA
Gria4	GluA4	CCAGTAGAGGACAACGCAATT	TGACAGAGTGAAGGTTACAGGAA
Grik1	GluK1	CACGAGACGGCTGCTGAA	ACCACTGTACCTGTAGAGTTCCA
Grik2	GluK2	ACAATCAACAGGAACAGGACTCT	TGCTGATGAACTGTGTGAAGGA
Grik3	GluK3	GCTCAGAGGTGGTGGAGAATA	GCCGTGTAGGAGGAGATGAT
Grik4	GluK4	CGCATGGTAGAATTGGAAGGT	AAGAGACTGTCAGAGATGTTGGA
Grik5	GluK5	CCACCTTGTCCTCCGTAA	CTCCACGATACCATCCAGAT
Grin1	GluN1	AGATAGTGACAATCCACCAAGAAC	ACCATTGACTGTGAACTCCTC
Grin2a	GluN2A	GACCAGATGCTTCAGGAGACAG	CTTGAGGCTTATGCTACGAGAGG
Grin2b	GluN2B	GGTGTTTAACAACTCCGTACCT	GAAACCTGGTCCACATACTCCTC
Grin2c	GluN2C	CGTGTGGTTAGTACCTAATCTG	TTCTGGCGTAGGCTAAGG
Grin2d	GluN2D	AACCGAGACTACTCCTTCAATGA	GCCATAGCGGGACCATAGA
Grin3a	GluN3A	GACAAAGCCCTTCTGGATTATGA	ATGTTAGAGGTCAACGGAGAGT
Grin3b	GluN3B	TGGTCGGGGACAAGACATTT	TCCGTGTGGAGTGGTAGGTG
Grm1	mGluR1	CGAGTGGAGTGACATAGAATC	TACCAGCCAGAATGATATAGCA
Grm3	mGluR3	CGACCACATATTCTCAGTCCTCT	AGCACTTCGTCTAACAGCCTATA
Grm5	mGluR5	CAGCTTAGATCGCAGCCACT	CAAGAATTTGGGTAAAATCACCA
Hcn1	HCN1	CTCAGTCTCTTGCGGTTATTACG	TGGCGAGGTCATAGGTCAT
Hcn2	HCN2	ATCGCATAGGCAAGAAGAACTC	CAATCTCCTGGATGATGGCATT
Hcn3	HCN3	GATGTTTGATGAAGAGAGCATCC	CCCGGCAGGTGAAGTTAATA
Hcn4	HCN4	GCATGATGCTTCTGCTGTGT	GCTTCCCCCAGGAGTTATTC
Kcna3	Kv1.3	GTAAGTCGGAGTATATGGTGAT	CAGTGAATATCTTCTTGATGTTGA
Kcna4	Kv1.4	CTGAATGACACCTCGGCAC	AGCATCGAACCACAAACTCA
Kcna5	Kv1.5	CGTGTCGGTCTTGGTCATTC	CGTAACAGCTCCCGTTCATC
Kcnj10	Kir4.1	AACTTGGGAGATTGAGATATGATATA	AAGTCTGAATACTTCCTTCTGTAC

Kcnj16	Kir5.1	CCTGTGTCTCCTCTTGAAGG	TGTGCTTAGGTGATACAATACGG
Kcnj2	Kir2.1	TCCCTCCCTTTCCCAAACAC	GAGGCTTGATTTTGAGACGC
Kcnk1	TWIK-1	GGGAAATTGGAATTGGGACTTCA	TGCCGATGACAGAGTAGATGAT
Kcnk10	TREK-2	CACTGTGGCTATCTCCTTAACC	GGCTGAGGCGGTGTAATC
Kcnk2	TREK-1	ATTCGTATCATCTCCACCATCATC	CACACCACAGGCTTGTAGAA
Nes	Nestin	AGCAACTGGCACACCTCAA	GGTATTAGGCAAGGGGGAAG
Pdgfra	PDGFαR	AAGAGACCCTCCTTCTACCAC	TATCAGAGTCCACCCGCAT
S100b	S100β	TCTAACTCAGGACCGAGAATCA	GGAGCAAGGAAGATACAACTAACT
Slc1a3	GLAST	ATCGTCCTGCCTCTCCTCTAC	GTCCACACCATTGTTCTCTTCCA
Snap25	SNAP25	TCATCTGGTGGCTCTAATTCCTAA	AACAGCACATTGAGCATTCCTAA
Trpv4	TRPV4	AGAGACAAGTGGCGTAAGTT	GCTGATAGTAGGCGGTGAG
Vim	Vimentin	TGCCAACCTTTTCTTCCCTG	TCTCTGGTCTCAACCGTCTT

Table 3. Primer sequences

3.7 Preamplification and qPCR

The applied preamplification protocol was verified on samples from three mice. The RNA was extracted and cDNA was prepared to test the preamplification protocol. Each reaction contained 25 µl of iQ Supermix (BioRad), 5 µl of a mix of all primers (final concentration 25 nM each), 5 µl of non-diluted cDNA, and water added to a final volume of 50 µl. The temperature profile was 95°C for 3 min followed by 18 cycles of amplification (95°C for 20 s, 57°C for 4 min and 72°C for 20 s on Biorad CFX96). The samples were diluted 5 times in water and analyzed by the qPCR protocol described above.

3.8 High throughput qPCR

The sample reaction mixture had a volume of 5 µl and contained 2.24 µl of diluted preamplified cDNA, 0.25 µl of DNA Binding Dye Sample Loading Reagent (Fluidigm, San Francisco, CA, USA), 2.5 µl SsoFast EvaGreen Supermix (Biorad, Hercules, CA, USA), and 0.01 µl ROX (Invitrogen, CA, USA). The primer reaction mixture had a final volume of 5 µl and contained 2.5 µl Assay Loading Reagent (Fluidigm) and 2.5 µl of a mix of reverse and

forward primers, corresponding to a final concentration of 4 μM. The chip was first primed with an oil solution in the NanoFlex™ 4-IFC Controller (Fluidigm) to fill the control wells of the dynamic array. The sample reaction mixture (5 μl) was loaded into each sample well, and 5 μl of the primer reaction mixtures was loaded into each assay well of the 48x48 dynamic array. The dynamic array was then placed in the NanoFlex™ 4-IFC Controller for automatic loading and mixing. After 55 min the dynamic array was transformed to the BioMark qPCR platform (Fluidigm). The cycling program was 3 min at 95°C for activation, followed by 35 cycles of denaturation at 95°C for 15 s, annealing at 60°C for 15 s, and elongation at 72°C for 20 s. After PCR, melting curves were collected between 60°C and 95°C with 0.5°C increments.

3.9 Data pre-processing

qPCR data were pre-processed for expression analysis using GenEx (MultiD, version 5.3) as follows: quantification cycle (Cq) values registered from amplifications that generated melting curves with aberrant melting temperatures were removed, Cq values larger than 26 were replaced with 26, and Cq values with products giving rise to a double peak in melting curves (corresponding to a mixture of expected and aberrant PCR products) were replaced with 26. All missing data, for each gene separately, were then replaced with the highest Cq+2, effectively assigning a concentration of 25% of the lowest measured concentration to the off-scale values. The Cq data were, for each gene separately, converted into relative quantities expressed relative to the sample with the lowest expression (maximum Cq) and finally converted to a logarithmic scale with base 2. The data were not normalized to any reference genes because of the large variation of all transcript levels among individual cells (Ståhlberg and Bengtsson 2010); with this pre-processing, the expression levels are expressed per cell.

3.10 Analysis of data obtained from the reverse transcription quantitative polymerase chain reaction (RT-qPCR)

Basic statistics were calculated. The non-parametric Mann-Whitney test was used to compare the expression of individual genes between groups of cells. Kohonen self-organizing maps (SOM) of size 3x1, forcing dividing of the samples into three groups according to the similarity in their gene expression profiles, were trained using GenEx with the following parameters: 0.10 learning rate, 3 neighbors and 5000 iterations. The SOM analysis was

repeated eight times with identical classification of the samples in six of the repeats. This stable classification of samples into three groups was accepted and verified with principal component analysis (PCA), in which were the samples grouped similarly as in the SOM analysis. For Kohonen SOMs and PCA gene expression, the data were mean-centered to reduce the effect of variation in the overall expression levels of the different genes. The Spearman correlation coefficients between transcripts were calculated for each group separately (SAS version 9.2) using all data, including the managed off-scale data. Only correlation coefficients for genes expressed in at least 50% of cells and having a p-value < 0.05 were considered for further analysis.

3.11 Immunohistochemistry

The mice were deeply anesthetized with PTB (100 mg/kg, i.p.) and perfused transcardially with 20 ml of saline followed by 20 ml of cooled 4% paraformaldehyde (PFA) in 0.1 M phosphate buffer. Brains were dissected out, post-fixed for 18 hours and placed stepwise in solutions with gradually increasing sucrose concentrations (10%, 20%, 30%) for cryoprotection. Coronal 30 µm thick slices were prepared using a microtome (HM550, Microm International, Germany). The slices were incubated with 5% Chemiblocker (Millipore, MA, USA) and 0.2% Triton in phosphate-buffered saline. This blocking solution was also used as the diluent for the antisera. The slices were incubated with the primary antibodies at 4-8°C overnight and then the secondary antibodies were applied for 2 hours. The primary antibodies we used are summarized in **Table 4.** As the secondary antibody we employed goat anti-rabbit IgG conjugated with Alexa Fluor 594 (1:200; Molecular Probes, CA, USA, A-11012). The slices were mounted using Aqua Poly/Mount (Polysciences Inc., Germany). All chemicals were purchased from Sigma–Aldrich, unless otherwise stated.

Antibody	Dilution	Reference number	Company
GluN1	1:500	AB28669	Abcam, Cambridge, UK
GluN2A	1:400	AB106957	Abcam, Cambridge, UK
GluN2B	1:400	AB65875	Abcam, Cambridge, UK
GluN2C	1:400	AGC-018	Alomone Labs, Jerusalem, Israel
GluN2D	1:400	AGC-020	Alomone Labs, Jerusalem, Israel
GluN3A	1:400	AB111226	Abcam, Cambridge, UK

GluN3B	1:500	AB35677	Abcam, Cambridge, UK

Table 4. Primary antibodies

A Zeiss 510DUO LSM confocal microscope equipped with Arg/HeNe lasers was used for immunohistochemical analyses. Stacks of consecutive confocal images taken at intervals of 3 µm were acquired sequentially with two lasers to avoid cross-talk between fluorescent labels. The background noise of each confocal image was reduced by averaging four image inputs. For each image stack the gain and detector offset were adjusted to minimize saturated pixels, yet still permit the detection of weakly stained cell processes. Co-localization images were made using a Zeiss LSM Image Browser.

3.12 Preparation of primary cultures

Primary cultures of GFAP/EGFP$^+$ glial cells were prepared from 40-57-day-old mice, either controls or D13-14 mice. The mice were deeply anesthetized with PTB (100 mg/kg, i.p) and perfused transcardially with cold (4–8°C) NMDG isolation solution containing (in mM): 110 NMDG-Cl, 2.5 KCl, 24.5 $NaHCO_3$, 1.25 Na_2HPO_4, 0.5 $CaCl_2$, 7 $MgCl_2$, 20 glucose (pH 7.4, osmolality 290 mOsm/kg). The brain was sliced into 200 µm coronal sections and the cortical tissue was dissected out. In D14 mice, the dissected tissue consisted of the ischemic core and its surrounding tissue (cca ½ of the injured hemisphere). The isolated tissue was transferred into 1 ml of artificial cerebrospinal fluid (aCSF) solution containing (in mM): 122 NaCl, 3 KCl, 1.3 $MgCl_2$, 1.5 $CaCl_2$, 28 $NaHCO_3$, 1.25 Na_2HPO_4, 10 glucose (pH 7.4, osmolality 305 mOsm/kg), which was supplemented with 0.05% trypsin (Life technologies), and incubated with continuous shaking at 37°C for 30 minutes. After incubation, the tissue was transferred into 1 ml of trypsin inhibitor (Sigma-Aldrich) and dissociated by gentle trituration using a 1 ml pipette. Subsequently, the cells were plated in a volume of 0.15 ml onto 6 coverslips in a 24-well plate, and 0.5 ml of fresh cultivation medium was added into each well. The cultivation medium consisted of high glucose Dulbecco's Modified Eagle Medium (Life Technologies) supplemented with 15% fetal bovine serum (PAA Laboratories GmbH, Austria), 2 mM L-Glutamine (Sigma-Aldrich) and Antibiotic-Antimycotic (Life Technologies) containing penicillin, streptomycin and amphotericin B. Cells were cultured in an incubator (100% humidity, 5% CO_2) at 37°C for 5-6 days without medium exchange.

3.13 Calcium imaging measurements

In situ measurements were performed in the somatosensory cortex of 35-59-day-old GFAP/EGFP mice, either controls or D13-14 mice. Transversal brain slices (200 μm thick) were cut in cold (4-8°C) NMDG isolation solution using a vibration microtome and were kept at room temperature in aCSF solution. The slices were then mounted in a microscope superfusion chamber, which was continually perfused with HEPES-based aCSF containing (in mM): 135 NaCl, 2.7 KCl, 1 $MgCl_2$, 2.5 $CaCl_2$, 1 Na_2HPO_4, 10 Glucose, 10 HEPES (pH 7.4, osmolality 305 mOsm/kg, equilibrated with O_2) at a flow rate of 2.5 ml/min. The regions with GFAP/$EGFP^+$ cells, which were 10-20 μm below the surface of the slice, were then found and their positions were saved based on their x, y and z coordinates displayed on a micromanipulator (SM5, Luigs & Neumann, Germany). The loading procedure was performed at room temperature in the measurement chamber for 40 min in 3 ml of HEPES-based aCSF (the flow was interrupted during this period) containing 1 μM Oregon Green 488 BAPTA-1, AM, cell permeant (OGB-1 AM) with 0.02% Pluronic F-127 and continually bubbled with O_2 to avoid ischemic conditions. After the loading, the flow of HEPES-based aCSF was re-established and the measurements were performed with the cells found prior to the loading. The solutions [NMDA, L-glutamic acid (glutamate), glycine, memantine hydrochloride (memantine), 2,3-dihydroxy-6-nitro-7-sulfamoyl-benzo[f]quinoxaline-2,3-dione (NBQX) and pyridoxalphosphate-6-azophenyl-2',4'-disulfonic acid (PPADS) from Sigma-Aldrich, Germany; DL-2-amino-5-phosphonovaleric acid (DL-APV) from Ascent Scientific, UK; and TTX from Alomone labs, Israel] were applied through a capillary with an internal diameter of 250 μm located 0.5 – 1 mm from the measurement region and connected to a Perfusion Pressure Kit, a pressurized application system with a flow rate of 600 μl/min controlled by a ValveBank II controller (AutoMate Scientific, Inc., Berkeley, CA, USA). The fast switching between applications (0.01 s) and low dead volume of the removable application capillary (2-3 μl) ensured rapid exchange of applied solutions (< 0.3 s). The HEPES-based aCSF was applied via the application system throughout the entire experiment to ensure that the Ca^{2+} responses were not influenced by the application itself and to accelerate the solution exchange in the vicinity of recorded cells. OGB-1 fluorescence was detected with a TILL Photonics Imaging System (FEI company, OR, USA) installed on a Zeiss Axioskop 2 FS Plus microscope equipped with a long-distance 40x objective (IR Achroplan 0.8 W, Zeiss, Germany). A digital camera (PCO Sensicam, Kelheim, Germany) was controlled by TILLvisION software (FEI company, OR, USA). The excitation light (488

nm) was generated by a Polychrome V (TILL Photonics GmbH, Gräfelfing, Germany), filtered by a BP 450-490 excitation band-pass filter, reflected by a FT 510 beam splitter and the emitted light was filtered by a LP 515 long-pass filter (Filter Set 09, Zeiss, Germany). Images were acquired at 0.83 Hz and were analyzed offline. Fluorescence intensity (F) was measured in the cell bodies and expressed after background correction as F-Fb, where Fb was the background fluorescence intensity in the proximity of the analyzed cell. The baseline F-Fb signal was then normalized to 100%, and the area under the curve was measured during 1 minute from the onset of application (expressed in arbitrary units). For measuring the delay of the response and percentage of responding cells, the signal threshold for Ca^{2+} responses *in situ* was 200% of the amplitude of the noise signal, and the responses were taken into account only if they occurred within 1 minute from the onset of application.

In vitro Ca^{2+} imaging measurements were performed similarly to *in situ* measurements with the exception of the OGB-1 AM loading procedure. Coverslips with 5–6-day-old cell cultures were incubated for 45 min in 0.5 ml of cultivation medium containing 1.5 μM OGB-1 AM and 0.03% Pluronic F-127 (Life Technologies) at 37°C in an incubator (100% humidity, 5% CO_2). Fluorescence intensity (F) was measured in the cell bodies, if not stated otherwise, and the area under the curve was measured from fluorescence intensity F (without background correction) during 1 minute from the onset of application (expressed in arbitrary units). Since noise signal in Ca^{2+} imaging *in vitro* was minimal, for measuring the delay of the response and percentage of responding cells, the threshold for Ca^{2+} responses was set to 120% of the baseline fluorescence, and responses were taken into account only if they occurred within 1 minute from the onset of application.

3.14 Statistics

If not stated otherwise, the results are expressed as the mean ± S.E.M. Statistical analyses of the differences between groups were performed using one-way ANOVA for multiple comparisons with Bonferroni post-hoc test or paired/unpaired Student's t-test, when appropriate. Values of $p < 0.05$ were considered significant, $p < 0.01$ very significant and $p < 0.001$ extremely significant.

4. RESULTS:

We performed a complex study of the glutamate receptors in astrocytes. First, we measured mRNA expression of AMPA, kainate, NMDA and metabotropic glutamate receptors in single GFAP/EGFP$^+$ glial cells. The cells were isolated from cortices of GFAP/EGFP mice during development (postnatal day 10-50; P10-50), ageing (P30-600) and 3, 7 and 14 days after MCAO.

4.1 Detection and quantification of mRNA expression in individual GFAP/EGFP$^+$ glial cells

RT-qPCR is currently a standard tool for detection and quantification of mRNA in biological samples. The advances in the field enabled to successfully utilize this method also in single cell samples, which is advantageous especially due to possible cell heterogeneity in studied population of the cells. In this work, we therefore used single cell RT-qPCR technique to measure mRNA expression in cortical astrocytes isolated from GFAP/EGFP mice.

4.1.1 Validation of experimental procedure

For the profiling of a large number of genes it is necessary to preamplify the cDNA. For this purpose, we have extensively optimized and validated the preamplification protocol. Our validation scheme was based on three samples that are profiled with and without preamplification and the measured Cq values were compared. In unbiased preamplification, the difference between Cq values measured in samples with and without preamplification (ΔCq) should be the same for all of the genes. The reproducibility of the preamplification was reflected by the standard deviation (SD) of the three ΔCq replicates measured for each gene. For our panel and protocol the SD was below 0.5 Cq values and ΔCq was between 9 to 11 for almost all the genes (**Fig. 15**). If ΔCq for some of the genes markedly differed or showed a large SD (e.g. *Grin2d* in **Fig. 15**), the primers needed to be redesigned.

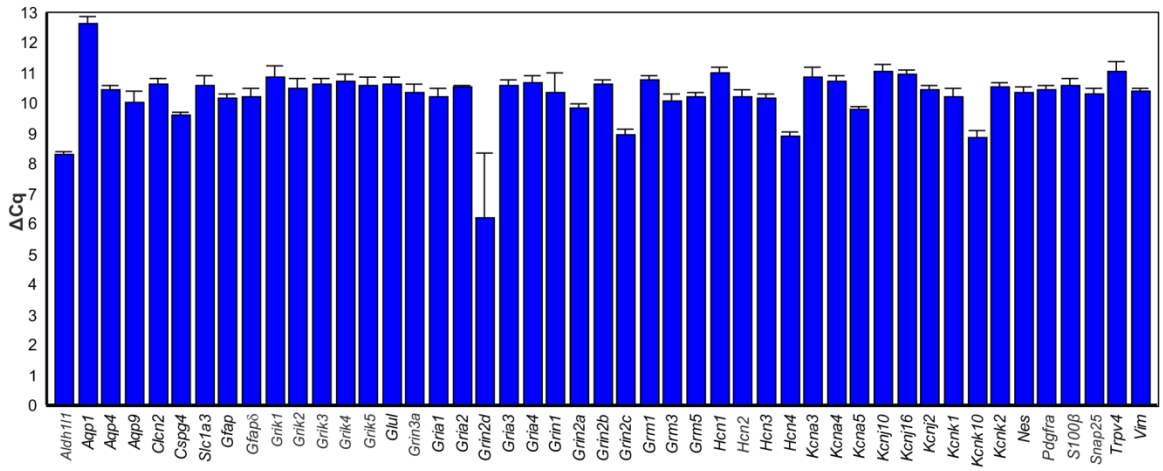


Figure 15. Validation of preamplification. Three separate RNA samples were isolated from the cortex of three different mice, transcribed and preamplified. Levels of cDNA were measured with preamplification (P) and without preamplification (NP). The average difference (ΔCq) and the standard deviation of the difference between P and NP for each gene were calculated for each of the three RNA samples.

We compared results obtained from single cell samples with those obtained from bulk samples containing thousands of FACS-sorted GFAP/EGFP^{+} glial cells per mouse. This comparison was performed on a large data set containing astrocytes isolated from cortices of 12 GFAP/EGFP mice, for which 693 single cells and 12 bulk samples (with an average of ~20000 cells per bulk sample) were collected and tested for the expression of 95 genes. The aim was to validate results from single cells by showing correlation with data obtained from bulk samples. First, we correlated average Cq values from normalized bulk samples for each gene with the percentage of positive cells of the corresponding single cell samples (**Fig. 16**). This dependence was modeled by a sigmoidal function using formula:

$$y = \frac{1}{1 + \exp((EC50 - \mathrm{x}) * slope)}$$

, where *EC50* represents bulk Cq value corresponding to 50% of gene expressing single cells and *slope* represents the slope of the sigmoidal curve in the point corresponding to *EC50*. The *EC50* calculated from sigmoidal curve fitting was 14.85 and the value for the *slope* was -1.12. Sigmoidal fit shows that these data are in a good correlation. Next, we compared the bulk Cq values with the average of the single cell gene expression, expressed as 28 – Cq (as 28 cycles is considered the detection limit corresponding to a single template molecule, or less for samples analyzed on the Biomark platform; negative values were replaced with 0). To reduce bias introduced when calculating average Cq values for the transcripts in the single cells due to missing data, these were replaced by the largest Cq measured for the particular gene in a single cell + 2 (Ståhlberg et al. 2013a). This should be ideally in a linear

dependence which was confirmed also with our data (**Fig. 17**). However, for genes with bulk Cq values above ~18, the amount of mRNA was too low to detect expression of this gene in single cells, even though it was still enough for detecting it in bulk samples containing thousands of cells. This comparison thus shows that results from single cell RT-qPCR data, which we used in this work, are in a good correlation with bulk samples; however, there is a detection limit of this approach, since genes with low expression might be below the single cell RT-qPCR detection limit.

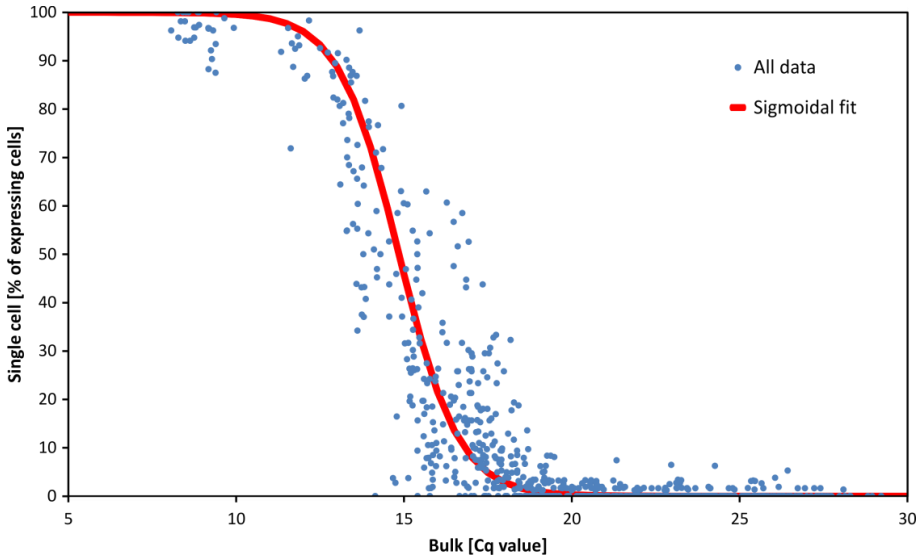


Figure 16. Validation of single cell RT-qPCR results by comparison with results obtained from bulk samples. The dependence of percentage of gene expressing single cells (y-axis) on the bulk Cq values (x-axis) could be described by a sigmoidal function.

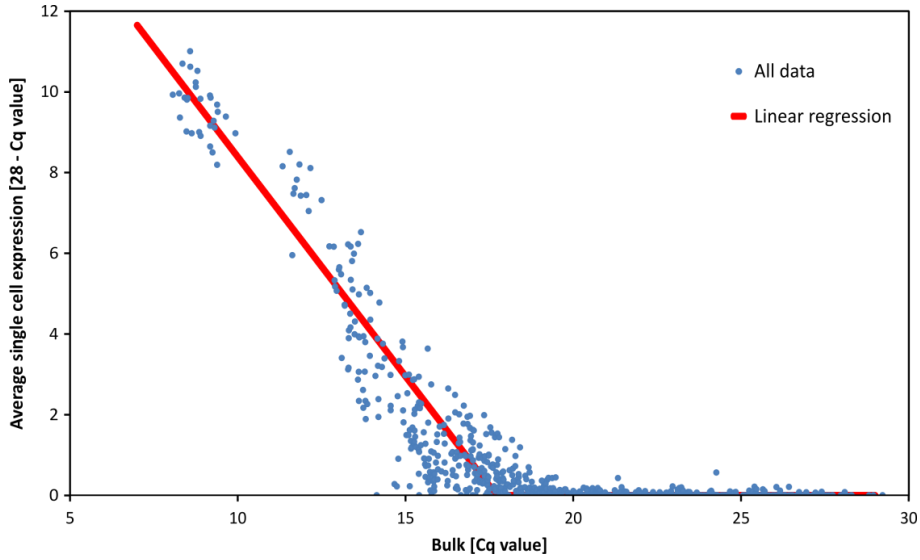


Figure 17. Validation of single cell RT-qPCR results by comparison with results obtained from bulk samples. The dependence of average single cell expression (calculated as 28 – Cq value; y-axis) on the bulk Cq values (x-axis) exhibited a linear character for genes with bulk Cq values < ~18.

4.1.2 Gene expression profile of GFAP/EGFP$^+$ glial cells changes during development and following ischemic injury

In the gene expression profiling of GFAP/EGFP$^+$ glial cells we measured expression of genes coding glial cell markers, developmental markers, aquaporins, subunits of glutamate receptors, outwardly rectifying K^+ channels, inwardly rectifying K^+ channels, two-pore domain K^+ channels, hyperpolarization-activated cyclic nucleotide-gated channels, voltage-gated chloride channels, transient receptor potential channels and synaptosomal-associated protein (**Table 3**). Measurement of such a gene set enabled us to analyze in detail GFAP/EGFP$^+$ glial cells, which are considered to be predominantly astrocytes.

Analyzing expression of mRNA that code glial cell markers revealed that GFAP/EGFP$^+$ cells do not express only markers of astrocytes but express also NG2 glial markers *Cspg4* and *Pdgfra*. The amount of GFAP/EGFP$^+$ cells expressing at least one of these NG2 glial markers decreased during development and in P50 mice it represented only 6% of all tested cells. During ageing, in P90 and P300 mice was this ratio 7% and 5% and interestingly, in P600 mice it increased to 15% (**Fig. 18**). Another interesting result was observed after induction of MCAO, as amount of GFAP/EGFP$^+$ cells expressing at least one of the NG2 glial markers increased to 48% in D3 mice in D14 mice was this ratio 24% (**Fig. 19**).

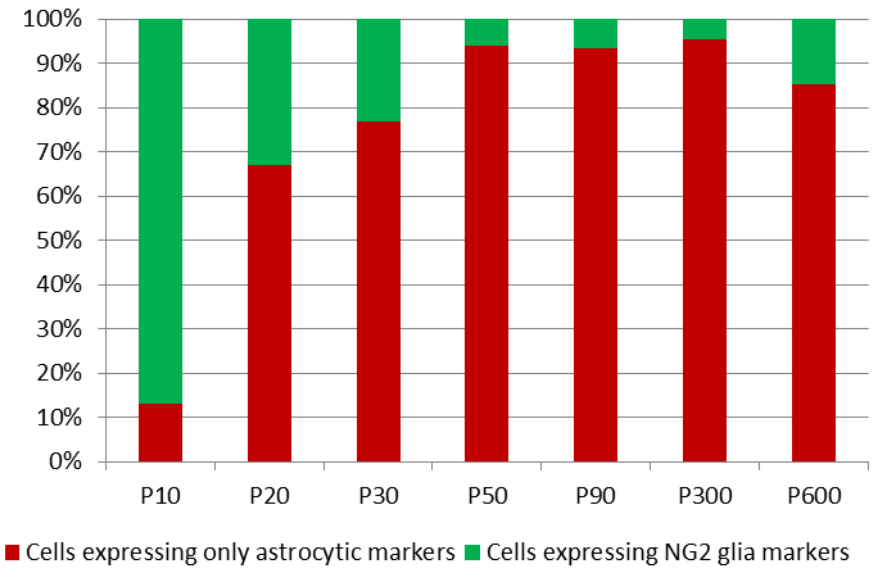


Figure 18. Characteristics of GFAP/EGFP$^+$ cells in the cortex of GFAP/EGFP mice during development P10-P50 (postnatal day 10-50) and during ageing P90-P600. Percentage of GFAP/EGFP$^+$ cells expressing NG2 glial markers *Cspg4* and/or *Pdgfra* are shown in green, while cells expressing only astrocytic markers *Slc1a3* and/or *Glul* are shown in red. The total numbers of the investigated cells were 137 for P10, 94 for P20, 157 for P30, 50 for P50, 123 for P90, 170 for P300 and 216 for P600.

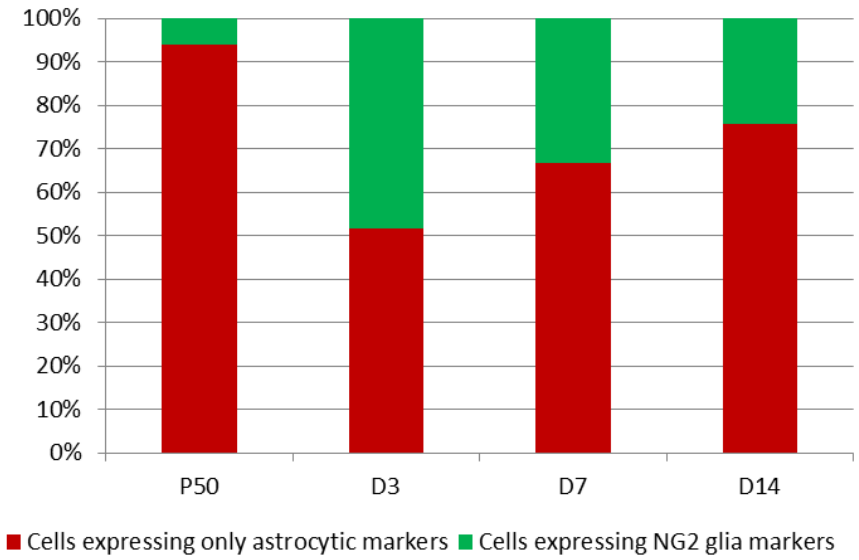


Figure 19. Characteristics of GFAP/EGFP$^+$ cells in the cortex of uninjured 50-day-old GFAP/EGFP mice (P50) and 3, 7 and 14 days after middle cerebral artery occlusion (D3, D7 and D14). Percentage of GFAP/EGFP$^+$ cells expressing NG2 glial markers *Cspg4* and/or *Pdgfra* are shown in green, while cells expressing only astrocytic markers *Slc1a3* and/or *Glul* are shown in red. The total numbers of the investigated cells were 50 for P50, 148 for D3, 96 for D7 and 136 for D14.

We were interested to find out whether GFAP/EGFP$^+$ cells expressing NG2 glial markers could be identified according to their EGFP fluorescence, but EGFP fluorescence of these cells (green dots in **Fig. 20**) was similar to those which expressed only astrocytic markers (red dots in **Fig. 20**). Such overlap of NG2 glial and astrocytic markers detected on mRNA level was also confirmed by immunohistochemical analyses, since in P20 mice and D14 mice, an overlap of EGFP fluorescence and PDGFαR staining was observed (arrowheads in **Fig. 21**).

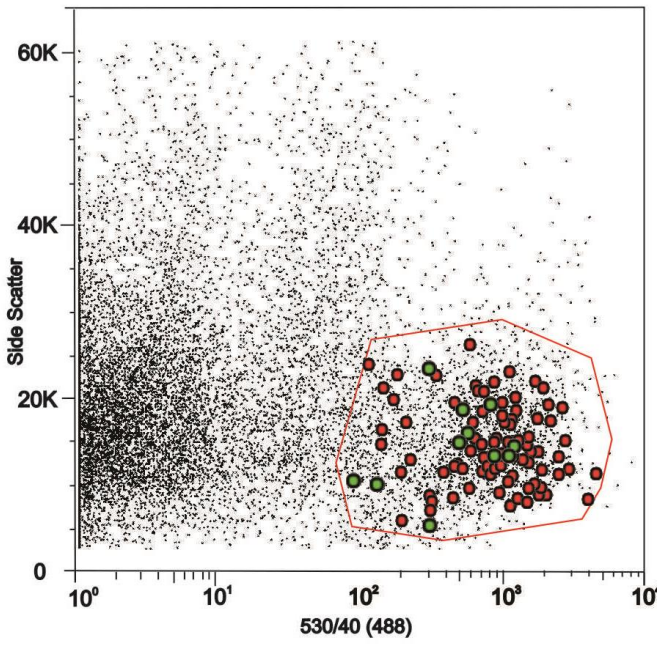


Figure 20. Flow cytometry analysis of GFAP/EGFP$^+$ cells isolated from the cortex of 20-day-old GFAP/EGFP mouse. GFAP/EGFP$^+$ cells were sorted according to their EGFP fluorescence (x-axis) and side scatter intensity reflecting cell size (y-axis). The red line indicates the sorter gate and each dot represents one cell. Cells positive for *Cspg4* and/or *Pdgfra* are indicated in green while those positive only for *Slc1a3* and/or *Glul* are shown in red. The small black dots represent all the cells from which we selected our samples.

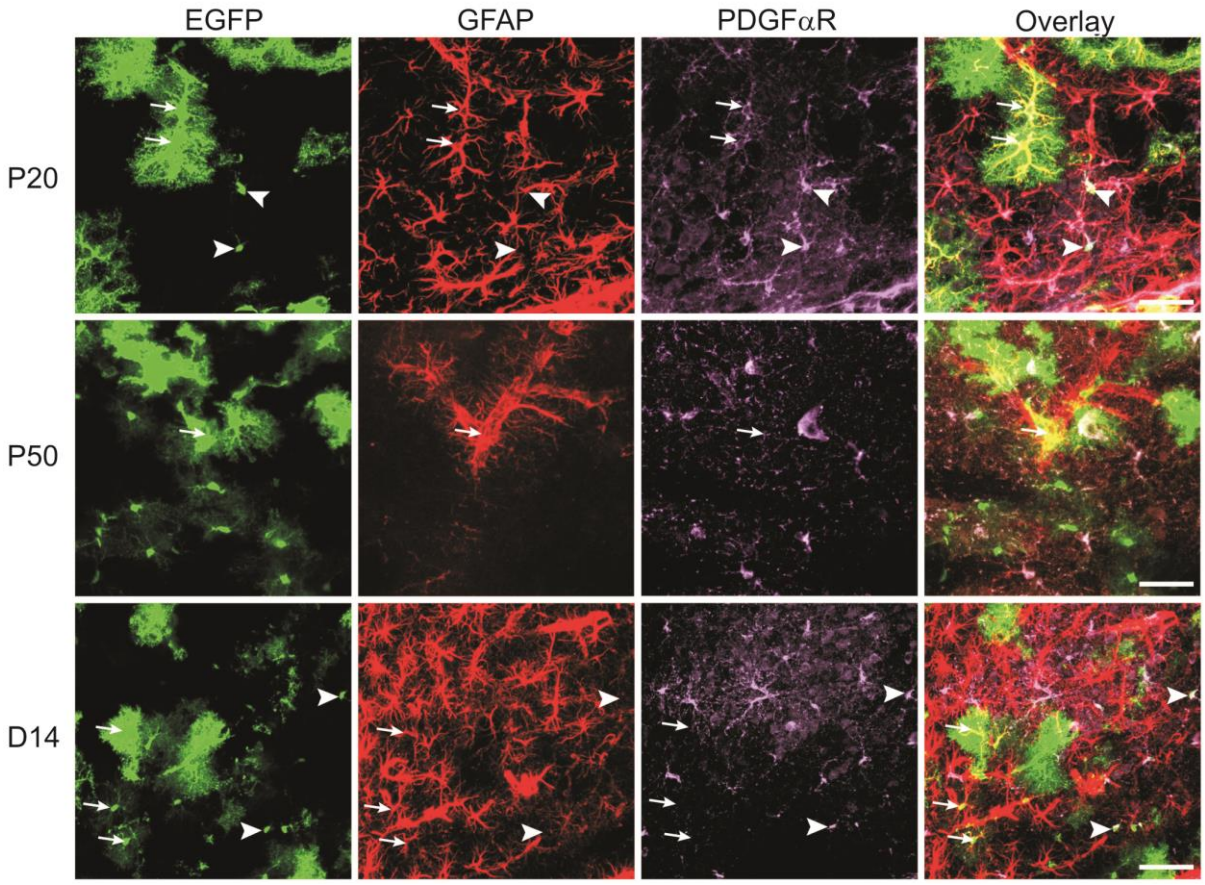


Figure 21. Immunohistochemical analysis of cortical GFAP/EGFP$^+$ cells. The analysis was performed in 20- and 50-day-old GFAP/EGFP mouse (P20 and P50, respectively), as well as in 50-day-old GFAP/EGFP mouse 14 days after middle cerebral artery occlusion (D14). The picture shows EGFP fluorescence (green), immunohistochemical staining against GFAP (red), and PDGFαR (violet) and an overlay image. Arrowheads indicate cells co-expressing EGFP and PDGFαR, and arrows indicate cells positive for EGFP and GFAP. Note that at P20 there are cells positive for all three markers. Scale bars, 50 mm.

There have been several recent studies demonstrating the heterogeneity of GFAP/EGFP$^+$ cells (Serrano et al. 2008; Benesova et al. 2009; Ståhlberg et al. 2011). The single cell RT-qPCR is a perfect tool for analysis of heterogeneity, since the expression of all genes are measured in each of the analyzed cells and such approach enables to perform PCA dividing the cells into subpopulations according to their gene expression profile. PCA can be further supplemented by SOM analyses to prove stable division into subpopulations. The examination of our single cell RT-qPCR data from the P10-50 GFAP/EGPF mice divided these cells into three subpopulations, A1-A3, which differed in their gene expression profile (**Fig. 22**). The subpopulation A1 which was formed mostly by cells isolated from young animals (P10-P20 mice) was characterized by high levels of gene expression and interestingly, cells in this subpopulation expressed markers of both, astrocytes and NG2 glia.

The second subpopulation, A2, mainly consisted from cells isolated from P20 mice, and was transcriptionally less active. The third subpopulation, A3, represented predominantly cells from older animals (P30-P50 mice) and expressed astrocytic markers (*Slc1a3*, *Glul*, *Aqp4*) but none of the NG2 glial markers.

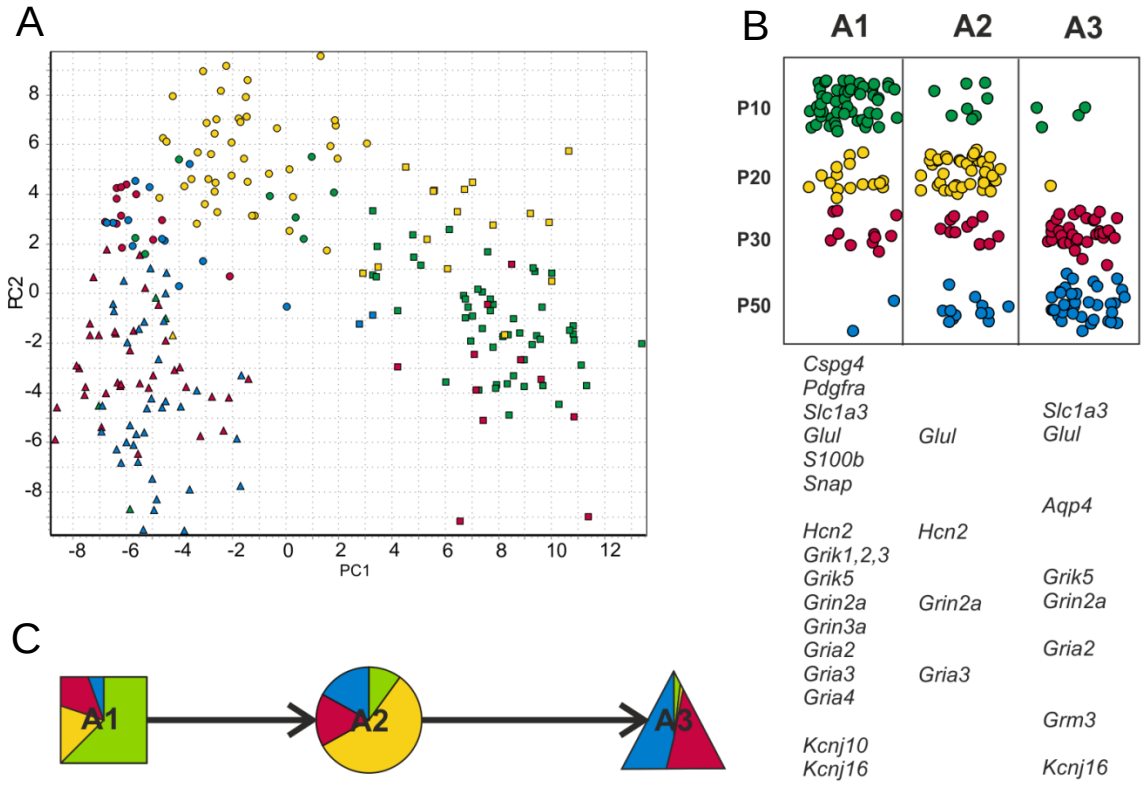


Figure 22. Gene expression profiling of cortical GFAP/EGFP$^+$ cells isolated from 10-, 20-, 30- and 50-day-old GFAP/EGFP mice (P10, P20, P30 and P50, respectively). (**A)** Principal component analysis (PCA) clustering of cells from all development stages (data mean-centered along genes). The stages are indicated in different colors (P10 green; P20 yellow; P30 red and P50 blue), and the three groups identified by Kohonen self-organizing maps (SOM) are indicated by symbols (squares for A1; circles for A2 and triangles for A3). (**B)** The incidence of cells from the three subpopulations at different postnatal developmental stages. The genes under the table indicate highly expressed genes (log2 relative average expression above 1.8 and at least 40% positive cells) in particular subpopulations. (**C)** The distribution of developmental stages in the subpopulations.

Similar analysis of cells isolated from P50 controls and D3, D7 and D14 mice also resulted in division of cells into three subpopulations, B1-B3 (**Fig. 23**). The subpopulation B1 represented resting astroglia (mainly from P50 and D3 mice) based on the fact that there were

only 7 highly expressed genes in this subpopulation. In the second subpopulation, B2, there were early reactive astroglia (partially from D3 and mainly from D7 mice) which were transcriptionally very active, since there were 26 highly expressed genes in this group, including markers of NG2 glia (*Cspg4* and *Pdgfra*). The third subpopulation, B3, was formed solely by cells from D14 mice and it represented group of permanent reactive astroglia also with high gene expression profile (25 highly expressed genes). The PCA and SOM analyses show that GFAP/EGFP^{+} cells exhibit heterogenous features during development as well as after MCAO, which depicts complexity of astrocytic population and should be taken into account in further analyses.

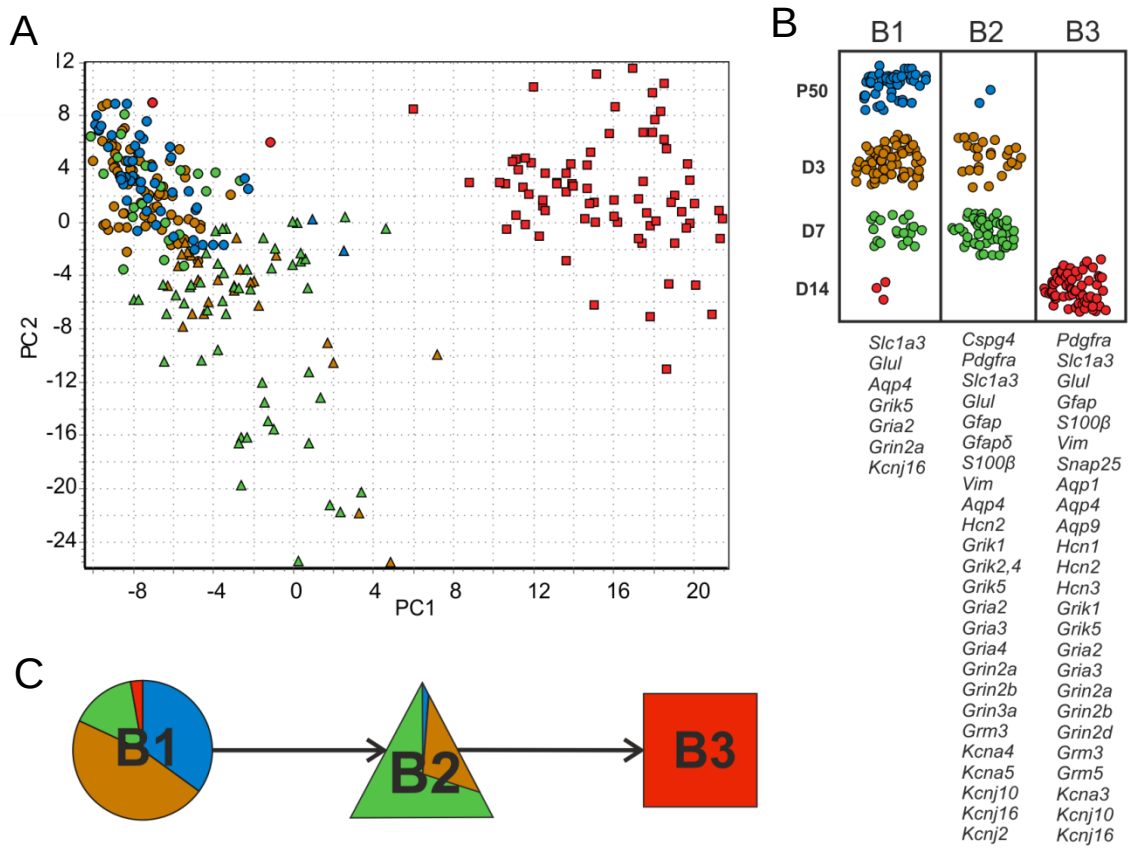


Figure 23. Change in the gene expression of GFAP/EGFP^{+} cells isolated from uninjured 50-day-old GFAP/EGFP mouse (P50) and mice 3, 7 and 14 days after middle cerebral artery occlusion (D3, D7 and D14, respectively). (**A**) Principal component analysis (PCA) clustering of cells from all post-ischemic stages and P50 (data mean-centered along genes). The stages are indicated in different colors (P50 blue, D3 orange, D7 green and D14 red), and the three groups identified by Kohonen self-organizing maps (SOM) are indicated by symbols (circles for B1, triangles for B2 and squares for B3). (**B**) The incidence of cells from the three subpopulations at post-ischemic stages and P50. The genes under the table indicate highly expressed genes (log2 relative average expression above 1.8 and at least 40% positive cells) in particular subpopulations. (**C**) The distribution of control and post-ischemic stages in individual subpopulations.

4.1.3 Glutamate receptors in GFAP/EGFP$^+$ glial cells

Since single cell RT-qPCR results provide information about expression of selected genes in each of the analyzed cells, the expression of subunits of glutamate receptors is presented as percentage of cells expressing given gene and also as an average gene expression level. We performed such analysis with GFAP/EGFP$^+$ cells isolated from cortices of mice during their development (P10-50 mice), in ageing (P90-600 mice) and after MCAO (D7-14 mice).

Expression profile of glutamate receptors during development and in ageing

In early development (P10-20), cortical GFAP/EGFP$^+$ cells are transcriptionally very active and show heterogeneous gene expression profile, which is already shown above (**Fig. 22**). Most of these cells co-express genes coding markers of astrocytes and NG2 glia; nevertheless, this tendency gradually changes and cells isolated from P50-600 mice express almost solely astrocytic markers (**Fig. 18**). The high expression level of genes in GFAP/EGFP$^+$ cortical cells during early development was also observed in the expression of genes coding glutamate receptors subunits (**Fig. 24**).

The expression of all subunits of AMPA receptors (*Gria1-4*) was in P10 mice very high (41% of tested cells expressed *Gria1*, 91% *Gria2*, 84% *Gria3* and 75% *Gria4*). Number of cells expressing *Gria1*, *Gria3* and *Gria4* decreased with age and they were expressed in less than 10% of cells isolated from P50-600 mice. This was not observed for *Gria2*, which was expressed in 50-80% of cells from aged groups. Interestingly, the GluA2 subunit, the protein product of the *Gria2* gene, is crucial for the Ca^{2+} permeability of the AMPA receptors and, for example, in cerebellar Bergmann glia is this subunit absent (Hollmann et al. 1991; Burnashev et al. 1992).

Similar trends as with *Gria1*, *Gria3* and *Gria4* were also observed with genes coding subunits of kainate receptors (**Fig. 24A**). High expression (40-75% of tested cells) in early development (P10-P20 mice) decreased in cells isolated from P50-P600 mice below 2% in the case of *Grik1*, *Grik3* and *Grik4*. Number of cells expressing *Grik2* was in P50-P600 mice between 7% and 15% and *Grik5* between 21% and 33%.

Expression of genes coding subunits of NMDA receptors *Grin2a*, *Grin2b* and *Grin3a* shows similar trend as most of the genes coding subunits of AMPA and kainate receptors - high number of expressing cells in early development (32-77%), which decreased below 10% during ageing (P90-P600 mice). The most stable expression among genes coding subunits of

NMDA receptors was observed with *Grin2c*, which was expressed in 8-26% of cells isolated from P10-P600 mice. *Grin2d* and *Grin3b* were expressed in fewest cells (*Grin3b* was not measured in cells isolated from P10 and P20 mice). The most interesting result regarding NMDA receptors was obtained with *Grin1* gene, which codes GluN1 subunit of NMDA receptors and which is to current knowledge the compulsory subunit in a functional NMDA receptor. Despite the assumption that this subunit is necessary for functional NMDA receptors, it was expressed only in 13-32% of cells isolated from developing mice (P10-P30 mice) and its expression dropped below 8% of cells isolated from P50-P600 mice.

We further studied expression of gene for the most abundant metabotropic receptor subunits in glial cells *Grm1,3,5* (D'Antoni et al. 2008; Loane et al. 2012). Expression of *Grm1* and *Grm5*, which both encode Group I metabotropic glutamate receptors, decreased with age of mice and the number of expressing cortical GFAP/EGFP^{+} glial cells isolated from P50-600 mice was below 10%. Opposite trend was observed in the expression of *Grm3*, which belongs to Group II metabotropic receptors and which was shown to prevent excitotoxic neuronal cell death (Bruno et al. 1998; D'Onofrio et al. 2001; Corti et al. 2007). Expression of *Grm3* was observed in 20% of cells isolated from P10 mice, 27% of P20 mice and it increased in cells isolated from P30-600 mice, since it was observed in majority of these cells (54-68%). In general we can conclude that number of cells expressing genes, which code glutamate receptors, stabilizes around day 50 of postnatal development of mice and does not significantly change during further ageing.

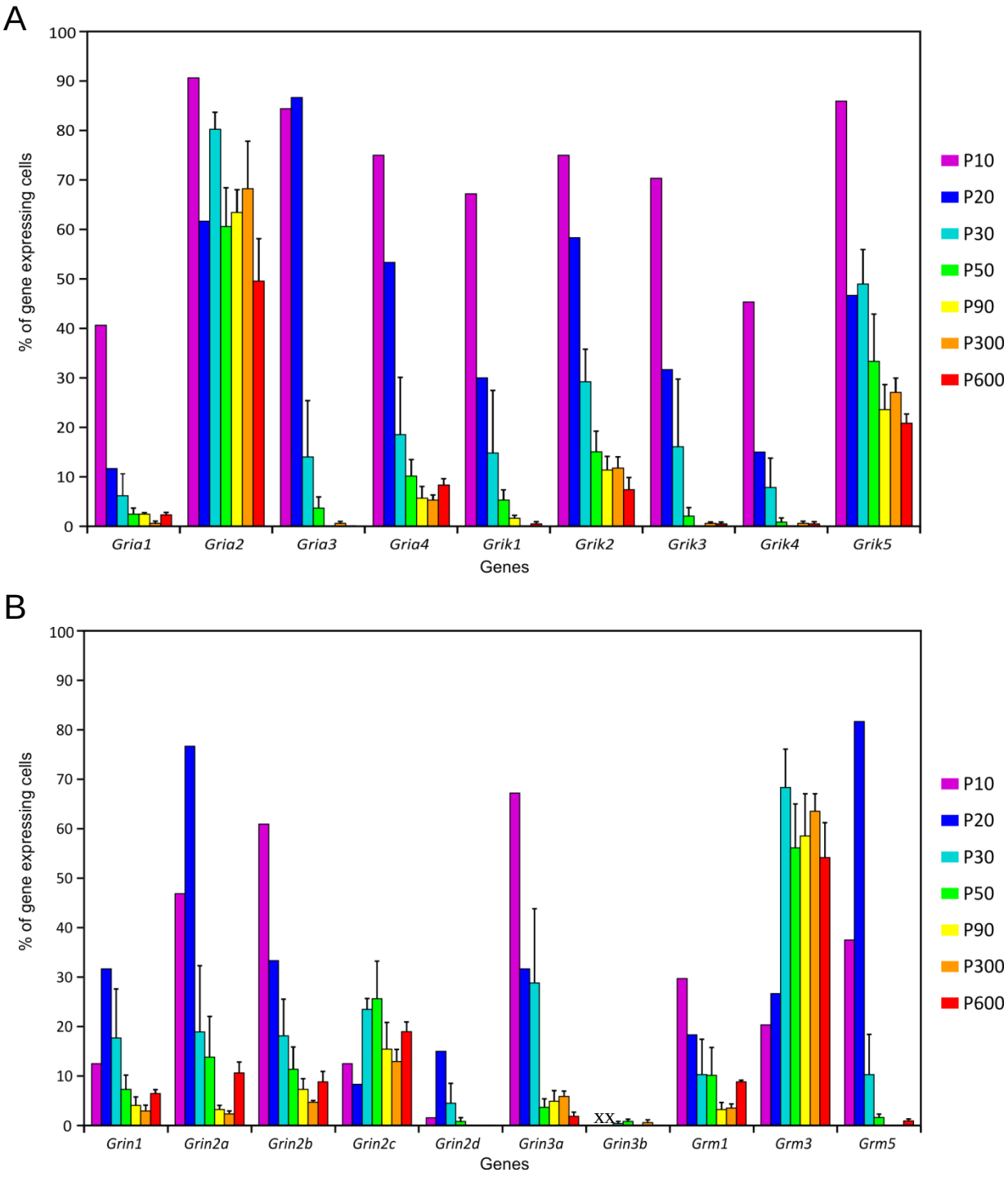


Figure 24. The percentage of GFAP/EGFP^{+} cells expressing genes coding individual subunits of glutamate receptors in mice during development and in ageing. Cells isolated from 10-, 20-, 30-, 50-, 90-, 300- and 600-day-old mice, (P10, 64 cells/1 mouse; P20, 60 cells/2 mice; P30, 243 cells/4 mice; P50, 246 cells/5 mice; P90, 123 cells/3 mice; P300, 170 cells/3 mice and P600, 216 cells/3 mice) were used. (**A**) Genes coding AMPA receptors (*Gria1-4*) and kainate receptors (*Grik1-5*). (**B**) Genes coding NMDA receptors (*Grin1-3b*) and metabotropic glutamate receptors (*Grm1,3,5*). The missing data in expression of *Grin3b* gene in P10 and P20 mice are marked with cross (x). Error bars represent S.E.M. and were calculated for groups containing at least 3 mice.

Expression profile of glutamate receptor subunits after MCAO

The incidence of cortical GFAP/EGFP^{+} cells expressing the genes coding particular glutamate receptors subunits was studied also after MCAO, which was shown to have a significant impact on the expression of glutamate receptors (**Fig. 25**).

The lowest number of cells expressing AMPA receptor subunits was observed in the *Gria1* gene, which was expressed only in 2% of cells isolated from P50 controls. In cells isolated from D7 and D14 mice was the incidence of cells expressing the *Gria1* gene higher, but did not exceed 12%. Interestingly, the expression of *Gria2* gene was not significantly changed after MCAO and the level was similar to P50 mice (61%). The *Gria3* gene was expressed in 4% of the cells from P50 mice; however, in cells isolated from D7 and D14 mice was the number of *Gria3*-expressing cells significantly increased (43% and 50%, respectively). The *Gria4* gene was expressed in 10% of cells from P50 mice, while the number of cells expressing this gene increased to 51% in cells from D7 and to 49% in cells from D14 mice. Thus, after MCAO the number of gene expressing cells was increased at least 4-fold for 3 out of 4 AMPA receptor subunits.

A similar trend was observed with genes coding kainate receptor subunits. The numbers of cells expressing *Grik1,2,3,4,5* were increased 10-, 3-, 9-, 15- and 2-fold after MCAO. The highest number of cells expressing *Grik3,4* was observed in D7 mice and the incidence of cells expressing *Grik1,2,5* was maximal in D14 mice.

The number of cells expressing the subunits of NMDA receptors underwent dramatic changes as well. The *Grin1* gene was present in 7% of the cells from P50 mice, and this number was increased to 30% and 43% in cells isolated from D7 and D14 mice, respectively. From among all of the *Grin2* genes, the only gene that displayed a significant increase in the number of expressing cells after MCAO was *Grin2d*. The *Grin3a* gene, which codes the recently discovered GluN3A subunit of NMDA receptors with a prominent effect on the Mg^{2+} block and Ca^{2+} permeability of NMDA receptors (Perez-Otano et al. 2001; Cavara and Hollmann 2008), was expressed in 7-12-fold more cells isolated from mice after ischemic insult when compared to cells isolated from P50 mice (30% and 50% of cells isolated from D7 and D14 mice, respectively, compared to 4% of cells from P50 mice). The number of cells expressing *Grin3b* gene was very low; we detected it only in 1% of cells from P50 mice and 2% of cells from D7 mice, while there was no expression in cells from D14 mice.

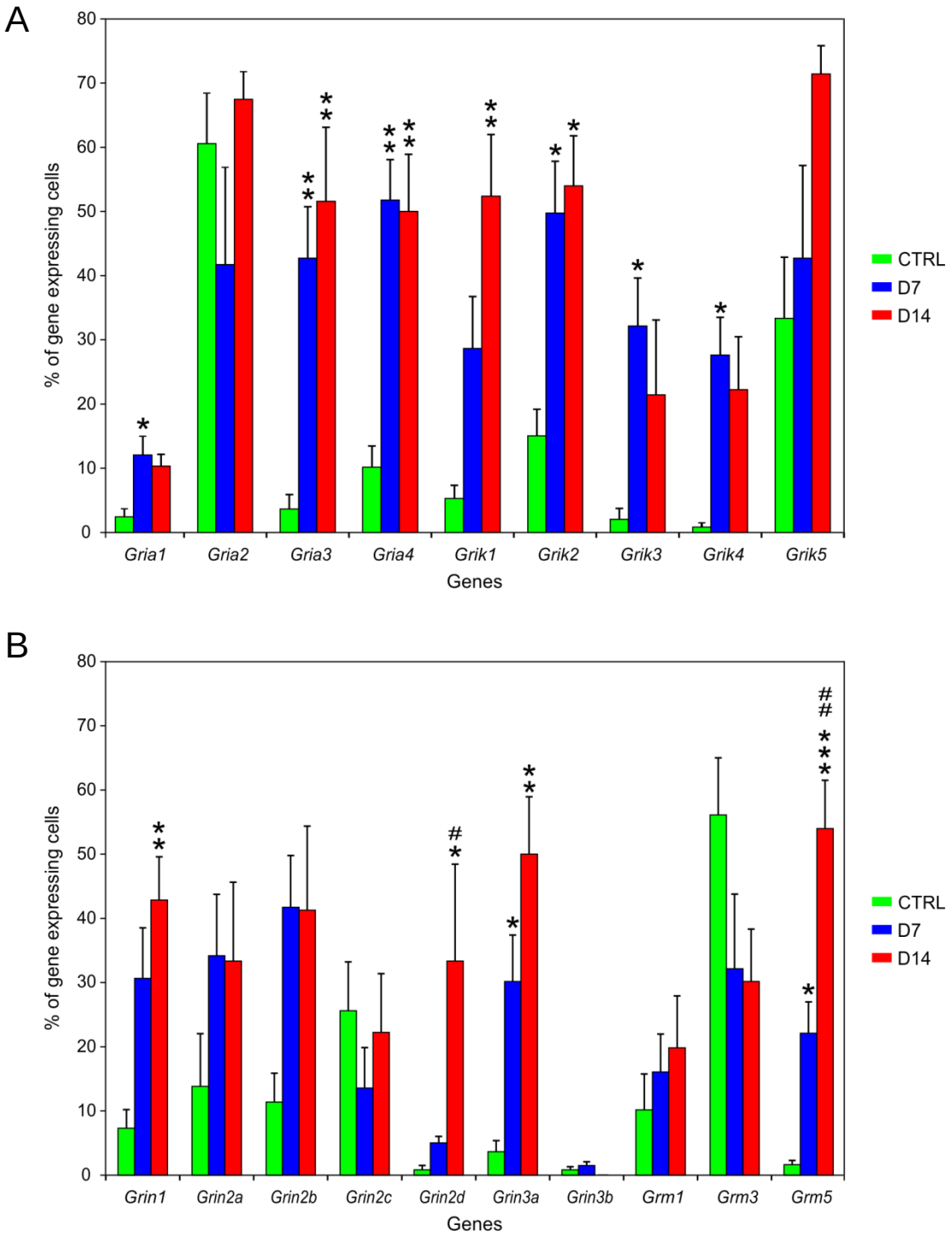


Figure 25. The percentage of GFAP/EGFP^{+} cells expressing genes coding individual subunits of glutamate receptors in control mice and in mice after MCAO. Cells isolated from 50-day-old uninjured control mice, (CTRL, 246 cells/5 mice) and from mice 7 and 14 days after middle cerebral artery occlusion (D7, 196 cells/4 mice and D14, 125 cells/3 mice) were used. (**A**) Genes coding AMPA receptors (*Gria1-4*) and kainate receptors (*Grik1-5*); (**B**) genes coding NMDA receptors (*Grin1-3b*) and metabotropic glutamate receptors (*Grm1,3,5*). Error bars represent S.E.M. Significant differences between D7/D14 compared to CTRL (* - $p < 0.05$, ** - $p < 0.01$, *** - $p < 0.001$) and D14 compared to D7 (# - $p < 0.05$, ## - $p < 0.01$) were calculated by one-way ANOVA followed by the Bonferroni post-test.

We also studied the expression of genes coding metabotropic glutamate receptor subunits *Grm1,3,5*. Ten percent of cells isolated from P50 mice expressed *Grm1*, and this incidence did not significantly change after MCAO. The number of cells expressing *Grm3* shifted from 56% in cells from P50 mice to 30-32% of cells isolated from mice after MCAO. The largest increase in the percentage of cells expressing a particular gene after MCAO was observed with *Grm5*, which was detected in only 1.6% of cells isolated from P50 mice. Following ischemic injury the incidence increased 13-fold and 33-fold in cells isolated from D7 and D14 mice, respectively. This is in accordance with other studies showing the absence of *Grm5* in adult astrocytes under physiological conditions (Sun et al. 2013) and an increased presence of *Grm5* mRNA and mGluR5 protein in reactive astrocytes (Ulas et al. 2000; Aronica et al. 2000). Moreover, *Grm5* together with *Grin2d* were the only genes which were expressed in significantly higher number of cells isolated from D14 mice when compared to cells isolated from D7 mice.

In general, we can conclude that number of cells expressing most of the genes coding glutamate receptors was increased after MCAO, so the glutamate receptors expression profile after MCAO was similar to the profile observed in early development (P10-P20 mice) (**Fig. 24**).

Gene expression profiling of distinct subpopulations of GFAP/EGFP$^+$ cells after MCAO with respect to glutamate receptors

We already showed that GFAP/EGFP$^+$ cells are heterogeneous in their gene expression profile after MCAO (**Fig. 24**). Next, we were interested in how expression of glutamate receptors contributes to this heterogeneity. Therefore, we performed a PCA using data which included only genes coding glutamate receptors (*Gria1-4, Grik1-5, Grin1-3a* and *Grm1,3,5),* markers of astrocytes (*Slc1a3, Glul, Gfap* and *Aqp4*) and markers of NG2 glia (*Cspg4* and *Pdgfra*) to find three distinct subpopulations (SP1-SP3) among a pool of cells isolated from P50, D7 and D14 mice (**Fig. 26A**). The SOM analysis, which forced the division of the cells into three groups, confirmed the stable classification of these subpopulations. There was an interesting tendency in the representation of cells isolated from P50, D7 and D14 mice in these subpopulations (**Fig. 26B**). Subpopulation SP1 mostly comprised cells from P50 mice, SP2 contained 30% of cells from P50 mice but mostly cells from D7 mice, and SP3 was formed almost solely by cells isolated from mice MCAO (42% and 54% of cells isolated from D7 and D14 mice, respectively).

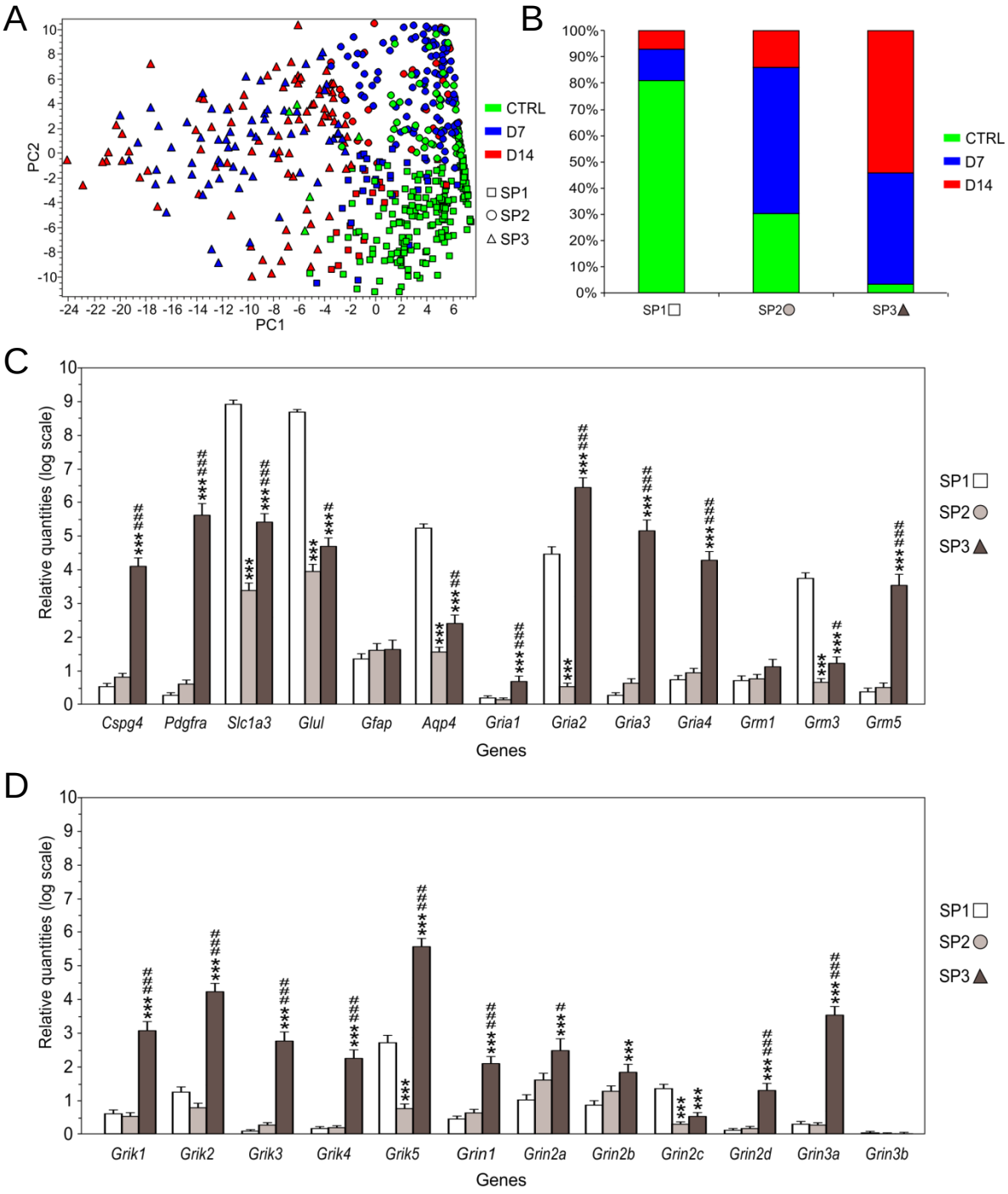


Figure 26. Gene expression profiling of distinct subpopulations of GFAP/EGFP$^+$ cells isolated from the cortex of GFAP/EGFP mice. (**A**) Principal component analysis (PCA) of cells from uninjured 50-day-old control mice (CTRL, 246 cells/5 mice) and mice 7 and 14 days after middle cerebral artery occlusion (D7, 199 cells/4 mice; D14, 126 cells/3 mice). The data were mean-centered according to the genes. The cells were divided into three groups by Kohonen self-organizing maps (SOM) and are marked by different symbols (squares for subpopulation SP1, circles for subpopulation SP2 and triangles for subpopulation SP3). (**B**) Percentage representation of cells isolated from CTRL, D7 and D14 mice in the subpopulations SP1-3. (**C, D**) Bar plot with S.E.M. showing the relative expression of the analyzed genes in subpopulations SP1-3. Significant differences between SP2/SP3 compared to SP1 (*** - $p < 0.001$) and SP3 compared to SP2 (# - $p < 0.05$, ## - $p < 0.01$, ### - $p < 0.001$) were calculated by one-way ANOVA followed by the Bonferroni post-test.

From the bar plot showing the expression levels of genes in the SP1-SP3 subpopulations (**Fig. 26C, D**), it is evident that the highest gene transcript levels were in subpopulation SP3, which consisted especially of cells from D7 and D14 mice, indicating the role of glutamate receptors after ischemia. This also corresponded with the increased percentage of cells expressing genes coding glutamate receptors after MCAO (**Fig. 25**).

Correlation between the expression of glial markers and glutamate receptors subunits

Even though there is heterogeneity among GFAP/EGFP$^+$ cells, there were still some trends in gene expression patterns when comparing cells isolated from P50, D7 and D14 mice. In the next step, we focused on their detailed classification. For this purpose, the Spearman correlation coefficients between pairs of genes were calculated. Positive correlation between the expressions of two genes indicates that in any of the analyzed cells, high expression of the first gene is accompanied by high expression of the second gene and vice versa. On the other hand, negative correlation between two genes indicates that high expression of the first gene is accompanied by low or no expression of the second gene. Since the GFAP/EGFP$^+$ cells, which we analyzed, expressed genes coding astrocytic markers *Slc1a3*, *Glul*, *Gfap* and/or *Aqp4* as well as the NG2 glial markers *Cspg4* and/or *Pdgfra* as previously shown (Rusnakova et al. 2013), we were able to assess significant correlations between genes coding glutamate receptors and astrocytic and NG2 glial markers (**Fig. 27**).

The lowest number of correlations was observed in cells isolated from P50 mice. Six genes (*Gria1*, *Gria3*, *Grik5*, *Grin2d*, *Grin3b* and *Grm5*) did not correlate with any of the astrocytic or NG2 glial markers in this group, while the remaining 13 genes correlated positively with at least one of the NG2 glial marker. Positive correlations with at least 2 out of 4 astrocytic markers were observed only with 3 genes (*Gria2*, *Grin2c* and *Grm3*), whereas negative correlations were found with 4 genes (*Gria4*, *Grik3*, *Grin2a* and *Grm1*). In cells isolated from P50 mice we can summarize that most of the glutamate receptors were especially present in GFAP/EGFP$^+$ cells, which expressed NG2 glial markers.

The correlation coefficients in cells isolated from D7 mice showed a strong positive correlation of AMPA and kainate receptor subunits with NG2 glial markers, which was not observed for NMDA receptor subunits (a positive correlation only with *Grin1*, *Grin3a* and marginally also with *Grin2d*) and metabotropic glutamate receptors (a positive correlation with *Grm5* only). In contrast to cells isolated from P50 mice, almost all glutamate receptor subunits displayed a positive correlation with astrocytic markers in cells isolated from D7

mice. Surprisingly, a positive correlation was also observed between the astrocytic marker *Slc1a3* and the NG2 glial markers *Cspg4* and *Pdgfra* (data not shown), which reflects the complex changes accompanying reactive astrogliosis 7 days after MCAO.

In cells isolated from D14 mice was the situation much more comprehensible. There was no positive correlation between genes coding NG2 glial and astrocytic markers (data not shown), and also most of the genes coding glutamate receptor subunits correlated positively only with NG2 glial or astrocytic markers. For AMPA receptors the correlation coefficients were similar to those in cells isolated from P50 mice. The only difference was in the *Gria3* gene, which was positively correlated with astrocytic markers in cells isolated from D14 mice. Kainate receptors also showed a similar trend as in cells from P50 mice, since they were mostly correlated with NG2 glial markers. Intriguingly, NMDA and metabotropic glutamate receptors showed a very distinct correlation pattern, as *Grin2a-d* and *Grm3,5* showed a strong negative correlation with NG2 glial markers and a positive correlation with astrocytic markers. The only genes coding NMDA receptor subunits that positively correlated with NG2 glial markers were *Grin1* and *Grin3a*.

	CTRL						D7						D14					
	Cspg4	*Pdgfra*	*Slc1a3*	*Glul*	*Gfap*	*Aqp4*	*Cspg4*	*Pdgfra*	*Slc1a3*	*Glul*	*Gfap*	*Aqp4*	*Cspg4*	*Pdgfra*	*Slc1a3*	*Glul*	*Gfap*	*Aqp4*
Gria1							0,28	0,28	0,31	0,16								
Gria2	0,19		**0,28**	**0,47**		**0,45**	0,60	0,56	**0,48**	**0,14**		**0,20**	0,41	0,45	**0,28**			
Gria3							0,66	0,65	0,46			0,15			0,28	0,31		
Gria4	0,19		-0,13	-0,13			0,50	0,51	0,39			0,15	0,39	0,48				-0,25
Grik1	0,18	**0,35**					0,37	**0,37**	0,36	0,14		0,23	0,22	**0,29**	0,32			
Grik2	0,20				0,16		0,45	0,44	0,30	0,27	-0,15	0,15	0,39	0,42				-0,19
Grik3		**0,29**	-0,18	-0,16		-0,14	0,53	**0,50**	0,25				0,37	**0,32**				-0,28
Grik4	0,22	0,23					0,51	0,50	0,34				0,36	0,48		-0,20		-0,25
Grik5							0,43	0,44	0,48	0,31		0,34	0,31	0,37	0,37	0,27		
Grin1	**0,30**				0,14		**0,30**	0,21	0,19			0,19	**0,23**	0,23				
Grin2a	0,23		-0,34	-0,22		-0,13			0,17	0,20	0,22	0,17	-0,45	-0,42	0,37	0,54		0,25
Grin2b	0,16		-0,14										-0,24	-0,20				0,27
Grin2c	0,14			0,18		0,21			0,14	0,25		0,28	-0,24	-0,25	0,42	0,36		0,42
Grin2d							0,17				-0,19		-0,26	-0,21		0,20		0,24
Grin3a	0,19	**0,30**					0,63	**0,67**	0,51			0,17	0,55	**0,62**	0,18			
Grin3b																		
Grm1	0,18		**-0,25**	-0,23		-0,13					0,15	0,22				0,21		0,27
Grm3		0,16	**0,25**	**0,46**		**0,40**			**0,27**	**0,48**	0,28	**0,35**	-0,24	-0,27	**0,50**	**0,54**		**0,47**
Grm5							0,50	0,46	0,25				-0,30	-0,24	0,47	0,55		0,20

Figure 27. Spearman correlation coefficients between genes coding glutamate receptor subunits and markers of NG2 glia/astrocytes in cells isolated from uninjured 50-day-old mice (CTRL) and in cells isolated from mice 7 and 14 days after middle cerebral artery occlusion (D7 and D14, respectively). The correlation coefficients were calculated from all cells including those without any expression of the studied genes. Positive correlations are highlighted in green, negative in red. All the values of the correlation coefficients are significant with $p < 0.05$. Correlation coefficients with $p < 0.001$ are in bold.

4.2 Immunohistochemical protein detection of NMDA receptor subunits

The single cell RT-qPCR studies provided us with information about the levels of mRNA transcripts in single GFAP/EGFP$^+$ cells. As the next step, we performed an immunohistochemical analysis of mouse cortical tissue to verify that these transcripts were translated into proteins. For this analysis we chose NMDA receptors since there are many unresolved questions about their presence and function in glial cells which we would like to unravel (Dzamba et al. 2013).

We analyzed staining of cortical GFAP/EGFP$^+$ glial cells for individual NMDA receptor subunits (GluN1, GluN2A-D and GluN3A-B) in brain slices from controls and from D14 mice, in which the images were taken from the ischemic rim (**Fig. 28A**). The analysis revealed that there were GFAP/EGFP$^+$ cells positively stained for the GluN1 subunits in D14 mice (**Fig. 28B**). As for the GluN2A subunit, we were not able to detect any GFAP/EGFP$^+$ cells positive for this subunit; the only positive cells morphologically resembled neurons (**Fig. 29**). The immunostaining analysis of GluN2B, GluN2C and GluN2D subunits showed similar results as with GluN1 subunit, since GluN2B-D positive GFAP/EGFP$^+$ cells were detected only in D14 mice and not in controls (**Fig. 29** and **Fig. 30**). The GluN3A subunit was the only NMDA receptor subunit, in which we observed an overlap with EGFP fluorescence from GFAP/EGFP$^+$ glial cells under control conditions; however, these cells had relatively low EGFP fluorescence and did not show a typical bushy-like astrocytic morphology (**Fig. 31**). The number of GFAP/EGFP$^+$ glial cells positive for GluN3A staining was in D14 mice much higher than in controls (**Fig. 31**). As for the GluN3B immunostaining, there were positive cells in subcortical regions (data not shown), but none of the cells in the cortex were positive, either in controls or D14 mice (**Fig. 31**).

The immunohistochemical analysis revealed that especially after MCAO, there are GFAP/EGFP$^+$ cells positive for most of the NMDA receptor subunits. This correlates with single cell RT-qPCR results which also showed increase of NMDA receptor subunits expression after MCAO. Nonetheless, the single cell RT-qPCR results showed that even under control conditions, the GFAP/EGFP$^+$ glial cells did express mRNA of NMDA receptor subunits, but these were not detected by immunostaining analysis (except for GluN3A subunit). This might be due to the fact that under control conditions, astrocytes have a bushy-like morphology with many fine processes, which are too small for immunohistochemical co-

localization utilizing confocal microscopy. The discussion regarding this discrepancy is in the Discussion part of this PhD thesis, where the inability to detect GluN2A subunit by immunostaining is also commented.

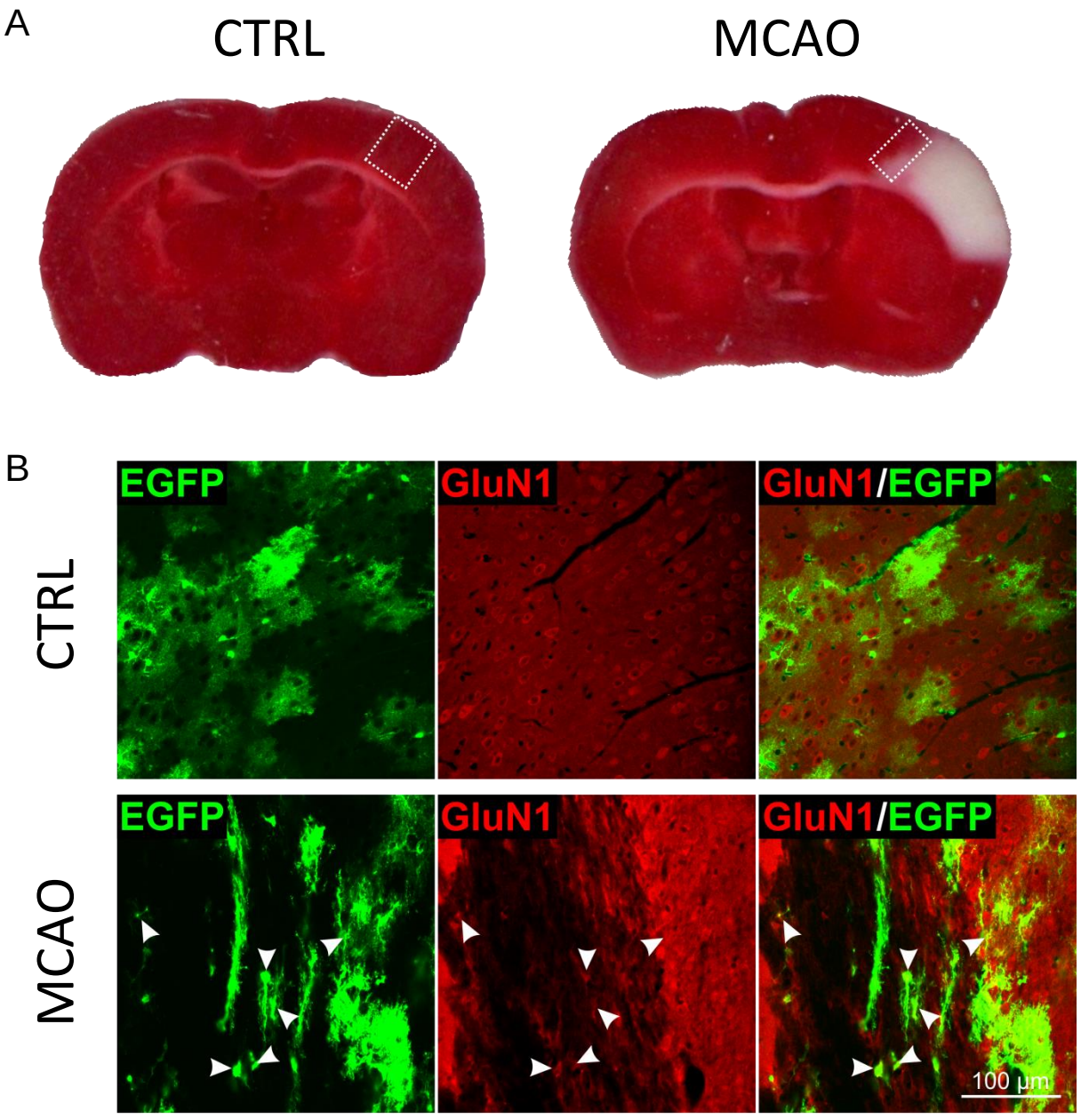


Figure 28. Immunohistochemical analysis of the GluN1 subunit of the NMDA receptors in the cortex of adult GFAP/EGFP mice under control conditions (CTRL) and 14 days after middle cerebral artery occlusion (MCAO). (**A**) Coronal brain sections from CTRL and MCAO animals stained with triphenyltetrazolium chloride. The white color in MCAO brain section indicates the volume of ischemic tissue after focal ischemia. The boxed areas indicate the regions in which the immunohistochemical analysis was performed. (**B**) The arrowheads indicate the overlay of GFAP/EGFP^{+} cells and GluN1 staining. Note the overlap of the EGFP signal with GluN1 staining in MCAO. The same scale bar applies to all images in part B.

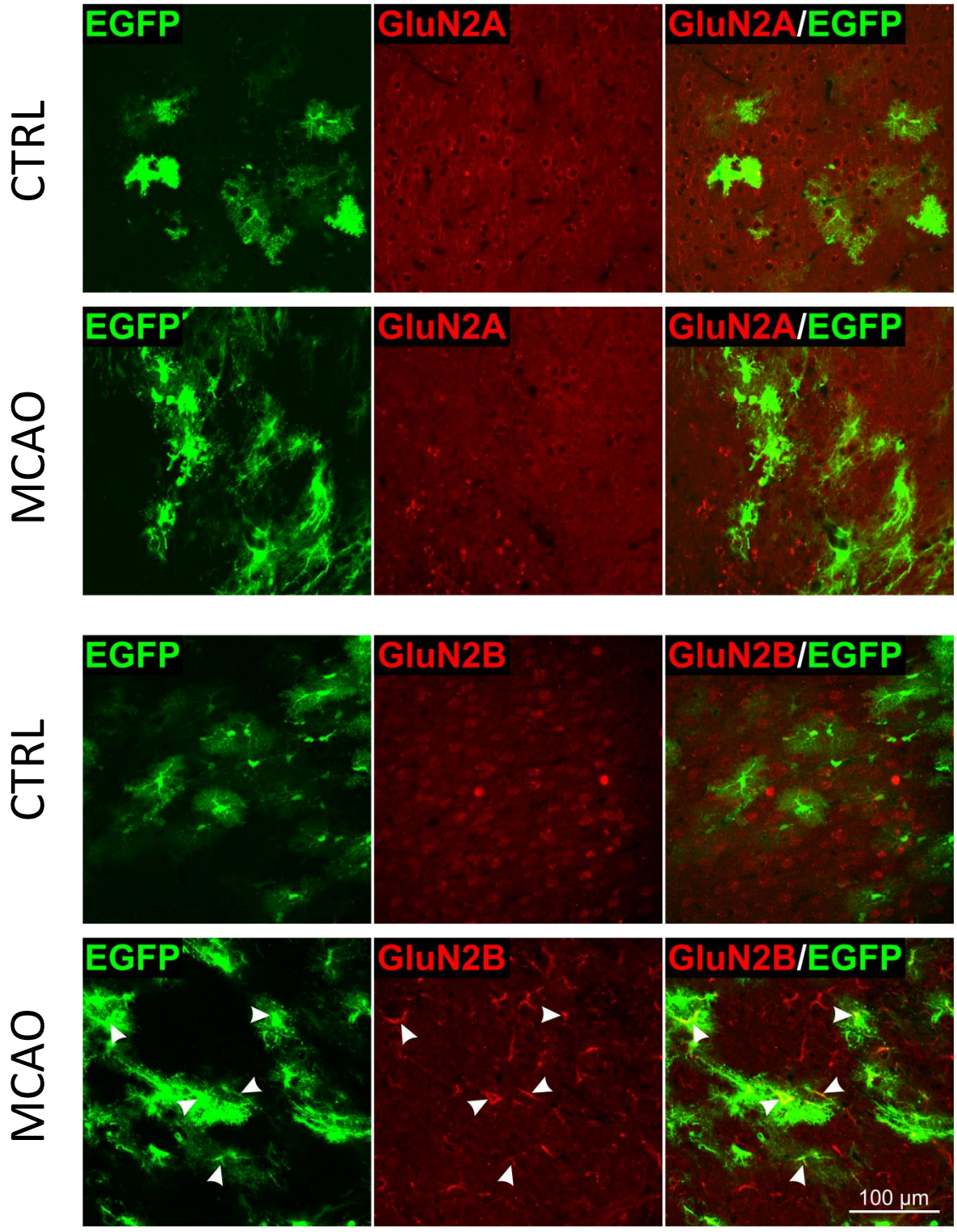


Figure 29. Immunohistochemical analysis of the GluN2A-B subunits of the NMDA receptors in the cortex of adult GFAP/EGFP mice under control conditions (CTRL) and 14 days after middle cerebral artery occlusion (MCAO). The arrowheads indicate the overlay of GFAP/EGFP^{+} cells and GluN2A-B staining. Note the overlap of the EGFP signal with GluN2B staining in MCAO. The same scale bar applies to all images.

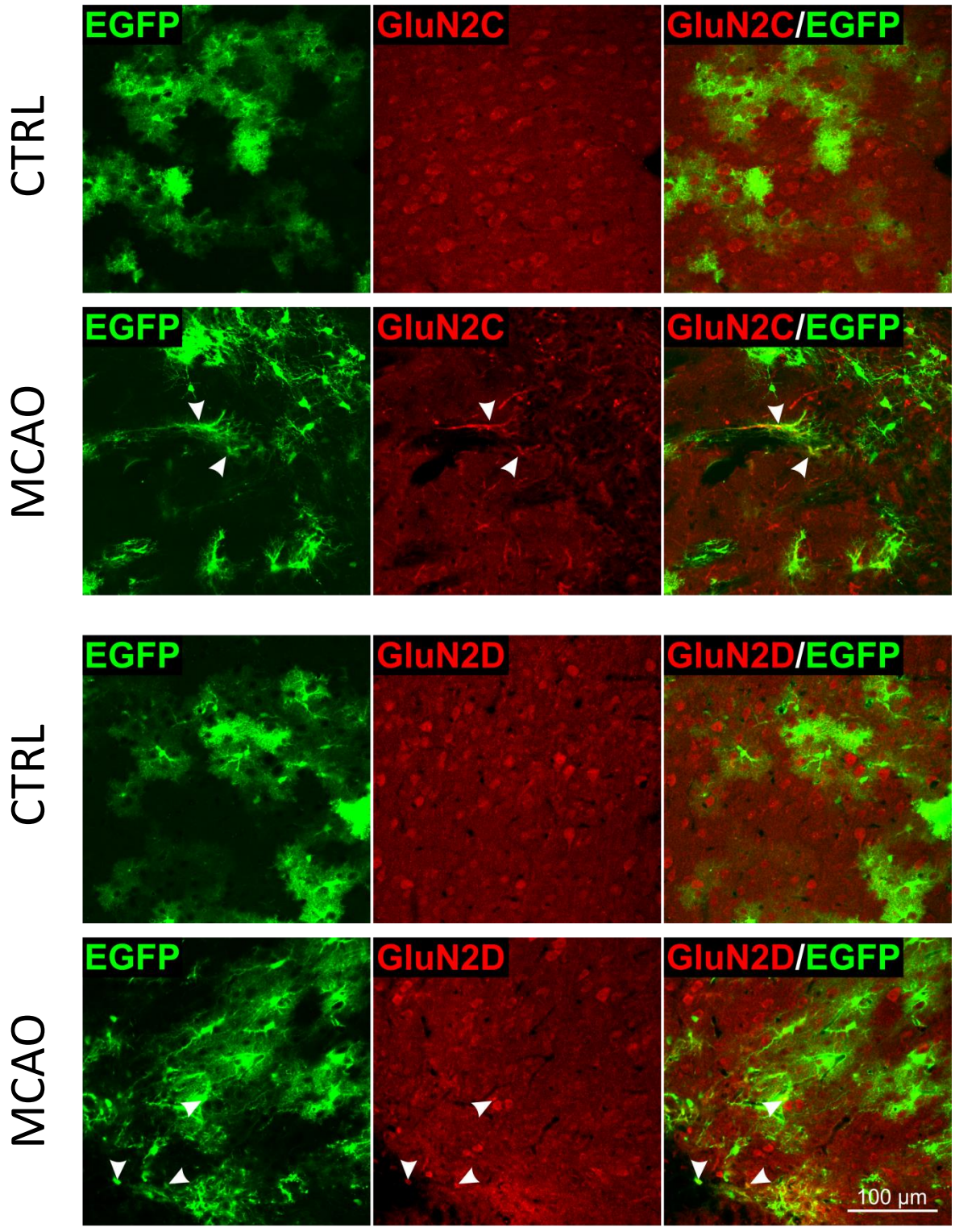


Figure 30. Immunohistochemical analysis of the GluN2C-D subunits of the NMDA receptors in the cortex of adult GFAP/EGFP mice under control conditions (CTRL) and 14 days after middle cerebral artery occlusion (MCAO). The arrowheads indicate the overlay of GFAP/EGFP^{+} cells and GluN2C-D staining. Note the overlap of the EGFP signal with GluN2C and GluN2D staining in MCAO. The same scale bar applies to all images.

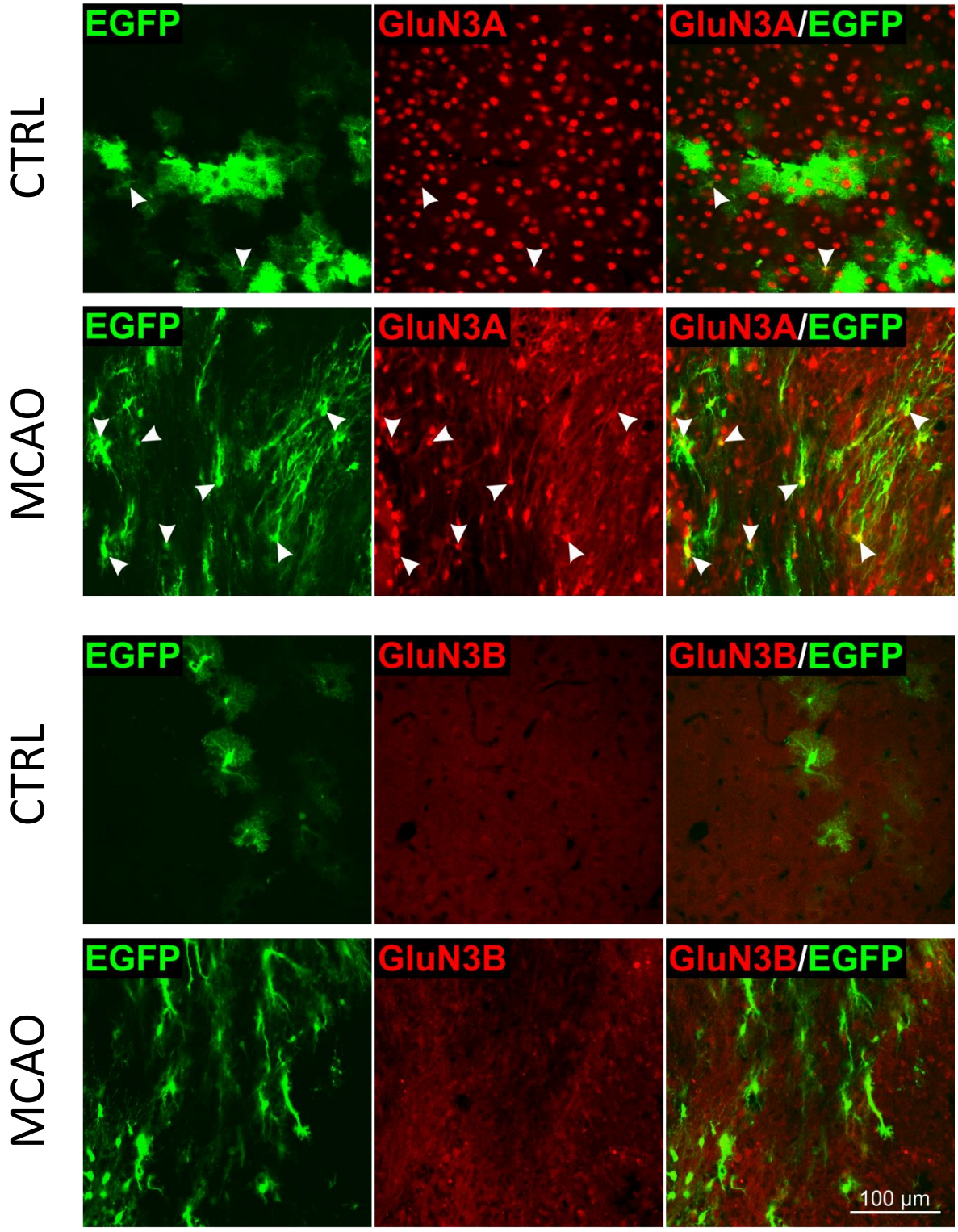


Figure 31. Immunohistochemical analysis of the GluN3A-B subunits of the NMDA receptors in the cortex of adult GFAP/EGFP mice under control conditions (CTRL) and 14 days after middle cerebral artery occlusion (MCAO). The arrowheads indicate the overlay of GFAP/EGFP^{+} cells and GluN3A staining. Note the overlap of the EGFP signal with GluN3A staining in CTRL tissue and in MCAO. The same scale bar applies to all images.

4.3 Functional properties of NMDA receptors under physiological conditions and following ischemia

The single cell RT-qPCR results and immunohistochemical analysis revealed that cortical GFAP/EGFP$^+$ glial cells express subunits of NMDA receptors and that these subunits are, especially after MCAO, detectable also on the protein level. Based on these results, we decided to perform a functional study of NMDA receptors in GFAP/EGFP$^+$ glial cells using Ca^{2+} imaging technique, as NMDA receptors are known to be Ca^{2+} permeable and this permeability is dependent on their subunit composition. The experiments were carried out in brain slices prepared from GFAP/EGFP mice (*in situ*) as well as in cell cultures (*in vitro*).

4.3.1 Calcium imaging measurements in brain slices (*in situ*)

We studied the Ca^{2+} elevations in GFAP/EGFP$^+$ glial cells after application of 100 µM NMDA (**Fig. 32A**). Since we noticed that the Ca^{2+} responses were not always detected immediately after the application of 100 µM NMDA, we quantified the delay of the NMDA-evoked Ca^{2+} responses (**Fig. 32B**). For this purpose, we set the signal threshold for Ca^{2+} responses to 200% of the amplitude of the noise signal, and the responses were taken into account only if they occurred within 1 minute from the onset of the application. The average delay of the onset of Ca^{2+} responses following an application of 100 µM NMDA was 32.4 s and the responses were more or less normally distributed around this value. Another analyzed parameter was the area under the curve which was measured during 1 minute from the start of application and was expressed in arbitrary units. The distribution of the area under the curve after application of 100 µM NMDA shows that the Ca^{2+} responses did not reveal any heterogeneity in the magnitude of the responses (**Fig. 32C**). Nonetheless, we can summarize that the 100 µM NMDA-evoked Ca^{2+} responses *in situ* differed in their kinetics as they displayed a large variability ranging from fast transient Ca^{2+} spikes to gradual changes of Ca^{2+} concentration indicating sustained Ca^{2+} entry (**Fig. 32A**).

Next, we aimed to elucidate to what extent are NMDA-evoked intracellular Ca^{2+} elevations dependent on NMDA concentration (**Fig. 33**). As expected, the Ca^{2+} elevations increased with the concentration of NMDA applied. The number of responding cells followed this trend even though it was not statistically significant (**Fig. 33B**). Nonetheless, the analysis of the area under the curve showed that 4 µM and 20 µM NMDA-evoked responses were lower by 78% and 42%, respectively, when compared to the application of 100 µM NMDA,

with statistically significant difference between application of 4 µM and 100 µM NMDA (**Fig. 33C**).

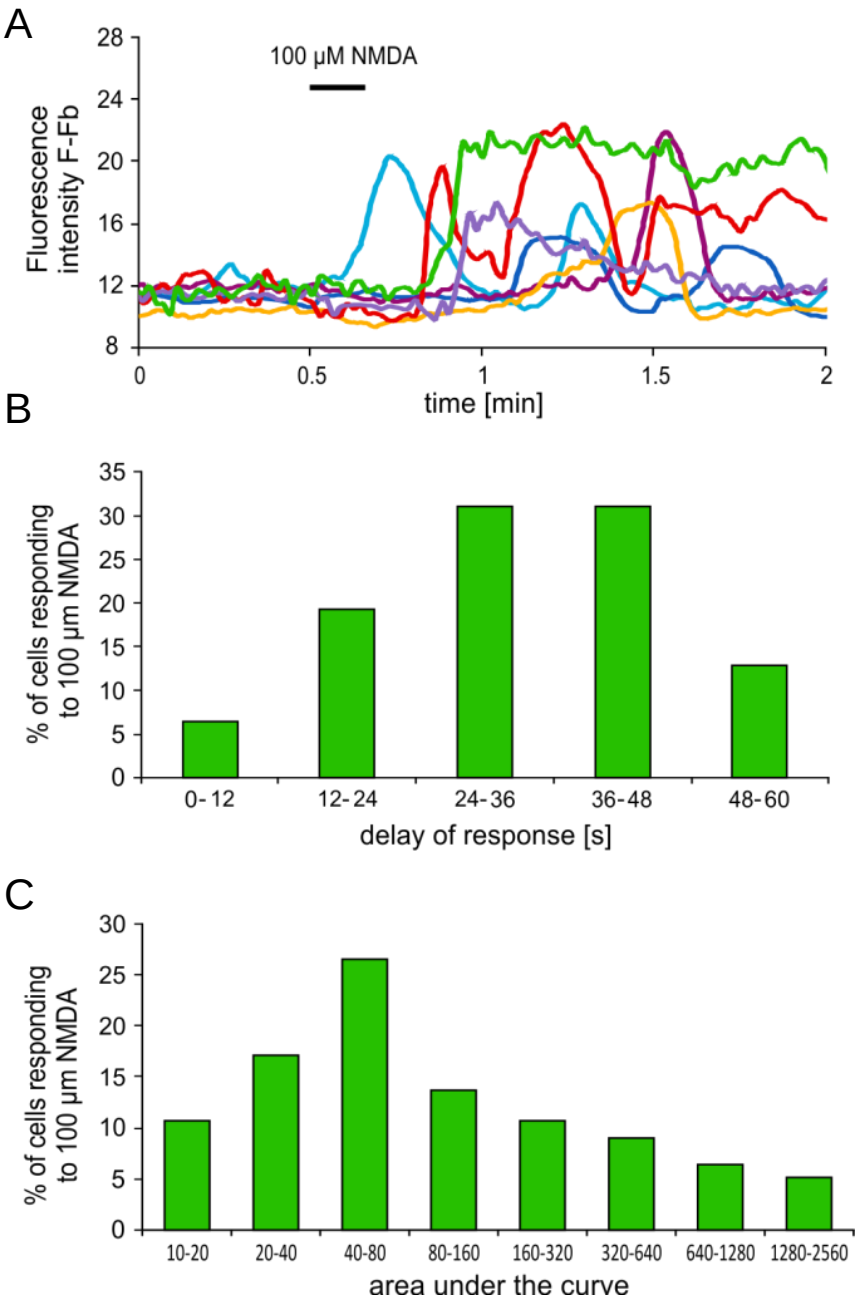


Figure 32. Calcium imaging measurements of cortical GFAP/EGFP^{+} glial cells from GFAP/EGFP mice *in situ* – description of Ca^{2+} responses. (**A**) Example traces showing kinetics of the responses to the application of 100 µM NMDA. (**B**) Quantification of the delay of the response onset shows that the average delay was ~30 s (n = 94). (**C**) A histogram of the distribution of Ca^{2+} responses evoked by the application of 100 µM NMDA. Only cells with responses having the area under the curve higher than 10 were analyzed (n = 232).

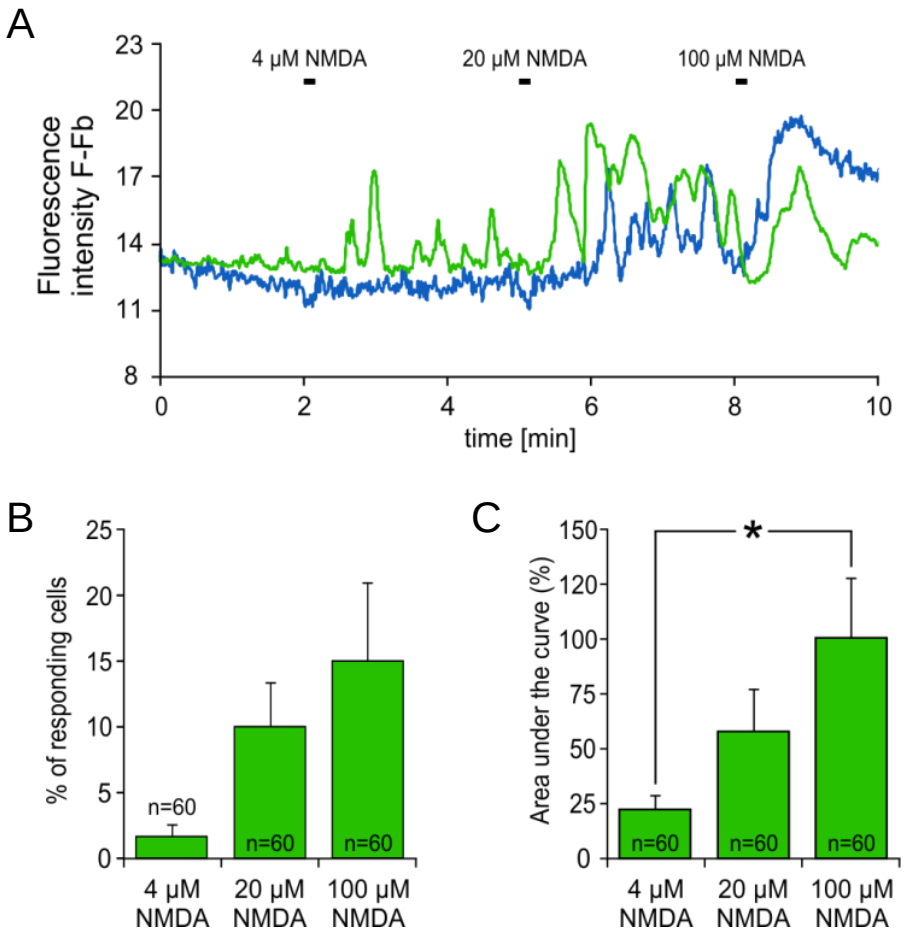


Figure 33. Calcium imaging measurements of cortical GFAP/EGFP$^+$ glial cells from GFAP/EGFP mice *in situ* - the NMDA concentration dependence. (**A**) Example traces showing responses to application of 4, 20 and 100 µM NMDA. (**B**) Percentage of cells responding to application of different concentrations of NMDA. (**C**) Quantification of the area under the curve of Ca^{2+} responses after application of different concentrations of NMDA. Error bars represent S.E.M. Significant differences (* - $p < 0.05$) were calculated by one-way ANOVA followed by the Bonferroni post-test; n indicates the number of cells.

One of the major issues of *in situ* measurements is that the measured cells are influenced by the cells in their surroundings. In our case were the most problematic element neurons, which possess NMDA receptors and are thus able to respond to application of NMDA and subsequently influence glial cells. To check to what extend our measurements on GFAP/EGFP$^+$ glial cells were influenced by the presence of neurons, we co-applied 1 µM TTX with 100 µM NMDA, as TTX inhibits the firing of action potentials in neurons by binding to the voltage-gated Na^+ channels. Our results show that co-application of 1 µM TTX did not result in any significant decrease in the Ca^{2+} responses evoked by 100 µM NMDA (**Fig. 34A**).

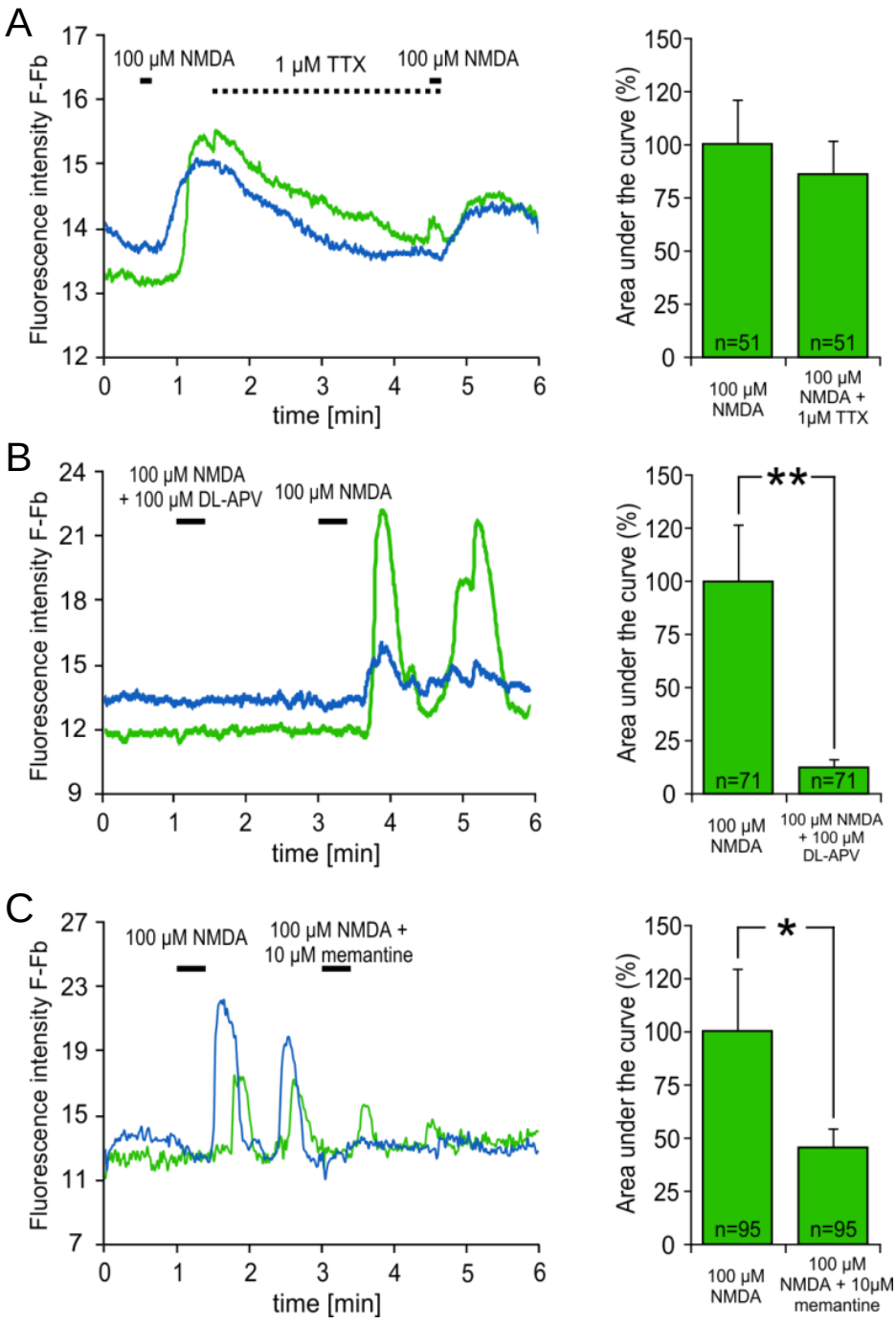


Figure 34. Calcium imaging measurements of cortical GFAP/EGFP^{+} glial cells from GFAP/EGFP mice *in situ* – pharmacology. (**A**) The co-application of 1 µM TTX did not reveal any significant change in the Ca^{2+} responses evoked by 100 µM NMDA. (**B**) The selective NMDA receptor blocker DL-APV markedly blocked the Ca^{2+} elevations evoked by the application of 100 µM NMDA. (**C**) The co-application of memantine decreased the NMDA-evoked Ca^{2+} elevations, which indicates the presence of GluN2C-D subunits in the NMDA receptors. Error bars represent S.E.M. Significant differences (* - $p < 0.05$ and ** - $p < 0.01$) were calculated by a paired t-test; n indicates the number of cells.

Furthermore, the responses to the application of 100 µM NMDA were sensitive to the selective NMDA receptor antagonist DL-APV, which markedly blocked Ca^{2+} elevations (**Fig. 34B**). To clarify the subunit composition of the NMDA receptors, we further tested the effect of 10 µM memantine, inhibiting preferentially GluN2C- and GluN2D-containing NMDA receptors (Kotermanski and Johnson 2009; Palygin et al. 2011). The co-application of memantine led to a significant diminishing of the NMDA-evoked Ca^{2+} elevations which might be due to the presence of GluN2C and/or GluN2D subunits in the NMDA receptors present in GFAP/$EGFP^{+}$ glial cells (**Fig. 34C**).

One of the main objectives of this thesis was to describe changes in NMDA receptors under pathophysiological conditions of focal cerebral ischemia. To study the impact of MCAO, we compared the Ca^{2+} responses of GFAP/$EGFP^{+}$ glial cells in controls with those in D13-14 mice (**Fig. 35**). The application of 100 µM NMDA evoked a markedly lower Ca^{2+} influx in the GFAP/$EGFP^{+}$ cells after MCAO and the number of responding cells was also significantly reduced when compared to cells in control mice. This result shows, that after MCAO the Ca^{2+} influx in cortical GFAP/$EGFP^{+}$ glial cells through NMDA receptors is blocked, which might be due to their different subunit composition after MCAO leading to impermeability for Ca^{2+}. Results from single cell RT-qPCR and immunohistochemical analyses suggest increased presence of the GluN3A subunit in NMDA receptors after MCAO, which would lead to lower Ca^{2+} permeability of NMDA receptors (Perez-Otano et al. 2001; Cavara and Hollmann 2008). The application of 100 µM glycine, a co-agonist of NMDA receptors, evoked responses in ~3% of cells from controls and no response was observed in cells from D13-14 mice (the threshold for a response was 200% of the amplitude of the noise signal). Analysis of the area under curve showed significant decrease in cells from D13-14 mice when compared to cells from controls. The same trend was observed also in application of 100 µM glutamate; nonetheless, ~12% of responding cells from mice after MCAO indicated that apart from NMDA receptors there are also other Ca^{2+} permeable glutamate receptors present in cortical GFAP/$EGFP^{+}$ glial cells. These might be AMPA, kainate or metabotropic glutamate receptors, which are all activated by glutamate. However, even though the amount of cells responding to application of 100 µM glutamate was not significantly decreased in cells from mice after MCAO, the area under the curve reflecting total Ca^{2+} influx was significantly decreased (**Fig. 35B**).

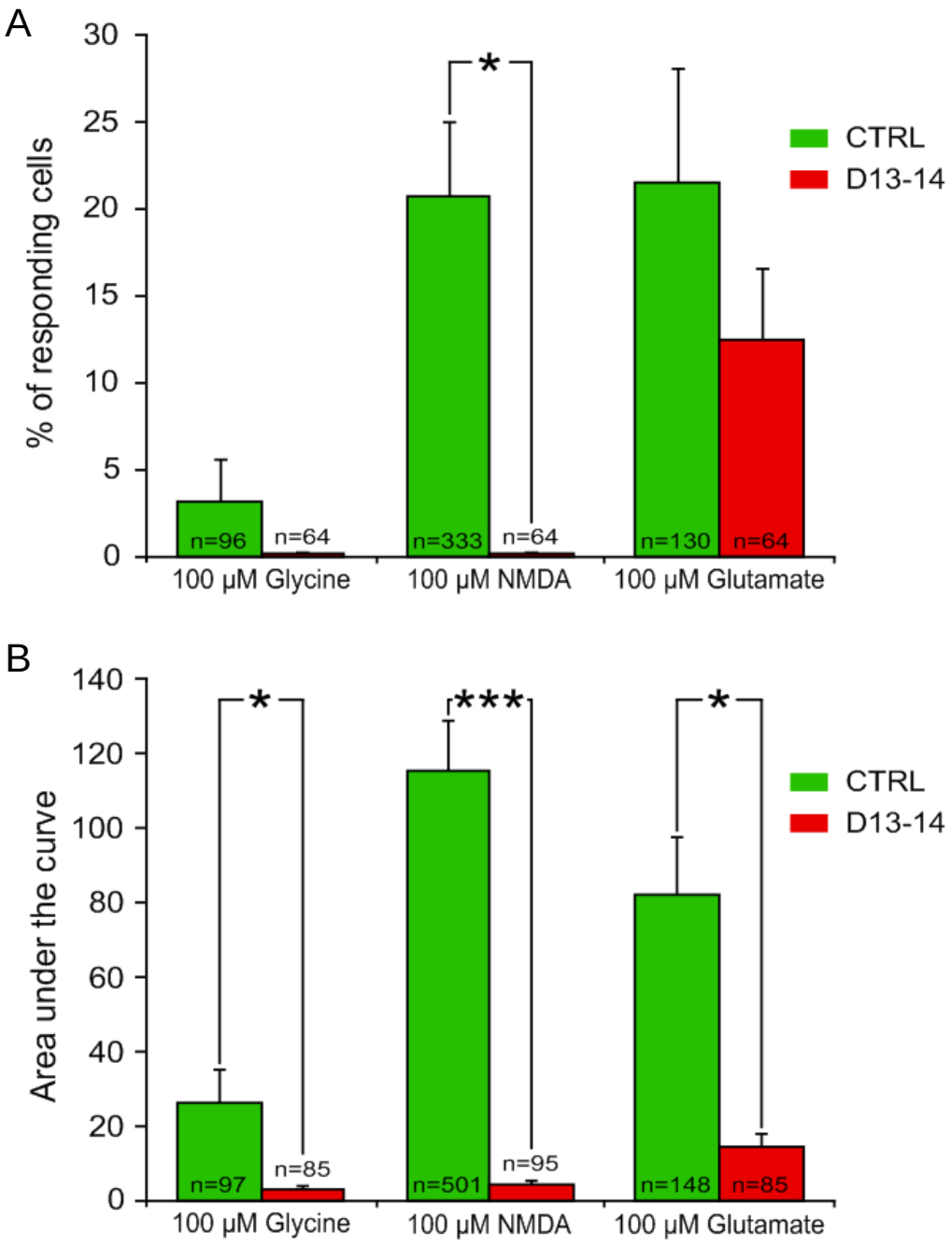


Figure 35. Calcium imaging measurements of cortical GFAP/EGFP$^+$ glial cells from GFAP/EGFP mice *in situ* – impact of middle cerebral artery occlusion (MCAO). (**A**) A comparison of the percentage of responding cells to the application of 100 µM glycine, 100 µM NMDA and 100 µM glutamate in cells from uninjured control mice (CTRL) and in cells from mice 13-14 days after MCAO (D13-14). (**B**) A comparison of the area under the curve after the application of 100 µM glycine, 100 µM NMDA and 100 µM glutamate in CTRL and D13-14. Error bars represent S.E.M. Significant differences (* - $p < 0.05$, ** - $p < 0.01$ and *** - $p < 0.001$) were calculated by an unpaired t-test; n indicates the number of cells.

4.3.2 Calcium imaging measurements in cell cultures (*in vitro*)

It is well known that recordings *in situ* are affected by interactions between cells, particularly by neuron-glia interactions. To address this issue, we characterized the NMDA responses in individual GFAP/EGFP^{+} glial cells isolated from the somatosensory cortices of controls or D13-14 mice and cultured for 5-6 days. The NMDA receptor co-agonist glycine was routinely added to the application of NMDA at 100 µM concentration in *in vitro* measurements since there was no endogenous source of glycine, but its addition did not cause any significant differences probably due to the fact that its low concentration was already present in the solutions as contamination. The kinetics of the Ca^{2+} responses in the cultured cells was different from those recorded *in situ*. In 77% of cells, the responses occurred within 12 s following the co-application of 500 µM NMDA and 100 µM glycine (95% within 24 s), and fast transient Ca^{2+} spikes were not observed (**Fig. 36**).

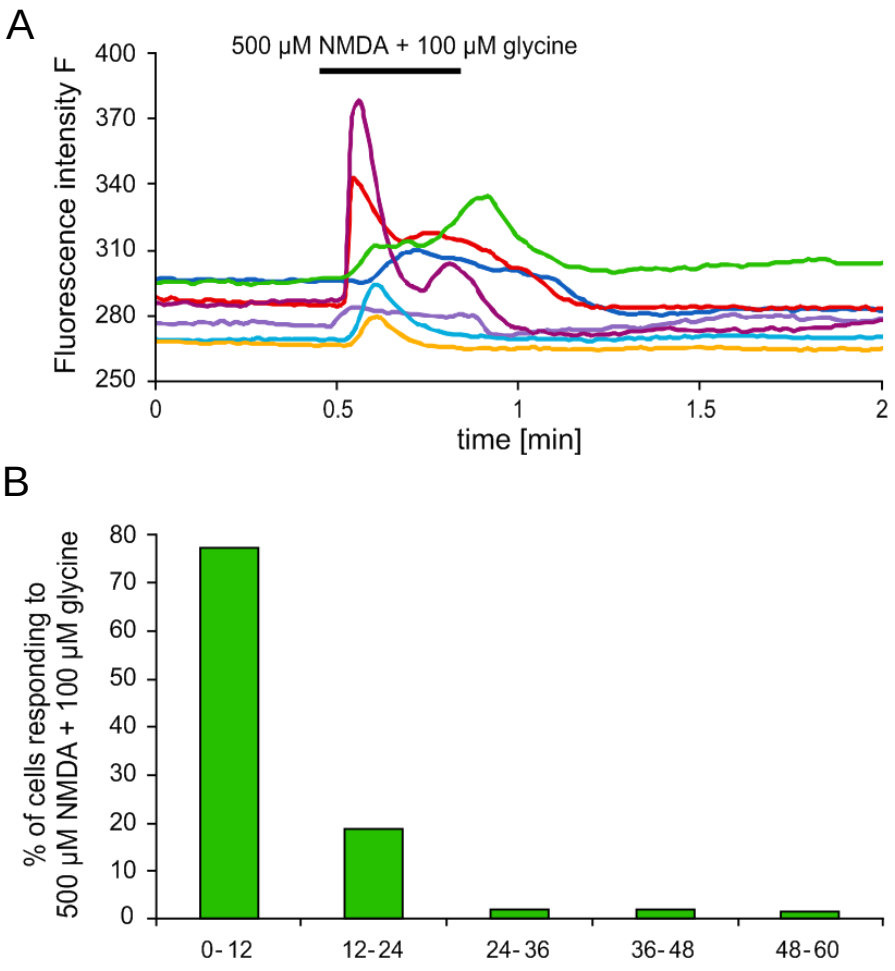


Figure 36. Calcium imaging measurements of cortical GFAP/EGFP^{+} glial cells from GFAP/EGFP mice *in vitro* – description of Ca^{2+} responses. (**A**) Example traces showing kinetics of the responses to the co-application of 500 µM NMDA and 100 µM glycine. (**B**) Quantification of the

delay of the response onset shows that 77% of cells responded within 12 s from the onset of application (n = 65).

In cells isolated from controls, 13.6% responded to the application of 100 µM NMDA, which increased to 36.4% when 500 µM NMDA was applied. The co-application of 100 µM glycine did not result in a higher response rate; however, 100 µM glycine alone evoked Ca^{2+} responses in 4.5% of GFAP/EGFP^{+} glial cells (**Fig. 37A**). To confirm the specificity of the NMDA responses, we used 100 µM DL-APV, which markedly decreased or completely blocked the Ca^{2+} responses evoked by co-application of 500 µM NMDA and 100 µM glycine in all tested cells (**Fig. 37B**).

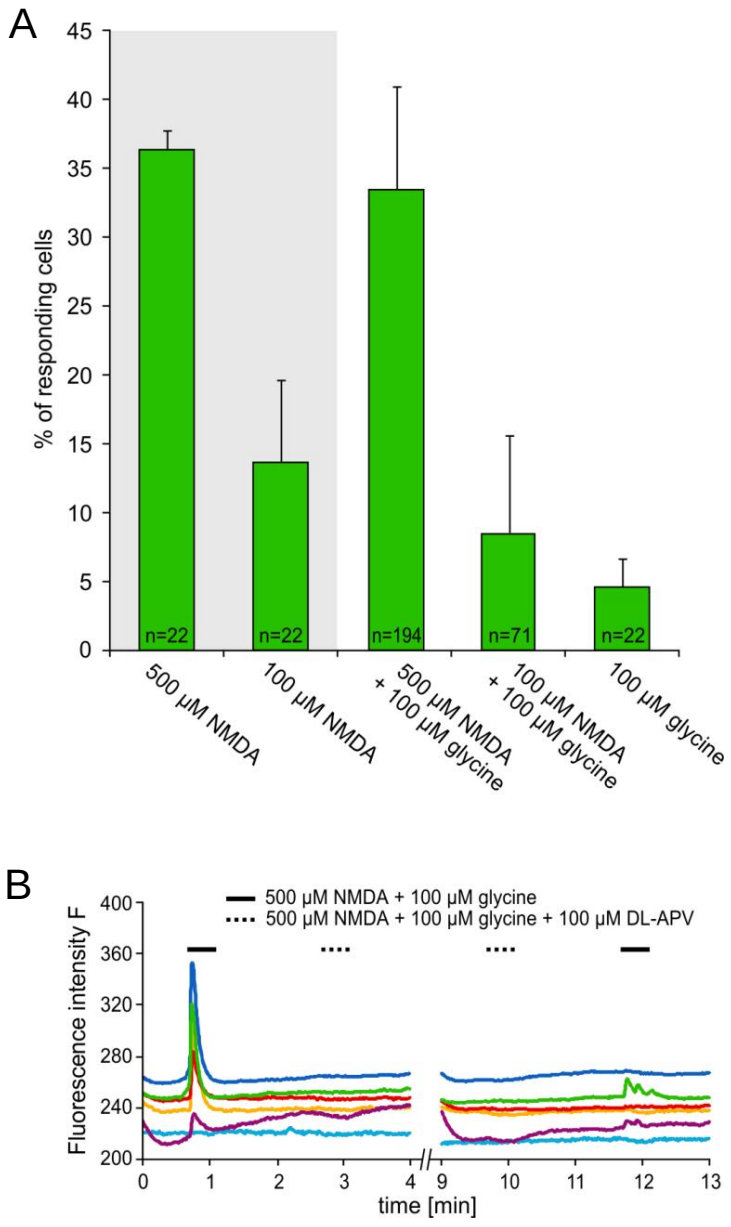


Figure 37. Calcium imaging measurements of cortical GFAP/EGFP^{+} glial cells from GFAP/EGFP mice *in vitro*. (**A**) Incidences of control cells responding to the application of the

NMDA receptor agonists NMDA and glycine in different concentrations and combinations. (**B**) The selective NMDA receptor blocker DL-APV blocked the Ca^{2+} elevations evoked by the co-application of 500 µM NMDA and 100 µM glycine (n = 33).

The ischemic insult had a significant impact on NMDA-evoked responses as only 8.4% of cells isolated from the injured cortical tissue of D13-14 mice responded to the co-application of 500 µM NMDA and 100 µM glycine compared to 33.5% of cells isolated from controls (**Fig. 38A**). This difference was also apparent from the analysis of the area under the curve (**Fig. 38B**). The diminished intracellular Ca^{2+} elevations after NMDA application observed *in situ* in post-ischemic GFAP/$EGFP^{+}$ glial cells were thus preserved even after 5-6 days of *in vitro* cultivation. Since *in vitro* Ca^{2+} imaging enabled the measurement of Ca^{2+} responses from single cells at much better resolution than *in situ*, we observed in large ramified cells that the responses to the application of 500 µM NMDA with 100 µM glycine did not occur uniformly in all of the processes, but were present in only some of the processes (**Fig. 39**).

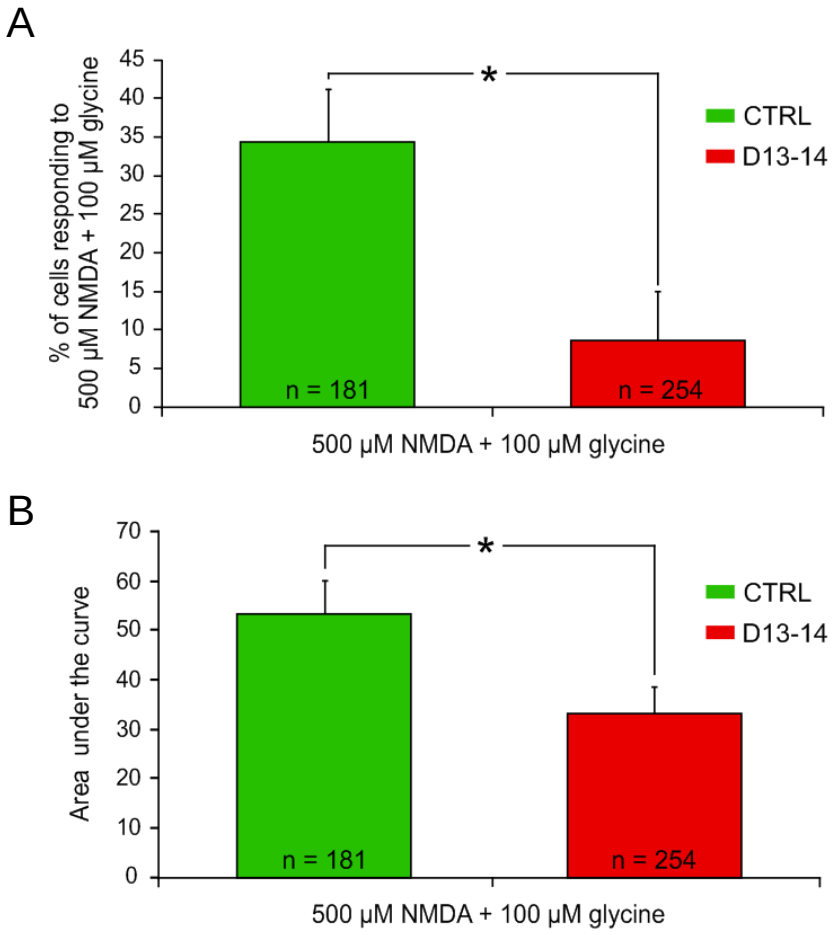


Figure 38. Calcium imaging measurements of cortical GFAP/$EGFP^{+}$ glial cells from GFAP/EGFP mice *in vitro* - impact of middle cerebral artery occlusion (MCAO). (**A**) A comparison of the percentage of responding cells to the co-application of 500 µM NMDA and 100

μM glycine in cells isolated from uninjured mice (CTRL) and in cells from mice 13-14 days after MCAO (D13-14). (**B**) A comparison of the area under the curve measured after co-application of 500 μM NMDA and 100 μM glycine in CTRL and D13-14. Error bars represent S.E.M. Significant differences (* - $p < 0.05$) were calculated by an unpaired t-test; n indicates the number of cells.

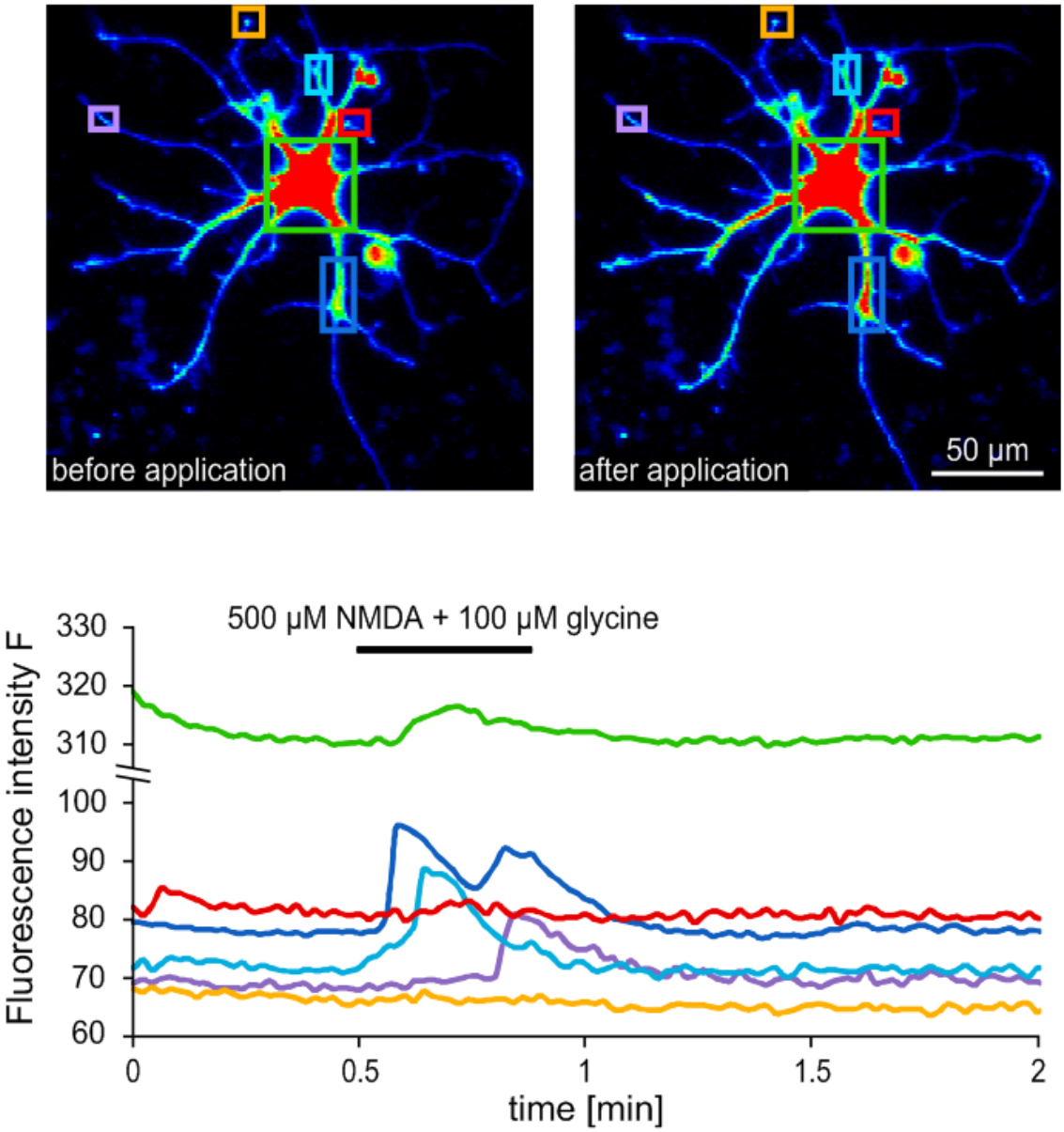


Figure 39. Calcium imaging measurements of cortical GFAP/EGFP$^+$ glial cells from GFAP/EGFP mice *in vitro* – Ca^{2+} responses are specific to cell processes. Imaging of the Ca^{2+} elevation induced by the co-application of 500 μM NMDA and 100 μM glycine with a focus on the cell processes. Traces in different colors (bottom) correspond to the imaged regions in the image of the GFAP/EGFP$^+$ glial cell (top). Note that Ca^{2+} elevations were not detected in all of the processes.

5. DISCUSSION:

In the present work we have analyzed the expression of glutamate receptors in glial cells isolated from cortices of GFAP/EGFP mice. This analysis was performed during development, ageing and after MCAO. We have shown that astrocytes undergo marked changes in the expression of genes coding glutamate receptors during their development and following ischemia. Our immunohistochemical analysis confirmed the presence of NMDA receptor subunits in GFAP/EGFP^{+} glial cells, and Ca^{2+} imaging measurements confirmed that changes in the expression of NMDA receptor subunits are also reflected in the functional properties of glial NMDA receptors.

5.1 Analysis of gene expression

5.1.1 Relationship between RT-qPCR data obtained from single cells and bulk samples

Gene expression experiments are in neuroscience traditionally performed using brain tissue samples which contain heterogenous cell types. In such approach, all cells present in the tissue are analyzed and it does not allow analysis of one particular group of cells. Fluorescent labeling of cells, such as in the GFAP/EGFP mice, enabled to purify the analyzed samples to contain only cells expressing EGFP. The samples can be analyzed as bulks containing thousands of cells; however, such results provide only information about an average gene expression in all cells (Wills et al. 2013). Therefore, a relatively new technique for gene expression profiling, single cell RT-qPCR, has been introduced (Bengtsson et al. 2005). The advantages of single cell RT-qPCR experiments have been several times proven - they enable to identify and characterize rare cells, explore population heterogeneity and find true correlations between the expression of transcripts in cells (Ståhlberg et al. 2011; Ståhlberg et al. 2013b; Ståhlberg and Kubista 2014).

Since single cell RT-qPCR studies are still very challenging type of measurement (Ståhlberg et al. 2013a), there might be concerns about the informative value of the obtained results, especially when experiments are not performed under strict requirements for high quality data. To eliminate these concerns, we analyzed gene expression in astrocytes during ageing, in which we analyzed and compared gene expression in single cells and bulk samples.

We showed that the single cell data are in a very good agreement with those obtained from bulk samples (**Fig. 16-17**), which confirmed validity of our results.

5.1.2 Identification of GFAP/EGFP$^+$ glial cells

GFAP/EGFP$^+$ glial cells are today routinely used for studying astrocytes by several research groups (Hinton et al. 2014; Höft et al. 2014; Kamphuis et al. 2015; Vanzulli and Butt 2015). Nonetheless, these cells express also markers of other cell types, especially of NG2 glial cells (*Cspg4* and *Pdgfra*). The single cell RT-qPCR method enabled us to quantify the amount of GFAP/EGFP$^+$ glial cells which express markers of NG2 glia. Our results show, that especially during early development is proportion of NG2 glia in GFAP/EGFP$^+$ glial cells relatively high – 87%, 33% and 23% in cells isolated from P10, P20 and P30 mice, respectively (**Fig. 18**). In P50-300 mice is the amount of cortical GFAP/EGFP$^+$ glial cells which express also NG2 glial markers below 7% and this ratio slightly increases to 15% in the oldest analyzed P600 mice. The induction of MCAO in P50 mice resulted in the increased expression of NG2 glial markers in GFAP/EGFP$^+$ glial cells (48%, 33% and 24% in cells isolated from D3, D7 and D14 mice, respectively, **Fig. 19**). These gene expression results were further supported by the immunohistochemical analysis (**Fig. 21**), which proved that the expression of genes coding NG2 glial markers was also translated into proteins. The observation that GFAP/EGFP$^+$ glial cells comprise two distinct types of cells in young, P6-20, mice was published already in 2003 by Mathias and colleagues (Matthias et al. 2003). In this work, they were able to roughly distinguish these two types of cells by their morphology, current profile measured by patch-clamp and intensity of their EGFP fluorescence. Therefore, in our experiments we analyzed intensity of EGFP in FACS-sorted GFAP/EGFP$^+$ glial cells; however, we did not observe any correlation between the EGFP intensity and the expression of NG2 glial markers (**Fig. 20**), which might be due to the cell isolation procedure.

The results thus indicate, that GFAP/EGFP$^+$ glial cells isolated from cortices of young mice (P10-20) or mice 3-7 days after MCAO (D3-7) are not suitable for studying of astrocytes since at least one third of these cells express NG2 glial markers. However, a more detailed analysis of this issue shows that the problem is much more complicated. First of all, the above mentioned GFAP/EGFP$^+$ glial cells express also markers of astrocytes (*Slc1a3, Glul*, *Gfap* or *Aqp4*), so simple removal of these cells from analyses would not be correct either. The main point for the discussion is therefore the definition of particular glial cell types, such as astrocytes or NG2 glia, which is currently missing. There exist markers of

these glial cell types, but unfortunately, there is no agreement in how to deal with cells, which express markers of more than one cell type. This problem is not present only in GFAP/EGFP mice, but occurs also in other mouse strains used for studying astrocytes, in Slc1a3/Tomato mice (unpublished data) or Cx43kiECFP mice, in which overlaps with microglia are reported (Theodoric et al. 2012). Zhang and colleagues performed an extensive study in which they measured RNA-Seq transcriptome of glial cell types, neurons, and vascular cells of the cerebral cortex (Zhang et al. 2014). From their study it is evident that even the currently most specific astrocytic markers, such as *Aldh1l1, Slc1a2, Slc1a3* or *Aqp4* are to some extend expressed also in cell types other than astrocytes. Interestingly, the gene they identified to be the most specific to astrocytes, is *Hgf* gene, coding hepatocyte growth factor, which has not been identified as an astrocytic marker, so far.

The categorization of glial cell types is necessary for better orientation in the research of glial cells. Nonetheless, the effort to make strict boundaries between the glial cell types is fully artificial from the biological point of view, especially in the early developing brain and in brain after injury. Nonetheless, we believe that complicated situation in glial cell markers could be, on the other hand, utilized in better exploration and understanding of the processes occurring during brain development or brain injury.

5.1.3 Expression of glutamate receptors in GFAP/EGFP$^+$ glial cells

The single cell RT-qPCR experiments provided us with information about the expression levels of genes coding glutamate receptors in single GFAP/EGFP$^+$ glial cells. Under physiological conditions, we analyzed GFAP/EGFP$^+$ glial cells isolated from P10-600 mice and we can conclude that the highest expression of genes coding glutamate receptors was observed in cells isolated from P10-20 mice (**Fig. 24**). The only exceptions were *Grin2c* and G*rm3* genes, which did not follow such tendency. Our results thus indicate that glutamate receptors are highly expressed in immature astrocytes isolated from P10-20 GFAP/EGFP$^+$ mice, which often express also markers of NG2 glia (**Fig. 18**). The glutamate receptors are according to the study of Zhang and colleagues expressed more in NG2 glia, when compared to astrocytes, as shown in **Fig. 40** (Zhang et al. 2014). Furthermore, according to our data, *Gria2, Grik5, Grin2c* and *Grm3* genes exhibit the highest expression among genes coding glutamate receptors in adult cortical GFAP/EGFP$^+$ glial cells (**Fig. 24**). Interestingly, these are the genes, which were shown to have higher or equal expression level in astrocytes when

compared to NG2 glia according to the above mentioned study (**Fig. 40**). We could thus speculate that *Gria2*, *Grin2c* and *Grm3* genes might have a role specific to astrocytes.

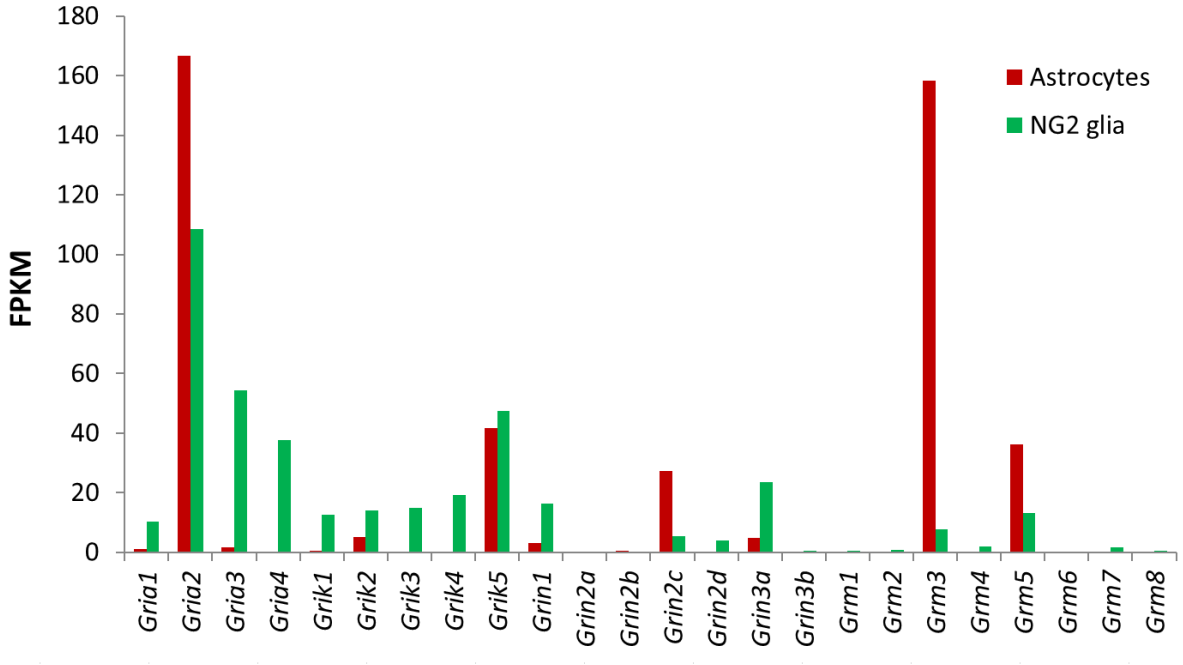


Figure 40. Comparison of expression of genes coding glutamate receptors in astrocytes (isolated from P7 mice) and NG2 glia (isolated from P17 mice), as published by Zhang and colleagues (Zhang et al. 2014). The presented data were selected from the supplementary data provided on http://web.stanford.edu/group/barres_lab/barreslab_rnaseq.xlsx.

Most of the genes coding subunits of glutamate receptors increased their expression after MCAO (**Fig. 25**). The largest increase of gene expression was observed in *Grm5* gene. This is an interesting result since the mGluR5 receptor, coded by the *Grm5* gene, is crucial in modulating neuronal activity and in the functioning of tripartite synapses. Our result is in accordance with a recent study showing that the expression of *Grm5* in astrocytes was undetectable after postnatal week 3, in contrast to *Grm3* which was expressed at all developmental stages (Sun et al. 2013). Our data show that the number of GFAP/EGFP^{+} glial cells expressing the *Grm1* and *Grm3* genes did not significantly change after MCAO; however, *Grm5* became detectable in the majority of these cells, which indicates the importance of this receptor in post-ischemic glia. Since the activation of mGluR5 receptors was shown to result in glutamate, ATP and/or D-serine release from glial cells, they might modulate neuronal activity in the post-ischemic brain (Haydon and Carmignoto 2006). However, mGluR5 receptors were also shown to modulate the expression and function of

glutamate transporters in glia and thus participate in regulating extracellular glutamate concentration (Aronica et al. 2003; Vermeiren et al. 2005; D'Antoni et al. 2008). Another interesting result was regarding the *Gria2* gene, which was present in 61% of cells isolated from controls, a result that did not significantly change after MCAO. This subunit is crucial for Ca^{2+} permeability of AMPA receptors as its presence markedly diminishes their Ca^{2+} permeability (Hollmann et al. 1991; Burnashev et al. 1992). As for the NMDA receptors, the presence of genes coding NMDA receptor subunits was increased in cells after MCAO when compared to controls. The role of NMDA receptors in glial cells is still not fully elucidated, and our data might contribute to unraveling their function, which is presumably also involved in CNS pathologies, such as ischemia or tumors (Aronica et al. 2001). One of their possible roles could be the activation of survival signaling pathways (Hetman and Kharebava 2006) or, as recently shown, astrocytic NMDA receptors can control the exocytosis of gliotransmitters and thus control synaptic transmission and plasticity (Lalo et al. 2014). It is also worth noting that in our study, there were 568 cells that expressed at least one gene coding NMDA receptor subunit; however, 399 of them (70%) did not express the *Grin1* gene encoding the GluN1 subunit, which according to the current knowledge is obligatory in NMDA receptor formation. A similar result was reported by Cahoy and colleagues, who reported presence of *Grin2c* and *Grin3a* but absence of *Grin1* in cortical astrocytes (Cahoy et al. 2008). This might be due to the high protein stability of the GluN1 subunit compared to the GluN2-3 subunits as previously reported (Atlason et al. 2007). Moreover, there are indications that murine NMDA receptors can be also co-assembled without the GluN1 subunit (Perez-Otano et al. 2001; Matsuda et al. 2003), but their functional properties are debatable.

The division of cells isolated from P50, D7 and D14 mice into three subpopulations according to their gene expression showed that cells isolated from D7 and especially from D14 mice have the highest relative expression of most of the genes coding subunits of glutamate receptors (subpopulation SP3), which distinguishes them from cells isolated from P50 controls. However, in subpopulation SP2, formed mainly by cells isolated from D7 and also D14 mice, the relative expression of glutamate receptor subunits was lower, indicating that cells after MCAO are not homogeneous (**Fig. 26**).

5.1.4 Correlation between genes coding glutamate receptors and glial cell markers changes following ischemia

Interesting results were obtained from the Spearman correlation coefficients analysis between expression of genes in cells isolated from P50 controls, D7 and D14 mice (**Fig. 27**). Since we used a GFAP/EGFP$^+$ glial cell population in this study, which among astrocytic markers expressed also NG2 glial markers in some cells, we were able to study the correlations between particular genes coding glutamate receptor subunits with genes coding markers of astrocytes and NG2 glia.

Most of the AMPA receptors are heterotetrameric, consisting of two GluA2 and two GluA1, GluA3 or GluA4 subunits. Since *Gria2* correlated positively with both astrocytic and NG2 glial markers, our results suggest the presence of AMPA receptors is not cell-type specific. An interesting finding was obtained in cells isolated from D14 mice in which *Gria3* positively correlated with astrocytic markers, indicating the presence of AMPA receptors of GluA2/GluA3 type in these cells, and *Gria4* correlated with NG2 glial markers, indicating AMPA receptors of GluA2/GluA4 type in these cells.

Several studies have shown that astrocytes possess kainate receptors (Seifert and Steinhäuser 2001; Brand-Schieber et al. 2004), which we also showed in the present work. Moreover, our results suggest that genes coding kainate receptor subunits correlated mostly with those GFAP/EGFP$^+$ cells that expressed NG2 glial markers, which would also confirm the results of the study demonstrating functional kainate receptors in NG2 glia (Kukley and Dietrich 2009; Haberlandt et al. 2011). In cells isolated from D7 mice we observed a strong positive correlation with astrocytic markers, but in cells isolated from D14 mice, most of the genes coding kainate receptor subunits again positively correlated with NG2 glial markers.

An interesting correlation pattern was observed with genes coding NMDA receptor subunits. In cells isolated from P50 controls, these genes positively correlated mostly with NG2 glial markers; only *Grin1* and *Grin2c* were also partially correlated with astrocytic markers. In cells isolated from D7 mice was the number of NMDA subunits correlating with NG2 glial markers reduced, and their correlation with astrocytic markers was increased. The most intriguing correlation pattern was found in cells isolated from D14 mice, where cells expressing NG2 glial markers were positively correlated with *Grin1* and *Grin3a* and, moreover, negatively correlated with *Grin2a-d*. This strongly indicates that 14 days after

MCAO, the composition of NMDA receptors in the NG2 glial markers expressing GFAP/EGFP$^+$ cells is of the GluN1/GluN3A type. On the other hand, *Grin2a-d* genes were positively correlated with astrocytic markers.

As for the metabotropic glutamate receptors, cells isolated from P50 controls, which expressed astrocytic markers seemed to possess mGluR3 receptors but not mGluR1, whereas genes coding both of these receptors also partially correlated with NG2 glial markers. This situation changed completely in cells isolated from D14 mice, in which genes coding metabotropic glutamate receptors correlated positively with astrocytic and negatively with NG2 glial markers.

5.2 Immunohistochemical analysis revealed presence of NMDA receptor subunits in GFAP/EGFP$^+$ glial cells

To study glutamate receptors also on the protein level, we performed an immunohistochemical analysis of the entire set of the 7 currently known NMDA receptor subunits of GFAP/EGFP$^+$ glial cells in the adult mouse cortex. To the best of our knowledge, our analysis provides the first immunohistochemical evidence that GFAP/EGFP$^+$ glial cells in the cortex possess GluN3A subunits, which has been previously discussed in many works (Verkhratsky and Kirchhoff 2007b; Palygin et al. 2011; Kehoe et al. 2013). Under control conditions, we did not observe GFAP/EGFP$^+$ cells positive for any NMDA receptor subunit, apart from GluN3A. This might be due to the fact that under control conditions, astrocytes have a bushy-like morphology with many fine processes. It was previously shown by electron microscopy that the GluN1 and GluN2A/B NMDA receptor subunits are present in astrocytes especially in the processes and not in the cellular bodies (Conti et al. 1996). The fluorescent immunohistochemical method is not able to distinguish NMDA receptor subunit positivity in fine processes from the background signal. On the other hand, reactive astrocytes present in the cortices of GFAP/EGFP mice 14 days after MCAO have a fibrous morphology with sharp edges separating them from the surrounding tissue, which enables the detection of positive staining for NMDA receptor subunits in these cells. Our immunohistochemical analysis clearly showed the positivity of cortical GFAP/EGFP$^+$ cells for the GluN1, GluN2B-D and GluN3A subunits 14 days after MCAO, which indicates the importance of NMDA receptors in glial cells under ischemic conditions. The GluN2A subunit was detected in cells that morphologically resembled neurons, but not in GFAP/EGFP$^+$ cells. Since the single cell RT-qPCR results indicate that GFAP/EGFP$^+$ cells should contain this subunit, we hypothesize

that it was not detected due to some post-translational modifications of the GluN2A protein or miRNA regulation, which might be specific to glia. In summary, the immunohistochemical analysis confirmed the presence of NMDA receptor subunits in GFAP/EGFP$^+$ glial cells, especially after ischemia.

5.3 Functional NMDA receptors in GFAP/EGFP$^+$ glial cells

The NMDA receptors in GFAP/EGFP$^+$ glial cells were also subjected to a functional study utilizing Ca^{2+} imaging technique. Calcium responses to the application of 100 µM NMDA were delayed *in situ* by ~30 s on average, as also reported in other studies (Porter and McCarthy 1995; Serrano et al. 2006; Serrano et al. 2008). We attribute this delay to the slow diffusion of NMDA in the brain tissue, which is supported by the fact that there were immediate responses in cultivated cells. Moreover, experiments with freshly isolated cells exhibited also immediate NMDA-evoked calcium responses (Palygin et al. 2010; Palygin et al. 2011). There have been several studies showing a TTX-mediated partial reduction of NMDA-evoked responses (Schipke et al. 2001; Serrano et al. 2006; Serrano et al. 2008). Similar to a study of oligodendrocytic NMDA receptors (Káradóttir et al. 2005), we did not observe any significant changes associated with the use of TTX, which might also be due to the fact that our application was relatively short and locally focused, in contrast to the above-mentioned studies showing a TTX-mediated effect (bath application for several minutes).

As for the subunit composition of NMDA receptors, our results suggest a tri-heteromeric composition of the GluN1/GluN2C/GluN3A type. This is supported by the weak Mg^{2+} block observed for NMDA receptors containing the GluN3A subunit (Sasaki et al. 2002; Kehoe et al. 2013), as we observed Ca^{2+} elevations in aCSF that contained Mg^{2+} without the need for cell depolarization. Based on our single cell RT-qPCR (**Fig. 25**) and immunohistochemical analyses (**Fig. 31**) showing low mRNA levels of *Grin3b* and the absence of GluN3B immunoreactivity, we do not assume the inclusion of the GluN3B subunit in the NMDA receptors. Di-heteromeric GluN1/GluN3A receptors have, however, no binding site for glutamate or NMDA, so the inclusion of the GluN2 subunit is also needed. Our data with memantine, which inhibits preferentially GluN2C and GluN2D-containing NMDA receptors (Kotermanski and Johnson 2009), suggest the incorporation of one of these subunits as well. Based on our single cell RT-qPCR data, which show much higher expression of *Grin2c* in comparison to *Grin2d* in cells from P50 controls (**Fig. 25**), we suppose that at least in these cells, the NMDA receptors contain mainly the GluN2C subunit. Nonetheless, we cannot

exclude the possibility that GFAP/EGFP$^+$ glial cells also possess GluN1/GluN2 NMDA receptors. We hypothesize that these could provide an amplification of the Ca^{2+} signal upon local depolarization, which would release the Mg^{2+} block. The application of NBQX and PPADS did not support the hypothesis that this local depolarization would be provided via AMPA, Kainate or P2X receptors.

Both *in situ* and *in vitro* experiments showed that the application of NMDA evoked significantly lower Ca^{2+} elevations in GFAP/EGFP$^+$ glial cells 13-14 days after MCAO when compared to cells in controls, which we hypothesize is due to the increased involvement of the GluN3A subunit as shown by our single cell RT-qPCR and immunohistochemical analyses. The decreased Ca^{2+} permeability of NMDA receptors can be further caused by the incorporation of the GluN2D subunit in NMDA receptors (Burnashev et al. 1995; Paoletti 2011; Evans et al. 2012), which was also highly upregulated 14 days after MCAO. Another reason for decreased Ca^{2+} permeability of NMDA receptors might be their internalization, which was shown to be regulated by the particular subunit compositions (Lavezzari et al. 2004), and for example GluN3A internalization is regulated via phosphorylation of a tyrosine residue (Y971) within the GluN3A intracellular C-terminal tail (Chowdhury et al. 2013). Therefore, we cannot completely rule out the possibility that NMDA receptors in GFAP/EGFP$^+$ glial cells are internalized or inactivated by the Ca^{2+}-calmodulin complex after MCAO (Ehlers et al. 1996). An alternative explanation of these results could be an indirect influence of neurons which promote NMDA-evoked Ca^{2+} signals in GFAP/EGFP$^+$ glial cells and which are missing in the penumbra region after MCAO. However, this explanation is in our opinion unlikely since it does not correspond with our *in vitro* results and with the results of Palygin and colleagues who demonstrated NMDA-evoked Ca^{2+} elevations in freshly isolated astrocytes (Palygin et al. 2010; Palygin et al. 2011).

Interestingly, the Ca^{2+} permeability of astrocytic NMDA receptors after ischemia is region-specific, since, as shown by Krebs and colleagues, acutely isolated hippocampal astrocytes displayed NMDA-evoked Ca^{2+} elevations 20 days after global cerebral ischemia (Krebs et al. 2003). The number of cells responding to the application of 100 µM glutamate *in situ* was also decreased after MCAO, but some Ca^{2+} influx was still detected, which is probably due to the presence of Ca^{2+}-permeable non-NMDA glutamate receptors. These could be ionotropic AMPA or kainate glutamate receptors (Burnashev et al. 1992), but also metabotropic mGluR5 glutamate receptors (coded by the *Grm5* gene), which became strongly

expressed in cells from D14 mice and which mediate intracellular Ca^{2+} elevations by releasing Ca^{2+} from intracellular stores (Nakahara et al. 1997).

In vitro cultivated GFAP/EGFP^{+} glial cells isolated from young adult mice enabled us to study NMDA-evoked responses in detail. Calcium imaging measurements revealed that the responses were process-specific, which corresponds with recent studies showing microdomains within astrocytic territories (Shigetomi et al. 2013). Moreover, this suggests that the response rates in our *in situ* experiments might be slightly underestimated since we recorded signal only from the cellular bodies and not from the processes, where the responses probably originate (Schipke et al. 2001). The results obtained by Ca^{2+} imaging measurements thus supplement the data from single cell RT-qPCR and immunohistochemical analyses and underline the changes of NMDA receptors in post-ischemic GFAP/EGFP^{+} glial cells.

In summary, our study provides an overall picture of ionotropic and metabotropic glutamate receptor expression in cortical GFAP/EGFP^{+} glial cells. We show how the expression of particular subunits of these receptors changes after focal cerebral ischemia. On the functional level, we further show that NMDA-mediated Ca^{2+} elevations significantly decrease after ischemia in GFAP/EGFP^{+} glial cells, which is presumably due to the involvement of the GluN3A subunit. We believe that our study thus adds a new piece of the puzzle to the picture, from which we will eventually understand all of the complex processes, including neuron-glia interaction or glutamate-mediated signaling in glial cells and which might serve as a guide for research into precisely targeted therapeutics.

6. CONCLUSIONS:

1) To reveal the changes in the expression of mRNA coding AMPA, kainate, NMDA and metabotropic glutamate receptors in cortical astrocytes during development, ageing and following MCAO model of focal cerebral ischemia employing single cell RT-qPCR.

To complete the first aim of this study, we employed single cell RT-qPCR method, which allowed us to create an overall picture of gene expression profile of glutamate receptors in GFAP/EGFP$^+$ glial cells under physiological and pathophysiological conditions. According to our results, the expression of most of the genes coding glutamate receptors is highest in juvenile mice and decreases with age. The highest gene expression was observed in *Gria2, Grik5, Grin2c* and *Grm3* genes. Our results further confirmed increased expression of most of the genes coding glutamate receptors 7-14 days after MCAO when compared to controls.

2) To identify NMDA receptor subunits in cortical astrocytes under physiological conditions and following MCAO, utilizing immunohistochemistry.

Utilizing immunohistochemical analyses for all 7 currently known NMDA receptor subunits, we were unable to detect cortical GFAP/EGFP$^+$ glial cells positive for any NMDA receptor subunits under control conditions, apart from the GluN3A subunit. In reactive astrocytes present in the cortices of GFAP/EGFP mice 14 days after MCAO, our results clearly confirmed the positivity of cortical GFAP/EGFP$^+$ glial cells for the GluN1, GluN2B-D and GluN3A subunits staining.

3) To investigate functional properties of astrocytic NMDA receptors in cortical tissue slices and to identify possible changes in their function following MCAO using Ca^{2+} imaging *in situ*.

For the study of the functional properties of NMDA receptors in cortical astrocytes we used *in situ* Ca^{2+} imaging measurements on GFAP/EGFP$^+$ glial cells. Under control conditions, we observed that application of NMDA evoked Ca^{2+} elevations in ~1/5 of the analyzed cells. These responses were delayed in average by ~30 s, NMDA-concentration dependent and blocked by NMDA receptor antagonists. The application of NMDA did not evoke any Ca^{2+} elevations in GFAP/EGFP$^+$ glial cells after MCAO, which we hypothesize is due to the increased involvement of GluN3A subunit in NMDA receptors leading to Ca^{2+} impermeability.

4) To verify results obtained from *in situ* functional study (Ca^{2+} imaging) by *in vitro* experiments without possible influence of other cellular elements.

The Ca^{2+} imaging measurements performed in cultivated GFAP/$EGFP^{+}$ glial cells confirmed *in situ* results, since cells cultivated from mice after MCAO displayed significantly diminished Ca^{2+} responses after co-application of NMDA with glycine when compared to cells isolated from controls. Moreover, *in vitro* experiments enabled to visualize Ca^{2+} responses in better detail, which revealed process-specific Ca^{2+} elevations corresponding with recent studies demonstrating microdomains within astrocytic territories.

7. REFERENCES:

Abbracchio MP, Ceruti S (2006) Roles of P2 receptors in glial cells: Focus on astrocytes. Purinergic Signal 2:595–604.

Adermark L, Lovinger DM (2008) Electrophysiological properties and gap junction coupling of striatal astrocytes. Neurochem Int 52:1365–1372.

Akazawa C, Shigemoto R, Bessho Y, et al (1994) Differential expression of five N-methyl-D-aspartate receptor subunit mRNAs in the cerebellum of developing and adult rats. J Comp Neurol 347:150–60.

Anderova M, Antonova T, Petrík D, et al (2004) Voltage-dependent potassium currents in hypertrophied rat astrocytes after a cortical stab wound. Glia 48:311–26.

Aoki C, Venkatesan C, Go CG, et al (1994) Cellular and subcellular localization of NMDA-R1 subunit immunoreactivity in the visual cortex of adult and neonatal rats. J Neurosci 14:5202–22.

Araque A, Parpura V, Sanzgiri RP, Haydon PG (1999) Tripartite synapses: Glia, the unacknowledged partner. Trends Neurosci 22:208–215.

Aronica E, Gorter J a., Ijlst-Keizers H, et al (2003) Expression and functional role of mGluR3 and mGluR5 in human astrocytes and glioma cells: opposite regulation of glutamate transporter proteins. Eur J Neurosci 17:2106–2118.

Aronica E, Leenstra S, Jansen GH, et al (2001) Expression of brain-derived neurotrophic factor and tyrosine kinase B receptor proteins in glioneuronal tumors from patients with intractable epilepsy: colocalization.

Aronica E, van Vliet E a, Mayboroda O a, et al (2000) Upregulation of metabotropic glutamate receptor subtype mGluR3 and mGluR5 in reactive astrocytes in a rat model of mesial temporal lobe epilepsy. Eur J Neurosci 12:2333–44.

Atlason PT, Garside ML, Meddows E, et al (2007) N-Methyl-D-aspartate (NMDA) receptor subunit NR1 forms the substrate for oligomeric assembly of the NMDA receptor. J Biol Chem 282:25299–307.

Backus K, Kettenmann H, Schachner M (1989) Pharmacological characterization of the glutamate receptor in cultured astrocytes.

Baraldo F (2002) NMDA Receptors. http://flipper.diff.org/app/pathways/info/3778.

Benesova J, Hock M, Butenko O, et al (2009) Quantification of astrocyte volume changes during ischemia in situ reveals two populations of astrocytes in the cortex of GFAP/EGFP mice. J Neurosci Res 87:96–111.

Benesova J, Rusnakova V, Honsa P, et al (2012) Distinct expression/function of potassium and chloride channels contributes to the diverse volume regulation in cortical astrocytes of GFAP/EGFP mice. PLoS One 7:e29725.

Bengtsson M, Ståhlberg A, Rorsman P, Kubista M (2005) Gene expression profiling in single cells from the pancreatic islets of Langerhans reveals lognormal distribution of mRNA levels. Genome Res 15:1388–92.

Blackshaw LA, Page AJ, Young RL (2011) Metabotropic glutamate receptors as novel therapeutic targets on visceral sensory pathways. Front Neurosci 5:40.

Bockstaele EJ, Colago EE (1996) Selective distribution of the NMDA-R1 glutamate receptor in astrocytes and presynaptic axon terminals in the nucleus locus coeruleus of the rat brain: an immunoelectron microscopic study. J Comp Neurol 369:483–96.

Bordey a, Lyons S a, Hablitz JJ, Sontheimer H (2001) Electrophysiological characteristics of reactive astrocytes in experimental cortical dysplasia. J Neurophysiol 85:1719–1731.

Bowman C, Kimelberg H (1984) Excitatory amino acids directly depolarize rat brain astrocytes in primary culture.

Brand-Schieber E, Lowery SL, Werner P (2004) Select ionotropic glutamate AMPA/kainate receptors are expressed at the astrocyte-vessel interface. Brain Res 1007:178–82.

Bruno V, Battaglia G, Casabona G, et al (1998) Neuroprotection by glial metabotropic glutamate receptors is mediated by transforming growth factor-beta. J Neurosci 18:9594–9600.

Burnashev N, Khodorova a, Jonas P, et al (1992) Calcium-permeable AMPA-kainate receptors in fusiform cerebellar glial cells. Science 256:1566–70.

Burnashev N, Zhou Z, Neher E, Sakmann B (1995) Fractional calcium currents through recombinant GluR channels of the NMDA, AMPA and kainate receptor subtypes. J Physiol 485 (Pt 2:403–18.

Bush TG, Puvanachandra N, Horner CH, et al (1999) Leukocyte infiltration, neuronal degeneration, and neurite outgrowth after ablation of scar-forming, reactive astrocytes in adult transgenic mice. Neuron 23:297–308.

Butenko O, Dzamba D, Benesova J, et al (2012) The increased activity of TRPV4 channel in the astrocytes of the adult rat hippocampus after cerebral hypoxia/ischemia. PLoS One 7:e39959.

Cahoy JD, Emery B, Kaushal A, et al (2008) A transcriptome database for astrocytes, neurons, and oligodendrocytes: a new resource for understanding brain development and function. J Neurosci 28:264–78.

Cavara N a, Hollmann M (2008) Shuffling the deck anew: how NR3 tweaks NMDA receptor function. Mol Neurobiol 38:16–26.

Conti F, Barbaresi P, Melone M, Ducati a (1999) Neuronal and glial localization of NR1 and NR2A/B subunits of the NMDA receptor in the human cerebral cortex. Cereb Cortex 9:110–20.

Conti F, DeBiasi S, Minelli a, Melone M (1996) Expression of NR1 and NR2A/B subunits of the NMDA receptor in cortical astrocytes. Glia 17:254–8.

Conti F, Minelli a, Molnar M, Brecha NC (1994) Cellular localization and laminar distribution of NMDAR1 mRNA in the rat cerebral cortex. J Comp Neurol 343:554–65.

Corti C, Battaglia G, Molinaro G, et al (2007) The use of knock-out mice unravels distinct roles for mGlu2 and mGlu3 metabotropic glutamate receptors in mechanisms of neurodegeneration/neuroprotection. J Neurosci 27:8297–8308.

D'Antoni S, Berretta A, Bonaccorso CM, et al (2008) Metabotropic glutamate receptors in glial cells. Neurochem Res 33:2436–43.

D'Onofrio M, Cuomo L, Battaglia G, et al (2001) Neuroprotection mediated by glial group-II metabotropic glutamate receptors requires the activation of the MAP kinase and the phosphatidylinositol-3-kinase pathways. J Neurochem 78:435–445.

Daikhin Y, Yudkoff M (2000) Compartmentation of brain glutamate metabolism in neurons and glia. J Nutr 130:1026S–31S.

Deitmer JW, Rose CR (1996) pH regulation and proton signalling by glial cells. Prog Neurobiol 48:73–103.

Dirnagl U, Iadecola C, Moskowitz M a (1999) Pathobiology of ischaemic stroke: an integrated view. Trends Neurosci 22:391–7.

Dzamba D, Honsa P, Anderova M (2013) NMDA Receptors in Glial Cells: Pending Questions. Curr Neuropharmacol 11:250–62.

Ehlers MD, Zhang S, Bernhadt JP, Huganir RL (1996) Inactivation of NMDA receptors by direct interaction of calmodulin with the NR1 subunit. Cell 84:745–55.

Eriksson M, Nilsson A, Froelich-Fabre S, et al (2002) Cloning and expression of the human N-methyl-D-aspartate receptor subunit NR3A. Neurosci Lett 321:177–81.

Evans PD, Reale V, Merzon RM, Villegas J (1992) N-methyl-D-aspartate (NMDA) and non-NMDA (metabotropic) type glutamate receptors modulate the membrane potential of the Schwann cell of the squid giant nerve fibre. J Exp Biol 173:229–249.

Evans RC, Morera-Herreras T, Cui Y, et al (2012) The effects of NMDA subunit composition on calcium influx and spike timing-dependent plasticity in striatal medium spiny neurons. PLoS Comput Biol 8:e1002493.

Farb CR, Aoki C, Ledoux JE (1995) Differential localization of NMDA and AMPA receptor subunits in the lateral and basal nuclei of the amygdala: a light and electron microscopic study. J Comp Neurol 362:86–108.

Fiacco T a, McCarthy K (2006) Astrocyte Calcium Elevations: Properties, Propagation, and Effects on Brain Signaling. Glia 54:676–690.

Fraser DD, Mudrick-Donnon L a, MacVicar B a (1994) Astrocytic GABA receptors. Glia 11:83–93.

Gallo V, Ghiani C a (2000) Glutamate receptors in glia: new cells, new inputs and new functions. Trends Pharmacol Sci 21:252–8.

Ganat YM, Silbereis J, Cave C, et al (2006) Early postnatal astroglial cells produce multilineage precursors and neural stem cells in vivo. J Neurosci 26:8609–8621.

Gao HW, He CY, Fang XD, et al (2006) Localization of aquaporin-1 water channel in glial cells of the human peripheral nervous system. Glia 53:783–787.

Giaume C, Koulakoff A, Roux L, et al (2010) Astroglial networks: a step further in neuroglial and gliovascular interactions. Nat Rev Neurosci 11:87–99.

Gordon GR, Mulligan SJ, MacVicar B (2007) Astrocute Control of the Cerebrovasculature. Glia 55:1214–1221.

Gottlieb M, Matute C (1997) Expression of ionotropic glutamate receptor subunits in glial cells of the hippocampal CA1 area following transient forebrain ischemia. J Cereb Blood Flow Metab 17:290–300.

Gracy KN, Pickel VM (1995) Comparative ultrastructural localization of the NMDAR1 glutamate receptor in the rat basolateral amygdala and bed nucleus of the stria terminalis. J Comp Neurol 362:71–85.

Haberlandt C, Derouiche A, Wyczynski A, et al (2011) Gray matter NG2 cells display multiple Ca2+-signaling pathways and highly motile processes. PLoS One 6:e17575.

Hamill OP, Marty A, Neher E, et al (1981) Improved patch clamp techniques for high resolution current recording from cells and cell-free membranes. Pflügers Arch 391:85–100.

Hamilton NB, Attwell D (2010) Do astrocytes really exocytose neurotransmitters? Nat Rev Neurosci 11:227–238.

Haydon P, Carmignoto G (2006) Astrocyte control of synaptic transmission and neurovascular coupling. Physiol Rev 1009–1031.

Hetman M, Kharebava G (2006) Survival signaling pathways activated by NMDA receptors. Curr Top Med Chem 6:787–99.

Hinton DJ, Lee MR, Jang JS, Choi D-S (2014) Type 1 equilibrative nucleoside transporter regulates astrocyte-specific glial fibrillary acidic protein expression in the striatum. Brain Behav 4:903–914.

Höft S, Griemsmann S, Seifert G, Steinhäuser C (2014) Heterogeneity in expression of functional ionotropic glutamate and GABA receptors in astrocytes across brain regions : insights from the thalamus Heterogeneity in expression of functional ionotropic glutamate and GABA receptors in astrocytes across brain.

Hollmann M, Hartley M, Heinemann S (1991) Ca2+ permeability of KA-AMPA--gated glutamate receptor channels depends on subunit composition. Science 252:851–3.

Hollmann M, Heinmann S (1994) Cloned Glutamate Receptors. Annu Rev Neurosci 17:31–108.

Holzwarth J a, Gibbons SJ, Brorson JR, et al (1994) Glutamate receptor agonists stimulate diverse calcium responses in different types of cultured rat cortical glial cells. J Neurosci 14:1879–91.

Honsa P, Pivonkova H, Dzamba D, et al (2012) Polydendrocytes display large lineage plasticity following focal cerebral ischemia. PLoS One 7:e36816.

Honsa P, Pivonkova H, Harantova L, et al (2014) Increased expression of hyperpolarization-activated cyclic nucleotide-gated (HCN) channels in reactive astrocytes following ischemia. Glia.

Houades V, Koulakoff A, Ezan P, et al (2008) Gap junction-mediated astrocytic networks in the mouse barrel cortex. J Neurosci 28:5207–5217.

Chen H-SV, Lipton S a (2006) The chemical biology of clinically tolerated NMDA receptor antagonists. J Neurochem 97:1611–26.

Chen Y, Vartiainen NE, Ying W, et al (2001) Astrocytes protect neurons from nitric oxide toxicity by a glutathione-dependent mechanism. J Neurochem 77:1601–1610.

Chowdhury D, Marco S, Brooks IM, et al (2013) Tyrosine phosphorylation regulates the endocytosis and surface expression of GluN3A-containing NMDA receptors. J Neurosci 33:4151–64.

Ikonomidou C, Turski L (2002) Why did NMDA receptor antagonists fail clinical trials for stroke and traumatic brain injury? Lancet Neurol 1:383–386.

Jensen a M, Chiu SY (1990) Fluorescence measurement of changes in intracellular calcium induced by excitatory amino acids in cultured cortical astrocytes. J Neurosci 10:1165–75.

Jimenez-Blasco D, Santofimia-Castaño P, Gonzalez a, et al (2015) Astrocyte NMDA receptors' activity sustains neuronal survival through a Cdk5–Nrf2 pathway. Cell Death Differ 1–13.

Johnson JW, Ascher P (1987) Glycine potentiates the NMDA response in cultured mouse brain neurons. Nature 325:529–531.

Kalash R (2013) Astrocyte: Structure, Function and Disease. http://advneurobio.blogspot.cz/2013/09/astrocyte-structure-function-and-disease.html.

Kamphuis W, Kooijman L, Orre M, et al (2015) GFAP and vimentin deficiency alters gene expression in astrocytes and microglia in wild-type mice and changes the transcriptional response of reactive glia in mouse model for Alzheimer's disease. Glia n/a–n/a.

Káradóttir R, Cavelier P, Bergersen L, Attwell D (2005) NMDA receptors are expressed in oligodendrocytes and activated in ischaemia. Nature 438:1162–1166.

Kato H, Narita M, Miyatake M, et al (2006) Role of neuronal NR2B subunit-containing NMDA receptor-mediated Ca2+ influx and astrocytic activation in cultured mouse cortical neurons and astrocytes. Synapse 59:10–7.

Kehoe L a, Bernardinelli Y, Muller D (2013) GluN3A: An NMDA Receptor Subunit with Exquisite Properties and Functions. Neural Plast 2013:145387.

Kettenmann H, Backus KH, Schachner M (1984a) Aspartate, glutamate and gamma-aminobutyric acid depolarize cultured astrocytes. Neurosci Lett 52:25–29.

Kettenmann H, Gilbert P, Schachner M (1984b) Depolarization of cultured oligodendrocytes by glutamate and GABA. Neurosci Lett 47:271–276.

Kettenmann H, Schachner M (1985) Pharmacological Properties of γ-Aminobutyric acid-, glutamate-, and aspartate-induced depolarizations in cultured astrocytes.

Kimelberg HK (2007) Supportive or information-processing functions of the mature protoplasmic astrocyte in the mammalian CNS? A critical appraisal. Neuron Glia Biol 3:181–189.

Kofuji P, Newman E (2004) Potassium buffering in the central nervous system. Neuroscience 129:1045–1056.

Köller H, Schroeter M, Jander S, et al (2000) Time course of inwardly rectifying K(+) current reduction in glial cells surrounding ischemic brain lesions. Brain Res 872:194–198.

Kotermanski SE, Johnson JW (2009) Mg2+ imparts NMDA receptor subtype selectivity to the Alzheimer's drug memantine. J Neurosci 29:2774–2779.

Krebs C, Fernandes HB, Sheldon C, et al (2003) Functional NMDA receptor subtype 2B is expressed in astrocytes after ischemia in vivo and anoxia in vitro. J Neurosci 23:3364–72.

Kressin K, Kuprijanova E, Jabs R, et al (1995) Developmental regulation of Na+ and K+

conductances in glial cells of mouse hippocampal brain slices. Glia 15:173–187.

Kuffler SW (1967) Neuroglial cells: physiological properties and a potassium mediated effect of neuronal activity on the glial membrane potential. Proc R Soc Lond B Biol Sci 168:1–21.

Kukley M, Dietrich D (2009) Kainate receptors and signal integration by NG2 glial cells. Neuron Glia Biol 72076.

Labat-gest V, Tomasi S (2013) Photothrombotic ischemia: a minimally invasive and reproducible photochemical cortical lesion model for mouse stroke studies. J Vis Exp 1–6.

Lalo U, Palygin O, North RA, et al (2011) Age-dependent remodelling of ionotropic signalling in cortical astroglia. Aging Cell 10:392–402.

Lalo U, Pankratov Y, Kirchhoff F, et al (2006) NMDA receptors mediate neuron-to-glia signaling in mouse cortical astrocytes. J Neurosci 26:2673–83.

Lalo U, Rasooli-Nejad S, Pankratov Y (2014) Exocytosis of gliotransmitters from cortical astrocytes: implications for synaptic plasticity and aging. Biochem Soc Trans 42:1275–81.

Lavezzari G, McCallum J, Dewey CM, Roche KW (2004) Subunit-specific regulation of NMDA receptor endocytosis. J Neurosci 24:6383–6391.

Lee C-H, Lu W, Michel JC, et al (2014) NMDA receptor structures reveal subunit arrangement and pore architecture. Nature 511:191–197.

Lee M, Schwab C, Mcgeer PL (2011) Astrocytes are GABAergic cells that modulate microglial activity. Glia 59:152–165.

Lee M-C, Ting KK, Adams S, et al (2010) Characterisation of the expression of NMDA receptors in human astrocytes. PLoS One 5:e14123.

Loane DJ, Stoica B a, Faden AI (2012) Metabotropic glutamate receptor-mediated signaling in neuroglia. Wiley Interdiscip Rev Membr Transp Signal 1:136–150.

Luque J, Richards J (1995) Expression of NMDA 2B receptor subunit mRNA in Bergmann glia.

MacFarlane SN, Sontheimer H (2000) Changes in ion channel expression accompany cell cycle progression of spinal cord astrocytes. Glia 30:39–48.

Matsuda K, Fletcher M, Kamiya Y, Yuzaki M (2003) Specific assembly with the NMDA receptor 3B subunit controls surface expression and calcium permeability of NMDA receptors. J Neurosci 23:10064–73.

Matthias K, Kirchhoff F, Seifert G, et al (2003) Segregated expression of AMPA-type glutamate receptors and glutamate transporters defines distinct astrocyte populations in the mouse hippocampus. J Neurosci 23:1750–8.

McKinley M, O'Loughlin V (2005) Human Anatomy.

Muir KW (2006) Glutamate-based therapeutic approaches: clinical trials with NMDA antagonists. Curr Opin Pharmacol 6:53–60.

Murakami K, Kondo T, Kawase M, Chan PH (1998) The development of a new mouse model of global ischemia: focus on the relationships between ischemia duration, anesthesia,

cerebral vasculature, and neuronal injury following global ischemia in mice. Brain Res 780:304–10.

Nakahara K, Okada M, Nakanishi S (1997) The metabotropic glutamate receptor mGluR5 induces calcium oscillations in cultured astrocytes via protein kinase C phosphorylation. J Neurochem 69:1467–75.

Nedergaard M, Dirnagl U (2005) Role of glial cells in cerebral ischemia. Glia 50:281–6.

Nolte C, Matyash M, Pivneva T, et al (2001) GFAP promoter-controlled EGFP-expressing transgenic mice: a tool to visualize astrocytes and astrogliosis in living brain tissue. Glia 33:72–86.

Ogden KK, Traynelis SF (2011) New advances in NMDA receptor pharmacology. Trends Pharmacol Sci 32:726–33.

Oliveira JF, Riedel T, Leichsenring A, et al (2011) Rodent cortical astroglia express in situ functional P2X7 receptors sensing pathologically high ATP concentrations. Cereb Cortex 21:806–20.

Orkand RK, Nicholls JG, Kuffler SW (1966) Effect of nerve impulses on the membrane potential of glial cells in the central nervous system of amphibia. J Neurophysiol 29:788–806.

Palygin O, Lalo U, Pankratov Y (2011) Distinct pharmacological and functional properties of NMDA receptors in mouse cortical astrocytes. Br J Pharmacol 163:1755–66.

Palygin O, Lalo U, Verkhratsky A, Pankratov Y (2010) Ionotropic NMDA and P2X1/5 receptors mediate synaptically induced Ca2+ signalling in cortical astrocytes. Cell Calcium 48:225–31.

Paoletti P (2011) Molecular basis of NMDA receptor functional diversity. Eur J Neurosci 33:1351–65.

Pasti L, Volterra A, Pozzan T, Carmignoto G (1997) Intracellular calcium oscillations in astrocytes: a highly plastic, bidirectional form of communication between neurons and astrocytes in situ. J … 17:7817–7830.

Pekny M, Eliasson C, Siushansian R, et al (1999) The impact of genetic removal of GFAP and/or vimentin on glutamine levels and transport of glucose and ascorbate in astrocytes. Neurochem Res 24:1357–1362.

Pekny M, Wilhelmsson U, Pekna M (2014) The dual role of astrocyte activation and reactive gliosis. Neurosci Lett 565:30–8.

Pellerin L (2003) Lactate as a pivotal element in neuron-glia metabolic cooperation. Neurochem Int 43:331–338.

Perez-Otano I, Schulteis CT, Contractor a, et al (2001) Assembly with the NR1 subunit is required for surface expression of NR3A-containing NMDA receptors. J Neurosci 21:1228–37.

Perillán PR, Li X, Simard JM (1999) K+ inward rectifier currents in reactive astrocytes from adult rat brain. Glia 27:213–225.

Petralia R, Wenthold R (2008) NMDA Receptors.

Porter JT, McCarthy KD (1995) GFAP-positive hippocampal astrocytes in situ respond to

glutamatergic neuroligands with increases in [Ca2+]i. Glia 13:101–12.

Puro D, Yuan J, Sucher N (1996) Activation of NMDA receptor-channels in human retinal Müller glial cells inhibits inward-rectifying potassium currents.

Rafiki A, Bernard A, Medina I, et al (2000) Characterization in cultured cerebellar granule cells and in the developing rat brain of mRNA variants for the NMDA receptor 2C subunit. J Neurochem 74:1798–808.

Rossi DJ, Brady JD, Mohr C (2007) Astrocyte metabolism and signaling during brain ischemia. Nat Neurosci 10:1377–86.

Rouach N, Koulakoff A, Abudara V, et al (2008) Hippocampal Synaptic Transmission. Science (80-) 332:1551–1555.

Rusnakova V, Honsa P, Dzamba D, et al (2013) Heterogeneity of astrocytes: from development to injury - single cell gene expression. PLoS One 8:e69734.

Salt T (2012) Properties of glutamate receptors. http://www.ucl.ac.uk/~smgxt01/frameh.htm?page=glutamat.htm.

Sasaki YF, Rothe T, Premkumar LS, et al (2002) Characterization and comparison of the NR3A subunit of the NMDA receptor in recombinant systems and primary cortical neurons. J Neurophysiol 87:2052–2063.

Scimemi A (2013) A TRP among the astrocytes. J Physiol 591:9–15.

Seifert G, Hüttmann K, Binder DK, et al (2009) Analysis of astroglial K+ channel expression in the developing hippocampus reveals a predominant role of the Kir4.1 subunit. J Neurosci 29:7474–7488.

Seifert G, Steinhäuser C (2001) Ionotropic glutamate receptors in astrocytes. Prog Brain Res 132:287–99.

Serrano A, Haddjeri N, Lacaille J-C, Robitaille R (2006) GABAergic network activation of glial cells underlies hippocampal heterosynaptic depression. J Neurosci 26:5370–82.

Serrano A, Robitaille R, Lacaille J-C (2008) Differential NMDA-dependent activation of glial cells in mouse hippocampus. Glia 56:1648–63.

Shigetomi E, Bushong E a, Haustein MD, et al (2013) Imaging calcium microdomains within entire astrocyte territories and endfeet with GCaMPs expressed using adeno-associated viruses. J Gen Physiol 141:633–47.

Schipke CG, Ohlemeyer C, Matyash M, et al (2001) Astrocytes of the mouse neocortex express functional N-methyl-D-aspartate receptors. FASEB J 15:1270–2.

Schools GP, Zhou M, Kimelberg HK (2006) Development of gap junctions in hippocampal astrocytes: evidence that whole cell electrophysiological phenotype is an intrinsic property of the individual cell. J Neurophysiol 96:1383–1392.

Schousboe A, Waagepetersen HS (2005) Role of astrocytes in glutamate homeostasis: Implications for excitotoxicity. Neurotox Res 8:221–225.

Schröder W, Hager G, Kouprijanova E, et al (1999) Lesion-induced changes of electrophysiological properties in astrocytes of the rat dentate gyrus. Glia 28:166–74.

Smothers CT, Woodward JJ (2007) Pharmacological Characterization of Glycine-Activated Currents in HEK 293 Cells Expressing N-Methyl- D -aspartate NR1 and NR3 Subunits.

322:739–748.

Sontheimer H (1994) Voltage-dependent ion channels in glial cells. Glia 11:156–72.

Sontheimer H, Kettenmann H, Backus KH, Schachner M (1988) Glutamate opens Na+/K+ channels in cultured astrocytes. Glia 1:328–36.

Ståhlberg A, Andersson D, Aurelius J, et al (2011) Defining cell populations with single-cell gene expression profiling: correlations and identification of astrocyte subpopulations. Nucleic Acids Res 39:e24.

Ståhlberg A, Bengtsson M (2010) Single-cell gene expression profiling using reverse transcription quantitative real-time PCR. Methods 50:282–8.

Ståhlberg A, Kubista M (2014) The workflow of single-cell expression profiling using quantitative real-time PCR. Expert Rev Mol Diagn 14:323–31.

Ståhlberg A, Rusnakova V, Forootan A, et al (2013a) RT-qPCR work-flow for single-cell data analysis. Methods 59:80–88.

Ståhlberg A, Rusnakova V, Kubista M (2013b) The added value of single-cell gene expression profiling. Brief Funct Genomics 12:81–89.

Steinhauser C, Berger T, Frotscher M, Kettenmann H (1992) Heterogeneity in the membrane current pattern of identified glial cells in the hippocampal slice. Eur J Neurosci 4:472–484.

Steinhäuser C, Kressin K, Kuprijanova E, et al (1994) Properties of voltage-activated Na+ and K+ currents in mouse hippocampal glial cells in situ and after acute isolation from tissue slices. Pflügers Arch Eur J Physiol 428:610–620.

Stewart TH, Eastman CL, Groblewski P a, et al (2010) Chronic dysfunction of astrocytic inwardly rectifying K+ channels specific to the neocortical epileptic focus after fluid percussion injury in the rat. J Neurophysiol 104:3345–3360.

Sun W, McConnell E, Pare J-F, et al (2013) Glutamate-dependent neuroglial calcium signaling differs between young and adult brain. Science 339:197–200.

Theodoric N, Bechberger JF, Naus CC, Sin WC (2012) Role of Gap Junction Protein Connexin43 in Astrogliosis Induced by Brain Injury. PLoS One.

Traystman RJ (2003) Animal models of focal and global cerebral ischemia. ILAR J 44:85–95.

Tse F, Fraser D, Duffy S, MacVicar B (1992) Voltage-activated K+ currents in acutely isolated hippocampal astrocytes. J Neurosci 1781–1788.

Ulas J, Satou T, Ivins KJ, et al (2000) Expression of metabotropic glutamate receptor 5 is increased in astrocytes after kainate-induced epileptic seizures. Glia 30:352–61.

Van Dongen A (2009) Biology of the NMDA Receptor.

Vanzulli I, Butt AM (2015) mGluR5 protect astrocytes from ischemic damage in postnatal CNS white matter. Cell Calcium.

Vargová L, Syková E (2008) Extracellular space diffusion and extrasynaptic transmission.

Verkhratsky A, Butt A (2007) Glial neurobiology.

Verkhratsky A, Kirchhoff F (2007a) Glutamate-mediated neuronal-glial transmission. J Anat

210:651–60. doi: 10.1111/j.1469-7580.2007.00734.x

Verkhratsky A, Kirchhoff F (2007b) NMDA Receptors in glia. Neuroscientist 13:28–37.

Vermeiren C, Najimi M, Vanhoutte N, et al (2005) Acute up-regulation of glutamate uptake mediated by mGluR5a in reactive astrocytes. J Neurochem 94:405–16.

Virchow R (1858) Die Cellularpathologie in ihrer Begründung auf physiologische and pathologische Gewebelehre. Verlag von August Hirschfeld, Berlin 1858.

Wallraff A, Köhling R, Heinemann U, et al (2006) The impact of astrocytic gap junctional coupling on potassium buffering in the hippocampus. J Neurosci 26:5438–5447.

Wallraff A, Odermatt B, Willecke K, Steinhäuser C (2004) Distinct types of astroglial cells in the hippocampus differ in gap junction coupling. Glia 48:36–43.

Wang DD, Bordey A (2008) The astrocyte odyssey. Prog Neurobiol 86:342–67.

Watkins JC, Jane DE (2006) The glutamate story. Br J Pharmacol 147 Suppl :S100–S108.

Westenbroek RE, Bausch SB, Lin RC, et al (1998) Upregulation of L-type Ca2+ channels in reactive astrocytes after brain injury, hypomyelination, and ischemia. J Neurosci 18:2321–2334.

Wills QF, Livak KJ, Tipping AJ, et al (2013) Single-cell gene expression analysis reveals genetic associations masked in whole-tissue experiments. Nat Biotechnol 31:748–52.

Zhang Q, Hu B, Sun S, Tong E (2003) Induction of increased intracellular calcium in astrocytes by glutamate through activating NMDA and AMPA receptors. J Huazhong Univ Sci Technolog Med Sci 23:254–257.

Zhang Y, Chen K, Sloan S a, et al (2014) An RNA-Sequencing Transcriptome and Splicing Database of Glia, Neurons, and Vascular Cells of the Cerebral Cortex. J Neurosci 34:11929–47.

Zhou M, Xu G, Xie M, et al (2009) TWIK-1 and TREK-1 are potassium channels contributing significantly to astrocyte passive conductance in rat hippocampal slices. J Neurosci 29:8551–8564.

Zhou Y, Li HL, Zhao R, et al (2010) Astrocytes express N-methyl-D-aspartate receptor subunits in development, ischemia and post-ischemia. Neurochem Res 35:2124–34.

Žiak D, Chvatal A, Sykova E (1998) Glutamate-, kainate-and NMDA-evoked membrane currents in identified glial cells in rat spinal cord slice.

8. ATTACHEMENTS:

1. **David Dzamba**, Pavel Honsa, Martin Valny, Jan Kriska, Lukas Valihrach, Vendula Novosadova, Mikael Kubista, Miroslava Anderova (2015), Quantitative analysis of glutamate receptors in glial cells from the cortex of GFAP/EGFP mice following ischemic injury – focus on NMDA receptors, Cellular and Molecular Neurobiology 35(8):1187-202, IF 2.201

2. **David Dzamba**, Pavel Honsa, Miroslava Anderova (2013), NMDA Receptors in Glial Cells: Pending Questions, Current Neuropharmacology 11, 250-262, IF 2.347

3. Vendula Rusnakova, Pavel Honsa, **David Dzamba**, Anders Ståhlberg, Mikael Kubista, Miroslava Anderova (2013), Heterogeneity of Astrocytes: From Development to Injury–Single Cell Gene Expression, PloS one 8 (8), IF 3.730

Cell Mol Neurobiol
DOI 10.1007/s10571-015-0212-8

ORIGINAL RESEARCH

Quantitative Analysis of Glutamate Receptors in Glial Cells from the Cortex of GFAP/EGFP Mice Following Ischemic Injury: Focus on NMDA Receptors

David Dzamba[1,2] · Pavel Honsa[1] · Martin Valny[1] · Jan Kriska[1,2] · Lukas Valihrach[3] · Vendula Novosadova[3] · Mikael Kubista[3] · Miroslava Anderova[1]

Received: 21 April 2015 / Accepted: 15 May 2015
© Springer Science+Business Media New York 2015

Abstract Cortical glial cells contain both ionotropic and metabotropic glutamate receptors. Despite several efforts, a comprehensive analysis of the entire family of glutamate receptors and their subunits present in glial cells is still missing. Here, we provide an overall picture of the gene expression of ionotropic (AMPA, kainate, NMDA) and the main metabotropic glutamate receptors in cortical glial cells isolated from GFAP/EGFP mice before and after focal cerebral ischemia. Employing single-cell RT-qPCR, we detected the expression of genes encoding subunits of glutamate receptors in GFAP/EGFP-positive (GFAP/EGFP$^+$) glial cells in the cortex of young adult mice. Most of the analyzed cells expressed mRNA for glutamate receptor subunits, the expression of which, in most cases, even increased after ischemic injury. Data analyses disclosed several classes of GFAP/EGFP$^+$ glial cells with respect to glutamate receptors and revealed in what manner their expression correlates with the expression of glial markers prior to and after ischemia. Furthermore, we also examined the protein expression and functional significance of NMDA receptors in glial cells. Immunohistochemical analyses of all seven NMDA receptor subunits provided direct evidence that the GluN3A subunit is present in GFAP/EGFP$^+$ glial cells and that its expression is increased after ischemia. In situ and in vitro Ca^{2+} imaging revealed that Ca^{2+} elevations evoked by the application of NMDA were diminished in GFAP/EGFP$^+$ glial cells following ischemia. Our results provide a comprehensive description of glutamate receptors in cortical GFAP/EGFP$^+$ glial cells and may serve as a basis for further research on glial cell physiology and pathophysiology.

Keywords Astrocytes · NG2 glia · MCAo · Single-cell RT-qPCR · Calcium imaging

Introduction

The era when glial cells were considered to be just passive bystanders of neuronal transmission was supplanted by a new era in which they are seen to actively communicate with neurons and participate in crucial processes, including the development of the nervous system, synaptic plasticity, and synaptogenesis. Glial cells of ectodermal origin are divided according to their function into astrocytes, NG2 glia (also called polydendrocytes or oligodendrocyte precursor cells—OPCs), oligodendrocytes, and ependymal cells. In this work, we studied GFAP/EGFP$^+$ glial cells, which mostly comprise astrocytes; however, there are indications of NG2 glia overlap, especially in juvenile animals (Matthias et al. 2003; Serrano et al. 2008).

Similarly to neurons, glial cells possess a variety of metabotropic and ionotropic glutamate receptors. Metabotropic glutamate receptors (mGluR1-8) regulate various intracellular signal cascades, and several of these

Electronic supplementary material The online version of this article (doi:10.1007/s10571-015-0212-8) contains supplementary material, which is available to authorized users.

✉ Miroslava Anderova
anderova@biomed.cas.cz

[1] Present Address: Department of Cellular Neurophysiology, Institute of Experimental Medicine, Academy of Sciences of the Czech Republic, Videnska 1083, Prague 4, Czech Republic

[2] 2nd Faculty of Medicine, Charles University, Prague, Czech Republic

[3] Laboratory of Gene Expression, Institute of Biotechnology, Academy of Sciences of the Czech Republic, Prague, Czech Republic

Published online: 21 May 2015

receptors have been identified in astrocytes, with mGluR3 and mGluR5 being the most abundant (Verkhratsky 2009; Loane et al. 2012). Ionotropic glutamate receptors are divided according to their specific agonists into three groups—AMPA, kainate, and NMDA. They differ in their subunit composition, functional properties such as desensitization rate or specificity in ion permeability, and also in their different occurrence in various brain cell types depending on the CNS region. AMPA receptor subunits (GluA1-4) are present in astrocytes in most brain regions (Seifert and Steinhäuser 2001), and their subunit composition determines their Ca^{2+} permeability (Hollmann et al. 1991; Burnashev et al. 1992). All kainate receptor subunits (GluK1-5) have been identified in astrocytes either on the mRNA or protein level (Brand-Schieber et al. 2004); however, the functional properties of these receptors have not been demonstrated so far. The last group of astrocytic glutamate receptors is NMDA receptors composed of GluN1-3B subunits, which is a highly debatable receptor family with a large therapeutic potential (for review see Verkhratsky and Kirchhoff 2007; Dzamba et al. 2013). In contrast to neuronal NMDA receptors, they do not possess a Mg^{2+} block (Lalo et al. 2006; Castillo et al. 2013), so they are also functional at resting membrane potential, which is probably due to their specific combination of subunits, including the most recently discovered GluN3A and GluN3B subunits. The impact of ischemia on NMDA receptors has been studied in hippocampal astrocytes (Gottlieb and Matute 1997; Krebs et al. 2003), but to the best of our knowledge, there are currently no data regarding cortical astrocytes after ischemia; therefore, we specifically focused on these receptors.

In this work, we used single-cell gene expression profiling, which is a novel and powerful method enabling us to study the correlation of transcript levels among individual cells (Ståhlberg and Bengtsson 2010), which is not possible using classical bulk samples composed of a large number of cells. The goal of this work was to characterize GFAP/EGFP-positive (GFAP/$EGFP^+$) cells in the cortex of GFAP/EGFP mice after focal cerebral ischemia and to present a detailed overall picture of glutamate receptors in individual GFAP/$EGFP^+$ glial cells with a main focus on NMDA receptors.

Materials and Methods

Induction of Focal Ischemic Injury in GFAP/EGFP Mice: Permanent Middle Cerebral Artery Occlusion (MCAo) Model

The experiments were performed on GFAP/EGFP transgenic mice [line designation TgN(GFAPEGFP)], in which the expression of EGFP is controlled by the human GFAP promoter (Nolte et al. 2001). All procedures involving the use of laboratory animals were performed in accordance with the European Communities Council Directive 24 November 1986 (86/609/EEC) and animal care guidelines approved by the Institute of Experimental Medicine, Academy of Sciences of the Czech Republic (Animal Care Committee on April 17, 2009; approval number 85/2009 and 036/2012).

Before the induction of focal ischemia, adult mice were anesthetized with 1.5 % isoflurane (Abbot, IL, USA) and maintained in 1 % isoflurane using a vaporizer (Tec-3, Cyprane Ltd., UK). A skin incision between the orbit and the external auditory meatus was made, and a hole (1–2 mm in diameter) was drilled through the frontal bone 1 mm rostral to the fusion of the zygoma and the squamosal bone and about 3.5 mm ventral to the dorsal surface of the brain. The dura was opened, gently removed, and the exposed middle cerebral artery was occluded by a short coagulation with bipolar tweezers (SMT, Czech Republic) at a proximal location, followed by transection of the vessel to ensure permanent occlusion. During the surgery, heating pad was used to maintain the mouse's body temperature at 37 ± 1 °C (Honsa et al. 2012).

Preparation of Cell Suspensions from the Cortex of GFAP/EGFP Mice

Before the collection of single GFAP/$EGFP^+$ cells utilizing flow cytometry, the cortical tissue was dissociated using papain treatment. In the experiment, the cells were collected from uninjured mice (5 mice, 63–108 days old; 246 cells), mice 7 days after MCAo (4 mice, 57–64 days old; 199 cells), and mice 14 days after MCAo (3 mice, 64 days old; 126 cells). The animals were deeply anesthetized with pentobarbital (PTB, 100 mg/kg, i.p.; Sigma-Aldrich, MO, USA) and perfused transcardially with cold (4–8 °C) isolation buffer containing (in mM) NaCl 136.0, KCl 5.4, HEPES 10.0, glucose 5.5, and osmolality 290 ± 3 mOsm/kg. To isolate the cerebral cortex, a part of the brain (+2 to −2 mm rostro-caudally from bregma) was sliced into 400-μm coronal sections using an HM650V vibrating microtome (MICROM International GmbH, Germany), and the dorsal cerebral cortex was carefully dissected out from the ventral white matter tracks. In mice after MCAo, the ischemic core with its surrounding tissue (cca 1/2 of the injured hemisphere) was used. The tissue was incubated with continuous shaking at 37 °C for 45–60 min in 5 ml of a papain solution (20 U/ml) and 0.2 ml DNase (both from Worthington, NJ, USA) prepared in isolation buffer. After papain treatment, the tissue was mechanically dissociated by gentle trituration using a 1-ml pipette. According to the manufacturer's instructions, the dissociated cells were

layered on top of 5 ml of ovomucoid inhibitor solution and harvested by centrifugation (140×*g* for 6 min). Cell aggregates were removed by filtering with a 30-µm cell strainer (Becton–Dickinson, NJ, USA), and the cells were kept on ice until sorting. This method routinely yielded $\sim 2 \times 10^6$ cells per mouse brain.

Collection of Single GFAP/EGFP$^+$ Cells by Flow Cytometry

The collection of single cells was performed using flow cytometer (BD Influx, CA, USA), which was manually calibrated to deposit single cells in the center of each well of 96-well plates (Life Technologies, CA, USA) that were placed on a pre-cooled rack. Only viable and GFAP/EGFP$^+$ cells were collected. The viability of the cells was checked using Hoechst 33258 (Life Technologies). Single cells were collected into 5 µl nuclease-free water with bovine serum albumin (1 mg/µl; Fermentas, IL, USA)) and RNaseOut (20 U; Life Technologies). Collected cells in 96-well plates were stored at −80 °C immediately after sorting.

Single-Cell Gene Expression Profiling of Mouse Astrocytes

The gene expression profiling of single GFAP/EGFP$^+$ glial cells was performed according to the protocol described in (Rusnakova et al. 2013). Briefly, RNA from single cells was transcribed into cDNA in the wells of 96-well plates. To increase the sensitivity of RT-qPCR, the cDNA from one-half of the cells were first pre-amplified. Subsequently, such pre-processed samples were analyzed for the expression of 25 genes of interest (for primer sequences see (Rusnakova et al. 2013), *Grin3b* forward primer TGGTCGGGGACAAGACATTT, reverse primer TCCGTGTGGAGTGGTAGGTG) using the BioMark qPCR platform (Fluidigm, San Francisco, CA, USA). Data were analyzed in GenEx v.6 software (MultiD, Sweden) utilizing the Kohonen self-organizing maps (SOM) method and principal component analysis (PCA), which divided all cells into three subpopulations according to the expression of these 25 genes. The Spearman correlation coefficients between genes were calculated in SAS v.9.3 software using all data, including the managed off-scale data. Only correlation coefficients for genes having a p value <0.05 are presented in the results.

Immunohistochemistry

The mice were deeply anesthetized with PTB (100 mg/kg, i.p.) and perfused transcardially with 20 ml of saline followed by 20 ml of cooled 4 % paraformaldehyde (PFA) in 0.1 M phosphate buffer. Brains were dissected out, post-fixed for 18 h, and placed stepwise in solutions with gradually increasing sucrose concentrations (10, 20, 30 %) for cryoprotection. Coronal 30-µm-thick slices were prepared using a microtome (HM550, Microm International, Germany). The slices were incubated with 5 % Chemiblocker (Millipore, MA, USA) and 0.2 % Triton in phosphate-buffered saline. This blocking solution was also used as the diluent for the antisera. The slices were incubated with the primary antibodies at 4–8 °C overnight, then the secondary antibodies were applied for 2 h. As primary antibodies, we used anti-GluN1 (1:500; Abcam, Cambridge, UK, AB28669), anti-GluN2A (1:400; Abcam, AB106957), anti-GluN2B (1:400; Abcam, AB65875), anti-GluN2C (1:400; Alomone Labs, Jerusalem, Israel, AGC-018), anti-GluN2D (1:400; Alomone Labs, AGC-020), anti-GluN3A (1:400; Abcam, AB111226), and anti-GluN3B (1:500; Abcam, AB35677). As the secondary antibody, we used goat anti-rabbit IgG conjugated with Alexa Fluor 594 (1:200; Molecular Probes, CA, USA, A-11012). The slices were mounted using Aqua Poly/Mount (Polysciences Inc., Germany). All chemicals were purchased from Sigma-Aldrich, unless otherwise stated.

A Zeiss 510DUO LSM confocal microscope equipped with Arg/HeNe lasers was used for immunohistochemical analysis. Stacks of consecutive confocal images taken at intervals of 3 µm were acquired sequentially with two lasers to avoid cross-talk between fluorescent labels. The background noise of each confocal image was reduced by averaging four image inputs. For each image stack the gain and detector offset were adjusted to minimize saturated pixels, yet still permit the detection of weakly stained cell processes. Colocalization images were made using a Zeiss LSM Image Browser.

Preparation of Primary Cultures

Primary cultures of GFAP/EGFP$^+$ glial cells were prepared from 40- to 57-day-old mice, either uninjured or those 13–14 days after MCAo. The animals were deeply anesthetized with PTB (100 mg/kg, i.p) and perfused transcardially with cold (4–8 °C) NMDG isolation solution containing (in mM) 110 NMDG-Cl, 2.5 KCl, 24.5 $NaHCO_3$, 1.25 Na_2HPO_4, 0.5 $CaCl_2$, 7 $MgCl_2$, and 20 glucose (pH 7.4, osmolality 290 mOsm/kg). The brain was sliced into 200-µm coronal sections as described above, and the cortical tissue was dissected out. In mice 14 days after MCAo, the dissected tissue consisted of the ischemic core and its surrounding tissue (cca 1/2 of the injured hemisphere). The isolated tissue was transferred into 1 ml of artificial cerebrospinal fluid (aCSF) solution containing (in mM) 122 NaCl, 3 KCl, 1.3 $MgCl_2$, 1.5 $CaCl_2$, 28 $NaHCO_3$, 1.25 Na_2HPO_4, and 10 glucose (pH 7.4,

osmolality 305 mOsm/kg), which was supplemented with 0.05 % trypsin (Life technologies), and incubated with continuous shaking at 37 °C for 30 min. After incubation, the tissue was transferred into 1 ml of trypsin inhibitor (Sigma-Aldrich) and dissociated by gentle trituration using a 1-ml pipette. Subsequently, the cells were plated in a volume of 0.15 ml onto 6 coverslips in a 24-well plate, and 0.5 ml of fresh cultivation medium was added into each well. The cultivation medium consisted of high-glucose Dulbecco's Modified Eagle Medium (Life Technologies) supplemented with 15 % fetal bovine serum (PAA Laboratories GmbH, Austria), 2 mM L-glutamine (Sigma-Aldrich), and antibiotic–antimycotic containing penicillin, streptomycin, and amphotericin B (Life Technologies). Cells were cultured in an incubator (100 % humidity, 5 % CO_2) at 37 °C for 5–6 days without medium exchange.

Calcium Imaging Measurements

In situ measurements were performed in the somatosensory cortex of 35–59-day-old GFAP/EGFP mice, either uninjured or mice 13–14 days after MCAo. Transversal brain slices (200 μm thick) were cut in cold (4–8 °C) NMDG isolation solution using a vibration microtome and were kept at room temperature in aCSF solution. The slices were then mounted in a microscope superfusion chamber, which was continually perfused with HEPES-based aCSF containing (in mM) 135 NaCl, 2.7 KCl, 1 $MgCl_2$, 2.5 $CaCl_2$, 1 Na_2HPO_4, 10 Glucose, and 10 HEPES (pH 7.4, osmolality 305 mOsm/kg, equilibrated with O_2) at a flow rate of 2.5 ml/min. The regions with GFAP/EGFP$^+$ cells, which were 10–20 μm below the surface of the slice, were then found and their positions were recorded. The loading procedure was performed at room temperature in the measurement chamber for 40 min in 3 ml of HEPES-based aCSF (the flow was interrupted during this period) containing 1 μM OGB-1 AM with 0.02 % Pluronic F-127 and continually bubbled with O_2 to avoid ischemic conditions. After the loading, the flow of HEPES-based aCSF was reestablished and the measurements were performed with the cells found prior to the loading. The solutions [*N*-methyl-D-aspartate (NMDA), L-glutamic acid (glutamate), glycine, memantine hydrochloride (memantine), NBQX, and PPADS from Sigma-Aldrich, Germany; DL-2-amino-5-phosphonovaleric acid (DL-APV) from Ascent Scientific, UK; and tetrodotoxin (TTX) from Alomone labs, Israel] were applied through a capillary with an i.d. of 250 μm located 0.5–1 mm from the measurement region and connected to a Perfusion Pressure Kit pressurized application system with a flow rate of 600 μl/min controlled by a ValveBank II controller (AutoMate Scientific, Inc., Berkeley, CA, USA). The HEPES-based aCSF was applied via the application system throughout the entire experiment to ensure that the Ca^{2+} responses were not influenced by the application itself and to accelerate the solution exchange in the vicinity of recorded cells. OGB-1 fluorescence was detected with a TILL Photonics Imaging System installed on a Zeiss Axioskop 2 FS Plus microscope equipped with a long-distance ×40 objective (IR Achroplan 0.8 W, Zeiss, Germany). A digital camera (PCO Sensicam, Kelheim, Germany) was controlled by TILLvisION software. The excitation light (488 nm) was generated by a Polychrome V (TILL Photonics GmbH, Gräfelfing, Germany), filtered by a BP 450–490 excitation band-pass filter, reflected by a FT 510 beam splitter, and the emitted light was filtered by a LP 515 long-pass filter (Filter Set 09, Zeiss, Germany). Images were acquired at 0.83 Hz and were analyzed offline. Fluorescence intensity (F) was measured in the cell bodies and expressed after background correction as $F - F_b$, where F_b was the background fluorescence intensity in the proximity of the analyzed cell. The baseline $F - F_b$ signal was then normalized to 100 %, and the area under the curve was measured during 1 min from the onset of application (expressed in arbitrary units). For measuring the delay of the response, the signal threshold for Ca^{2+} responses in situ was 200 % of the amplitude of the noise signal, and the responses were taken into account only if they occurred within 1 min from the onset of application.

In vitro Ca^{2+} imaging measurements were performed similarly to in situ measurements with the exception of the OGB-1 AM loading procedure. Coverslips with 5–6-day-old cell cultures were incubated for 45 min in 0.5 ml of cultivation medium containing 1.5 μM OGB-1 AM and 0.03 % Pluronic F-127 (Life Technologies) at 37 °C in an incubator (100 % humidity, 5 % CO_2). Fluorescence intensity (F) was measured in the cell bodies, if not stated otherwise, and the area under the curve was measured from fluorescence intensity F during 1 min from the onset of application (expressed in arbitrary units). Since noise signal in Ca^{2+} imaging in vitro was minimal, for measuring the delay of the response, the threshold for Ca^{2+} responses was set to 120 % of the baseline fluorescence, and responses were taken into account only if they occurred within 1 min from the onset of application.

Results

In this study, GFAP/EGFP$^+$ glial cells isolated from the cortices of GFAP/EGFP mice were studied in young adult uninjured mice (controls) and in mice 7 and 14 days after MCAo. Employing a single-cell RT-qPCR technique, we were able to detect changes in the expression of the genes coding particular subunits of glutamate receptors following ischemia. For this purpose, the cells were isolated using

papain dissociation, sorted on a flow cytometer according to their EGFP fluorescence and individually analyzed by single-cell analysis.

Expression Profile of Glutamate Receptor Subunits in Uninjured and Post-ischemic Mouse Brains

At first, we analyzed the incidence of GFAP/EGFP^{+} cells expressing the genes of particular ionotropic glutamate receptor subunits of the AMPA (*Gria1-4*), kainate (*Grik1–5*), and NMDA (*Grin1–3b*) types and of metabotropic glutamate receptors (*Grm1,3,5*) in controls and mice 7 and 14 days after MCAo (Fig. 1). The majority of GFAP/EGFP^{+} cells (567 out of 571) expressed typical astrocytic markers, such as *Slc1a3, Glul, Gfap*, or *Aqp4*. Four cells, which expressed only markers of NG2 glia (*Cspg4* and/or *Pdgfra*) and did not express any astrocytic marker (*Slc1a3, Glul, Gfap*, and *Aqp4*), were excluded from the analysis; however, this did not lead to any substantial changes in the gene expression profiling.

The lowest expression from all AMPA receptor subunits was found with the *Gria1* gene, which was expressed only in 2 % of cells isolated from controls (control cells). In cells isolated from mice 7 and 14 days after induction of MCAo (D7 and D14 cells), the incidence of cells expressing the *Gria1* gene was higher, but did not exceed 12 %. Very interesting results were obtained in the case of the *Gria2* gene, which was present in numerous control cells (61 %) with no significant change in expression after MCAo. The GluA2 subunit, the protein product of the *Gria2* gene, is crucial for the Ca^{2+} permeability of the AMPA receptors and, for example, in cerebellar Bergmann glia this subunit is absent (Hollmann et al. 1991; Burnashev et al. 1992). The *Gria3* gene was expressed in 4 % of the control cells; however, in D7 and D14 cells its expression was significantly increased (43 and 50 %, respectively). The *Gria4* gene was expressed in 10 % of the control cells, while the number of cells expressing this gene increased to 51 % in D7 cells and to 49 % in D14 cells. Thus, after MCAo, the gene expression of 3 out of 4 AMPA receptor subunits was increased at least fourfold.

A similar trend was observed with genes coding kainate receptor subunits. The numbers of cells expressing *Grik1,2,3,4,5* were increased 10-, 3-, 9-, 15-, and 2-fold after MCAo. The maximum expression of *Grik3,4* was observed in D7 cells and that of *Grik1,2,5* in D14 cells.

The expression of genes coding the subunits of NMDA receptors underwent dramatic changes as well. The *Grin1* gene was present in 7 % of the control cells, and this number was increased to 30 % in D7 and 43 % in D14 cells. From among all of the *Grin2* genes, the only gene that displayed a significant increase in the number of expressing cells after MCAo was *Grin2d*. The *Grin3a* gene, which codes the recently discovered GluN3A subunit of NMDA receptors with a prominent effect on the Mg^{2+} block and Ca^{2+} permeability of NMDA receptors (Perez-

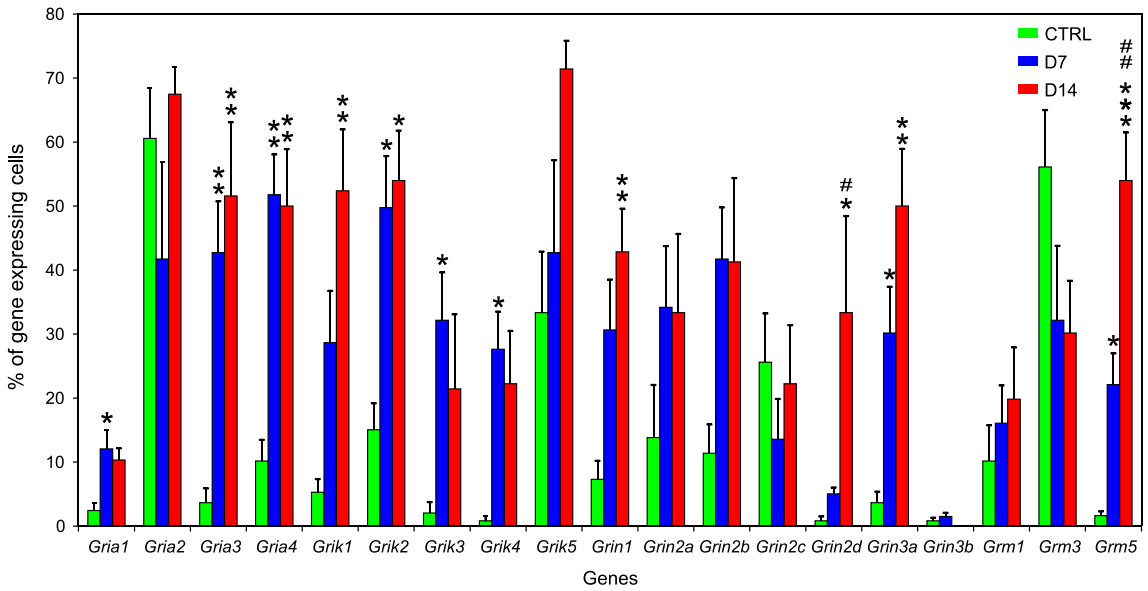


Fig. 1 The percentage of cells expressing genes coding individual subunits of glutamate receptors in control mice and in mice after MCAo. Cells isolated from control mice (CTRL, 5 mice, 246 cells) and from mice 7 and 14 days after MCAo (D7, 4 mice, 196 cells and D14, 3 mice, 125 cells) were used. Genes coding AMPA receptors (*Gria1-4*), kainate receptors (*Grik1–5*), NMDA receptors (*Grin1-3b*), and metabotropic glutamate receptors (*Grm1,3,5*) were studied. *Error bars* represent SEM. Significant differences between D7/D14 compared to CTRL ($^{*}p < 0.05$, $^{**}p < 0.01$, $^{***}p < 0.001$) and D14 compared to D7 ($^{\#}p < 0.05$, $^{\#\#}p < 0.01$) were calculated by one-way ANOVA followed by the Bonferroni post-test

Otano et al. 2001; Cavara and Hollmann 2008), was expressed in 7–12-fold more cells isolated from mice after ischemic insult when compared to control cells (30 % of D7 and 50 % of D14 cells compared to 4 % in control cells). The expression of the *Grin3b* gene was very low; we detected it only in 1 % of control cells and 2 % of D7 cells, while there was no expression in D14 cells.

Together with ionotropic glutamate receptors, we also studied the expression of genes coding the most abundant metabotropic receptor subunits in glial cells *Grm1,3,5* (D'Antoni et al. 2008). Ten percent of control cells expressed *Grm1,* and this incidence did not significantly change after MCAo. The number of cells expressing *Grm3* shifted from 56 % in control cells to 30–32 % after MCAo. The largest increase in the percentage of cells expressing a particular gene after MCAo was observed with *Grm5,* which was detected in only 1.6 % of the control cells. Following ischemic injury, its expression increased 13-fold in D7 cells and 33-fold in D14 cells. This is in accordance with other studies showing the absence of *Grm5* in adult astrocytes under physiological conditions (Sun et al. 2013) and an increased presence of *Grm5* mRNA and mGluR5 protein in reactive astrocytes (Ulas et al. 2000; Aronica et al. 2000). Moreover, *Grm5* together with *Grin2d* was the only genes with significantly increased expression in D14 cells when compared to D7 cells.

Gene Expression Profiling of Distinct Subpopulations of GFAP/EGFP$^+$ Cells

There have been several recent studies demonstrating the heterogeneity of GFAP/EGFP$^+$ cells (Serrano et al. 2008; Ståhlberg et al. 2011; Benesova et al. 2012; Rusnakova et al. 2013). The single-cell RT-qPCR method used in this work is suitable for studying such heterogeneity, since it provides information about the gene expression levels of several genes in individual cells, with the possibility to further analyze the division of the cells into subpopulations. In this study, PCA was used to find three distinct subpopulations (SP1–SP3) among a pool of control, D7, and D14 cells (Fig. 2a). The SOM analysis, which forced the division of the cells into three groups, confirmed the stable classification of these subpopulations. The division into subpopulations was performed according to the similarity in gene expression of glial cell markers (*Cspg4, Pdgfra, Slc1a3, Glul, Gfap, Aqp4*) and glutamate receptor subunits (*Gria1–4, Grik1–5, Grin1–3b, Grm1,3,5*). There was an interesting tendency in the representation of control, D7, and D14 cells in these subpopulations (Fig. 2b). Subpopulation SP1 mostly comprised control cells, SP2 contained 30 % of control cells but mostly D7 cells, and SP3 was formed almost solely by cells after MCAo (42 % of D7 cells and 54 % of D14 cells). From the bar plot showing the expression levels of genes in the SP1–SP3 subpopulations (Fig. 2c), it is evident that the highest gene transcript levels were in subpopulation SP3, which consisted especially of D7 and D14 cells, indicating the importance of glutamate receptors after ischemia. This also corresponded with the increased percentage of cells expressing genes coding glutamate receptors after MCAo (Fig. 1).

Spearman Correlation Coefficients

Even though there is heterogeneity among GFAP/EGFP$^+$ cells, there were still some trends in gene expression patterns when comparing control, D7, and D14 cells. In the next step, we focused on a detailed classification of control cells and those isolated at particular times after MCAo. For this purpose, the Spearman correlation coefficients between pairs of genes were calculated; all of the correlation coefficients are shown in Online Resource 1. Since some of the GFAP/EGFP$^+$ cells also expressed genes coding the NG2 glial markers *Cspg4* and/or *Pdgfra* as previously shown (Rusnakova et al. 2013), we were able to assess significant correlations between genes coding glutamate receptors and glial cells markers (Fig. 3).

The lowest number of correlations was observed in control cells. Six genes (*Gria1, Gria3, Grik5, Grin2d, Grin3b*, and *Grm5*) did not correlate with any glial marker in this group, while the remaining 13 genes correlated positively with at least one NG2 glial marker. Positive correlations with at least 2 out of 4 astrocytic markers were observed only with 3 genes (*Gria2, Grin2c,* and *Grm3*), whereas negative correlations were found with 4 genes (*Gria4, Grik3, Grin2a,* and *Grm1*). In control cells, we can summarize that most of the glutamate receptors were especially present in GFAP/EGFP$^+$ cells, which expressed NG2 glial markers.

The correlation coefficients in D7 cells showed a strong positive correlation of AMPA and kainate receptor subunits with NG2 glial markers, which was not true for NMDA receptor subunits (a positive correlation with only *Grin1, Grin3a,* and marginally *Grin2d*) and metabotropic glutamate receptors (a positive correlation with *Grm5* only). In contrast to control cells, almost all glutamate receptor subunits displayed a positive correlation with astrocytic markers in D7 cells. Surprisingly, a positive correlation was also observed between the astrocytic marker *Slc1a3* and the NG2 glial markers *Cspg4* and *Pdgfra* (see Online Resource 1), which reflects the complex changes accompanying reactive astrogliosis after an ischemic insult.

In D14 cells, the situation was much more comprehensible. There was no positive correlation between genes

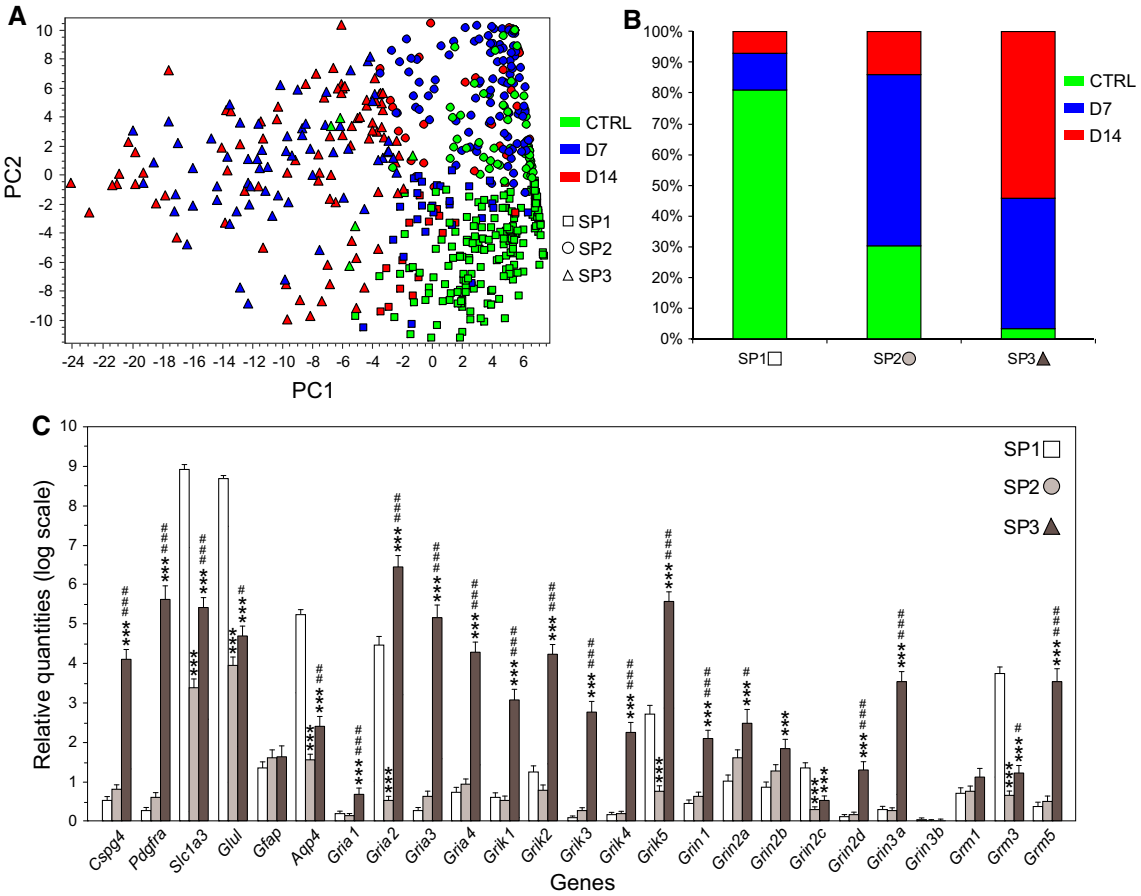


Fig. 2 Gene expression profiling of distinct subpopulations of GFAP/EGFP^{+} cells isolated from the cortex of GFAP/EGFP mice. **a** Principal component analysis (PCA) of cells from control mice (CTRL, 246 cells/5 mice) and those 7 and 14 days after MCAo (D7, 199 cells/4 mice; D14, 126 cells/3 mice). The data were mean-centered according to the genes. The cells were divided into three groups by Kohonen self-organizing maps (SOM) and are marked by different symbols (*squares* for subpopulation SP1, *circles* for subpopulation SP2, and *triangles* for subpopulation SP3). **b** Percentage representation of CTRL, D7, and D14 cells in the subpopulations SP1–3. **c** Bar plot with SEM showing the relative expression of the analyzed genes in subpopulations SP1–3. Significant differences between SP2/SP3 compared to SP1 ($^{***}p < 0.001$) and SP3 compared to SP2 ($^{\#}p < 0.05$, $^{\#\#}p < 0.01$, $^{\#\#\#}p < 0.001$) were calculated by one-way ANOVA followed by the Bonferroni post-test

coding NG2 glial and astrocytic markers (see Online Resource 1), and also most of the genes coding glutamate receptor subunits correlated positively only with NG2 glial or astrocytic markers. For AMPA receptors, the correlation coefficients were similar to those in control cells. The only difference was with the *Gria3* gene, which was positively correlated with astrocytic markers in D14 cells. Kainate receptors also showed a similar trend as in control cells, since they were mostly correlated with NG2 glial markers. Intriguingly, NMDA and metabotropic glutamate receptors showed a very distinct correlation pattern, as *Grin2a-d* and *Grm3,5* showed a strong negative correlation with NG2 glial markers and a positive correlation with astrocytic markers. The only genes coding NMDA receptor subunits that positively correlated with NG2 glial markers were *Grin1* and *Grin3a.*

Immunohistochemical Analysis of NMDA Receptor Subunits

The single-cell RT-qPCR studies provided us with information about the levels of mRNA transcripts in single cells. As the next step, we performed an immunohistochemical analysis to verify that these transcripts were translated into proteins. For this analysis, we chose NMDA receptors since there are many unresolved questions about their presence and function in glial cells (Dzamba et al. 2013).

The immunohistochemical analysis (Fig. 4) showed staining of cortical GFAP/EGFP^{+} glial cells for individual NMDA receptor subunits (GluN1, GluN2A-D, and GluN3A-B) in tissue slices from controls and from mice 14 days after MCAo, in which the images were taken from

CTRL

	Cspg4	Pdgfra	Slc1a3	Glul	Gfap	Aqp4
Gria1						
Gria2	0,19		**0,28**	**0,47**		**0,45**
Gria3						
Gria4	0,19		-0,13	-0,13		
Grik1	0,18	**0,35**				
Grik2	0,20				0,16	
Grik3		**0,29**	-0,18	-0,16		-0,14
Grik4	0,22	0,23				
Grik5						
Grin1	**0,30**				0,14	
Grin2a	0,23		-0,34	-0,22		-0,13
Grin2b	0,16		-0,14			
Grin2c	0,14			0,18		0,21
Grin2d						
Grin3a	0,19	**0,30**				
Grin3b						
Grm1	0,18		**-0,25**	-0,23		-0,13
Grm3		0,16	**0,25**	**0,46**		**0,40**
Grm5						

D7

	Cspg4	Pdgfra	Slc1a3	Glul	Gfap	Aqp4
Gria1	0,28	0,28	0,31	0,16		
Gria2	0,60	0,56	**0,48**	**0,14**		**0,20**
Gria3	0,66	0,65	0,46			0,15
Gria4	0,50	0,51	0,39			0,15
Grik1	0,37	**0,37**	0,36	0,14		0,23
Grik2	0,45	0,44	0,30	0,27	-0,15	0,15
Grik3	0,53	**0,50**	0,25			
Grik4	0,51	0,50	0,34			
Grik5	0,43	0,44	0,48	0,31		0,34
Grin1	**0,30**	0,21	0,19			0,19
Grin2a			0,17	0,20	0,22	0,17
Grin2b						
Grin2c			0,14	0,25		0,28
Grin2d	0,17				-0,19	
Grin3a	0,63	**0,67**	0,51			0,17
Grin3b						
Grm1					0,15	0,22
Grm3			**0,27**	**0,48**	0,28	**0,35**
Grm5	0,50	0,46	0,25			

D14

	Cspg4	Pdgfra	Slc1a3	Glul	Gfap	Aqp4
Gria1						
Gria2	0,41	0,45	**0,28**			
Gria3			0,28	0,31		
Gria4	0,39	0,48				-0,25
Grik1	0,22	**0,29**	0,32			
Grik2	0,39	0,42				-0,19
Grik3	0,37	**0,32**				-0,28
Grik4	0,36	0,48		-0,20		-0,25
Grik5	0,31	0,37	0,37	0,27		
Grin1	**0,23**	0,23				
Grin2a	-0,45	-0,42	0,37	0,54		0,25
Grin2b	-0,24	-0,20				0,27
Grin2c	-0,24	-0,25	0,42	0,36		0,42
Grin2d	-0,26	-0,21		0,20		0,24
Grin3a	0,55	**0,62**	0,18			
Grin3b						
Grm1				0,21		0,27
Grm3	-0,24	-0,27	**0,50**	**0,54**		**0,47**
Grm5	-0,30	-0,24	0,47	0,55		0,20

Fig. 3 Spearman correlation coefficients between genes coding glutamate receptor subunits and markers of NG2 glia/astrocytes in control cells (CTRL) and in cells 7 and 14 days after MCAo (D7, D14). The correlation coefficients were calculated from all cells including those without any expression of the studied genes. Positive correlations are highlighted in *green*, negative in *red*. All the values of the correlation coefficients are significant with $p < 0.05$. Correlation coefficients with $p < 0.001$ are in *bold* (Complete list of Spearman correlation coefficients is provided in Online Resource 1)

the ischemic rim (Fig. 4b). The analysis revealed that there were GFAP/EGFP$^+$ cells positively stained for the GluN3A subunit in controls; however, we did not observe any GFAP/EGFP$^+$ glial cells positively stained for other NMDA receptor subunits under control conditions. In contrast, 14 days after MCAo, we observed GFAP/EGFP$^+$ cells positive for the NMDA receptor subunits GluN1, GluN2B-D, and GluN3A close to the ischemic lesion. Immunohistochemical staining for the GluN2A subunit differed from that of the rest of the subunits since none of the GFAP/EGFP$^+$ cells were positive for GluN2A; the only positive cells morphologically resembled neurons. As for the GluN3B immunostaining, there were positive cells in subcortical regions (data not shown), but none of the cells in the cortex were positive, which correlates with the single-cell RT-qPCR results. Nonetheless, the immunohistochemical analysis revealed that especially after ischemia, many GFAP/EGFP$^+$ cells became positive for most of the NMDA receptor subunits.

NMDA Receptors in GFAP/EGFP$^+$ Glial Cells – Ca^{2+} Imaging Measurements In Situ

Based on the results obtained from single-cell RT-qPCR and immunohistochemical analysis, we also performed a functional study of NMDA receptors in GFAP/EGFP$^+$ glial cells using a Ca^{2+} imaging measurement technique. The experiments were carried out in tissue slices prepared from GFAP/EGFP mice, either in controls or mice 13–14 days after MCAo (D13–14 mice).

First of all, we aimed to clarify what is the delay of the NMDA-evoked Ca^{2+} responses and to what extent are NMDA-evoked intracellular Ca^{2+} elevations dependent on agonist concentration. The average delay of the onset of Ca^{2+} responses following an application of 100 μM NMDA was 32.4 s (Fig. 5a). Moreover, the Ca^{2+} responses also differed in their kinetics; they displayed a large variability ranging from fast transient Ca^{2+} spikes to gradual changes of Ca^{2+} concentration indicating sustained Ca^{2+} entry. As expected, the Ca^{2+} elevations increased with the concentration of NMDA applied, as 4 μM and 20 μM NMDA-evoked responses were lower by 78 and 42 %, respectively, when compared to the application of 100 μM NMDA (Fig. 5b). The distribution of Ca^{2+} responses evoked by 100 μM NMDA did not reveal any heterogeneity in the magnitude of the responses (Fig. 5c). The co-application of 1 μM TTX did not result in any significant decrease in the Ca^{2+} responses evoked by 100 μM NMDA (Fig. 5d). The responses to the application of 100 μM NMDA were sensitive to the selective NMDA receptor antagonist DL-APV, which markedly blocked Ca^{2+} elevations (Fig. 5e). To clarify the subunit composition of the NMDA receptors, we further tested the effect of 10 μM memantine, which is a very efficient inhibitor of GluN2C- and GluN2D-containing NMDA receptors. The co-application of memantine led to a significant diminishing of the

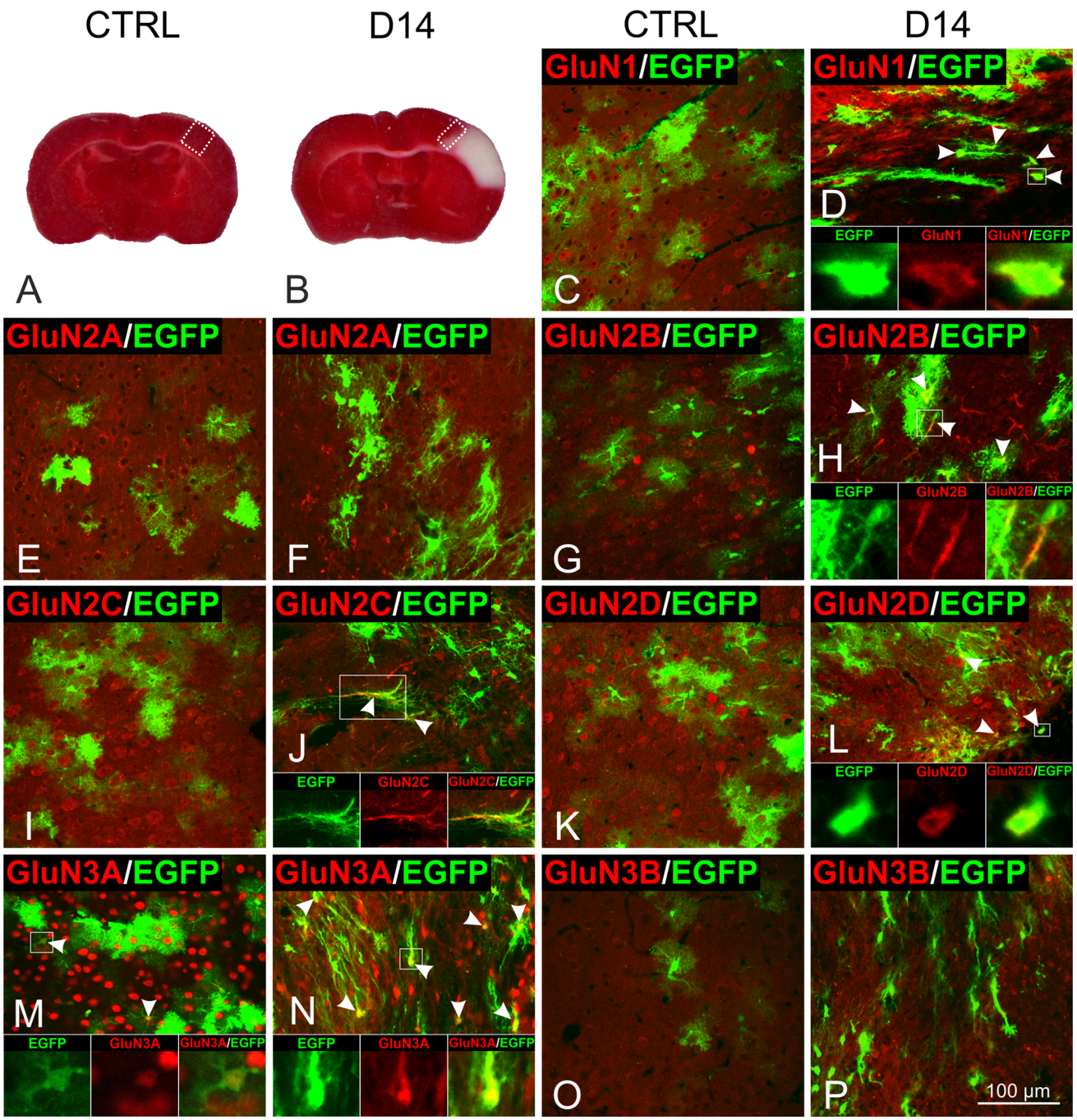
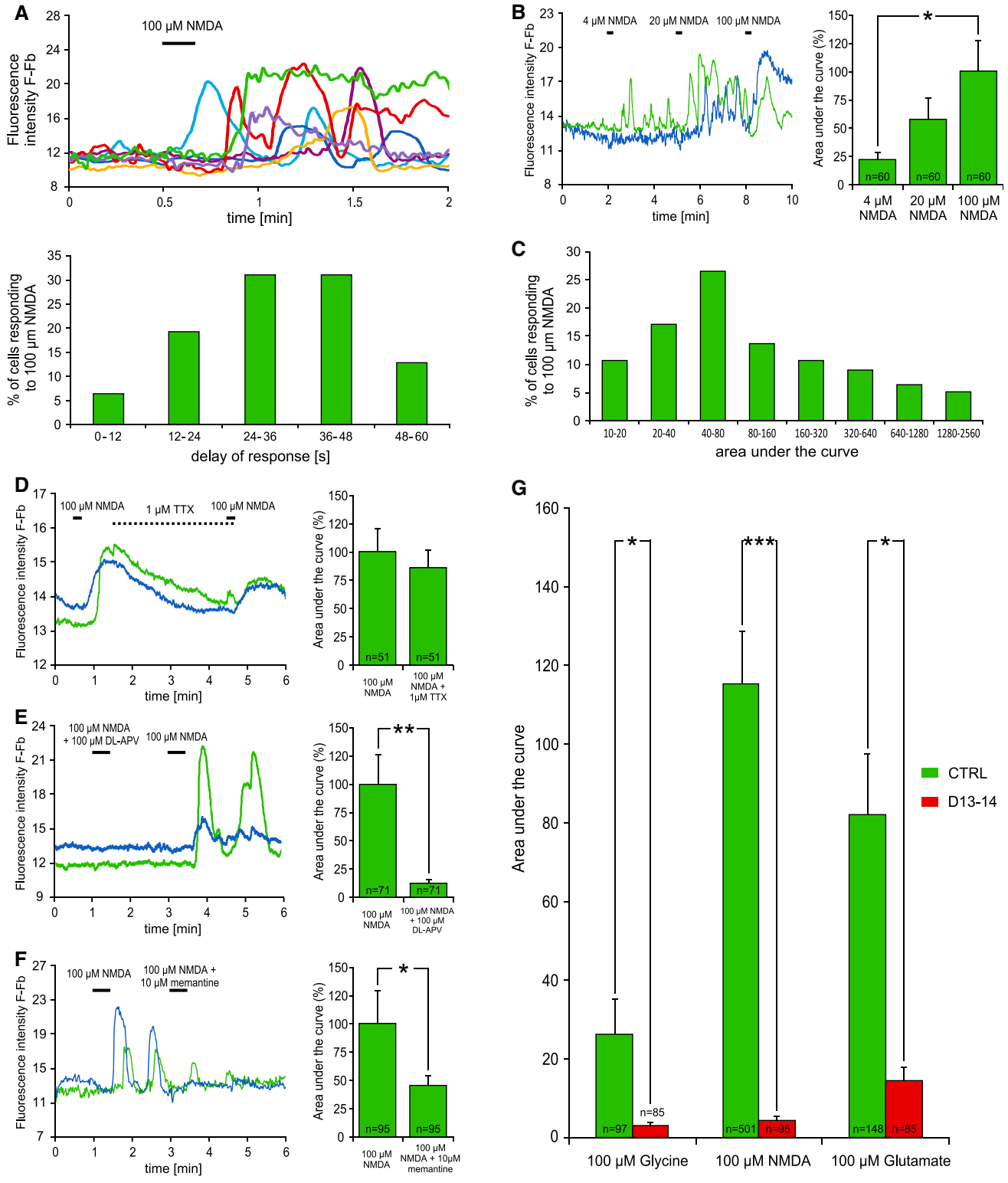


Fig. 4 Immunohistochemical analysis of the GluN1, GluN2A-D, and GluN3A-B subunits of the NMDA receptors in the cortex of adult GFAP/EGFP mice under control conditions (CTRL) and 14 days after MCAo (D14). Coronal brain sections from CTRL (**a**) and D14 (**b**) animals stained with triphenyl tetrazolium chloride. The *white color* in **b** indicates the volume of ischemic tissue at D14. The *boxed areas* indicate the regions in which the immunohistochemical analysis was performed. The *arrowheads* in **c**–**p** indicate the overlay of GFAP/EGFP$^+$ cells and NMDA subunit staining—see figure *insets* for detailed images of cells in *white rectangles*. Note the overlap of the EGFP signal with GluN3A staining in CTRL tissue and GluN1, GluN2B-D, and GluN3A staining at D14. The same *scale bar* applies to all non-inset images

NMDA-evoked Ca^{2+} elevations (Fig. 5f). On the other hand, the co-application of NBQX (AMPA and kainate receptors antagonist) and PPADS (P2X receptors antagonist) did not cause any changes (data not shown).

To study the impact of MCAo, we compared the Ca^{2+} responses in control and D13–14 mice (Fig. 5g). The application of 100 µM NMDA evoked a markedly lower Ca^{2+} influx in the GFAP/EGFP$^+$ cells after MCAo. We


A
100 µM NMDA
Fluorescence intensity F-Fb
time [min]
% of cells responding to 100 µm NMDA
delay of response [s]
0-12
12-24
24-36
36-48
48-60
B
4 µM NMDA
20 µM NMDA
100 µM NMDA
Fluorescence intensity F-Fb
time [min]
Area under the curve (%)
n=60
4 µM NMDA
20 µM NMDA
100 µM NMDA
C
% of cells responding to 100 µm NMDA
area under the curve
10-20
20-40
40-80
80-160
160-320
320-640
640-1280
1280-2560
D
100 µM NMDA
1 µM TTX
100 µM NMDA
Fluorescence intensity F-Fb
time [min]
Area under the curve (%)
n=51
n=51
100 µM NMDA
100 µM NMDA + 1µM TTX
E
100 µM NMDA + 100 µM DL-APV
100 µM NMDA
Fluorescence intensity F-Fb
time [min]
Area under the curve (%)
n=71
n=71
100 µM NMDA
100 µM NMDA + 100 µM DL-APV
F
100 µM NMDA
100 µM NMDA + 10 µM memantine
Fluorescence intensity F-Fb
time [min]
Area under the curve (%)
n=95
n=95
100 µM NMDA
100 µM NMDA + 10µM memantine
G
Area under the curve
CTRL
D13-14
n=97
n=85
n=501
n=95
n=148
n=85
100 µM Glycine
100 µM NMDA
100 µM Glutamate

◀**Fig. 5** Calcium imaging measurements of cortical GFAP/EGFP$^+$ glial cells from GFAP/EGFP mice in situ. **a** Kinetics of the responses to the application of 100 μM NMDA (*top*). Quantification of the delay of the response onset shows that the average delay was ~30 s (*bottom*) ($n = 94$). **b** The concentration dependence of control cells responding to the application of NMDA (4, 20, and 100 μM, *left*) with quantification of the responses (*right*). **c** A histogram of the distribution of Ca^{2+} responses evoked by the application of 100 μM NMDA. Only cells with responses having an area under the curve higher than ten were analyzed ($n = 232$). **d** The co-application of 1 μM TTX did not reveal any significant change in the Ca^{2+} responses evoked by 100 μM NMDA. **e** The selective NMDA receptor blocker DL-APV markedly blocked the Ca^{2+} elevations evoked by the application of 100 μM NMDA. **f** The co-application of memantine decreased the NMDA-evoked Ca^{2+} elevation, which indicates the presence of GluN2C–D subunits in the NMDA receptors. **g** A comparison of the Ca^{2+} responses to the application of 100 μM glycine, 100 μM NMDA, and 100 μM glutamate in control cells (CTRL) and in cells 13–14 days after MCAo (D13–14). *Error bars* represent SEM. Significant differences ($*p < 0.05$, $**p < 0.01$, and $***p < 0.001$) were calculated by one-way ANOVA followed by the Bonferroni post-test (**b**), a paired *t* test (**d–f**), and an unpaired *t* test (**g**); *n* indicates the number of cells

suggest that this might be due to the increased presence of the GluN3A subunit in NMDA receptors after MCAo, which leads to lower Ca^{2+} permeability of NMDA receptors (Perez-Otano et al. 2001; Cavara and Hollmann 2008). The application of 100 μM glycine or 100 μM glutamate followed the same trend as they both evoked lower responses in D13–14 cells when compared to controls (Fig. 5g).

NMDA Receptors in GFAP/EGFP$^+$ Glial Cells – Ca^{2+} Imaging Measurements In Vitro

It is well known that recordings in situ are affected by interactions between cells, particularly by neuron-glia interactions. To address this issue, we characterized the NMDA responses in individual GFAP/EGFP$^+$ glial cells isolated from the somatosensory cortices of control or D13-14 mice and cultured for 5–6 days. The NMDA receptor co-agonist glycine was routinely added to the application of NMDA at 100 μM concentration in in vitro measurements since there was no endogenous source of glycine, but its addition did not cause any significant differences. The kinetics of the Ca^{2+} responses in the cultured cells was different from those recorded in situ. In 77 %of cells, the responses occurred within 12 s following the application of 500 μM NMDA with 100 μM glycine (95 % within 24 s), and fast transient Ca^{2+} spikes were not observed (Fig. 6a). To confirm the specificity of the NMDA responses, we used 100 μM DL-APV, which blocked the Ca^{2+} responses evoked by 500 μM NMDA with 100 μM glycine in all tested cells (data not shown). The ischemic insult had a significant impact on NMDA-evoked responses as only 8.4 % of cells isolated from the injured cortical tissue of D13–14 mice responded to the application of 500 μM NMDA with 100 μM glycine compared to 33.5 % of cells isolated from controls (Fig. 6b). The diminished intracellular Ca^{2+} elevations after NMDA application observed in situ in post-ischemic GFAP/EGFP$^+$ glial cells were thus preserved even after 5-6 days of in vitro cultivation. Since in vitro Ca^{2+} imaging enabled the measurement of Ca^{2+} responses from single cells at much better resolution than in situ, in large ramified cells we observed that the responses to the application of 500 μM NMDA with 100 μM glycine did not occur uniformly in all of the processes, but were present in only some of the processes (Fig. 6c).

Discussion

In the present work, we have shown that post-ischemic glial cells undergo marked changes in the expression of subunits of ionotropic as well as metabotropic glutamate receptors. Our immunohistochemical analyses confirmed the presence of NMDA receptor subunits in GFAP/EGFP$^+$ glial cells, and Ca^{2+} imaging measurements confirmed that changes in the expression of NMDA receptor subunits are also reflected in the functional properties of glial NMDA receptors.

The single-cell RT-qPCR technique provided us with information about the expression levels of 25 genes in single GFAP/EGFP$^+$ glial cells under physiological conditions, but also following focal cerebral ischemia. Most of the genes coding subunits of glutamate receptors increased their expression after MCAo, and the largest increase was observed in *Grm5*. This is an interesting result since the mGluR5 receptor, coded by the *Grm5* gene, is crucial in modulating neuronal activity and in the functioning of tripartite synapses. Our result is in accordance with a recent study showing that the expression of *Grm5* in astrocytes was undetectable after postnatal week 3, in contrast to *Grm3* which was expressed at all developmental stages (Sun et al. 2013). In the current work, we show that the number of GFAP/EGFP$^+$ glial cells expressing the *Grm1* and *Grm3* genes did not significantly change after MCAo; however, *Grm5* became detectable in the majority of these cells, which indicates the importance of this receptor in post-ischemic glia. Since the activation of mGluR5 receptors was shown to result in glutamate, ATP and/or D-serine release from glial cells, they might modulate neuronal activity in the post-ischemic brain (Haydon and Carmignoto 2006). However, mGluR5 receptors were also shown to modulate the expression and function of glutamate transporters in glia and thus participate in regulating extracellular glutamate concentration (Aronica et al. 2003; Vermeiren et al. 2005; D'Antoni et al. 2008). Another

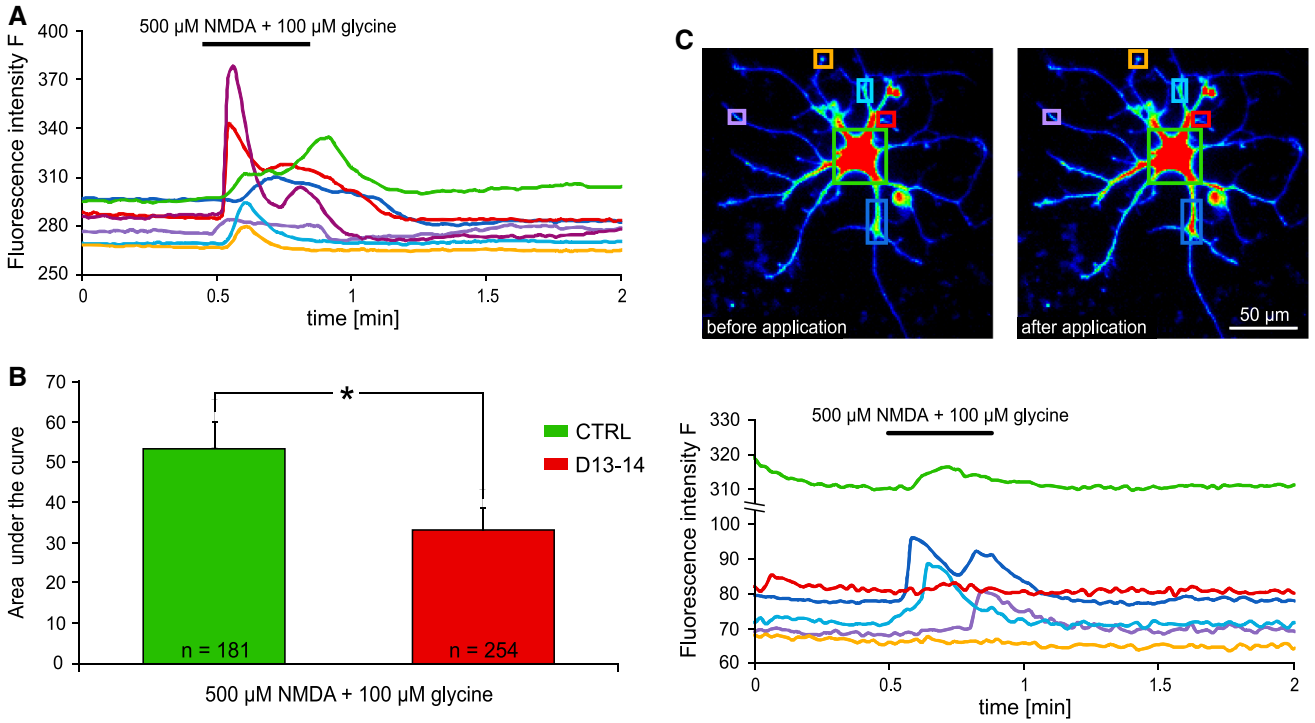


Fig. 6 Calcium imaging measurements of cortical GFAP/EGFP$^+$ glial cells from GFAP/EGFP mice in vitro. **a** Kinetics of the responses to the application of 500 µM NMDA + 100 µM glycine. **b** A comparison of the Ca^{2+} responses to the application of 500 µM NMDA + 100 µM glycine in cells isolated from control mice (CTRL) and those isolated from mice 13–14 days after MCAo (D13–14). *Error bars* represent SEM. *Asterisk* indicates a significant difference ($p < 0.05$) calculated by an unpaired *t* test; *n* indicates the number of cells. **c** Imaging of the Ca^{2+} elevation induced by the application of 500 µM NMDA + 100 µM glycine with a focus on the cell processes. Traces in different *colors* (*bottom*) correspond to the imaged regions in the image of the GFAP/EGFP$^+$ glial cell (*top*). Note that Ca^{2+} elevations were not detected in all of the processes

interesting result was regarding the *Gria2* gene, which was present in 61 % of control cells, a result that did not significantly change after MCAo. This subunit is crucial for Ca^{2+} permeability of AMPA receptors as its presence markedly diminishes their Ca^{2+} permeability (Hollmann et al. 1991; Burnashev et al. 1992). As for the NMDA receptors, the presence of genes coding NMDA receptor subunits was increased in cells after MCAo when compared to controls. The role of NMDA receptors in glial cells is still not fully elucidated, and our data might contribute to unraveling their function, which is presumably also involved in CNS pathologies, such as ischemia or tumors (Aronica et al. 2001). One of their possible roles could be the activation of survival signaling pathways (Hetman and Kharebava 2006) or, as recently shown, astrocytic NMDA receptors can control the exocytosis of gliotransmitters and thus control synaptic transmission and plasticity (Lalo et al. 2014). It is also worth noting that there were 356 cells that expressed at least one gene coding a NMDA receptor subunit in our study, and 236 of them did not express the *Grin1* gene encoding the GluN1 subunit, which according to current knowledge is obligatory in NMDA receptor formation. A similar result was reported by Cahoy and colleagues, who reported the presence of *Grin2c* and *Grin3a* but the absence of *Grin1* in cortical astrocytes (Cahoy et al. 2008). This might be due to the high protein stability of the GluN1 subunit compared to the GluN2-3 subunits as previously reported (Atlason et al. 2007). Moreover, there are indications that murine NMDA receptors can be also co-assembled without the GluN1 subunit (Perez-Otano et al. 2001; Matsuda et al. 2003), but their functional properties are debatable.

The division of control, D7, and D14 cells into three subpopulations according to their gene expression showed that D7 and especially D14 cells have the highest relative expression of most of the genes coding subunits of glutamate receptors (subpopulation SP3), which distinguishes them from control cells. However, in subpopulation SP2, formed mainly by D7 but also by D14 cells, the relative expression of glutamate receptor subunits is lower, indicating that cells after MCAo are not homogeneous.

Interesting results were obtained from the Spearman correlation coefficient analysis between genes in control, D7, and D14 cells. Since we used a GFAP/EGFP$^+$ glial cell population in this study, which among astrocytic markers expressed also NG2 glial markers in some cells, we were

able to study the correlations between particular genes coding glutamate receptor subunits with genes coding markers of astrocytes and NG2 glia. Most of the AMPA receptors are heterotetrameric, consisting of two GluA2 and two GluA1, GluA3, or GluA4 subunits. Since *Gria2* correlated positively with astrocytic and NG2 glial markers, our results indicate that the presence of AMPA receptors is without any preference to these markers. An interesting situation was observed in D14 cells, since *Gria3* positively correlated with astrocytic markers, indicating AMPA receptors of GluA2/GluA3 type in these cells, and *Gria4* correlated with NG2 glial markers, indicating AMPA receptors of GluA2/GluA4 type in these cells (Fig. 3). Several studies have shown that astrocytes possess kainate receptors (Seifert and Steinhäuser 2001; Brand-Schieber et al. 2004), which we also showed in the current work. Moreover, our results suggest that genes coding kainate receptor subunits correlated mostly with those GFAP/EGFP$^+$ cells that expressed NG2 glial markers, which would also confirm the results of a study demonstrating functional kainate receptors in NG2 glia (Kukley and Dietrich 2009; Haberlandt et al. 2011). In D7 cells, we observed a large positive correlation with astrocytic markers, but in D14 cells, most of the genes coding kainate receptor subunits again positively correlated with NG2 glial markers. An interesting correlation pattern was observed with genes coding NMDA receptor subunits. In control cells, these genes positively correlated mostly with NG2 glial markers; only *Grin1* and *Grin2c* were also partially correlated with astrocytic markers. In D7 cells, the number of NMDA subunits correlating with NG2 glial markers was reduced, and their correlation with astrocytic markers was increased. The most intriguing correlation pattern was found in D14 cells, where cells expressing NG2 glial markers were positively correlated with *Grin1* and *Grin3a* and moreover negatively correlated with *Grin2a-d*. This strongly indicates that 14 days after MCAo, the composition of NMDA receptors in the NG2 glial markers expressing GFAP/EGFP$^+$ cells is of the GluN1/GluN3A type. On the other hand, *Grin2a-d* genes were positively correlated with astrocytic markers. As for the metabotropic glutamate receptors, control cells expressing astrocytic markers seemed to possess mGluR3 receptors but not mGluR1, whereas genes coding both of these receptors also partially correlated with NG2 glial markers. This situation changed completely in D14 cells, where genes coding metabotropic glutamate receptors positively correlated with astrocytic and negatively with NG2 glial markers.

To study glutamate receptors also on the protein level, we performed an immunohistochemical analysis of the entire set of the 7 currently known NMDA receptor subunits of GFAP/EGFP$^+$ glial cells in the adult mouse cortex. To the best of our knowledge, our analysis provides the first immunohistochemical evidence that GFAP/EGFP$^+$ glial cells in the cortex possess GluN3A subunits, which has previously been discussed in many works (Verkhratsky and Kirchhoff 2007; Palygin et al. 2011; Kehoe et al. 2013). Under control conditions, we did not observe GFAP/EGFP$^+$ cells positive for any NMDA receptor subunit, apart from GluN3A. This might be due to the fact that under control conditions, astrocytes have a bushy-like morphology with many fine processes. It was previously shown by electron microscopy that the GluN1 and GluN2A/B NMDA receptor subunits are present in astrocytes especially in the processes and not in the cellular bodies (Conti et al. 1996). The fluorescent immunohistochemical method is not able to distinguish NMDA receptor subunit positivity in fine processes from the background signal. On the other hand, reactive astrocytes present in the cortices of GFAP/EGFP mice 14 days after MCAo have a fibrous morphology with sharp edges separating them from the surrounding tissue, which enables the detection of positive staining for NMDA receptor subunits in these cells. Our immunohistochemical analysis clearly showed the positivity of cortical GFAP/EGFP$^+$ cells for the GluN1, GluN2B-D, and GluN3A subunits 14 days after MCAo, which indicates the importance of NMDA receptors in glial cells under ischemic conditions. The GluN2A subunit was detected in cells that morphologically resembled neurons, but not in GFAP/EGFP$^+$ cells. Since the single-cell RT-qPCR results indicate that GFAP/EGFP$^+$ cells should contain this subunit, we hypothesize that it was not detected due to some post-translational modifications of the GluN2A protein or miRNA regulation, which might be specific to glia. In summary, the immunohistochemical analysis confirmed the presence of NMDA receptor subunits in GFAP/EGFP$^+$ glial cells, especially after ischemia.

The NMDA receptors in GFAP/EGFP$^+$ glial cells were also subjected to functional study utilizing a Ca^{2+} imaging technique. Calcium responses to the application of 100 μM NMDA were delayed in situ by ~30 s on average, as also reported in other studies (Serrano et al. 2008; Serrano et al. 2006; Porter and McCarthy 1995). We attribute this delay to the slow diffusion of NMDA in the brain tissue, which is supported by the fact that there were immediate responses in cultivated cells. There have been several studies showing a TTX-mediated partial reduction of NMDA-evoked responses (Schipke et al. 2001; Serrano et al. 2006, 2008). Similar to a study of oligodendrocytic NMDA receptors (Káradóttir et al. 2005), we did not observe any significant changes associated with the use of TTX, which might also be due to the fact that our application was relatively short and locally focused, in contrast to the above-mentioned studies showing a TTX-mediated effect (bath application for several minutes). As for the subunit composition of the

NMDA receptors, our results suggest a tri-heteromeric composition of the GluN1/GluN2C/GluN3A type. This is supported by the weak Mg^{2+} block observed for NMDA receptors containing the GluN3A subunit (Sasaki et al. 2002; Kehoe et al. 2013), as we observed Ca^{2+} elevations in aCSF that contained Mg^{2+} without the need for cell depolarization. Based on our single-cell RT-qPCR (Fig. 1) and immunohistochemical analyses (Fig. 4) showing low mRNA levels of *Grin3b* and the absence of GluN3B immunoreactivity, we do not assume the inclusion of the GluN3B subunit in the NMDA receptors. Di-heteromeric GluN1/GluN3A receptors have, however, no binding site for glutamate or NMDA, so the inclusion of the GluN2 subunit is also needed. Our data with memantine, which is an efficient inhibitor of GluN2C and GluN2D subunits (Kotermanski and Johnson 2009), suggest the incorporation of one of these subunits as well. Based on our single-cell RT-qPCR data, which show much higher expression of *Grin2c* in comparison to *Grin2d* in controls (Fig. 1), we suppose that at least in controls, the NMDA receptors contain mainly the GluN2C subunit. Nonetheless, we cannot exclude the possibility that GFAP/EGFP$^+$ glial cells also possess GluN1/GluN2 NMDA receptors. We hypothesize that these could provide an amplification of the Ca^{2+} signal upon local depolarization, which would release the Mg^{2+} block. The application of NBQX and PPADS did not support the hypothesis that this local depolarization would be provided via AMPA, Kainate, or P2X receptors.

Both in situ and in vitro experiments showed that the application of NMDA evoked significantly lower Ca^{2+} elevations in GFAP/EGFP$^+$ glial cells 13–14 days after MCAo when compared to control cells, which we hypothesize is due to the increased involvement of the GluN3A subunit as shown by our single-cell RT-qPCR and immunohistochemical analyses. The decreased Ca^{2+} permeability of NMDA receptors can be further caused by the incorporation of the GluN2D subunit in NMDA receptors (Burnashev et al. 1995; Paoletti 2011; Evans et al. 2012), which was also highly upregulated 14 days after MCAo. Another reason for decreased Ca^{2+} permeability of NMDA receptors might be their internalization, which was shown to be regulated by the particular subunit compositions (Lavezzari et al. 2004), and, for example, GluN3A internalization is regulated via phosphorylation of a tyrosine residue (Y971) within the GluN3A intracellular C-terminal tail (Chowdhury et al. 2013). Therefore, we cannot completely rule out the possibility that NMDA receptors in GFAP/EGFP$^+$ glial cells are internalized or inactivated by the Ca^{2+}-calmodulin complex after MCAo (Ehlers et al. 1996). Interestingly, the Ca^{2+} permeability of astrocytic NMDA receptors after ischemia is region-specific, since as shown by Krebs and colleagues, acutely isolated hippocampal astrocytes displayed NMDA-evoked Ca^{2+} elevations 20 days after global cerebral ischemia (Krebs et al. 2003). The number of cells responding to the application of 100 μM glutamate in situ was also decreased after MCAo, but some Ca^{2+} influx was still detected, which is probably due to the presence of Ca^{2+}-permeable non-NMDA glutamate receptors. These could be ionotropic AMPA or kainate glutamate receptors (Burnashev et al. 1992), but also metabotropic mGluR5 glutamate receptors coded by the *Grm5* gene, which becomes strongly expressed in D14 cells and which mediates intracellular calcium elevations by releasing calcium from intracellular stores (Nakahara et al. 1997). In vitro cultivated GFAP/EGFP$^+$ glial cells isolated from young adult mice enabled us to study NMDA-evoked responses in detail. Calcium imaging measurements revealed that the responses were process-specific, which corresponds with recent studies showing microdomains within astrocytic territories (Shigetomi et al. 2013). Moreover, this suggests that the response rates in our in situ experiments might be slightly underestimated since we recorded a signal only from the cellular body and not from the processes, where the responses probably originate (Schipke et al. 2001). The results obtained by Ca^{2+} imaging measurements thus supplement the data from single-cell RT-qPCR and immunohistochemical analysis and underline the changes of NMDA receptors in post-ischemic GFAP/EGFP$^+$glial cells.

In summary, our study provides an overall picture of ionotropic and metabotropic glutamate receptor expression in cortical GFAP/EGFP$^+$ glial cells. We show how the expression of particular subunits of these receptors changes after focal cerebral ischemia. On the functional level, we further show that NMDA-mediated Ca^{2+} elevations significantly decrease after ischemia in GFAP/EGFP$^+$ glial cells, which is presumably due to the involvement of the GluN3A subunit. We believe that our study thus adds a new piece of the puzzle to the picture, from which we will eventually understand all of the complex processes, including neuron-glia interaction or glutamate-mediated signaling, in glial cells and which might serve as a guide for research into precisely targeted therapeutics.

Acknowledgments This study was supported by the Grants GA CR P304/12/G069 and GACR 13-02154S from the Grant Agency of the Czech Republic, GAUK 604212 from the Grant Agency of the Charles University in Prague, CZ.1.05/1.1.00/02.0109 from the European Regional Development Fund, and CZ.1.07/2.3.00/30.0045 from the European Social Fund and the state budget of the Czech Republic.

Conflict of interest The authors declare that they have no conflict of interest.

References

Aronica E, van Vliet EA, Mayboroda OA et al (2000) Upregulation of metabotropic glutamate receptor subtype mGluR3 and mGluR5 in reactive astrocytes in a rat model of mesial temporal lobe epilepsy. Eur J Neurosci 12:2333–2344

Aronica E, Leenstra S, Jansen GH et al (2001) Expression of brain-derived neurotrophic factor and tyrosine kinase B receptor proteins in glioneuronal tumors from patients with intractable epilepsy: colocalization with N-methyl-D-aspartic acid receptor. Acta Neuropathol 101:383–392

Aronica E, Gorter JA, Ijlst-Keizers H et al (2003) Expression and functional role of mGluR3 and mGluR5 in human astrocytes and glioma cells: opposite regulation of glutamate transporter proteins. Eur J Neurosci 17:2106–2118. doi:10.1046/j.1460-9568.2003.02657.x

Atlason PT, Garside ML, Meddows E et al (2007) N-Methyl-D-aspartate (NMDA) receptor subunit NR1 forms the substrate for oligomeric assembly of the NMDA receptor. J Biol Chem 282:25299–25307. doi:10.1074/jbc.M702778200

Benesova J, Rusnakova V, Honsa P et al (2012) Distinct expression/function of potassium and chloride channels contributes to the diverse volume regulation in cortical astrocytes of GFAP/EGFP mice. PLoS One 7:e29725. doi:10.1371/journal.pone.0029725

Brand-Schieber E, Lowery SL, Werner P (2004) Select ionotropic glutamate AMPA/kainate receptors are expressed at the astrocyte-vessel interface. Brain Res 1007:178–182. doi:10.1016/j.brainres.2003.12.051

Burnashev N, Khodorova A, Jonas P et al (1992) Calcium-permeable AMPA-kainate receptors in fusiform cerebellar glial cells. Science 256:1566–1570

Burnashev N, Zhou Z, Neher E, Sakmann B (1995) Fractional calcium currents through recombinant GluR channels of the NMDA, AMPA and kainate receptor subtypes. J Physiol 485(Pt 2):403–418

Cahoy JD, Emery B, Kaushal A et al (2008) A transcriptome database for astrocytes, neurons, and oligodendrocytes: a new resource for understanding brain development and function. J Neurosci 28:264–278. doi:10.1523/JNEUROSCI.4178-07.2008

Castillo C, Norcini M, Martin Hernandez LA et al (2013) Satellite glia cells in dorsal root ganglia express functional NMDA receptors. Neuroscience 240:135–146. doi:10.1016/j.neuroscience.2013.02.031

Cavara NA, Hollmann M (2008) Shuffling the deck anew: how NR3 tweaks NMDA receptor function. Mol Neurobiol 38:16–26. doi:10.1007/s12035-008-8029-9

Chowdhury D, Marco S, Brooks IM et al (2013) Tyrosine phosphorylation regulates the endocytosis and surface expression of GluN3A-containing NMDA receptors. J Neurosci 33(9):4151–4164

Conti F, DeBiasi S, Minelli A, Melone M (1996) Expression of NR1 and NR2A/B subunits of the NMDA receptor in cortical astrocytes. Glia 17:254–258. doi:10.1002/(SICI)1098-1136(199607)17:3<254:AID-GLIA7>3.0.CO;2-0

D'Antoni S, Berretta A, Bonaccorso CM et al (2008) Metabotropic glutamate receptors in glial cells. Neurochem Res 33:2436–2443. doi:10.1007/s11064-008-9694-9

Dzamba D, Honsa P, Anderova M (2013) NMDA receptors in glial cells: pending questions. Curr Neuropharmacol 11:250–262. doi:10.2174/1570159X11311030002

Ehlers MD, Zhang S, Bernhadt JP, Huganir RL (1996) Inactivation of NMDA receptors by direct interaction of calmodulin with the NR1 subunit. Cell 84:745–755

Evans RC, Morera-Herreras T, Cui Y et al (2012) The effects of NMDA subunit composition on calcium influx and spike timing-dependent plasticity in striatal medium spiny neurons. PLoS Comput Biol 8:e1002493. doi:10.1371/journal.pcbi.1002493

Gottlieb M, Matute C (1997) Expression of ionotropic glutamate receptor subunits in glial cells of the hippocampal CA1 area following transient forebrain ischemia. J Cereb Blood Flow Metab 17:290–300. doi:10.1097/00004647-199703000-00006

Haberlandt C, Derouiche A, Wyczynski A et al (2011) Gray matter NG2 cells display multiple Ca^{2+}-signaling pathways and highly motile processes. PLoS One 6:e17575. doi:10.1371/journal.pone.0017575

Haydon P, Carmignoto G (2006) Astrocyte control of synaptic transmission and neurovascular coupling. Physiol Rev. doi:10.1152/physrev.00049.2005

Hetman M, Kharebava G (2006) Survival signaling pathways activated by NMDA receptors. Curr Top Med Chem 6:787–799

Hollmann M, Hartley M, Heinemann S (1991) Ca^{2+} permeability of KA-AMPA–gated glutamate receptor channels depends on subunit composition. Science 252:851–853

Honsa P, Pivonkova H, Dzamba D et al (2012) Polydendrocytes display large lineage plasticity following focal cerebral ischemia. PLoS One 7:e36816. doi:10.1371/journal.pone.0036816

Káradóttir R, Cavelier P, Bergersen L, Attwell D (2005) NMDA receptors are expressed in oligodendrocytes and activated in ischaemia. Nature 438:1162–1166. doi:10.1038/nature04302.NMDA

Kehoe LA, Bernardinelli Y, Muller D (2013) GluN3A: an NMDA receptor subunit with exquisite properties and functions. Neural Plast 2013:145387. doi:10.1155/2013/145387

Kotermanski SE, Johnson JW (2009) Mg^{2+} imparts NMDA receptor subtype selectivity to the Alzheimer's drug memantine. J Neurosci 29:2774–2779. doi:10.1523/JNEUROSCI.3703-08.2009

Krebs C, Fernandes HB, Sheldon C et al (2003) Functional NMDA receptor subtype 2B is expressed in astrocytes after ischemia in vivo and anoxia in vitro. J Neurosci 23:3364–3372

Kukley M, Dietrich D (2009) Kainate receptors and signal integration by NG2 glial cells. Neuron Glia Biol 5:13–20

Lalo U, Pankratov Y, Kirchhoff F et al (2006) NMDA receptors mediate neuron-to-glia signaling in mouse cortical astrocytes. J Neurosci 26:2673–2683. doi:10.1523/JNEUROSCI.4689-05.2006

Lalo U, Palygin O, Rasooli-Nejad S et al (2014) Exocytosis of ATP from astrocytes modulates phasic and tonic inhibition in the neocortex. PLoS Biol 12:e1001747. doi:10.1371/journal.pbio.1001747

Lavezzari G, McCallum J, Dewey CM et al (2004) Subunit-specific regulation of NMDA receptor endocytosis. J Neurosci 24(28):6383–6391

Loane DJ, Stoica BA, Faden AI (2012) Metabotropic glutamate receptor-mediated signaling in neuroglia. Wiley Interdiscip Rev Membr Transp Signal 1:136–150. doi:10.1002/wmts.30

Matsuda K, Fletcher M, Kamiya Y, Yuzaki M (2003) Specific assembly with the NMDA receptor 3B subunit controls surface expression and calcium permeability of NMDA receptors. J Neurosci 23:10064–10073

Matthias K, Kirchhoff F, Seifert G et al (2003) Segregated expression of AMPA-type glutamate receptors and glutamate transporters defines distinct astrocyte populations in the mouse hippocampus. J Neurosci 23:1750–1758

Nakahara K, Okada M, Nakanishi S (1997) The metabotropic glutamate receptor mGluR5 induces calcium oscillations in cultured astrocytes via protein kinase C phosphorylation. J Neurochem 69:1467–1475

Nolte C, Matyash M, Pivneva T et al (2001) GFAP promoter-controlled EGFP-expressing transgenic mice: a tool to visualize astrocytes and astrogliosis in living brain tissue. Glia 33:72–86

Palygin O, Lalo U, Pankratov Y (2011) Distinct pharmacological and functional properties of NMDA receptors in mouse cortical astrocytes. Br J Pharmacol 163:1755–1766. doi:10.1111/j.1476-5381.2011.01374.x

Paoletti P (2011) Molecular basis of NMDA receptor functional diversity. Eur J Neurosci 33:1351–1365. doi:10.1111/j.1460-9568.2011.07628.x

Perez-Otano I, Schulteis CT, Contractor A et al (2001) Assembly with the NR1 subunit is required for surface expression of NR3A-containing NMDA receptors. J Neurosci 21:1228–1237

Porter JT, McCarthy KD (1995) GFAP-positive hippocampal astrocytes in situ respond to glutamatergic neuroligands with increases in $[Ca^{2+}]_i$. Glia 13:101–112

Rusnakova V, Honsa P, Dzamba D et al (2013) Heterogeneity of astrocytes: from development to injury—single cell gene expression. PLoS One 8:e69734. doi:10.1371/journal.pone.0069734

Sasaki YF, Rothe T, Premkumar LS et al (2002) Characterization and comparison of the NR3A subunit of the NMDA receptor in recombinant systems and primary cortical neurons. J Neurophysiol 87:2052–2063. doi:10.1152/jn.00531.2001

Schipke CG, Ohlemeyer C, Matyash M et al (2001) Astrocytes of the mouse neocortex express functional N-methyl-D-aspartate receptors. FASEB J 15:1270–1272

Seifert G, Steinhäuser C (2001) Ionotropic glutamate receptors in astrocytes. Prog Brain Res 132:287–299. doi:10.1016/S0079-6123(01)32083-6

Serrano A, Haddjeri N, Lacaille J-C, Robitaille R (2006) GABAergic network activation of glial cells underlies hippocampal heterosynaptic depression. J Neurosci 26:5370–5382. doi:10.1523/JNEUROSCI.5255-05.2006

Serrano A, Robitaille R, Lacaille J-C (2008) Differential NMDA-dependent activation of glial cells in mouse hippocampus. Glia 56:1648–1663. doi:10.1002/glia.20717

Shigetomi E, Bushong EA, Haustein MD et al (2013) Imaging calcium microdomains within entire astrocyte territories and endfeet with GCaMPs expressed using adeno-associated viruses. J Gen Physiol 141:633–647. doi:10.1085/jgp.201210949

Ståhlberg A, Bengtsson M (2010) Single-cell gene expression profiling using reverse transcription quantitative real-time PCR. Methods 50:282–288. doi:10.1016/j.ymeth.2010.01.002

Ståhlberg A, Andersson D, Aurelius J et al (2011) Defining cell populations with single-cell gene expression profiling: correlations and identification of astrocyte subpopulations. Nucleic Acids Res 39:e24. doi:10.1093/nar/gkq1182

Sun W, McConnell E, Pare J-F et al (2013) Glutamate-dependent neuroglial calcium signaling differs between young and adult brain. Science 339:197–200. doi:10.1126/science.1226740

Ulas J, Satou T, Ivins KJ et al (2000) Expression of metabotropic glutamate receptor 5 is increased in astrocytes after kainate-induced epileptic seizures. Glia 30:352–361

Verkhratsky A (2009) Neuronismo y reticulismo: neuronal-glial circuits unify the reticular and neuronal theories of brain organization. Acta Physiol (Oxf) 195:111–122. doi:10.1111/j.1748-1716.2008.01926.x

Verkhratsky A, Kirchhoff F (2007) NMDA receptors in glia. Neuroscientist 13:28–37. doi:10.1177/1073858406294270

Vermeiren C, Najimi M, Vanhoutte N et al (2005) Acute up-regulation of glutamate uptake mediated by mGluR5a in reactive astrocytes. J Neurochem 94:405–416. doi:10.1111/j.1471-4159.2005.03216.x

Send Orders of Reprints at reprints@benthamscience.net

250 *Current Neuropharmacology*, **2013**, *11*, **250-262**

NMDA Receptors in Glial Cells: Pending Questions

David Dzamba, Pavel Honsa and Miroslava Anderova*

Department of Cellular Neurophysiology, Institute of Experimental Medicine AS CR, Prague, Czech Republic and Second Medical Faculty, Charles University, Prague, Czech Republic

Abstract: Glutamate receptors of the N-methyl-D-aspartate (NMDA) type are involved in many cognitive processes, including behavior, learning and synaptic plasticity. For a long time NMDA receptors were thought to be the privileged domain of neurons; however, discoveries of the last 25 years have demonstrated their active role in glial cells as well. Despite the large number of studies in the field, there are many unresolved questions connected with NMDA receptors in glia that are still a matter of debate. The main objective of this review is to shed light on these controversies by summarizing results from all relevant works concerning astrocytes, oligodendrocytes and polydendrocytes (also known as NG2 glial cells) in experimental animals, further extended by studies performed on human glia. The results are divided according to the study approach to enable a better comparison of how findings obtained at the mRNA level correspond with protein expression or functionality. Furthermore, special attention is focused on the NMDA receptor subunits present in the particular glial cell types, which give them special characteristics different from those of neurons – for example, the absence of Mg^{2+} block and decreased Ca^{2+} permeability. Since glial cells are implicated in important physiological and pathophysiological roles in the central nervous system (CNS), the last part of this review provides an overview of glial NMDA receptors with respect to ischemic brain injury.

Keywords: Astrocytes, ischemia, NG2 glia, NMDA receptors, oligodendrocyte progenitors, oligodendrocytes, polydendrocytes.

INTRODUCTION

NMDA Receptors

NMDA receptors are named after their selective agonist N-methyl-D-aspartate and belong to the family of ionotropic glutamate receptors. The receptors are heterotetramers comprising a combination of GluN1, GluN2A-D and GluN3A-B subunits. Splice variants have been reported for most of the NMDA receptor subunits, but the best studied is the GluN1 subunit with 8 different isoforms [1]. The main agonists are glutamate and NMDA, with their binding site on GluN2 subunits, while the binding site for the co-agonists D-serine and glycine is located on GluN1 and GluN3 subunits. The most common composition of functional NMDA receptors involves two GluN1 and two GluN2 subunits, or two GluN1, one GluN2 and one GluN3 subunits. NMDA receptors composed of GluN1 and GluN3 subunits are also functional, but they lack the glutamate/NMDA binding site [2]. The large variety in possible NMDA receptor compositions leads to a large variation in their functional properties such as conductivity, deactivation time, sensitivity to Mg^{2+} and antagonist specificity. Furthermore, the composition of NMDA receptors differs among brain regions and also depends on the developmental stages [3]. Activated NMDA receptors are permeable to Ca^{2+}, Na^{+} and K^{+}; however, their permeability to certain ions is strongly dependent on the subunit composition, e.g., including the GluN3 subunit leads to decreased Mg^{2+} block and reduced Ca^{2+} and overall current permeability [4]. Since NMDA receptors are present on the majority of neurons and play a key role in mediating signal transduction in neuronal networks, they are the target of several drugs used for anaesthesia or the treatment of neurodegenerative diseases [5,6]. Interestingly, in the last 25 years a number of studies have emerged describing the presence of NMDA receptors also on glial cells [7].

Glial Cells

It is not surprising that the first attempts to detect NMDA receptors on glial cells were performed on the most well-known and most abundant glial cell type – astrocytes. These cells consist of several subtypes based on the brain region and currently, researchers distinguish protoplasmic astrocytes in the grey matter, fibrillary astrocytes in the white matter, Bergmann glia in the cerebellum and Muller cells in the retina. The common property of these subtypes is their complex bushy morphology and the apparent larger size of their domains in larger–brained primates, possibly enabling the control of more synapses with fewer astrocytic somata [8]. The large surface area of astrocytes, their interconnection by gap junctions and their expression of leak potassium channels allow them to maintain K^{+} homeostasis in the CNS *via* K^{+} spatial buffering and thus to control neuronal activity [9]. In addition, astrocytes contribute to overall homeostasis in the neuronal tissue, including control of pH [10], the uptake of neurotransmitters [11], cerebral blood flow [12], the astrocyte-neuronal lactate shuttle [13], antioxidant function [14] and water transport [15]. An important feature of astrocytes is their ability to detect changes in their

*Address correspondence to this author at the Department of Cellular Neurophysiology, Institute of Experimental Medicine AS CR, Prague, Czech Republic and Second Medical Faculty, Charles University, Prague, Czech Republic; Tel: +420 241 062 050; Fax: +420 296 442 783;
E-mail: anderova@biomed.cas.cz

1875-6190/13 $58.00+.00 **©2013 Bentham Science Publishers**

surroundings through many types of receptors. Beside a variety of metabotropic receptors, astrocytes also express ionotropic receptors for a large number of common neurotransmitters including glutamate [16]. Astrocytic endfeet which contain AMPA and NMDA receptors enwrap synaptic clefts and are thus able to modulate synaptic plasticity [7]. AMPA and NMDA receptors serve as sensors in this process; since they differ in their sensitivity to glutamate and their desensitization rate, they provide information about the duration and concentration of glutamate in the synaptic cleft. Moreover, astrocytes are able to release various chemical transmitters in a Ca^{2+}-dependent manner [17]. Besides the classical types of astrocytes, there exist astrocyte-like adult neural stem cells (aNSC), which are localized in the SVZ and RMS and play an important role in the process of adult neurogenesis. Platel and co-authors described that neuroblasts use NMDA receptors to detect glutamate released in a Ca^{2+}-dependent manner from aNSC [18]; however, the presence of NMDA receptors in aNSC has never been proven.

Astrocytes also play an important role in many pathological processes. They react to injury by the increased expression of a variety of proteins, which causes their transformation into "reactive" astrocytes, a state with specific structural and functional characteristics. In CNS pathologies, reactive astrocytes represent a double-edged sword; on the one hand, they worsen the extent of injury due to the release of pro-apoptotic substances and Ca^{2+} to the surrounding healthy cells through gap-junctions, while on the other hand, they contribute to regenerative processes during the chronic phase of injury [19,20]. Unravelling the variety of newly expressed receptors and activated signalling pathways [21] that guide the activation of astrocytes may contribute to the development of therapies that could decrease the negative influence of astrocytes while enhancing their positive effect on the outcome of pathological processes.

When compared to the many complex functions of astrocytes, the role of oligodendrocytes in the CNS may appear to be less significant. However, this second most abundant glial cell population plays a crucial role in generating and maintaining myelin. By encapsulating neuronal axons with myelin, they enable the fast and efficient conduction of action potentials without any inappropriate increase in axonal diameter. Under pathological conditions oligodendrocytes, like neurons, are highly sensitive to damage by oxidative stress, trophic factor deprivation, the activation of apoptotic pathways and excitatory amino acids [22]. Such significant sensitivity to excitatory amino acids is probably caused by the expression and sustained activation of 2-amino-3-(3-hydroxy-5-methyl-isoxazol-4-yl) propanoic acid (AMPA), kainate or NMDA receptors, which initiate oligodendrocyte damage by cytoplasmic Ca^{2+} overload [23]. Describing the exact composition of these oligodendroglial receptors and discovering specific blockers could lead to the development of protective therapy in white matter pathologies without negative side effects on the neuronal population [24].

The third class of macroglia in the adult mammalian brain are cells expressing chondroitin sulphate proteoglycan NG2 [also known as oligodendrocyte precursor cells (OPCs), synantocytes or polydendrocytes]. These cells are widespread in the grey and white matter of the CNS; they comprise 8–9% of the total cell population in the white matter and 2–3% in the grey matter [25]. This glial cell population was first described more than 20 years ago [26]; however, only recently they have started to attract attention after the discovery of their special properties. Polydendrocytes are the most proliferative cells in the adult mammalian brain, as was shown in several studies that described that any given time, approximately half of them were in the interphase of the cell cycle [27-29]. A large number of studies sought to identify the reason for this extensive proliferative ability and found that a significant number of polydendrocytes change their phenotype and differentiate into other cell types. Polydendrocytes are able to divide symmetrically without retracting their processes or changing their morphology while giving rise to another polydendrocyte [27,30]; furthermore, these cells are also an important source of newly-derived postnatal oligodendrocytes [31]. Moreover, a number of studies have described the ability of these cells to differentiate not only into oligodendrocytes, but also into astrocytes and neuronal cells in the healthy [32] or injured CNS [33,34]. Another interesting feature of polydendrocytes is their ability to communicate with other cells. In contrast to astrocytes, which connect to each other by electrical synapses [35], polydendrocytes were shown to form classical chemical synapses with neighbouring neurons [36]; this may be an important communication channel that enables controlling polydendrocytic proliferation and/or differentiation. Polydendrocytes are equipped with a number of ionotropic ligand-gated receptors, predominantly AMPA or γ-aminobutyric acid (GABA) receptors; however, several studies also reported the surprising presence of receptors with properties similar to NMDA receptors.

ASTROCYTIC NMDA RECEPTORS

Expression of NMDA Receptor Subunits in Astrocytes

In the last two decades there have been several attempts to detect subunits of NMDA receptors in astrocytes. In one of the first studies, Conti *et al*. used *in situ* hybridization together with immunocytochemistry to detect a marker of astrocytes – glial fibrillary acidic protein (GFAP) – and showed that in adult rat cortical slices virtually no astrocytes contained mRNA transcripts of the GluN1 subunit [37]. Other *in situ* hybridization studies in adult rat cerebellar Bergmann glial cells confirmed the presence of GluN2C and GluN2B mRNA transcripts [3,38] which; however, cannot form functional NMDA receptors without the GluN1 subunit. The absence of GluN1 transcripts in cultivated as well as acutely isolated astrocytes from 1-17 day-old mice was also confirmed by Affymetrix GeneChip Arrays [39]. Nevertheless, in mature acutely isolated cortical astrocytes, Cahoy and co-authors confirmed the presence of GluN2C transcripts, which were statistically highly enriched when compared to their numbers in neurons or oligodendrocytes. It is very interesting that in all astrocytes tested, a high level of GluN3A subunit transcripts was detected. In the study of Cahoy both the genes coding GluN2C and GluN3A subunits were statistically augmented in acutely isolated astrocytes when compared to cultured ones. In contrast to these findings, there are also studies showing the presence of the

crucial GluN1 mRNA in astrocytes. In the first of these, reverse transcriptase polymerase chain reaction (RT-PCR) analysis of fluorescence-activated cell sorted astrocytes acutely isolated from the cortices of 2-week-old GFAP/EGFP transgenic mice revealed the presence of GluN1, GluN2B and GluN2C and the absence of GluN2A, GluN2D and GluN3 mRNA transcripts [40]. In another work studying astrocytes in primary cultures prepared from newborn mice, the authors showed the presence of GluN1 mRNA transcripts in these cells, which was significantly down-regulated after 2 weeks of cultivation [41]. On the other hand, the mRNA levels of GluN2A and GluN2B significantly increased with cultivation time for up to 4 weeks. Another very interesting result, especially with respect to human medicine, was obtained using end-point PCR results and showed that cultivated astrocytes isolated from both adult humans and human fetuses express the mRNA of all known NMDA receptor subunits, GluN1, GluN2A-D and GluN3A-B [42].

The first attempt to detect NMDA receptors in astrocytes on the protein level was performed in the rat visual cortex. GluN1 immunoreactivity in the astrocytic processes was detected by electron microscopy, especially in the deeper cortical layers starting at postnatal day 14. By postnatal day 30, the GluN1 immunoreactive profile in these layers became predominantly astroglial [43]. GluN1 and GluN2A/B immunoreactivity in adult rat cortical astrocytes was also confirmed by Conti and co-authors and was detected primarily in the astrocytic processes and occasionally in the cell bodies [44]. In astrocytic primary cultures prepared from the cortex of newborn mice, only a few astrocytes were GluN1- or GluN2B-positive, while the majority of them was negative [41]. The presence of NMDA receptor subunits seems to be brain region-specific, since in the CA1 region of the adult rat hippocampus, no GluN1 or GluN2A/B immunostaining was detected in astrocytes under physiological conditions [45,46]. In contrast to the hippocampus, the GluN1 protein was detected in adult rat astrocytes in the basolateral amygdala and the bed nucleus of the stria terminalis [47], the lateral and basal nuclei of the amygdala [48] and the nucleus locus coeruleus [49]. The results obtained in rat astrocytes are in accord with those reported from studies on human astrocytes. Conti *et al*. showed that the processes of human cortical astrocytes are immunopositive for GluN1, GluN2A and/or GluN2B subunits [50]. The study of Lee and colleagues confirmed the presence of all NMDA receptor subunits located on the membrane of cultivated astrocytes isolated from 16-19 week-old fetuses [42]. GluN1-positive cells were also found in cultured Muller glial cells isolated from the adult human retina, as confirmed by Western blots [51].

NMDA-specific Current/Ca^{2+} Entry in Astrocytes

There are a large number of functional studies providing insight into the astrocytic NMDA receptors enigma and clearly showing that astrocytic NMDA receptors are brain region-specific.

Cerebral Cortex

In the cerebral cortex, the first attempts to detect NMDA receptors in astrocytes were performed on murine cultures prepared from neonatal animals. Even though glutamate, aspartate, kainate and several other neurotransmitters evoked electrophysiological responses, in none of these studies were NMDA-specific responses detected in response to NMDA application [52-55]. Similar results were obtained in calcium imaging experiments on cultured cerebral astrocytes [56-58]. The only exception was the study of Zhang and co-authors, in which the NMDA receptor antagonist (2R)-amino-5-phosphonopentanoate (D-AP5) diminished the Ca^{2+} response to glutamate [59]. Completely different results were obtained when cortical astrocytes were studied in slices from juvenile and adult mice. The application of NMDA triggered inward currents in most astrocytes, which were partially reduced by Cd^{2+} and almost completely and irreversibly blocked by the NMDA receptor antagonist dizocipline (MK-801) [40]. Since a cocktail containing tetrodotoxine (TTX), L-trans-pyrollidine-2,4-dicarboxylic acid (PDC), Cd^{2+} and the competitive AMPA/kainite receptor antagonist 6-cyano-7-nitroquinoxaline-2,3-dione (CNQX) reduced NMDA-evoked responses by ~45%, Shipke and co-authors suggested that most of the NMDA-induced currents are due to an indirect effect *via* neuronal glutamate release and glial glutamate uptake, but there is still a component indicating the presence of intrinsic NMDA receptors in astrocytes. Calcium imaging experiments showing NMDA-evoked Ca^{2+} elevations, especially in distal astrocytic processes, in the presence of the above-mentioned cocktail of inhibitors leads to the same conclusion. The application of 4 mM Mg^{2+} abolished the NMDA-induced current, and this blockage could be overcome only by depolarizing the cell membrane. Recently, two studies proved the presence of NMDA receptors on astrocytes by measuring the glial synaptic currents evoked by stimulating neurons. These currents were blocked or partially blocked by the NMDA antagonists MK-801, D-AP5, UBP141 and memantine, but not by ifenprodil [60,61] and they were maximal at 6 months of age, then decreased with increasing age [62]. These results were also verified by calcium imaging measurements that showed Ca^{2+} elevations after NMDA application, with a maximal amplitude reached between 3 and 6 months of age [62,63]. Similarly, NMDA-evoked currents were detected in cerebral astrocytes [64], however without blocking neuronal activity by TTX. The only work that cast doubt on the presence of NMDA receptors on cortical astrocytes *in situ* was published in 1997 by Pasti and co-authors [65], who reported that Ca^{2+} elevations were delayed 20-30 s following NMDA application, in contrast to the immediate neuronal responses reported by other authors. This might be due to the fact that in contrast to previous studies, Pasti and colleagues carried out their experiments on relatively young animals (5-day-old mice). The ultimate proof of the presence of functional NMDA receptors on cerebral astrocytes was provided by astrocytes acutely isolated using a vibrating ball technique, studies in which the cells were isolated from the possible influence of other surrounding cells. In these cells, NMDA-induced inward currents were potentiated by the addition of glycine and the responses were blocked by MK-801 or partially blocked by UBP141, while ifenprodil had no influence [61,63]. In contrast to the data of Shipke and co-authors, these astrocytes were insensitive to blockage by

Mg^{2+}. The NMDA receptor-mediated currents were maximal at 6 months, followed by a decline with increasing age [62]. NMDA application also induced Ca^{2+} responses in these acutely isolated cerebral astrocytes with lower amplitudes than those evoked by glutamate, and they were D-AP5 sensitive [61,63]. As for the NMDA receptor subunit composition, the lack of Mg^{2+} block together with lower Ca^{2+} permeability strongly suggest the presence of GluN3 subunits. Pharmacological studies suggest the incorporation of GluN2C/D subunits in astrocytic NMDA receptors. Therefore, the most probable composition of the NMDA receptors in cortical astrocytes seems to be tri-heteromeric, containing GluN1, GluN2C/D and GluN3 subunits [61] (Fig. **1**). For an overall summary of NMDA receptor subunits in astrocytes, see Table **1**.

Hippocampus

The story of astrocytic NMDA receptors in the hippocampus seems to be much more complicated than in the cortex. The first experiments were performed on rat neonatal hippocampal cultures, and in contrast to glutamate, the application of NMDA or glycine did not evoke any Ca^{2+} responses in astrocytes [66]. This is in accord with another study performed on hippocampal astrocytes in cultures [46]. An interesting and so far unique result was obtained by Steinhauser and co-authors when they applied 5 mM NMDA to hippocampal astrocytes in slices prepared from juvenile mice, resulting in inward currents in 9 astrocytes, no response in 6 and outward currents in 7 cells tested. The measurements were performed without neuronal blocking, and similar results were obtained with 1 or 0.2 mM NMDA [67]. The hippocampal astrocytes in slices displayed an immediate NMDA-induced decrease in input resistance of 63%, which was significantly reduced by 43% in the presence of TTX [68]. However, the Ca^{2+} responses to NMDA application were delayed by at least 2 min in this study, raising a question about the cause of such a delay. In another work of Serrano and colleagues, a similar delay between the application of NMDA and the Ca^{2+} response of hippocampal astrocytes was observed with significantly reduced response amplitudes and even prolonged delays of the NMDA-evoked response in the presence of TTX [69]. In contrast, Porter and co-authors demonstrated that the Ca^{2+} responses of hippocampal astrocytes to NMDA are almost immediate, but the fact that TTX blocked 55% of these responses suggests that neuronal action potentials are also partially involved in triggering such increases in astrocytic intracellular Ca^{2+}. When glutamate was applied to hippocampal astrocytes in the presence of TTX, the co-application of D-AP5 reduced the peak amplitude of the Ca^{2+} responses by 10% [70], which is; however, only an indirect indication that these astrocytes possessed functional NMDA receptors. On the other side of the spectrum of studies focusing on NMDA receptors in hippocampal astrocytes is the work of Shelton and co-authors, in which no Ca^{2+} increase was observed in response to NMDA application in the presence of TTX in any of 56 cells tested [71]. These ambivalent results might be due to the inherent complexity of the problem, especially when the neurons in the surrounding tissue have to be taken into account. Acutely isolated hippocampal astrocytes should help to overcome

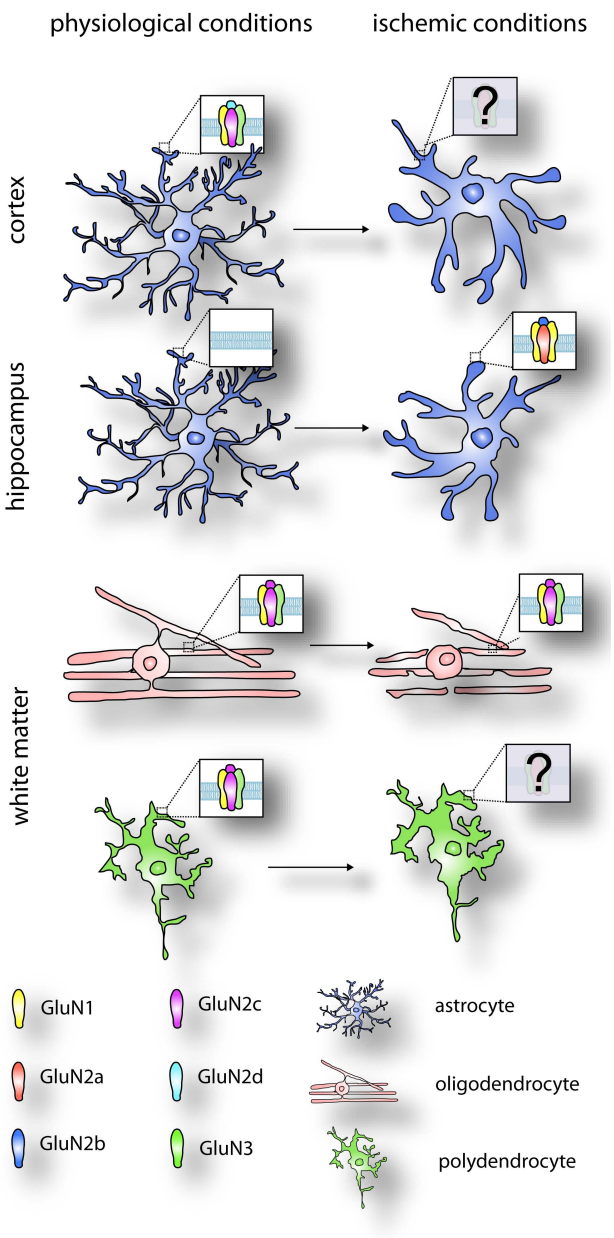


Fig. (1). The most probable composition of NMDA receptors in glial cells. The most probable composition of NMDA receptors in astrocytes, oligodendrocytes and polydendrocytes in particular CNS regions under physiological and pathological conditions, based on published data predominantly from functional studies. Question marks indicate unknown NMDA receptor composition. Note the presumed absence of NMDA receptors in hippocampal astrocytes under physiological conditions.

such a problem; however, NMDA complemented with glycine in Mg^{2+}-free medium did not evoke any increases in membrane currents [72] or in the extent of Ca^{2+} elevation [73], indicating that acutely isolated hippocampal astrocytes do not possess any functional NMDA receptors under physiological conditions. On the other hand, the impact of

Table 1. NMDA Receptor Subunits in Murine Glial Cells Under Physiological Conditions

	Level	Brain Area	NMDA Receptor Subunits							Reference
			GluN1	GluN2A	GluN2B	GluN2C	GluN2D	GluN3A	GluN3B	
astrocytes	mRNA	cortex	✗							Conti *et al*., 1994
			✓		✓	✓				Schipke *et al*., 2001
			✗			✓		✓		Cahoy *et al*., 2008
		cerebellum				✓				Akazawa *et al*., 1994
					✓					Luque *et al*., 1995
	protein	cortex	✓							Aoki *et al*., 1994
			✓	✓	✓					Conti *et al*., 1996
		hippocampus	✗	✗	✗					Gottlieb *et al*., 1997
			✗		✗					Krebs *et al*., 2003
		amygdala	✓							Gracy *et al*., 1995
			✓							Farb *et al*., 1995
		nucleus locus coeruleus	✓							Bockstaele *et al*., 1996
	function	cortex	✓			✓	✓	✓	✓	Palygin *et al*., 2010, 2011
oligodendrocytes	mRNA	optic nerve	✓			✓		✓		Salter and Fern, 2005
			✓	✓	✓	✓	✓	✓	✓	Burzomato *et al*., 2010
		forebrain	✗			✗		✓		Cahoy *et al*., 2008
	protein	optic nerve	✓	✓	✓	✓	✓	✓		Salter and Fern, 2005
			✓	✓	✓	✓	✓	✓	✓	Micu *et al*., 2006
			✓					✓	✓	Piňa-Crespo *et al*., 2010
		cerebellar white matter	✓			✓		✓	✓	Karadottir *et al*., 2005
			✓			✓		✓		Burzomato *et al*., 2010
	function	white matter	✓			✓		✓	✓	Karadottir *et al*., 2005
		cerebellar white matter	✓			✓		✓		Burzomato *et al*., 2010
		optic nerve	✓					✓	✓	Piňa-Crespo *et al*., 2010
polydendrocytes	mRNA	forebrain				✗		✓		Cahoy *et al*., 2008
	protein	white matter	✓							Manning *et al*., 2009
		cortex		✓		✓				Hamilton *et al*., 2010
	function	white matter	✓			✓		✓	✓	Karadottir *et al*., 2005
			✓							De Biase *et al*., 2011

The data were obtained from studies performed *in situ* and on freshly isolated glial cells, while those obtained *in vitro* were not included due to the possible influence of the cultivation process.

the isolation procedure should be also considered. Employing papain for tissue dissociation might result in damaging or removing the receptors from astrocytic processes. Taken together, the existence of NMDA receptors in hippocampal astrocytes is even after more than two decades of research, still a matter of debate.

Cerebellum

NMDA receptors have also been studied in Bergman glia in the cerebellum. Neither NMDA nor aspartate elicited any current responses in cultivated astrocytes prepared from 8-day-old rats even in the presence of glycine or in Mg^{2+}-free

solution [74]. Nevertheless, the *in situ* study of Muller and co-authors showed that the application of NMDA induces an inward current in 30% of Bergmann glial cells, which was blocked by ketamine. In contrast to neurons, the presence of Mg^{2+} did not alter the amplitude of the inward currents. The NMDA-induced currents were also not affected by the presence of glycine, although the application of glycine itself induced a small inward current. In calcium imaging measurements performed simultaneously with electro-physiological measurements, no Ca^{2+} elevations were observed upon NMDA application even in cells responding to this application by an inward current. [75]. In another study, the application of NMDA induced Ca^{2+} responses in Bergmann glia in slices, but these were reversibly inhibited by TTX, suggesting that the Bergmann glia responded to a substance(s) released from neurons after firing action potentials [76].

Spinal Cord

Cultured spinal cord astrocytes isolated from rat embryos produced only small Ca^{2+} elevations after the application of NMDA, and in Ca^{2+}-free solution NMDA application did not produce any Ca^{2+} responses at all [77]. Astrocytes in the spinal cord were also studied *in situ*. The application of NMDA induced a current in 95% of astrocytes with no sensitivity to Mg^{2+} or Ca^{2+}-free extracellular solutions. These responses were observed in astrocytes in the spinal cords of very young animals, and the NMDA-induced current amplitude decreased with age to almost zero in 13-day-old rats [78]. Glial cells in the red nucleus of the brain stem *in situ* did not display any increase in membrane currents following the application of NMDA [79].

Studies on Human Astrocytes

Functional studies of NMDA receptors in human astrocytes have revealed their peculiar behavior. In cultivated astrocytes isolated from human cerebral white matter surrounding a brain tumor, the application of NMDA generated currents potentiated by glycine, inhibited by 19% in Ca^{2+}-free extracellular solution and blocked by Mg^{2+}. The currents were not sensitive to the NMDA receptor antagonists D-AP5 or kynurenic acid. Interestingly, a broad G-protein inhibitor, GDPβS, inhibited the NMDA-induced currents to 82% of the original levels, which suggests regulation by an unknown G-protein-coupled receptor [80,81]. Human Muller cells freshly isolated from adult human retinas showed NMDA-evoked currents sensitive to D-AP5 in 6 out of 8 cells tested. When these cells were cultivated, the NMDA-induced currents were gradually less frequently observed with no detectable NMDA responses after 2.5 months of cultivation. Reduction of the Ca^{2+} concentration in the bathing solution or pre-treatment with the Ca^{2+} chelator BAPTA-AM reduced the effect of NMDA on the inward currents, which suggests that the activation of NMDA receptors in human Muller cells leads to an influx of Ca^{2+} [51].

Other Functional Studies

Apart from electrophysiological and Ca^{2+} measurements, interesting results were also obtained by biocytin dialysis of a single astrocyte in mice hippocampal slices. This revealed that a 2 min bath application of NMDA resulted in a significant increase in the number of coupled astrocytes; however, when TTX was pre-applied, the increase in coupling was much smaller [68,69]. The authors suggested that the NMDA-induced increase in astrocyte coupling is indirect and involves the activation of the neuronal network. Studying cortical astrocytes in neuron/glia co-cultures prepared from neonatal rats, Kato and colleagues revealed that treatment with glutamate increases the levels of GFAP immunoreactivity. This effect was reversed by NMDA receptor antagonists. However, in purified astrocytic cultures, glutamate-induced astrocytic activation was not suppressed by antagonists of NMDA receptors [58]. Similar results were obtained in human retinal Muller cells in culture in which NMDA treatment stimulated the proliferation of these cells, suggesting the presence of functional NMDA receptors [82].

NMDA RECEPTORS IN OLIGODENDROCYTES

Oligodendrocytes were thought to express predominantly non-NMDA glutamate ionotropic receptors, and initial reports also disclosed that oligodendrocytes do not respond to NMDA [83]. Nevertheless, oligodendrocyte NMDA receptors were shown to have an important role in controlling oligodendrocyte development [84], but also in oligodendroglial damage during pathological conditions.

Expression of NMDA Receptor Subunits in Oligodendrocytes

The first evidence of NMDA receptors in oligodendrocytes was found *in vitro* in 1996, when Yoshioka and co-authors described the expression of NMDA receptor subunits using RT-PCR and Southern blotting in the rat oligodendroglial lineage CG-4 [85]. They found gene transcripts of GluN1 and GluN2D, and after the differentiation of CG-4 cells into oligodendrocyte-like cells, they found also transcripts of the GluN2B subunit. Despite the presence of the essential subunits for functional NMDA receptor formation, patch-clamp recordings revealed that NMDA application had no effect on this cell line [86]. Clear evidence of NMDA receptor expression in mature oligodendrocytes was provided by Salter and Fern, who demonstrated that cells of the oligodendrocyte lineage express different subunits of NMDA receptors [87]. In the white matter of CNP-GFP mice expressing green fluorescent protein (GFP) specifically in oligodendrocytes, RT-PCR analyses of NMDA receptor subunits disclosed the presence of mRNA coding the GluN1, GluN2A-D and GluN3A subunits. Moreover, mRNA quantification suggested that GluN1, GluN2C and GluN3A are the most abundant subunits in the optic nerve isolated from 7-13-day-old animals, while the levels of mRNA coding the GluN2B subunit were quite low and the GluN3B subunit was not present [87]. Similarly to previous reports, RT-PCR analyses of the adult rat optic nerve revealed the presence of mRNA coding the GluN1 subunit, namely three C terminal variants and two N terminal variants, as well as mRNA coding GluN2A-D and GluN3A [88]. Surprisingly, Burzomato and colleagues also detected mRNA coding the GluN3B subunit, a contrasting finding to that of Salter and Fern [87], a discrepancy that might originate from Salter and Fern's use

of the mouse optic nerve. Employing Affymetrix GeneChip Arrays, Cahoy and co-authors carried out gene expression profiling of glial cells and detected significant expression levels of only GluN3A transcripts in oligodendrocytes isolated from the forebrain of postnatal mice. Interestingly, other transcripts of NMDA receptor subunits were either not present or did not exceed the threshold level of significant expression [39].

The identification of oligodendroglial NMDA receptor subunits on the protein level and their localization were initially performed in optic nerves by Salter and Fern [87]. Using immunohistochemical analyses they found the clustered expression of the NMDA receptor subunit GluN1 along oligodendroglial processes, and they also observed GluN2A-D and GluN3A subunit expression with a high degree of co-localization with GluN1 and Glu2A subunits on oligodendrocyte processes. Concurrently, Micu and co-authors detected GluN1, GluN2 and GluN3 subunits appearing in discrete high densities in the myelin of larger axons in adult rat optic nerves [89]. Moreover, they were able to detect the GluN1 subunit on the rough endoplasmatic reticulum and Golgi membranes. Probing an isolated fraction of myelin from the adult rat optic nerve by immunoblotting with specific antibodies against NMDA receptor subunits provided evidence for GluN1/GluN3 but not GluN2/GluN3 complexes [90]. On the other hand, mature oligodendrocytes in the cerebellar white matter displayed strong immuno-reactivity for GluN1, GluN2C and GluN3, while weaker labeling was observed for the GluN2A, B and D subunits [91]. Double-labeling revealed that the GluN1 and GluN2C subunits, and also the GluN3 and GluN2C subunits, co-localize in oligodendrocyte processes. Additionally, post-embedding electron microscopic immunohistochemistry showed that GluN1 subunits are present in the myelinating processes of adult cerebellar oligodendrocytes, in both the outer- and innermost membranes as well as within the myelin; their quantification disclosed that NMDA receptor density throughout the myelin is comparable to that observed in mossy fibre-granule cell synapses or parallel fibre-Purkinje cell synapses. These authors also noticed that the density of immunogold particles seemed to be higher in the outer membrane of the myelin, where the receptors presumably sense glutamate released from neighbouring cells [91]. Similarly, co-immunoprecipitation revealed interactions between the GluN1, GluN2C and GluN3A subunits in rat cerebellar oligodendrocytes [88]. Nonetheless, as for the myelination process, there are several studies that have shown the importance of NMDA receptors in immature oligodendrocytes, since even small Ca^{2+} signals can influence the stabilization/retraction of the myelinating projections from oligodendrocytes due to the small intracellular space [87,91,92]. However, De Biase and co-authors showed that this role of NMDA receptors in the myelination process can be taken over by AMPA receptors, since GluN1 subunit deletion from oligodendrocyte precursor cells led to the enhanced expression of AMPA receptors, but did not alter the formation of white matter tracts [93].

Functional NMDA Receptors in Oligodendrocytes

Indirect evidence of functional NMDA receptors in oligodendrocytes came in 1993, when Matute and Miledi [94] described NMDA receptors in Xenopus leavis oocytes injected with mRNA from the corpus callosum. Supposing that oligodendrocytes represent the most abundant cell type in the corpus callosum, they suggested that in addition to AMPA/kainite receptors, these cells also express NMDA receptors. Using the whole-cell patch-clamp technique, NMDA-induced inward currents were detected in neuro-hypophysial O-2A cells, displaying properties similar to those of the neuronal NMDA receptor [95]. The NMDA-evoked currents were characterized by a range of activating NMDA concentrations from 5 to 100 μM, blockage by MK-801, and weak blockage by Mg^{2+}. In addition, the authors showed that NMDA-evoked increases in intracellular Ca^{2+} are sensitive to the specific antagonist D-AP5 as well as to Ca^{2+}-free solutions or high Mg^{2+} [95]. In grey matter oligodendrocytes, direct evidence of functional NMDA receptors was given by Ziak and co-authors in spinal cord slices of young 5-13-day-old rats [78]. They described significantly higher NMDA-evoked currents in oligodendro-cytes of the dorsal rather than the ventral horn and, moreover, an increase in NMDA-evoked currents during oligodendroglia maturation. Recently, in a few independent studies, functional NMDA receptors were clearly demonstrated in white matter oligodendrocytes in the cerebellum [91,96], corpus callosum [91] and adult rat optic nerve [89]. They showed that the NMDA-mediated responses were mostly restricted to the oligodendrocytic processes rather than to the cell somas and Karadottir and co-authors suggested that NMDA receptor expression might be a general feature of white matter oligodendrocytes [91]. NMDA-evoked currents recorded in oligodendrocytes of the corpus callosum and cerebellum were comparable in size to those evoked by AMPA or kainate, and based on pharmacological analyses of the NMDA-evoked currents, these authors proposed the presence of subunit combinations or even a mixture of NMDA receptors with different subunit compositions. Based on the pharmacological properties of the NMDA-evoked currents, their weak blockage by Mg^{2+} and immuno-histochemical analyses revealing the co-localization of GluN1 and GluN2C subunits and also GluN3 and GluN2C subunits, they suggested that oligodendrocyte NMDA receptors comprise at least GluN1, GluN2C and GluN3 (Fig. **1**). Similarly, by comparing NMDA-evoked currents in cerebellar oligodendrocytes with those evoked in HEK cells transfected with cDNAs encoding recombinant receptors (GluN1/GluN2C/GluN3A or GluN1/GluN2C), Burzomato and co-authors clearly demonstrated that NMDA-evoked currents in oligodendrocytes reflect the activation of receptors containing GluN1, GluN2C and GluN3A [88].

Generally, NMDA receptors are typically activated by a combination of glutamate and glycine; however, Piña-Crespo and co-authors recently described excitatory responses in optic nerve myelin, gated by glycine alone and mediated by GluN1/GluN3 NMDA receptor subunits. They suggested that D-AP5-insensitive/2,3-dihydroxy-6-nitro-7-sulfamoyl-benzo[f]quinoxaline-2,3-dione (NBQX)-sensitive GluN1/GluN3 receptors seem to be restricted to myelin [90], while D-AP5 sensitive GluN2-containing receptors are more widely distributed [87,89,91]. For an overall summary of NMDA receptor subunits in oligodendrocytes, see Table **1**.

NMDA RECEPTORS IN POLYDENDROCYTES

Expression of NMDA Receptor Subunits in Polydendrocytes

One of the first studies describing the presence of NMDA receptors on the mRNA level was performed on oligodendrocyte precursors that were isolated from neonatal rats and kept under *in vitro* conditions by Wang and co-authors [95]. mRNA coding the GluN1 subunit was clearly detected using *in situ* hybridization and RT-PCR; however, their analyses failed to prove the presence of GluN2A-D subunit transcripts. Strikingly, the number of studies that report the expression of NMDA receptor subunits on the mRNA level in polydendrocytes *in situ* is smaller than the numerous functional studies that report the same finding; nevertheless, Cahoy and colleagues [39] recently showed the strong expression of mRNA coding the GluN3A subunit in polydendrocytes acutely isolated from postnatal mice. Similarly to oligodendrocytes, they did not detect mRNA encoding other NMDA receptor subunits.

Another important step towards confirming the presence of NMDA receptors subunits in polydendrocytes was done on the protein level by Wang and co-authors. Their pioneer study was performed *in vitro* on neonatal rat oligodendrocyte precursors, in which the GluN1 subunit was detected on process-bearing cells [95]. Recently, two studies confirmed the expression of several NMDA receptor subunits in polydendrocytes *in situ*. Manning and colleagues [97] detected GluN1 subunits, which are required for assembling a functional NMDA receptor, on O4-positive polydendrocytes in the white matter of postnatal rats and in developing human tissue. The second study employed the transgenic mouse strain NG2-dsRed, where polydendrocytes labelled with red fluorescent protein in the 15-day-old cortex expressed, besides AMPA receptors, also GluN2A and GluN2C subunits in the cell bodies as well as in the primary processes. Some of these NMDA receptors co-localized with synaptophysin, an indicator of synaptic contacts [98].

Functional NMDA Receptors in Polydendrocytes

In contrast to the low number of studies describing the presence of NMDA receptors in polydendrocytes at the mRNA or protein level, numerous references exist in the literature that report functional properties indicating the presence of NMDA receptors on this glial cell type. Wang and co-authors [95] detected for the first time the capability of cultivated oligodendrocyte precursors to respond to an application of NMDA using the whole cell patch-clamp recordings *in vitro*. These cells displayed an inward current in the range of 20-100 pA that slowly inactivated upon prolonged application of NMDA and was inhibited by D-AP5, a selective competitive NMDA receptor antagonist. Interestingly, the responses were very similar to those measured in neurons, based on a significant Mg^{2+} block and strong Ca^{2+} permeability, as revealed by calcium imaging. Another important advance in identifying functional NMDA receptors was done on white matter polydendrocytes *in situ* in 1-2-week-old rats. This type of cell responded to the application of glutamate by an inward current that was partially blocked by D-AP5 or MK-801 and fully blocked by NBQX, thus demonstrating the significant contribution of NMDA receptors to glutamate-evoked currents in addition to the strong activation of AMPA receptors [91]. Moreover, these data point to NMDA receptors of unusual subunit composition (probably GluN1, GluN2C and GluN3 subunits, Fig. **1**) with a weak Mg^{2+} block that are, however, more prominent in pre-myelinating and mature oligodendrocytes. Using another NMDA receptor antagonist, (+/-)-3-(2-carboxypiperazin-4-yl)-propyl-1-phosphonic acid (D,L-CPP), revealed that more than 60% of polydendrocytes in the white matter of adult Ng2-dsRed mice produce currents in response to NMDA application that were sensitive to this NMDA antagonist [99]. In contrast to previous reports, Ziskin and colleagues showed that NMDA currents in polydendrocytes are also blocked by Mg^{2+} at their resting potential, indicating that substantial depolarization would be required to allow Ca^{2+} influx through these receptors. It is worth noting that another study, which examined the NMDA-evoked currents in polydendrocytes from the cerebellum of 7-day-old rats, distinguished two different groups of polydendrocytes with distinct responses to the application of NMDA. One group comprised cells with non-detectable voltage-activated sodium TTX-sensitive currents that responded only weakly to the application of NMDA, while the second group consisted of polydendrocytes with large Na^{+} currents and NMDA-evoked inward currents that were significantly higher than those observed in the first group [100]. The optic nerve was another region of the CNS where the expression of polydendrocytic NMDA receptors was examined. In this region approximately 22% of measured cells showed an increased intracellular concentration of Ca^{2+}, based on Fura-2 calcium imaging, and these responses were sensitive to D-AP5 antagonist [98]. One of the most conclusive approaches was used by De Biase and co-authors [93], who generated triple transgenic mice (called PDGFαR–CreER;$NR1^{flox/flox}$;Z/EG) that enabled conditional tamoxifen-inducible knock-out of obligatory GluN1 subunits in PDGFαR-expressing polydendrocytes. The application of tamoxifen resulted in the genetic deletion of GluN1 subunits of the NMDA receptor specifically in polydendrocytes, and subsequent electrophysiological measurements in the white matter of 30-day-old mice showed the disappearance of D,L-CPP-sensitive NMDA currents after this conditional knock-out. For an overall summary of NMDA receptor subunits in polydendrocytes, see Table **1**. Nevertheless, the aim of this study was to reveal the function of NMDA receptors in the oligodendrocyte lineage, and it was clearly demonstrated that NMDA receptor ablation did not affect any physiological or morphological properties of polydendrocytes or their synaptic connections, survival or differentiation. These findings raise questions about the function and significance of NMDA receptors in polydendrocytes in the mammalian brain.

As shown above, a number of convincing indications exist on mRNA, protein and functional levels that prove the presence and functionality of NMDA receptors on polydendrocytes in a number of CNS regions during several developmental stages as well as in adulthood. Nevertheless, it seems that NMDA receptors are not the major mediators of

glutamate signals from surrounding cells. This role is evidently conveyed by Ca^{2+} permeable AMPA receptors, which respond to this excitatory neurotransmitter with stronger responses while NMDA receptors probably serve as a feedback control of AMPA receptor function [93]. However, some properties of polydendrocytic NMDA receptors are striking. Although there are several contradictory results in the literature, it seems that their subunit composition differs from that found in the majority of neurons, which could result in different functional properties compared to neuronal NMDA receptors, such as a lack of Mg^{2+} block at resting membrane potential or decreased permeability for Ca^{2+}. These unusual properties of NMDA receptors in polydendrocytes may be one of the reasons for their being overlooked for an extended period in the past.

GLIAL NMDA RECEPTORS IN THE PATHOLOGY OF ISCHEMIA

Excessive activation of ionotropic glutamate receptors occurring under ischemic conditions is harmful to neurons but also to glial cells. There have been two studies examining NMDA receptors in astrocytes after an ischemic insult, both in the hippocampus. Transient forebrain ischemia in rats resulted in the appearance of GluN2A/B but not GluN1 immunolabeling in cells with the characteristic morphological features of astrocytes, with the maximum expression levels appearing several weeks after ischemia [45]. The second study of Krebs and colleagues showed that transient forebrain ischemia resulted in the increased expression of both GluN1 and GluN2B subunits in GFAP-positive hippocampal astrocytes, reaching a maximum 14 to 28 days after ischemia [46] (Fig. **1**). Hippocampal astrocytes isolated from 2-4-day-old rats and cultivated in the presence of neurons were not immunopositive for any NMDA subunit, but after anoxia, which led to neuronal death, the GluN1 and GluN2B subunits became expressed in the remaining GFAP-positive glial cells. It is worth noting that when these astrocytes were cultivated in the absence of neurons, they were not positive for either GluN1 or GluN2B prior to or after anoxia. These authors further demonstrated that astrocytes co-cultivated with neurons 3 days after anoxia responded to the application of NMDA by an oscillatory increase in intracellular Ca^{2+} levels, which was reversibly blocked by D-AP5. The authors speculated that the expression of NMDA receptors in cultivated hippocampal astrocytes is probably a response related to the accompanying neuronal death. The final proof of ischemia-induced NMDA receptor appearance in hippocampal astrocytes was shown in cells acutely isolated from brains 20 days after transient forebrain ischemia, in which NMDA application elicited an increase in intracellular Ca^{2+} levels that was partially blocked by ifenprodil and fully blocked by D-AP5 [46]. Nevertheless, the impact of an ischemic insult on NMDA receptors in other brain regions has yet not been studied.

Among glia, oligodendrocytes are the most sensitive cells to excitotoxicity mediated by glutamate. Ca^{2+} entry, which is mediated by glutamate receptors, ultimately leads to oligodendroglial cell death *via* Ca^{2+} accumulation in the mitochondria, their depolarization and the release of pro-apoptotic factors [5]. Despite the fact that AMPA/kainate receptors were described as the major mediators of excitotoxic death in mature oligodendrocytes due to GluA4 expression, which is associated with the high Ca^{2+} permeability of AMPA/kainate receptors [101-105], a large number of studies have emphasized the role of NMDA receptors in oligodendroglial pathophysiology following ischemic injury; for a review see [23]. Nevertheless, the mechanisms that are triggered by NMDA receptor overactivation and that lead to oligodendroglial damage have not yet been elucidated. In 2005 Salter and Fern reported that in oxygen-glucose deprived optic nerves, the activation of NMDA receptors results in the fast Ca^{2+}-dependent detachment and disintegration of oligodendroglial processes in the white matter of CNP-GFP mice and that blocking the NMDA receptors prevents injury to oligodendrocytic processes [87]. They also found the differential expression of NMDA and AMPA/kainate receptors, which explains the early damage of myelin sheaths due to NMDA receptor activation, while AMPA/kainate receptor activation mediates cytotoxicity. Such detachment/disintegration of oligodendroglial processes was observed at an age corresponding to the onset of myelination as well as at the end of this process. Using an *in vitro* model of chemical ischemia, Micu and co-authors demonstrated that Ca^{2+} increases in myelin in adult rat optic nerves are abolished by NMDA antagonists, such as MK-801 or D-AP5, while those evoked in cell bodies are completely blocked by the AMPA/kainate receptor antagonist NBQX [89,106]. Additionally, it has been shown that ischemia leads to the development of an inward current in oligodendrocytes of the cerebellar cortex [91], corpus callosum and optic nerve [107], which is partially blocked by memantine or MK-801 and thus carried by NMDA receptors. NMDA receptor blockade with memantine was shown to attenuate white matter injury in a rat model of periventricular leukomalacia, a white matter injury resulting from hypoxia-ischemia in premature infants [97,108]. Although the protective effects of NMDA receptor antagonists were demonstrated *in vitro*, *in situ* as well as *in vivo* [87,89,91,97,106,107], the application of such antagonists might be somewhat problematic in human patients due to the significant side-effects of NMDA antagonists, such as interference with synaptic function. Nevertheless, all of these results show that inhibiting NMDA receptors alone is sufficient to protect against white matter injury and that the use of NMDA antagonists might be considered for clinical applications. However, the development of new selective agonists or antagonists should rather focus on the unusual subunit composition found in myelin/white matter oligodendroglia.

Despite increasing interest in polydendrocytes, the impact of ischemia on NMDA receptors in these cells has not yet been studied.

THE ROLE OF GLIAL NMDA RECEPTORS IN CELL DEATH

Besides the most common type of CNS injury, which is the above-described ischemia, NMDA receptors play an important role in many other CNS pathologies such as traumatic brain injury, multiple sclerosis [23], as well as certain neurodegenerative diseases, such as Huntington's [109]. In general, excessive glutamate release in the CNS can

lead to the necrotic or apoptotic cell death of neurons as well as glial cells, and which of these two pathways prevails, depends mostly on the severity of the insult. As mentioned above, severe insults lead to necrosis due to excessive Ca^{2+} influx through NMDA receptors, which is taken up by mitochondria and causes an initial depolarization of the mitochondria. Overloading mitochondria with Ca^{2+} causes necrotic cell death and might induce the production of reactive oxygen species that damage either mitochondrial respiratory processes or impair Ca^{2+} extrusion and membrane potential maintenance. The substantial depletion of cytosolic ATP levels caused by the reversal of mitochondrial ATP synthase in depolarized mitochondria further limits the ability of cells to regulate their intracellular Ca^{2+} levels [110]. On the other hand, apoptotic cell death occurs if the NMDA receptor-dependent insult is less intensive, mitochondrial depolarization is incomplete and intracellular ATP levels are sufficient to support the active processes associated with apoptosis. The mechanisms underlying NMDA receptor-dependent apoptosis are not certain, but are likely to involve the release of apoptotic factors – such as cytochrome c – from mitochondria and the activation of stress-induced pathways such as that of p38 MAP kinase or c-Jun N-terminal kinase [110].

Finally, glutamatergic signaling is not mediated only by NMDA currents. Many other glutamate receptors and transporters exist in glial cells. Simultaneously with NMDA receptor activation, glutamate binds and activates other glutamate receptors (AMPA, kainate) and transporters, including eight metabotropic glutamate receptor subtypes and the excitatory amino acid transporters 1,2 [7]. The activation of each of these receptors or transporters has the capacity to initiate cells death. Extensive studies in recent years have demonstrated that NMDA receptor subunits are capable of binding PDZ-domains, which not only ensures their proper targeting but may also play a critical role in coupling NMDA receptors to intracellular proteins and signaling enzymes [111-113]. This tight organization may thus facilitate the individual toxic signal mechanisms downstream of the receptors during glutamate over-activity. Evidence exists showing that the downstream signals of NMDA receptors activate proteins such as nitric oxide synthase, an enzyme that produces superoxide; the resultant oxidative stress participates in cell death. Another downstream activated signaling molecule is PARP-1, which plays a crucial role in apoptotic cell death [114].

Before the discovery of NMDA receptors in glial cells, a theory existed that excitotoxic damage of glial cells (predominantly oligodendrocytes) was related to the over-activation of AMPA and kainate receptors [115]. This theory was controversial because of the rapid desensitization of AMPA receptors, which inactivates them when exposed to glutamate for a long time. The discovery of NMDA receptors in glial cells made them prime suspects for such excitotoxicity. Based on glial-specific NMDA receptor subunit composition, these receptors have different pharmacokinetics, without Mg^{2+} block and lower Ca^{2+} permeability, when compared to neuronal NMDA receptors [7]. Although the overall Ca^{2+} influx through glial NMDA receptors could be minor under physiological conditions, the absence of Mg^{2+} block and a hyperpolarized glial resting membrane potential compared to neurons would provide for a larger and significant Ca^{2+} influx under pathologic conditions as a consequence of excessive extracellular glutamate concentration.

CONCLUSION

In summary, it seems that astrocytes, oligodendrocytes as well as polydendrocytes express NMDA receptors of quite similar composition, mainly containing the GluN1 and GluN2 subunits, but more importantly, the unusual GluN3A subunit as well (Fig. **1**). The co-assembly of these subunits within glial NMDA receptors markedly alters their properties, resulting in a weak or even absent sensitivity to Mg^{2+}; as a result, glial NMDA receptors may be potentially active at the resting membrane potential, which is in contrast to neurons. Nevertheless, many published and surely many more unpublished studies have failed to prove the expression of NMDA receptors on glial cells, a phenomenon that could, however, be connected to the clear regional specificity in the expression of NMDA receptors on glial cells in the CNS and moreover, also to their probable age-dependent expression. It should also be taken into account that before discovering the composition and properties of NMDA receptors on glial cells, many studies were considered negative due to the expectation of observing NMDA-specific responses typical of neurons, which are not, in fact, characteristic of glial cells. Under physiological conditions, astroglial NMDA receptors were shown to be involved in neuronal-glial signalling [7]; nevertheless, the role of NMDA receptors in oligodendrocytes and polydendrocytes needs to be elucidated. On the other hand, the pathogenic potential of NMDA receptors was clearly demonstrated in oligodendrocytes during ischemic injury, while the role of astrocytic and polydendrocytic NMDA receptors in CNS pathologies such as ischemia remains unknown. NMDA-mediated Ca^{2+} entry might be one of the key players triggering polydendrocyte migration, proliferation and/or differentiation and may also contribute to the onset of events initiating the development of reactive astrocytes. All of the processes connected with NMDA receptors in glial cells described in this review, including their role in ischemia and the myelination process, naturally bring promising pharmacological perspectives [116,117]. There were several attempts to utilize antagonists of NMDA receptors in clinical trials; however, most of them were high-affinity antagonists that impede normal brain activity and lead to intolerable side effects. The exceptions are memantine derivatives, since these are open-channel uncompetitive antagonists with a relatively fast “off rate”, parameters that do not impede physiological neurotransmission, thus making them clinically tolerable [6,97,118-121]. Another reason why many clinical trials with NMDA receptor antagonists were unsuccessful is, in our opinion, their strong focus on neuronal NMDA receptors while neglecting these receptors in glial cells due to the relatively recent discoveries in this field. Nonetheless, thanks to the unusual composition of glial NMDA receptors (especially GluN2C and GluN3A subunits), we believe that new antagonists specific for glial NMDA receptors will emerge soon and will enable selective targeted intervention with weaker/fewer side effects. Although many questions about NMDA receptors in the

human brain have been answered, numerous questions are still pending. Future research should thus unravel the exact role of glial NMDA receptors in CNS physiology/pathology since this will significantly contribute to the future treatment of many serious brain pathologies.

CONFLICT OF INTEREST

The author(s) confirm that this article content has no conflict of interest.

ACKNOWLEDGEMENTS

The authors thank James Dutt for helpful comments and suggestions.

SUPPORTED BY

This study was supported by the grants GACR: 309/08/1381 and GACR P304/12/G069 from the Grant Agency of the Czech Republic and by the grant GAUK 604212 from the Grant Agency of the Charles University in Prague.

REFERENCES

[1] Petralia, R.S., Wenthold, R.J. NMDA receptors. 2008 In: Gereau R.W. and Swanson, G.T. Eds., Glutamate receptors. Humana press, a part of Springer Science+Business Media, LLC. pp. 45-98, **2008**.

[2] Smothers, C.T., Woodward, J.J. Pharmacological characterization of glycine-activated currents in HEK 293 cells expressing N-methyl-D-aspartate NR1 and NR3 subunits. *J. Pharmacol. Exp. Ther*., **2007**, *322*, 739-748.

[3] Akazawa, C., Shigemoto, R., Bessho, Y., Nakanishi, S., Mizuno, N. Differential expression of five N-methyl-D-aspartate receptor subunit mRNAs in the cerebellum of developing and adult rats. *J. Comp. Neurol*., **1994**, *347*, 150-160.

[4] Cavara, N.A., Hollmann, M. Shuffling the deck anew: how NR3 tweaks NMDA receptor function. *Mol. Neurobiol*., **2008**, *38*, 16-26.

[5] Matute, C. Oligodendrocyte NMDA receptors: a novel therapeutic target. *Trends Mol. Med*., **2006**, *12*, 289-292.

[6] Lipton, S.A. NMDA receptors, glial cells, and clinical medicine. *Neuron*, **2006**, *50*, 9-11.

[7] Verkhratsky, A., Kirchhoff, F. NMDA Receptors in glia. *Neuroscientist*, **2007**, *13*, 28-37.

[8] Kimelberg, H.K., Nedergaard M. Functions of astrocytes and their potential as therapeutic targets. *Neurotherapeutics*, **2010**, *7*, 338-353.

[9] Kofuji, P., Newman, E.A. Potassium buffering in the central nervous system. *Neuroscience*, **2004**, *129*, 1045-1056.

[10] Deitmer, J.W., Rose, C.R. Ion changes and signalling in perisynaptic glia. *Brain Res. Rev*., **2010**, *63*, 113-129.

[11] Anderson, C.M., Swanson, R.A. Astrocyte glutamate transport: review of properties, regulation, and physiological functions. *Glia*. **2000**, *32*, 1-14.

[12] Iadecola, C., Nedergaard, M. Glial regulation of the cerebral microvasculature. *Nat. Neurosci*., **2007**, *10*, 1369-1376.

[13] Magistretti P.J. Role of glutamate in neuron-glia metabolic coupling. *Am. J. Clin. Nutr*., **2009**, *90*, 875S-880S.

[14] Jou, M.J. Pathophysiological and pharmacological implications of mitochondria-targeted reactive oxygen species generation in astrocytes. *Adv. Drug Deliv. Rev*., **2008**, *60*, 1512-1526.

[15] Amiry-Moghaddam, M., Williamson, A., Palomba, M., Eid, T., de Lanerolle, N.C., Nagelhus, E.A., Adams M.E., Froehner S.C., Agre P., Ottersen O.P. Delayed K+ clearance associated with aquaporin-4 mislocalization: phenotypic defects in brains of alpha-syntrophin-null mice. *Proc. Natl. Acad. Sci. U. S. A.*, **2003**, *100*, 13615-13620.

[16] Kimelberg, H.K., O'Connor, E. Swelling of astrocytes causes membrane potential depolarization. *Glia*, **1988**, *1*, 219-224.

[17] Halassa, M.M., Fellin, T., Haydon, P.G. The tripartite synapse: roles for gliotransmission in health and disease. *Trends Mol. Med*., **2007**, 13, 54-63.

[18] Platel, J.C., Dave, K.A., Gordon, V., Lacar, B., Rubio, M.E., Bordey A. NMDA receptors activated by subventricular zone astrocytic glutamate are critical for neuroblast survival prior to entering a synaptic network. *Neuron*, **2010**, *65*, 859-872.

[19] Pekny, M., Nilsson, M. Astrocyte activation and reactive gliosis. *Glia*, **2005**, *50*, 427-434.

[20] Sidoryk-Wegrzynowicz, M., Wegrzynowicz, M., Lee, E., Bowman, A.B., Aschner M. Role of astrocytes in brain function and disease. *Toxicol Pathol*., **2011**, *39*, 115-123.

[21] Verkhratsky, A. Neurotransmitter receptors in astrocytes. In: Parpura, V., Haydon, P.G. Eds., Astrocytes in (Patho)Physiology of the Nervous System. Springer Science and Business Media, LLC. pp. 49-67.**2009**,

[22] Dewar, D., Underhill, S.M., Goldberg M.P. Oligodendrocytes and ischemic brain injury. *J. Cereb. Blood Flow Metab*., **2003**, *23*, 263-274.

[23] Matute, C. Glutamate and ATP signalling in white matter pathology. *J Anat.* **2011**, *219*, 53-64.

[24] Wolosker, H., Dumin, E., Balan, L., Foltyn, V.N. D-amino acids in the brain: D-serine in neurotransmission and neurodegeneration. *FEBS J*. **2008**, *275*, 3514-3526.

[25] Dawson, M.R., Polito, A., Levine, J.M., Reynolds, R. NG2-expressing glial progenitor cells: an abundant and widespread population of cycling cells in the adult rat CNS. *Mol. Cell Neurosci*., **2003**, *24*, 476-488.

[26] Stallcup, W.B., Beasley, L. Bipotential glial precursor cells of the optic nerve express the NG2 proteoglycan. *J. Neurosci*., **1987**, *7*, 2737-2744.

[27] Kukley, M., Kiladze, M., Tognatta, R., Hans, M., Swandulla, D., Schramm, J., Dietrich, D. Glial cells are born with synapses. *FASEB J*. **2008**, 22, 2957-2969.

[28] Psachoulia, K., Jamen, F., Young, K.M., Richardson, W.D. Cell cycle dynamics of NG2 cells in the postnatal and ageing brain. *Neuron Glia Biol*., **2009**, *5*, 57-67.

[29] Simon, C., Gotz, M., Dimou, L. Progenitors in the adult cerebral cortex: cell cycle properties and regulation by physiological stimuli and injury. *Glia*, **2011**, *59*, 869-881.

[30] Ge, W.P., Zhou, W., Luo, Q., Jan, L.Y., Jan, Y.N. Dividing glial cells maintain differentiated properties including complex morphology and functional synapses. *Proc. Natl. Acad. Sci. U. S. A*., **2009**, *106*, 328-333.

[31] Kang, S.H., Fukaya, M., Yang, J.K., Rothstein, J.D., Bergles, D.E. NG2+ CNS glial progenitors remain committed to the oligodendrocyte lineage in postnatal life and following neurodegeneration. *Neuron*, **2010**, *68*, 668-681.

[32] Rivers, L.E., Young, K.M., Rizzi, M., Jamen, F., Psachoulia, K., Wade, A., Kessaris, N., Richardson W.D. PDGFRA/NG2 glia generate myelinating oligodendrocytes and piriform projection neurons in adult mice. *Nat. Neurosci*., **2008**, *11*, 1392-1401.

[33] Honsa, P., Pivonkova, H., Dzamba, D., Filipova, M., Anderova, M. Polydendrocytes display large lineage plasticity following focal cerebral ischemia. *PLoS One*, **2012**, *7*, e36816.

[34] Komitova, M., Serwanski, D.R., Lu Q.R., Nishiyama, A. NG2 cells are not a major source of reactive astrocytes after neocortical stab wound injury. *Glia*, **2011**, *59*, 800-809.

[35] Theis, M., Giaume, C. Connexin-based intercellular communication and astrocyte heterogeneity. *Brain Res*., **2012**,

[36] Bergles, D.E., Jabs, R., Steinhauser, C. Neuron-glia synapses in the brain. *Brain Res. Rev*., **2010**, *63*, 130-137.

[37] Conti F., Minelli, A., Molnar, M., Brecha, N.C. Cellular localization and laminar distribution of NMDAR1 mRNA in the rat cerebral cortex. *J. Comp. Neurol.* **1994**, 343, 554-565.

[38] Luque, J.M., Richards, J.G. Expression of NMDA 2B receptor subunit mRNA in Bergmann glia. *Glia*, **1995**, *13*, 228-232.

[39] Cahoy, J.D., Emery, B., Kaushal, A., Foo, L.C., Zamanian, J.L., Christopherson, K.S., Xing, Y., Lubischer, J.L., Krieg P.A., Krupenko, S.A., Thompson, W.J., Barres, B.A. A transcriptome database for astrocytes, neurons, and oligodendrocytes: a new resource for understanding brain development and function. *J. Neurosci*., **2008**, *28*, 264-278.

[40] Schipke, C.G., Ohlemeyer, C., Matyash, M., Nolte, C., Kettenmann H., Kirchhoff F. Astrocytes of the mouse neocortex express functional N-methyl-D-aspartate receptors. *FASEB J*. **2001**, 15, 1270-1272.

[41] Zhou, Y., Li, H.L., Zhao, R., Yang, L.T., Dong, Y., Yue, X., Ma, Y.Y., Wang, Z., Chen, J., Cui, C.L., Yu, A.C. Astrocytes express N-methyl-D-aspartate receptor subunits in development, ischemia and post-ischemia. *Neurochem. Res*., **2010**, *35*, 2124-2134.

[42] Lee, M.C., Ting, K.K., Adams, S., Brew B.J., Chung R., Guillemin G.J. Characterisation of the expression of NMDA receptors in human astrocytes. *PLoS One*, **2010**, *5*, e14123.

[43] Aoki, C., Venkatesan, C., Go, C.G., Mong, J.A., Dawson, T.M. Cellular and subcellular localization of NMDA-R1 subunit immunoreactivity in the visual cortex of adult and neonatal rats. *J. Neurosci*., **1994**, *14*, 5202-5222.

[44] Conti, F., DeBiasi, S., Minelli, A., Melone, M. Expression of NR1 and NR2A/B subunits of the NMDA receptor in cortical astrocytes. *Glia*, **1996**, *17*, 254-258.

[45] Gottlieb, M., Matute, C. Expression of ionotropic glutamate receptor subunits in glial cells of the hippocampal CA1 area following transient forebrain ischemia. *J. Cereb. Blood Flow Metab*. **1997**, *17*, 290-300.

[46] Krebs, C., Fernandes, H.B., Sheldon, C., Raymond, L.A., Baimbridge, K.G. Functional NMDA receptor subtype 2B is expressed in astrocytes after ischemia *in vivo* and anoxia *in vitro*. *J. Neurosci*., **2003**, *23*, 3364-3372.

[47] Gracy, K.N., Pickel, V.M. Comparative ultrastructural localization of the NMDAR1 glutamate receptor in the rat basolateral amygdala and bed nucleus of the stria terminalis. *J. Comp. Neurol*., **1995**, *362*, 71-85.

[48] Farb, C.R., Aoki, C., Ledoux, J.E. Differential localization of NMDA and AMPA receptor subunits in the lateral and basal nuclei of the amygdala: a light and electron microscopic study. *J. Comp. Neurol*., **1995**, *362*, 86-108.

[49] Van Bockstaele, E.J., Colago, E.E. Selective distribution of the NMDA-R1 glutamate receptor in astrocytes and presynaptic axon terminals in the nucleus locus coeruleus of the rat brain: an immunoelectron microscopic study. *J. Comp. Neurol*., **1996**, *369*, 483-496.

[50] Conti, F., Barbaresi, P., Melone, M., Ducati, A. Neuronal and glial localization of NR1 and NR2A/B subunits of the NMDA receptor in the human cerebral cortex. *Cereb Cortex*, **1999**, *9*, 110-120.

[51] Puro, D.G., Yuan, J.P., Sucher, N.J. Activation of NMDA receptor-channels in human retinal Muller glial cells inhibits inward-rectifying potassium currents. *Vis Neurosci*., **1996**, *13*, 319-326.

[52] Backus, K.H., Kettenmann, H., Schachner, M. Pharmacological characterization of the glutamate receptor in cultured astrocytes. *J. Neurosci. Res*., **1989**, *22*, 274-282.

[53] Bowman, C.L., Kimelberg, H.K. Excitatory amino acids directly depolarize rat brain astrocytes in primary culture. *Nature*, **1984**, *311*, 656-659.

[54] Kettenmann, H., Schachne, M. Pharmacological properties of gamma-aminobutyric acid-, glutamate-, and aspartate-induced depolarizations in cultured astrocytes. *J. Neurosci*., **1985**, *5*, 3295-3301.

[55] Sontheimer, H., Kettenmann, H., Backus, K.H., Schachner M. Glutamate opens Na+/K+ channels in cultured astrocytes. *Glia*, **1988**, *1*, 328-336.

[56] Holzwarth, J.A., Gibbons, S.J., Brorson, J.R., Philipson, L.H., Miller R.J. Glutamate receptor agonists stimulate diverse calcium responses in different types of cultured rat cortical glial cells. *J. Neurosci*., **1994**, *14*, 1879-1891.

[57] Jensen, A.M., Chiu, S.Y. Fluorescence measurement of changes in intracellular calcium induced by excitatory amino acids in cultured cortical astrocytes. *J. Neurosci*., **1990**, *10*, 1165-1175.

[58] Kato, H., Narita, M., Miyatake, M., Yajima, Y., Suzuki, T. Role of neuronal NR2B subunit-containing NMDA receptor-mediated Ca2+ influx and astrocytic activation in cultured mouse cortical neurons and astrocytes. *Synapse*,**2006**, *59*, 10-17.

[59] Zhang, Q., Hu, B., Sun, S., Tong, E. Induction of increased intracellular calcium in astrocytes by glutamate through activating NMDA and AMPA receptors. *J. Huazhong. Uni. Sci. Technolog Med Sci.* **2003**, *23*, 254-257.

[60] Lalo, U., Pankratov, Y., Kirchhoff, F., North, R.A., Verkhratsky, A. NMDA receptors mediate neuron-to-glia signaling in mouse cortical astrocytes. *J. Neurosci*., **2006**, *26*, 2673-2683.

[61] Palygin O., Lalo, U., Pankratov, Y. Distinct pharmacological and functional properties of NMDA receptors in mouse cortical astrocytes. *Br. J. Pharmacol*., **2011**, *163*, 1755-1766.

[62] Lalo, U., Palygin, O., North, R.A., Verkhratsky, A., Pankratov, Y. Age-dependent remodelling of ionotropic signalling in cortical astroglia. *Aging Cell*, **2011**, *10*, 392-402.

[63] Palygin O., Lalo U., Verkhratsky, A., Pankratov, Y. Ionotropic NMDA and P2X1/5 receptors mediate synaptically induced Ca2+ signalling in cortical astrocytes. *Cell Calcium*, **2010**, *48*, 225-231.

[64] Oliveira, J.F., Riedel, T., Leichsenring, A., Heine, C., Franke, H., Krugel, U., Norenberg, W., Illes, P. Rodent cortical astroglia express *in situ* functional P2X7 receptors sensing pathologically high ATP concentrations. *Cereb. Cortex*, **2011**, *21*, 806-820.

[65] Pasti, L., Volterra, A., Pozzan, T., Carmignoto, G. Intracellular calcium oscillations in astrocytes: a highly plastic, bidirectional form of communication between neurons and astrocytes *in situ*. *J. Neurosci*., **1997**, *17*, 7817-7830.

[66] Cornell-Bell, A.H., Finkbeiner, S.M., Cooper, M.S., Smith, S.J. Glutamate induces calcium waves in cultured astrocytes: long-range glial signaling. *Science*,**1990**, *247*, 470-473.

[67] Steinhauser, C., Jabs, R., Kettenmann, H. Properties of GABA and glutamate responses in identified glial cells of the mouse hippocampal slice. *Hippocampus*, **1994**, *4*, 19-35.

[68] Serrano, A., Robitaille, R., Lacaille, J.C. Differential NMDA-dependent activation of glial cells in mouse hippocampus. *Glia*, **2008**, *56*, 1648-1663.

[69] Serrano, A., Haddjeri, N., Lacaille, J.C., Robitaille, R. GABAergic network activation of glial cells underlies hippocampal heterosynaptic depression. *J. Neurosci*., **2006**, *26*, 5370-5382.

[70] Latour, I., Gee, C.E., Robitaille, R., Lacaille, J.C. Differential mechanisms of Ca2+ responses in glial cells evoked by exogenous and endogenous glutamate in rat hippocampus. *Hippocampus*, **2001**, *11*, 132-145.

[71] Shelton, M.K., McCarthy, K.D. Mature hippocampal astrocytes exhibit functional metabotropic and ionotropic glutamate receptors in situ. *Glia*, **1999**, *26*, 1-11.

[72] Seifert, G., Steinhauser, C. Glial cells in the mouse hippocampus express AMPA receptors with an intermediate Ca2+ permeability. *Eur. J. Neurosci*., **1995**, *7*, 1872-1881.

[73] Cai, Z., Kimelberg, H.K. Glutamate receptor-mediated calcium responses in acutely isolated hippocampal astrocytes. *Glia*, **1997**, 21, 380-389.

[74] Usowicz, M.M., Gallo, V., Cull-Candy, S.G. Multiple conductance channels in type-2 cerebellar astrocytes activated by excitatory amino acids. *Nature*,**1989**, *339*, 380-383.

[75] Muller, T., Grosche, J., Ohlemeyer, C., Kettenmann, H. NMDA-activated currents in Bergmann glial cells. *Neuroreport*, **1993**, *4*, 671-674.

[76] Shao, Y., McCarthy, K.D. Responses of Bergmann glia and granule neurons in situ to N-methyl-D-aspartate, norepinephrine, and high potassium. *J Neurochem*. **1997**, 68, 2405-2411.

[77] Ahmed, Z., Lewis, C.A., Faber, D.S. Glutamate stimulates release of Ca2+ from internal stores in astroglia. *Brain Res*., **1990**, *516*, 165-169.

[78] Ziak, D., Chvatal, A., Sykova, E. Glutamate-, kainate- and NMDA-evoked membrane currents in identified glial cells in rat spinal cord slice. *Physiol. Res.*,**1998**, *47*, 365-375.

[79] Akopian, G., Kuprijanova, E., Kressin, K., Steinhuser C. Analysis of ion channel expression by astrocytes in red nucleus brain stem slices of the rat. *Glia*, **1997**, *19*, 234-246.

[80] Kondoh, T., Nishizaki, T., Aihara, H., Tamaki, N. NMDA-responsible, APV-insensitive receptor in cultured human astrocytes. *Life Sci*., **2001**, *68*, 1761-1767.

[81] Nishizaki, T., Matsuoka, T., Nomura, T., Kondoh, T., Tamaki, N., Okada Y. Store Ca2+ depletion enhances NMDA responses in cultured human astrocytes. *Biochem. Biophys. Res. Commun*., **1999**, *259*, 661-664.

[82] Uchihori, Y., Puro, D.G. Glutamate as a neuron-to-glial signal for mitogenesis: role of glial N-methyl-D-aspartate receptors. *Brain, Res*., **1993**, *613*, 212-220.

[83] Cull-Candy, S.G., Wyllie, D.J. Glutamate-receptor channels in mammalian glial cells. *Ann. N. Y. Acad. Sci*., **1991**, *633*, 458-474.

[84] Yuan, X., Eisen, A.M., McBain, C.J., Gallo, V. A role for glutamate and its receptors in the regulation of oligodendrocyte development in cerebellar tissue slices. *Development*, **1998**, *125*, 2901-2914.

[85] Yoshioka, A., Ikegaki, N., Williams, M., Pleasure, D. Expression of N-methyl-D-aspartate (NMDA) and non-NMDA glutamate

receptor genes in neuroblastoma, medulloblastoma, and other cells lines. *J. Neurosci. Res*., **1996**, *46*, 164-178.

[86] Gallo, V., Patneau, D.K., Mayer, M.L., Vaccarino, F.M. Excitatory amino acid receptors in glial progenitor cells: molecular and functional properties. *Glia*, **1994**, *11*, 94-101.

[87] Salter, M.G., Fern, R. NMDA receptors are expressed in developing oligodendrocyte processes and mediate injury. *Nature*, **2005**, *438*, 1167-1171.

[88] Burzomato V., Frugier G., Perez-Otano I., Kittler J.T., Attwell D. The receptor subunits generating NMDA receptor mediated currents in oligodendrocytes. *J Physiol.* **2010**, 588, 3403-3414.

[89] Micu, I., Jiang, Q., Coderre, E., Ridsdale, A., Zhang, L., Woulfe, J., Yin, X., Trapp, B.D., McRory, J.E., Rehak, R., Zamponi, G.W., Wang, W., Stys, P.K. NMDA receptors mediate calcium accumulation in myelin during chemical ischaemia. *Nature*, **2006**, *439*, 988-992.

[90] Pina-Crespo, J.C., Talantova, M., Micu, I., States, B., Chen, H.S., Tu, S., Nakanishi, N., Tong, G., Zhang, D., Heinemann, S.F., Zamponi, G.W., Stys, P.K., Lipton, S.A. Excitatory glycine responses of CNS myelin mediated by NR1/NR3 "NMDA" receptor subunits. *J Neurosci*., **2010**, *30*, 11501-11505.

[91] Karadottir, R., Cavelier, P., Bergersen, L.H., Attwell, D. NMDA receptors are expressed in oligodendrocytes and activated in ischaemia. *Nature*, **2005**, *438*, 1162-1166.

[92] Wong, R. NMDA receptors expressed in oligodendrocytes. *Bioessays*, **2006**, *28*, 460-464.

[93] De Biase, L.M., Kang, S.H., Baxi, E.G., Fukaya, M., Pucak, M.L., Mishina, M., Calabresi, P.A., Bergles, D.E. NMDA receptor signaling in oligodendrocyte progenitors is not required for oligodendrogenesis and myelination. *J. Neurosci*., **2011**, *31*, 12650-12662.

[94] Matute, C., Miledi, R. Neurotransmitter receptors and voltage-dependent Ca2+ channels encoded by mRNA from the adult corpus callosum. *Proc. Natl. Acad. Sci. U. S. A*., **1993**, *90*, 3270-3274.

[95] Wang, C., Pralong, W.F., Schulz, M.F., Rougon, G., Aubry, J.M., Pagliusi, S., Robert, A., Kiss, J.Z. Functional N-methyl-D-aspartate receptors in O-2A glial precursor cells: a critical role in regulating polysialic acid-neural cell adhesion molecule expression and cell migration. *J. Cell Biol.*, **1996**, *135*, 1565-1581.

[96] Kolodziejczyk, K., Hamilton, N.B., Wade, A., Karadotti, R., Attwell, D. The effect of N-acetyl-aspartyl-glutamate and N-acetyl-aspartate on white matter oligodendrocytes. *Brain*, **2009**, *132*, 1496-1508.

[97] Manning, S.M., Talos, D.M., Zhou, C., Selip, D.B., Park, H.K., Park C.J., Volpe, J.J., Jensen F.E. NMDA receptor blockade with memantine attenuates white matter injury in a rat model of periventricular leukomalacia. *J. Neurosci*., **2008**, *28*, 6670-6678.

[98] Hamilton, N., Vayro, S., Wigley, R., Butt, A.M. Axons and astrocytes release ATP and glutamate to evoke calcium signals in NG2-glia. *Glia*, **2010**, *58*, 66-79.

[99] Ziskin, J.L., Nishiyama, A., Rubio, M., Fukaya, M., Bergles, D.E. Vesicular release of glutamate from unmyelinated axons in white matter. *Nat. Neurosci*., **2007**, *10*, 321-330.

[100] Karadottir, R., Hamilton, N.B., Bakiri, Y., Attwell, D. Spiking and nonspiking classes of oligodendrocyte precursor glia in CNS white matter. *Nat. Neurosci*., **2008**, *11*, 450-456.

[101] Alberdi, E., Sanchez-Gomez, M.V., Marino, A., Matute, C. Ca(2+) influx through AMPA or kainate receptors alone is sufficient to initiate excitotoxicity in cultured oligodendrocytes. *Neurobiol. Dis*., **2002**, *9*, 234-243.

[102] Leuchtmann, E.A., Ratner, A.E., Vijitruth, R., Qu, Y., McDonald J.W. AMPA receptors are the major mediators of excitotoxic death in mature oligodendrocytes. *Neurobiol. Dis*., **2003**, *14*, 336-348.

[103] Matute, C., Alberdi, E., Domercq M., Perez-Cerda, F., Perez-Samartin, A., Sanchez-Gomez, M.V. The link between excitotoxic oligodendroglial death and demyelinating diseases. *Trends Neurosci*., **2001**, *24*, 224-230.

[104] Matute, C., Alberdi, E., Ibarretxe, G., Sanchez-Gomez, M.V. Excitotoxicity in glial cells. *Eur. J. Pharmacol*., **2002**, *447*, 239-246.

[105] McDonald, J.W., Althomsons, S.P., Hyrc, K.L., Choi, D.W., Goldberg, M.P. Oligodendrocytes from forebrain are highly vulnerable to AMPA/kainate receptor-mediated excitotoxicity. *Nat. Med*., **1998**, *4*, 291-297.

[106] Micu, I., Ridsdale, A., Zhan, L., Woulfe, J., McClintock J., Brantner C.A., Andrews S.B., Stys P.K. Real-time measurement of free Ca2+ changes in CNS myelin by two-photon microscopy. *Nat. Med*., **2007**, *13*, 874-879.

[107] Bakiri Y., Hamilton, N.B., Karadottir, R., Attwell, D. Testing NMDA receptor block as a therapeutic strategy for reducing ischaemic damage to CNS white matter. *Glia*, **2008**, *56*, 233-240.

[108] Manning S.M., Boll, G., Fitzgerald, E., Selip, D.B., Volpe, J.J., Jensen F.E. The clinically available NMDA receptor antagonist, memantine, exhibits relative safety in the developing rat brain. *Int. J. Dev. Neurosci*., **2011**, *29*, 767-773.

[109] Hardingham, G.E. Coupling of the NMDA receptor to neuroprotective and neurodestructive events. *Biochem. Soc. Trans*., **2009**, *37*, 1147-1160.

[110] Hardingham, G.E., Bading, H. The Yin and Yang of NMDA receptor signalling. *Trends Neurosci*., **2003**, *26*, 81-89.

[111] Brenman, J.E., Chao D.S., Gee S.H., McGee A.W., Craven S.E., Santillano, D.R., Wu, Z., Huang, F., Xia, H., Peters, M.F., Froehner S.C., Bredt D.S. Interaction of nitric oxide synthase with the postsynaptic density protein PSD-95 and alpha1-syntrophin mediated by PDZ domains. *Cell*, **1996**, *84*, 757-767.

[112] Sheng, M., Sala, C. PDZ domains and the organization of supramolecular complexes. *Annu. Rev. Neurosci*., **2001**, *24*, 1-29.

[113] Cui, H., Hayashi, A., Sun, H.S., Belmares, M.P., Cobey, C., Phan, T., Schweizer, J., Salter, M.W., Wang, Y.T., Tasker R.A., Garman D., Rabinowitz, J., Lu, P.S., Tymianski, M. PDZ protein interactions underlying NMDA receptor-mediated excitotoxicity and neuroprotection by PSD-95 inhibitors. *J. Neurosci*., **2007**, *27*, 9901-9915.

[114] Aarts, M.M., Tymianski, M. Molecular mechanisms underlying specificity of excitotoxic signaling in neurons. *Curr. Mol. Med*., **2004**, *4*, 137-147.

[115] Alberdi, E., Sanchez-Gomez, M.V., Matute, C. Calcium and glial cell death. *Cell Calcium*, **2005**, *38*, 417-425.

[116] Chen, H.S., Lipton, S.A. The chemical biology of clinically tolerated NMDA receptor antagonists. *J. Neurochem.*, **2006**, *97*, 1611-1626.

[117] Gogas, K.R. Glutamate-based therapeutic approaches: NR2B receptor antagonists. *Curr. Opin. Pharmacol*., **2006**, *6*, 68-74.

[118] Lipton, S.A. Paradigm shift in neuroprotection by NMDA receptor blockade: memantine and beyond. *Nat. Rev. Drug Discov*., **2006**, *5*, 160-170.

[119] Muir, K.W. Glutamate-based therapeutic approaches: clinical trials with NMDA antagonists. *Curr. Opin. Pharmacol*., **2006**, *6*, 53-60.

[120] Parsons, C.G., Gilling, K. Memantine as an example of a fast, voltage-dependent, open channel N-methyl-D-aspartate receptor blocker. *Methods Mol. Biol*., **2007**, *403*, 15-36.

[121] Parsons, C.G., Stoffler, A., Danysz, W. Memantine: a NMDA receptor antagonist that improves memory by restoration of homeostasis in the glutamatergic system--too little activation is bad, too much is even worse. *Neuropharmacology*, **2007**, *53*, 699-723.

Received: December 04, 2012 Revised: January 08, 2013 Accepted: February 02, 2013

OPEN ACCESS Freely available online

PLOS ONE

Heterogeneity of Astrocytes: From Development to Injury – Single Cell Gene Expression

Vendula Rusnakova[1], Pavel Honsa[2], David Dzamba[2], Anders Ståhlberg[3], Mikael Kubista[1], Miroslava Anderova[2]*

1 Laboratory of Gene Expression, Institute of Biotechnology, Academy of Sciences of the Czech Republic, Prague, Czech Republic, **2** Department of Cellular Neurophysiology, Institute of Experimental Medicine, Academy of Sciences of the Czech Republic, Prague, Czech Republic, **3** Sahlgrenska Cancer Center, Department of Pathology, Sahlgrenska Academy at the University of Gothenburg, Gothenburg, Sweden

Abstract

Astrocytes perform control and regulatory functions in the central nervous system; heterogeneity among them is still a matter of debate due to limited knowledge of their gene expression profiles and functional diversity. To unravel astrocyte heterogeneity during postnatal development and after focal cerebral ischemia, we employed single-cell gene expression profiling in acutely isolated cortical GFAP/EGFP-positive cells. Using a microfluidic qPCR platform, we profiled 47 genes encoding glial markers and ion channels/transporters/receptors participating in maintaining K^+ and glutamate homeostasis per cell. Self-organizing maps and principal component analyses revealed three subpopulations within 10–50 days of postnatal development (P10–P50). The first subpopulation, mainly immature glia from P10, was characterized by high transcriptional activity of all studied genes, including polydendrocytic markers. The second subpopulation (mostly from P20) was characterized by low gene transcript levels, while the third subpopulation encompassed mature astrocytes (mainly from P30, P50). Within 14 days after ischemia (D3, D7, D14), additional astrocytic subpopulations were identified: resting glia (mostly from P50 and D3), transcriptionally active early reactive glia (mainly from D7) and permanent reactive glia (solely from D14). Following focal cerebral ischemia, reactive astrocytes underwent pronounced changes in the expression of aquaporins, nonspecific cationic and potassium channels, glutamate receptors and reactive astrocyte markers.

Citation: Rusnakova V, Honsa P, Dzamba D, Ståhlberg A, Kubista M, et al. (2013) Heterogeneity of Astrocytes: From Development to Injury – Single Cell Gene Expression. PLoS ONE 8(8): e69734. doi:10.1371/journal.pone.0069734

Editor: Michal Hetman, University of Louisville, United States of America

Received April 26, 2013; **Accepted** June 12, 2013; **Published** August 5, 2013

Copyright: © 2013 Rusnakova et al. This is an open-access article distributed under the terms of the Creative Commons Attribution License, which permits unrestricted use, distribution, and reproduction in any medium, provided the original author and source are credited.

Funding: This work was supported by the Academy of Sciences of the Czech Republic IBT AS CR [AVOZ50520701] and UEM AS CR [AV0Z50390703]; by Grant Agency of the Czech Republic [P303/13/02154S]; by an EMBO Short Term Fellowship [ASTF 110-2011] and an ESF Functional Genomics Short Visit Grant [2426]. The funders had no role in study design, data collection and analysis, decision to publish, or preparation of the manuscript.

Competing Interests: The authors have declared that no competing interests exist.

* E-mail: anderova@biomed.cas.cz

Introduction

Astrocytes comprise a heterogeneous cell type with several subgroups; for review see [1]. Even within the same brain region multiple astrocytic subgroups have been observed [2]. In addition to morphological differences, astrocytes show diversity in Ca^{2+} signalling, gap junction coupling, and the expression of membrane proteins such as K^+ channels, glutamate receptors and transporters; for review see [3]. It was recently shown that astrocyte heterogeneity also rests on the expression of inwardly rectifying (KIR) and two-pore-domain K^+ (K2P) channels [4]. In our recent work we demonstrated the presence of two distinct subpopulations of astrocytes that respond differently to oxygen-glucose deprivation, probably due to their different expression of chloride channels (ClC2), inwardly rectifying K^+ channels (KIR4.1) and K2P channels, such as TREK-1 and TWIK-1 [5]. Astrocytes also change their properties during development. In contrast to neurons, astrocytes are formed at late stages of embryogenesis (from E16 and onward) and during the first postnatal weeks [6], and the mouse cortex is not fully developed until between the 3rd and 4th week after birth [7]. The origin of astrocytes is not fully known; possibly they arise from distinct groups of progenitors [8], and some subpopulations may be generated from NG2 glia cells [9]. NG2 glia are characterized by their expression of NG2 chondroitin sulphate proteoglycan (CSPG4) and platelet-derived growth factor α receptor (PDGFαR). After their discovery, NG2 glia were found to be oligodendrocyte progenitor cells [10]. Later, NG2 glia were also shown to be progenitors of some groups of reactive astrocytes [11,12], which appear after CNS injury. This process, termed astrogliosis, is characterized by the increased expression of glial fibrillary acidic protein (GFAP) and Nestin, followed by the elevated expression of vimentin [13]. Another characteristic of astrogliosis is the high expression of aquaporins, especially of AQP1 and AQP9, which are proteins rarely expressed in healthy tissue [14,15]. Several publications have reported reactive astrocytes expressing proteoglycans [16,17] and glutamate metabotropic receptor 5 (*Grm5*) [18,19]. Traditionally, astrocytes are identified by the expression of GFAP [20]. However GFAP is not always expressed in non-reactive astrocytes, and GFAP is frequently not immunohistochemically detected in astrocytes in healthy tissue [21]. Other complementary markers are therefore used to identify astrocytes, including S100β [22], excitatory amino acid transporter 1 and 2 (EAAT1 and 2) [23], glutamine synthetase (GS) [24] and aldehyde dehydrogenase 1 family member L1 (ALDH1L1) [25]. Since non-glial cells also express some of these markers, detecting a combination of markers is needed for the reliable identification of astrocytes [26].

Altogether, there is evidence of astrocyte heterogeneity between, as well as within, CNS regions. To characterize the different types of astrocytes that appear under various conditions, single-cell studies are necessary. Single cell gene expression profiling is a novel and powerful method to study cell heterogeneity [27]. It has already been used to establish the presence of distinct subpopulations of astrocytes in a seemingly homogenous macroscopic population [5,28]. Single cell expression profiling is challenging because of the limited amount of RNA present in a single cell. Very efficient reverse transcription is needed, and for the analysis of more than some 10 genes preamplification is required. Cells express mRNAs in bursts [29,30], resulting in large natural variation in the number of any transcript among cells, which can be modelled with a lognormal distribution [31]. To obtain biologically relevant and statistically significant conclusions, rather large numbers of cells must be analysed [32]. A particularly powerful approach to distinguish different cells and subtypes of cells is to study the correlation of transcript levels within individual cells [33]. This kind of information is not available when studying classical samples composed of many cells.

Our goal was to characterize astrocytes based on changes in their gene expression profiles throughout development and after focal cerebral ischemia. We used single cell RT-qPCR profiling to analyse EGFP-positive ($EGFP^+$) cells collected by fluorescence-activated cell sorting (FACS) from the cortex of GFAP/EGFP transgenic mice with the objective of identifying and characterizing subpopulations of astrocytes. We focus our profiling effort on glial glutamate transporters and receptors as well as on ion channels, which are critical for the maintenance of the ionic/neurotransmitter homeostasis of neurons and glial cells under physiological conditions as well as in pathological states.

Materials and Methods

Induction of an Ischemic Lesion in Adult GFAP/EGFP Mice

All experiments were performed on cells from acutely isolated brains of GFAP/EGFP transgenic mice [line designation TgN(GFAPEGFP)], in which the expression of EGFP is controlled by the human GFAP promoter [34]. All procedures involving the use of laboratory animals were performed in accordance with the European Communities Council Directive 24 November 1986 (86/609/EEC) and animal care guidelines approved by the Institute of Experimental Medicine, Academy of Sciences of the Czech Republic (Animal Care Committee on April 17, 2009; approval number 85/2009).

Prior to the induction of focal ischemia, 50-day-old (P50) mice were anaesthetized with 1.5% isoflurane (Abbot) and maintained in 1% isoflurane using a vaporizer (Tec-3, Cyprane Ltd., Keighley). A skin incision between the orbit and the external auditory meatus was made, and a 1–2 mm hole was drilled through the frontal bone 1 mm rostral to the fusion of the zygoma and the squamosal bone and about 3.5 mm ventral to the dorsal surface of the brain. The middle cerebral artery (MCA) was exposed after the dura was opened and removed. The MCA was occluded by short coagulation with bipolar tweezers (SMT, Czech Republic) at a proximal location, followed by transection of the vessel to ensure permanent occlusion. The mice received 0.5 ml saline solution subcutaneously, and during the surgery the body temperature was maintained at $37\pm1^{\circ}C$ using a heating pad.

Immunohistochemistry

The mice were deeply anaesthetized with pentobarbital (PTB, 100 mg/kg, i.p.) and perfused transcardially with 20 ml of saline followed by 20 ml of cooled 4% paraformaldehyde in 0.1 M phosphate buffer. Brains were dissected out, fixed with paraformaldehyde overnight, cryoprotected with sucrose and sliced into 30 μm coronal slices using a microtome (HM550, Microm International). The slices were incubated with 5% Chemiblocker (Millipore) and 0.2% Triton in PBS then with the primary antibodies at $4^{\circ}C$ overnight. As primary antibodies, we used anti-GFAP (1:800, Sigma-Aldrich, mouse, conjugated with Cy3), anti-GFAP (1:800, Sigma-Aldrich, mouse), anti-NG2 (1:400, Chemicon, rabbit) and anti-PDGFαR (1:200, Santa Cruz, rabbit). Finally, the secondary antibody was applied for 2 hours, either goat anti-mouse IgG or goat anti-rabbit IgG conjugated with Alexa Fluor 660 (Molecular Probes). A Zeiss 510DUO LSM confocal microscope equipped with Arg/HeNe lasers was used for immunohistochemical analysis. Colocalization images and their maximum z projections were made using a Zeiss LSM Image Browser.

Preparation of Cell Suspensions from the Cortex of GFAP/EGFP Mice

GFAP/EGFP transgenic mice 10, 20, 30 and 50 days old (P10, P20, P30, P50) or 3, 7, and 14 days after middle cerebral artery occlusion (MCAO) (D3, D7, D14) were deeply anesthetized with PTB (100 mg/kg, i.p.) and perfused transcardially with cold (4–$8^{\circ}C$) isolation buffer containing (in mM): NaCl 136.0, KCl 5.4, Hepes 10.0, glucose 5.5, osmolarity 290 ± 3 mOsmol/kg. The forebrain was isolated by the removal of the olfactory lobes, cerebellum, and midbrain/hindbrain structures by dissection. To isolate the cerebral cortex, the brain (+2 mm to −2 mm from bregma) was sliced into 400 μm coronal sections using a vibrating microtome HM650V (MICROM International GmbH), and the dorsal cerebral cortex was carefully dissected out from the ventral white matter tracks. The tissue was incubated with continuous shaking at $37^{\circ}C$ for 90 minutes in 5 ml of a papain solution (20 U/ml) and 0.2 ml DNase (both from Worthington) prepared in isolation buffer. After papain treatment, the tissue was mechanically dissociated by gentle trituration using a 1 ml pipette. Dissociated cells were layered on the top of 5 ml of Ovomucoid inhibitor solution (Worthington) and harvested by centrifugation ($140\times g$ for 6 minutes). This method routinely yielded $\sim2\times10^6$ cells per mouse. Cell aggregates were removed by filtering with a 30 μm cell strainer (Becton Dickinson), and the cells were kept on ice until sorting.

Collection of Single $EGFP^+$ Cells

Single cells were sorted using flow cytometry (BD Influx). The flow cytometer was manually calibrated to deposit a single cell in the centre of each collection tube. Hoechst 33258 (Life Technologies) was added to the suspension of cells to check viability. Initially, cell sorting was performed with a negative control (no fluorescent cells) in order to set the fluorescence threshold for collecting $EGFP^+$ cells and to avoid auto-fluorescent cells. After setting the threshold, all $EGFP^+$ cells that crossed this level of fluorescence were collected. Single cells were collected into 96-well plates (Life Technologies) containing 5 μl nuclease-free water with bovine serum albumin (1 mg/μl, Fermentas) and RNaseOut 20 U (Life Technologies). Plates were placed on a pre-cooled rack. The glial cells collected were positive for EGFP and viable. Collected cells in 96-well plates were immediately placed at $-80^{\circ}C$. For analysing individual developmental or post-ischemic stages, the cells were isolated from 1 mouse (P10), 2 mice (P20), 1 mouse (P30), 1 mouse (P50), 2 mice (D3), 2 mice (D7) and 1 mouse (D14).

cDNA Synthesis

cDNA synthesis was performed with SuperScript III RT (Life Technologies). Lysed single cells in 5 µl water containing 0.5 µM dNTP (Promega), 1.0 µM oligo (dT15) (Invitrogen) and 1.0 µM random hexamers (Eastport) were incubated at 70°C for 5 min. 50 mM Tris–HCl, 75 mM KCl, 3 mM $MgCl_2$, 5 mM dithiothreitol, 20 U RNaseOut and 100 U SuperScript III (all Life Technologies) were added to a final volume of 10 µl. Reverse transcription was performed at 25°C for 5 min, then at 50°C for 60 min, followed by 55°C for 15 min and finally terminated by heating at 70°C for 15 min. Four µl from each sample was diluted 4 times and used for pre-testing. Five µl of cDNA was used for preamplification.

qPCR

Primers were designed using BeaconDesigner (version 7.91, Premier Biosoft International) as previously described [5]. Primer sequences are provided in Table S1. All single cells were pre-tested for the expression of glutamate transporter (*Eaat2*), glutamine synthetase (*Glul*), which are markers of astrocytes, and chondroitin sulphate proteoglycan (*Cspg4*) and platelet-derived growth factor α receptor (*Pdgfra*), which are markers of NG2 glia, to select samples for further gene expression profiling using assays for 47 genes. A CFX384 (Biorad) was used for all qPCR measurements. To each reaction (10 µl) containing iQ SYBR Green Supermix (BioRad) and 400 nM of each primer (EastPort), we added 3 µl of diluted cDNA. The temperature profile was 95°C for 3 min followed by 50 cycles of amplification (95°C for 15 s, 60°C for 15 s and 72°C for 20 s). All samples were subjected to melting curve analysis. The same experimental setup was used to test preamplification.

Preamplification and qPCR

The applied preamplification protocol was verified on samples from three animals. The RNA was extracted and cDNA was prepared to test the preamplification protocol. Each reaction contained 25 µl of iQ Supermix (BioRad), 5 µl of a mix of all primers (final concentration 25 nM each), 5 µl of non-diluted cDNA, and water added to a final volume of 50 µl. The temperature profile was 95°C for 3 min followed by 18 cycles of amplification (95°C for 20 s, 57°C for 4 min and 72°C for 20 s on a Biorad CFX96). The samples were diluted 5 times in water. The expression of all genes was measured in preamplified and non-preamplified samples. The average difference between preamplified and non-preamplified samples and the standard deviations of the differences were calculated. The same setup was then used for the preamplification of single cells.

High Throughput qPCR

The sample reaction mixture had a volume of 5 µl and contained 2.4 µl of diluted preamplified cDNA, 0.25 µl of DNA Binding Dye Sample Loading Reagent (Fluidigm), 2.5 µl SsoFast EvaGreen Supermix (Biorad), and 0.01 µl ROX (Invitrogen). The primer reaction mixture had a final volume of 5 µl and contained 2.5 µl Assay Loading Reagent (Fluidigm) and 2.5 µl of a mix of reverse and forward primers, corresponding to a final concentration of 4 µM. The chip was first primed with an oil solution in the NanoFlex™ 4-IFC Controller (Fluidigm) to fill the control wells of the dynamic array. The reaction mixture (5 µl) was loaded into each sample well, and 5 µl of the primer reaction mixtures was loaded into each assay well of the 48×48 dynamic array. The dynamic array was then placed in the NanoFlex™ 4-IFC Controller for automatic loading and mixing. After 55 min the dynamic array was transformed to the BioMark qPCR platform (Fluidigm). The cycling program was 3 min at 95°C for activation, followed by 40 cycles of denaturation at 95°C for 5 s, annealing at 60°C for 15 s, and elongation at 72°C for 20 s. After PCR, melting curves were collected between 60°C and 95°C with 0.5°C increments.

Data Pre-processing

qPCR data were pre-processed for expression analysis using GenEx (MultiD, version 5.3) as follows: Cq values registered from amplifications that generated melting curves with aberrant Tm were removed, Cq values larger than 26 were replaced with 26, and Cq values with products giving rise to a double peak in melting curves (corresponding to a mixture of expected and aberrant PCR products) were replaced with 26. All missing data, for each gene separately, were then replaced with the highest Cq +2, effectively assigning a concentration of 25% of the lowest measured concentration to the off-scale values. The Cq data were, for each gene separately, converted into relative quantities expressed relative to the sample with the lowest expression (maximum Cq) and finally converted to a logarithmic scale with base 2. The data were not normalized to any reference genes because of the large variation of all transcript levels among individual cells [33]; with this pre-processing, the levels are expressed per cell.

Analysis

Basic statistics were calculated. The non-parametric Mann-Whitney test was used to compare the expression of individual genes between groups of cells. Kohonen self-organizing maps (SOM) of size 3×1, dividing the cells into three groups, were trained using GenEx with the following parameters: 0.10 learning rate, 3 neighbors and 5000 iterations. The SOM analysis was repeated eight times with identical classification of the cells in six of the repeats. This classification of cells into three groups was substantiated with principal component analysis (PCA). The division of cells into three groups by SOM does not imply that there are three distinct subtypes of cells; the cells may also be changing their expression pattern from one state to another, and the SOM then divides the cells into different phases: those just starting to change, those that have undergone substantial change, and finally cells approaching completion. Distinct subtypes, when such are present, appear as separated clusters in PCA. For Kohonen SOM and PCA the data were mean-centered to reduce the effect of variation in the overall expression levels of the different genes. The Spearman correlation coefficients between genes were calculated for each group separately (SAS vers. 9.2) using all data, including the managed off-scale data, and then also for the truly positive expression values only. Only correlation coefficients for genes expressed in at least 50% of cells and having a p-value <0.05 were considered for further analysis. Indirect correlations between genes were established by calculating partial Spearman correlation coefficients (only genes expressed in at least 80% of the cells were considered). An interaction was considered indirect when the correlation coefficient lost significance (at 95% confidence) or was reduced to below 0.4 [28].

Results

$EGFP^+$ cells from GFAP/EGFP transgenic mice are today routinely used by several research groups [4,35] and characterizing their gene expression profile is highly desirable. Because of the possible heterogeneity of astrocytes, single cells were collected by flow cytometry, lysed, and analyzed individually by RT-qPCR. For preamplification and further analysis we selected $EGFP^+$ cells

that were also positive for the astrocytic markers *Glul* and/or *Eaat2* and EGFP$^+$ cells that were also positive for *Cspg4* and/or *Pdgfra*, which are markers of NG2 glia. In these cells the gene expression of the following markers was measured: glial cell markers (*Eaat1, Gfap, Gfapδ, Glul, S100b, Pdgfra, Cspg4*), developmental markers nestin and vimentin (*nes and vim*), aquaporins (*Aqp1, Aqp4, Aqp9*), subunits of glutamate ionotropic AMPA receptors (*Gria1, Gria2, Gria3, Gria4*), glutamate ionotropic NMDA receptors (*Grin1, Grin2a, Grin2b, Grin2c, Grin2d, Grin3a*), glutamate ionotropic kainate receptors (*Grik1, Grik2, Grik3, Grik4, Grik5*), glutamate metabotropic receptors (*Grm1, Grm3, Grm5*), outwardly rectifying K^+ channels (*Kcna3, Kcna4, Kcna5*), inwardly rectifying K^+ channels (*Kcnj2, Kcnj10, Kcnj16*), two pore domain K^+ channels (*Kcnk1, Kcnk2, Kcnk10*) and hyperpolarization-activated cyclic nucleotide-gated channels (*Hcn1, Hcn2, Hcn3, Hcn4*), voltage-gated chloride channels (*Clcn2*), transient receptor potential channels (*Trpv4*), and *Snap25* encoding synaptosomal-associated protein SNAP-25. The markers were selected based on our previous work [5], which revealed significant differences between astrocytic subpopulations in the expression of genes coding for membrane proteins.

For the profiling of a large number of genes on the Biomark platform, it is necessary to preamplify the cDNA; in this regard, we have extensively optimized and validated the preamplification protocol. Our validation scheme is based on three samples that are profiled with and without preamplification and the measured Cq values are compared. Unbiased preamplification should result in the same ΔCq for all of the genes. The reproducibility of the preamplification is reflected by the standard deviation (SD) of the three ΔCq replicates measured for each gene. For our panel and protocol the SD was below 0.5 cycles for almost all genes. Only one gene (*Grin2d*) showed a large standard deviation (SD = 3.7 cycles) (Figure S1) and was omitted in the expression analysis. Inspecting the validation results, we did not find correlation between assay efficiency and ΔCq.

All cells collected from the cortex were analysed for the expression of *Eaat2*, *Glul*, *Cspg4*, and *Pdgfra* to estimate the ratio between cells that express only astrocytic markers (*Eaat2* and *Glul*) and cells that also express at least one of the NG2 glia markers (Figure 1). The number of cells that expressed only astrocytic markers increased, while the number of cells that also expressed NG2 glia markers decreased during postnatal development. After ischemic injury there was a distinct increase in the number of cells expressing NG2 glia markers 3 days after MCAO, but their number decreased again at later post-ischemic stages. In neither system did the expression profile depend on the EGFP intensity of the cells or on their size. Notably, cells expressing NG2 glia markers were distributed across the entire sorter gate (Figure 2, green dots). For single cell qPCR expression profiling 64 cells were collected from P10, 60 cells from P20, 89 cells from P30, 50 cells from P50, 90 cells from D3, 74 cells from D7, and 78 cells from D14. The cDNA produced from these cells was preamplified and measured on the Biomark platform.

Characteristics of EGFP$^+$ Cells Collected from Different Stages of Postnatal Development

The majority of EGFP$^+$ cells isolated from P10 mice expressed *Cspg4* and/or *Pdgfra* (87%) and *S100b* (80%). More than 70% of these cells also expressed *Eaat1*, *Grik1-3*, *5*, *Gria2-4* and *Kcnj16* (Figure 3A). Generally, cells at P10 were transcriptionally very active (Table 1). The expression profile of cells collected at P20 was different. *Cspg4* and/or *Pdgfra* were expressed in only 32% of the cells, and the expressions of *Kcnj16*, *Eaat1*, *Grik1*, *Grik3*, *Grik5*, *Gria2*, and *Gria4* were also reduced. *Gria3* expression remained high and the expression of *Hcn2*, *Grm5* and *Grin2a* increased. Cells at P30 and P50 displayed very similar expression patterns (Figure 3B). The expression of most genes was lower than at the earlier stages; only *Eaat1*, *Glul*, *Grin2a*, *Gria2* and *Aqp4* showed high expression. The fraction of cells positive for *Pdgfra* and/or *Cspg4* decreased to only 22% and 6% at P30 and P50, respectively.

Cells collected between P10 and P50 were divided by SOM into 3 groups based on their expression profiles (Figure 3C). This SOM classification was fully reproducible - repeated independent classifications predicted the same groups. This shows that the collection of cells is not homogeneous. SOM itself cannot tell if there are distinctly different groups or gradual changes, but the cells can be divided reproducibly into three subpopulations. The spatial separation between the clusters in the PCA suggests that the subpopulations are distinct (Figure 3B). Dividing the cells into more than three groups with SOM did not reveal any additional differences and was not supported by the PCA. We compared the average expression of the individual genes in the three subpopulations, which we henceforth refer to as A1, A2 and A3 (Table S2). Subpopulation A1 was characterized by the high expression of *Pdgfra*, *Cspg4*, *Grik1-3*, *Grik5*, *Gria2-4*, *Grin2a*, *Grin3a*, *Kcnj16*, *Eaat1*, *Glul*, *S100b*, *Snap25* and *Kcnj10* (Figure 3C) and was comprised mainly of P10 cells (composition: 64%, 19%, 13% and 2% of P10, P20, P30 and P50, respectively; Figure 3D). Subpopulation A2 was characterized by the low expression of most genes, including *Eaat1*, *Cspg4*, *Pdgfra*, *Grik5*, *Gria2* and *Grin3a*; only *Glul*, *Hcn2*, *Gria3* and *Grin2a* were highly expressed. Subpopulation A2 was comprised mainly of P20 cells (57%); cells from the other stages (P10, P30 and P50) were present at similarly low levels (Figure 3D). In addition to the classical astrocyte markers *Eaat1*, *Glul*, Aqp4, subpopulation A3 also expressed *Grik5*, *Gria2-3*, *Grin2a*, *Grm3* and *Kcnj16* at high levels and was comprised mainly of P30 and P50 cells (46% of each).

The relation between the expressions of different genes among the individual cells can be evaluated by calculating correlation coefficients. The calculation can include all cells, including those that did not express the genes of interest, or only those cells that had measurable expression. When all cells are considered, the dominant effect is whether a cell expresses both genes or not, while when cells with missing data are filtered out, the correlation coefficient is dominated by the expression levels of genes (Table S3, S4 and S5, Figure S2A–C). Although 95% of all cells in subpopulation A1 expressed *Pdgfra* as well as *Cspg4*, the correlation between their expressions was weak (r = 0.44), which means that they are expressed independently of each other in individual cells. We hypothesize that their expression might be regulated by different transcriptional factors and/or that such a weak correlation between *Pdgfra* and *Cspg4* expression might reflect the different stages of astrocyte maturation even within the A1 subpopulation, which comprises EGFP$^+$ cells from P10 and P20. The correlation between the expression of *Gria2* and *Cspg4* was negligible, while *Gria2* expression correlated with *Pdgfra* (r = 0.60) (Table S3). In subpopulation A3, correlated expression was found between *Glul* and *Eaat1* (r = 0.59) when considering only cells with valid expression data (74 cells) and between *Eaat1* and *Gria2* (r = 0.73). Notably, the correlation of *Eaat1* with *Glul* and of *Eaat1* with *Gria2* in subpopulations A1 and A2 was much lower, thus the increasing correlation between *Glul* and *Eaat1* clearly mirrors the maturation process of astrocytes.

Interestingly, gene expression profiling revealed that a large number of EGFP$^+$ cells express *Cspg4* as well as *Pdgfra* at P10, while at P50 we detected only a negligible number of EGFP$^+$ cells that co-expressed these markers (Figure 1). Furthermore, we also detected the co-expression of *Gfap* and *Cspg4*/*Pdgfra* in most of the cells at P10; this co-expression gradually decreased at P20 and

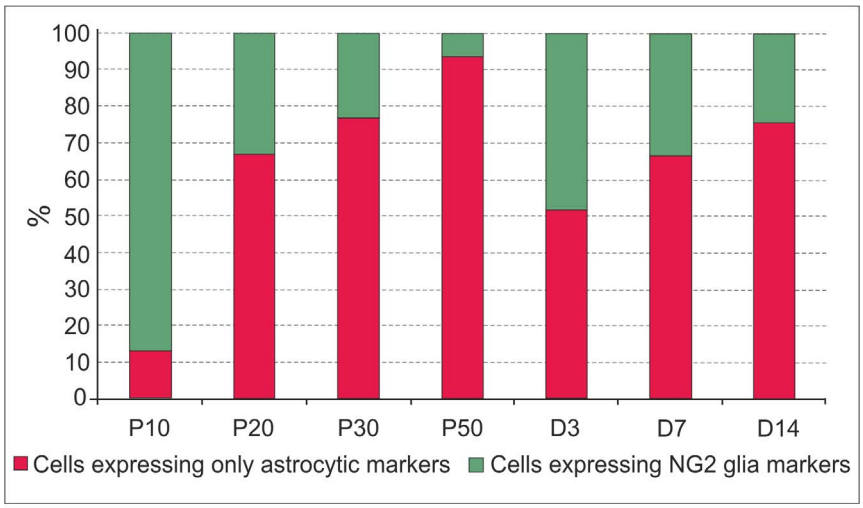


Figure 1. Characteristics of EGFP$^+$ cells in the cortex of GFAP/EGFP mice. (**A**) Percentage of EGFP$^+$ cells expressing either predominantly astrocytic or NG2 glia markers during postnatal development (P10, P20, P30, and P50) and at 3, 7 and 14 days (D3, D7 and D14) following focal cerebral ischemia. Cells expressing *Cspg4* and/or *Pdgfra* receptor are shown in green, while cells expressing only *Eaat2* and/or *Glul* are shown in red. The total numbers of the investigated cells were 137 for P10, 94 for P20, 157 for P30, 50 for P50, 148 for D3, 96 for D7 and 136 for D14.
doi:10.1371/journal.pone.0069734.g001

P30, and at P50 there was no co-expression detected. In order to confirm this observation on the protein level, we carried out immunohistochemical analyses, which revealed the co-expression of GFAP and PDGFαR or of GFAP and NG2 in EGFP$^+$ cells only at P10 and P20, but not at P50 (Figure 4, Figure S3).

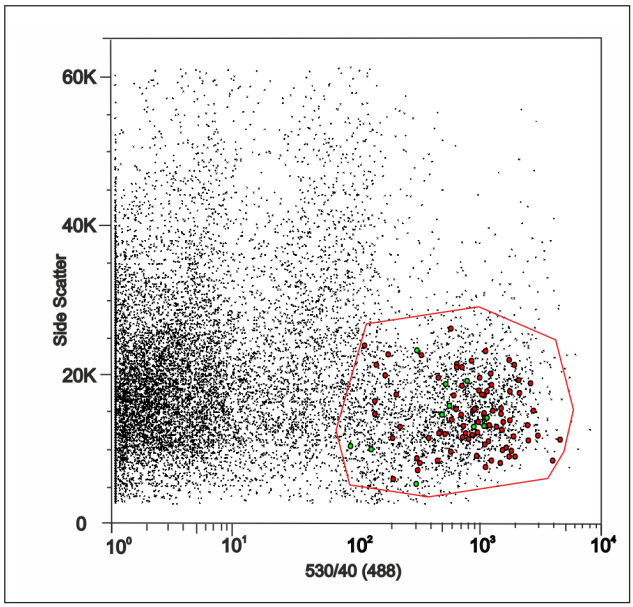


Figure 2. FACS analysis of EGFP$^+$ cells isolated from the cortex of 20-day-old mice. EGFP$^+$ cells sorted based on EGFP intensity (x axis) and side scatter intensity reflecting cell size (y axis). During the selection of cells by FACS, their position is automatically saved in the plot, and thus it is possible to determine the expression profile of each individual cell in the plot after qPCR analysis. The red line indicates the sorter gate and each dot represents one cell. Cells positive for *Cspg4* and/or *Pdgfra* are indicated in green while those positive only for *Eaat1* and/or *Glul* are shown in red. The latter are also drawn larger for better resolution. The small black dots represent all of the cells from which we selected our samples.
doi:10.1371/journal.pone.0069734.g002

Expression Profiling of Reactive Glia Following Focal Cerebral Ischemia

Three days after ischemia the expression profiles of the cells had changed. Approximately 50% of all EGFP$^+$ cells began to express *Pdgfra*, *Vim*, and *Grik5*, while *Aqp4*, *Glul* and *Eaat1* expression was decreased. Seven days after ischemia the cells were transcriptionally more active with particularly high expression of *Pdgfra*, *Vim*, *S100b*, *Eaat1*, *Glul*, *Gria2-4*, *Grin2a*, *Grin2b*, *Grik2*, *Grik5*, potassium channels *Kcna4*, *Kcna5*, *Kcnj10*, *Kcnj16*, *Aqp4* and *Hcn2*. Furthermore, the cells also began to express *Gfap* and *Gfapδ*. At this time, the expression of *Glul* returned to the basal level (P50, Figure 5A). Fourteen days after ischemia, the difference in expression compared to control (P50) was the largest. The expression of *Vim*, *Gfap*, *Gfapδ*, *Aqp4*, *S100b* and *Grm3* had dramatically decreased, while the expression of *Hcn1*, *Hcn2*, *Hcn3*, *Aqp1*, *Aqp9*, *Grm5*, *Gria3*, *Grin2a*, *Grin2d*, *Snap25* and *Kcna3* had markedly increased. At all post-ischemic stages, we found some cells expressing *Cspg4* and *Pdgfra*.

All cells (P50, D3, D7 and D14) were divided by SOM into 3 subpopulations and confirmed by PCA to have different expression profiles (Figure 5B). We will refer to these subpopulations as B1, B2 and B3. To characterize these subpopulations, we compared the expressions of the genes individually in histograms and by conventional univariate statistics. Almost all cells from P50 were assigned to subpopulation B1 (48 out of 50) (Figure 5C), and they comprised 35% of the B1 cells. 47% of B1 cells were from D3, 15% from D7, and only 3 B1 cells were from D14 (Figure 5D). The B1 subpopulation displayed the lowest overall transcriptional activity; high expression was observed only for *Eaat1*, *Glul*, *Aqp4* and *Gria2*. Subpopulation B2 was more transcriptionally active with the high expression of genes encoding glutamate ionotropic receptors, K^+ channels, *Grm3*, *Aqp4*, *Hcn2*, *Gfap*, *Gfapδ*, *Glul*, *Eaat1*, *S100b*, *Vim*, *Cspg4*, and *Pdgfra*. Most B2 cells were from D7 (66%), 31% were from D3 and only 2 cells were from P50. Notably, the two P50 cells also expressed *Pdgfra* and *Cspg4*. Subpopulation B3 was composed of only D14 cells. The very high expression of many genes makes this group unique, and there is no overlap in the PCA between B3 and the other subpopulations. Clearly, the B3 subpopulation is distinct. We also noted that the EGFP

Table 1. Statistics describing gene expression in different postnatal developmental stages or post-ischemic stages.

	Percentage of positive cells							Average relative expression log_2						
Gene	**P10**	**P20**	**P30**	**P50**	**D3**	**D7**	**D14**	**P10**	**P20**	**P30**	**P50**	**D3**	**D7**	**D14**
All cells (count)	64	60	79	50	90	74	78							
Cspg4	77%	32%	46%	4%	49%	35%	38%	3.63	1.45	2.22	0.10	1.99	1.45	1.63
Pdgfra	78%	40%	51%	4%	49%	35%	42%	6.32	2.38	3.37	0.25	3.03	2.36	2.71
Eaat1	83%	65%	92%	90%	88%	80%	87%	4.21	2.35	5.41	6.00	4.48	4.84	5.81
Glul	63%	58%	92%	92%	76%	81%	92%	2.16	2.80	4.50	5.79	3.61	5.91	5.84
Gfap	8%	13%	27%	8%	40%	57%	40%	0.29	0.47	1.15	0.35	1.55	4.14	1.95
Gfap D	19%	20%	44%	32%	47%	64%	40%	0.40	0.55	1.27	0.75	1.66	3.75	1.40
S100b	80%	48%	62%	64%	72%	85%	82%	2.05	1.37	1.87	1.54	2.09	3.81	2.28
nestin	11%	3%	11%	0%	23%	16%	10%	0.24	0.11	0.46	0.00	0.92	0.68	0.45
Vim	31%	23%	30%	18%	60%	82%	55%	0.79	0.69	0.91	0.45	3.33	5.91	1.89
Snap25	61%	25%	35%	26%	27%	26%	77%	1.93	0.82	1.53	1.15	0.82	0.86	4.02
Aqp1	2%	50%	0%	0%	1%	4%	79%	0.03	1.13	0.00	0.00	0.02	0.13	4.89
Aqp4	33%	25%	65%	72%	48%	70%	59%	1.03	0.70	2.96	2.81	1.38	4.15	2.78
Aqp9	9%	40%	5%	2%	0%	8%	91%	0.24	1.26	0.22	0.04	0.00	0.23	6.77
Clcn2	27%	27%	22%	28%	33%	28%	31%	0.76	0.86	0.88	1.27	0.96	1.50	1.30
Hcn1	19%	43%	29%	12%	0%	22%	96%	0.46	2.21	1.24	0.48	0.00	0.94	8.81
Hcn2	59%	95%	0%	24%	43%	55%	95%	1.52	5.05	0.00	0.61	1.38	3.30	8.78
Hcn3	31%	62%	28%	10%	22%	34%	88%	0.65	2.08	0.74	0.26	0.51	0.84	6.55
Hcn4	67%	43%	84%	72%	24%	80%	27%	1.40	1.23	1.88	1.46	0.52	1.69	1.85
Trpv4	38%	17%	34%	28%	39%	34%	35%	1.17	0.40	1.16	0.81	1.13	1.27	1.25
Grik1	67%	30%	44%	14%	40%	47%	63%	2.37	0.91	1.70	0.43	1.28	1.89	2.26
Grik2	75%	58%	38%	30%	42%	61%	47%	2.67	1.65	1.39	0.90	1.31	2.87	1.52
Grik3	70%	32%	48%	8%	44%	31%	33%	2.54	1.11	2.17	0.21	1.62	1.28	1.25
Grik4	45%	15%	22%	4%	19%	30%	14%	1.14	0.42	0.76	0.08	0.53	1.12	0.37
Grik5	86%	47%	54%	72%	77%	68%	69%	3.45	1.42	2.14	2.38	3.26	3.39	3.07
Grin3a	67%	32%	61%	10%	43%	35%	51%	2.27	0.90	2.46	0.25	1.25	1.36	1.58
Gria1	41%	12%	16%	8%	18%	16%	28%	0.87	0.28	0.37	0.22	0.44	0.63	0.72
Gria2	91%	62%	52%	74%	76%	66%	77%	5.22	2.45	2.60	3.54	3.19	3.25	4.08
Gria4	75%	53%	44%	24%	44%	54%	42%	2.67	1.45	1.71	0.83	1.59	2.54	1.54
Grin1	13%	32%	39%	18%	28%	50%	50%	0.27	0.69	1.03	0.47	0.63	1.26	1.30
Grin2a	47%	77%	49%	48%	46%	54%	97%	1.67	3.20	2.45	2.58	1.71	3.11	8.56
Grin2b	61%	33%	33%	30%	44%	57%	59%	1.82	0.90	1.30	1.24	1.37	2.60	2.19
Grin2c	13%	8%	23%	48%	28%	30%	35%	0.29	0.17	0.57	1.55	0.79	0.96	0.94
Grin2d	2%	15%	14%	4%	8%	4%	64%	0.03	0.42	0.55	0.17	0.20	0.11	3.05
Gria3	84%	87%	41%	12%	53%	49%	100%	4.23	4.55	2.21	0.58	2.29	2.46	9.49
Grm1	30%	18%	27%	32%	37%	31%	31%	0.89	0.64	1.01	1.18	1.20	1.24	1.34
Grm3	20%	27%	33%	62%	44%	61%	41%	0.60	1.01	1.35	2.39	1.43	2.80	1.89
Grm5	38%	82%	29%	0%	30%	27%	92%	0.77	2.45	0.77	0.00	0.71	0.64	7.18
Kcna3	25%	67%	18%	14%	23%	27%	91%	0.52	1.47	0.33	0.31	0.52	0.68	6.00
Kcna4	33%	45%	38%	22%	19%	53%	37%	0.99	1.69	1.58	0.73	0.60	2.36	1.48
Kcna5	25%	30%	42%	22%	41%	64%	38%	0.79	0.89	1.58	0.64	1.29	2.83	1.33
Kcnj10	95%	45%	72%	74%	79%	82%	88%	2.05	1.12	1.33	1.48	1.92	3.04	1.96
Kcnj16	66%	30%	54%	52%	60%	55%	58%	2.37	0.96	2.11	2.15	2.25	2.64	2.38
Kcnj2	17%	17%	19%	14%	23%	49%	29%	0.51	0.56	0.73	0.44	0.81	2.12	0.96
Kcnk1	22%	15%	30%	24%	26%	11%	28%	0.53	0.44	1.10	0.65	0.62	0.43	0.94
Kcnk10	67%	25%	33%	20%	44%	50%	32%	1.54	0.55	0.78	0.48	1.02	1.23	0.79
Kcnk2	34%	17%	23%	4%	31%	12%	41%	1.09	0.41	0.80	0.16	0.87	0.42	1.35

doi:10.1371/journal.pone.0069734.t001

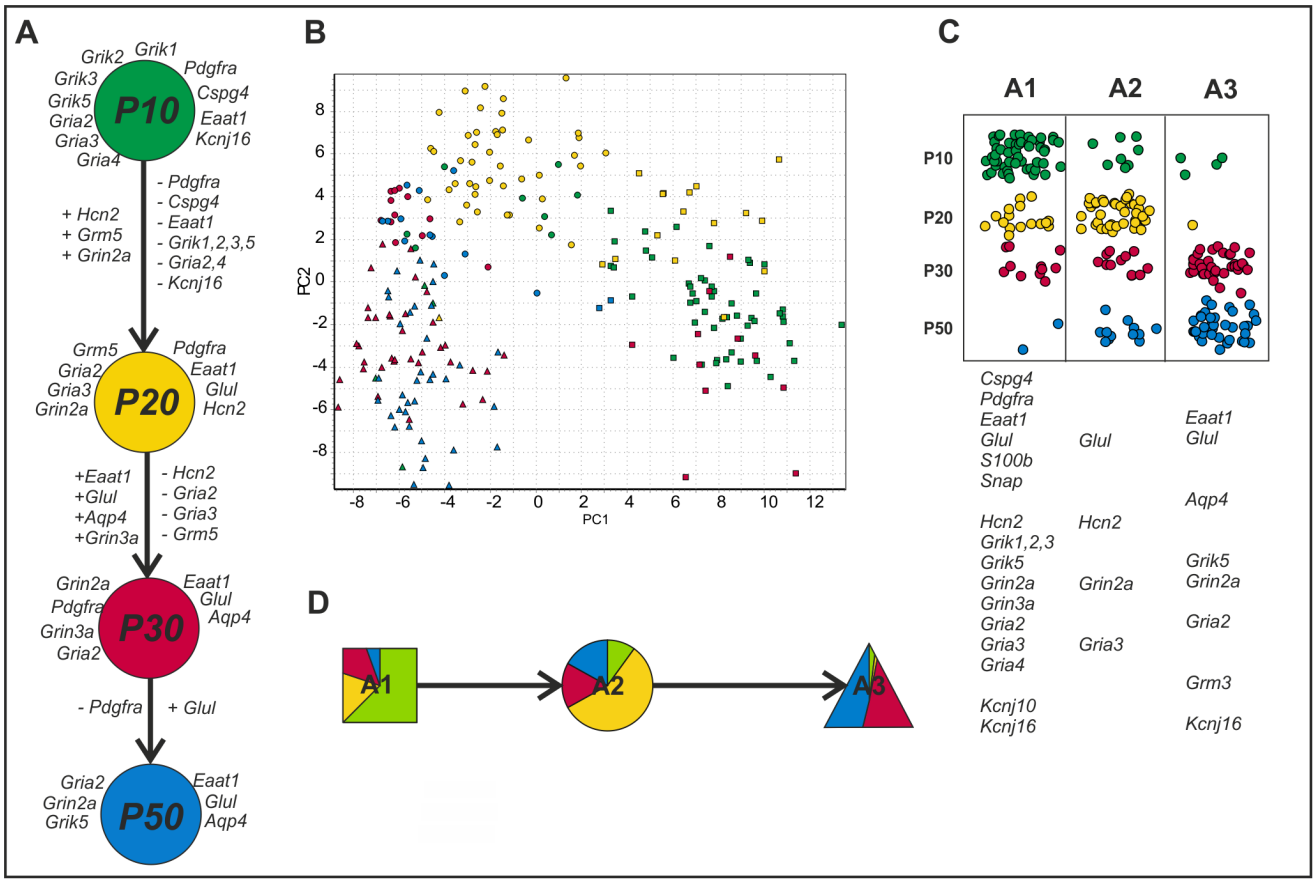


Figure 3. Gene expression profiling of cortical EGFP$^+$ cells during postnatal development. (**A**) Changes in the gene expression of highly expressed (log_2 relative average expression above 2.3 from all data) astrocytic/NG2 glia markers and membrane proteins at P10 (green), P20 (yellow), P30 (red), and P50 (blue). The listed genes show at least 2-fold up (+) or 2-fold down-regulation (−) between sequential developmental stages. (**B**) PCA clustering of cells from all development stages (data mean-centered along genes). The stages are indicated in color (P10 green; P20 yellow; P30 in red, and P50 in blue), and the three groups identified by SOM are indicated by symbols (squares for A1; circles for A2, and triangles for A3). (**C**) The incidence of cells from the three subpopulations at different postnatal developmental stages. The genes under the table indicate highly expressed genes (log2 relative average expression above 1.8 and at least 40% positive cells) in particular subpopulations. (**D**) The distribution of developmental stages in the subpopulations.
doi:10.1371/journal.pone.0069734.g003

fluorescence of these cells was much higher compared to that of cells classified as B1 and B2.

Generally, astrocytes isolated from post-ischemic stages (D3, D7 and D14) showed much higher gene expression than those collected from the postnatal developmental stages. Within each subpopulation B1-B3 we found many significant correlations. The strongest are listed in Tables S6, S7 and S8 and visualized in Figure S2D–F. Interestingly, the expression of *Pdgfra* and of *Cspg4* were strongly correlated when cells with non-measurable expression (r = 0.89, 0.71 and 0.87 in B1, B2 and B3) were included, but the correlation was lost when only cells with measurable expression were considered. The expressions of *Eaat1* and *Glul* in B1 and B3 were correlated (r = 0.66 and 0.79), and a correlation of *Eaat1* and *Aqp4* was found in B1, B2 and B3 (r = 0.43, 0.69, 0.81). A strong correlation was also found between the expressions of *Gfap* and *Gfapδ* in B1 and B2 (r = 0.76 and 0.87) and between the expressions of *Aqp1* and *Aqp9* in B3 (r = 0.78). The expressions of the latter two genes also correlated with those of *Hcn1*, *Hcn2*, *Hcn3*, *Hcn4*, *Grin2a*, *Grin2d*, *Gria3*, *Grm5*, *Kcna3*, *and Kcnk2*. In fact, the expressions of almost all of these genes were strongly correlated on the single cell level in B3 (r close to or larger than 0.7, Figure S4A). Such a strong correlation between the above-listed genes suggests significant alterations in the membrane properties of reactive astrocytes at D14, namely the appearance of *Hcn1-4*, which so far have been described only in neurons [36]. On the other hand, a significant negative correlation was found between the expressions of *Cspg4* or *Pdgfra* and *Glul*, *Aqp9*, *Hcn1*, *Grin2a* and *Gria3* (r<-0.55). This clearly demonstrates that astrocytes from D14 (B3 subpopulation) lose the expression of *Cspg4* and *Pdgfra* while they change into reactive astrocytes comprising a permanent glial scar.

The calculated partial Spearman correlation coefficients surprisingly indicated that there was no direct interaction between *Aqp9* and *Aqp1* (Figure S4B), but the observed correlation can be accounted for as being mediated via *Hcn2* or *Kcna3*. Further, *Aqp9* does not mediate any interaction between *Hcn1*, *Hcn2*, *Hcn3*, *Gria3*, *Grm5* and *Aqp1*. Out of the total 21 possible direct interactions, *Gria3* and *Hcn2* were involved in 10 (Figure S4C and S2D).

Further classification of the reactive glial cells in subpopulation B3 using SOM revealed that it is not a homogenous group; rather there are two subgroups, which we refer to as B3A and B3B. Their existence was clearly confirmed by PCA (Figure 6A). Viewing the data in a 3-dimensional PC1 vs. PC2 vs. PC3 space shows that the B3A/B3B subpopulations separate along PC3 (Figure 6B). Hence, the genes distinguishing B3A from B3B are those with high

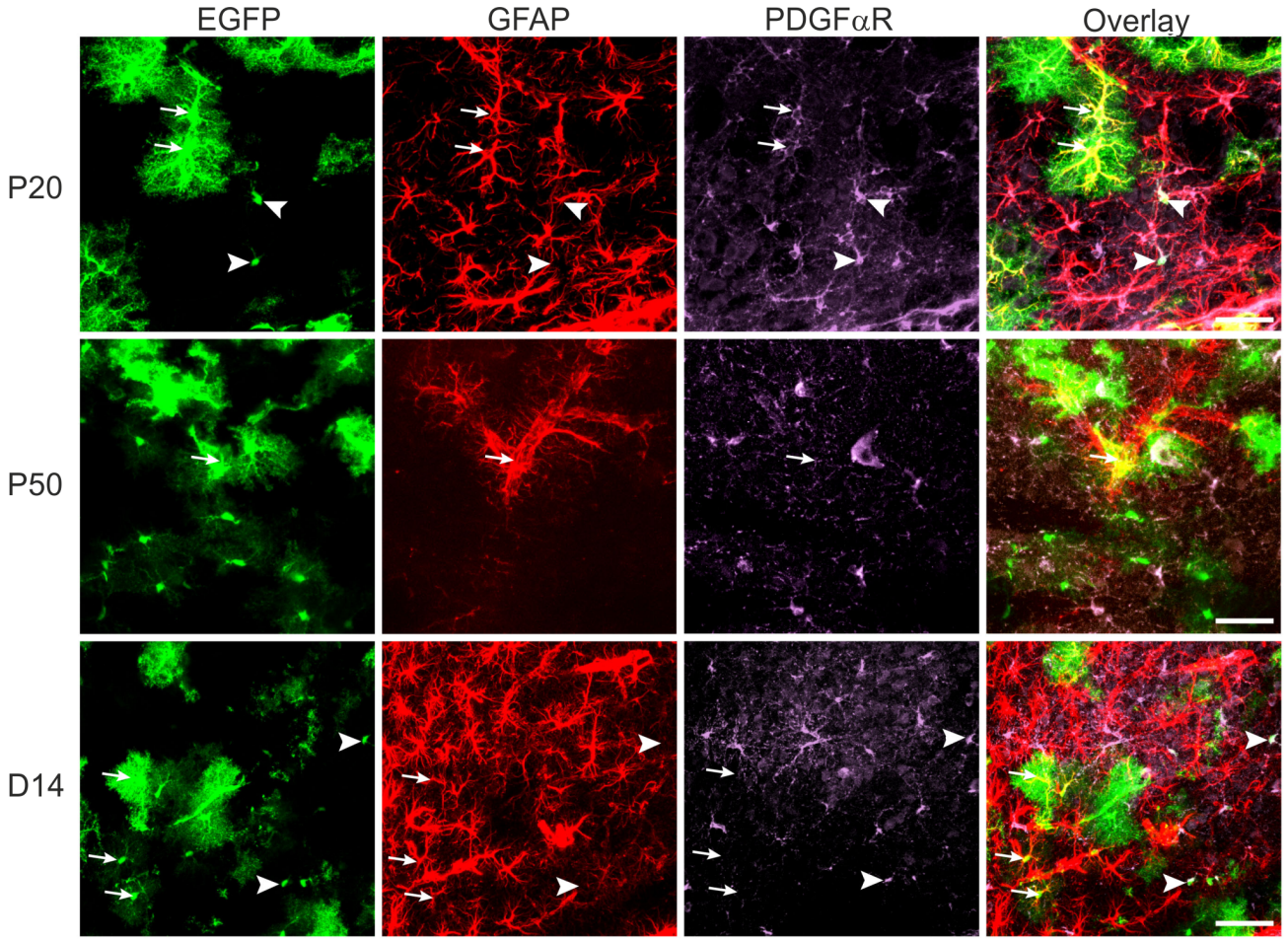


Figure 4. Immunohistochemical analysis of EGFP$^+$ cells. P20, P50, and D14 cells expressing EGFP (green), GFAP (red), and PDGFαR (violet). Arrowheads indicate cells co-expressing EGFP and PDGFαR, and arrows indicate cells positive for EGFP and GFAP. Note, at P20 there are cells positive for all three markers. Scale bars, 50 µm.
doi:10.1371/journal.pone.0069734.g004

weights in PC3, thus being different from the genes distinguishing B3 from B1/B2, which are those with high weights in PC1 and PC2. The expression of genes in the B3A and B3B subgroups were compared using the non-parametric Mann-Whitney test, and those with significant p-values after Bonferroni correction for multiple testing ($p<0.00109$) are shown in Figure 6C. The most important differences between the B3A and B3B subgroups are the down-regulation of *Pdgfra, Cspg4* and *Grik2* and the up-regulation of *Eaat1, Glul, Aqp1, Aqp4, Aqp9, Hcn1, Hcn2, Hcn3, Grin2a, Gria3, Grm3, Grm5* and *Kcna3* (Figure 6C).

Similarly as in the early stages of development, post-ischemic astrocytes also co-expressed *Gfap* and *Cspg4/Pdgfra* (approximately 40%); however, on the protein level we did not detect such co-expression (Figure 4).

Discussion

We show that cortical EGFP$^+$ cells collected during postnatal development as well as cells collected after focal cerebral ischemia are highly heterogeneous with respect to their gene expression profiles. Our findings demonstrate that the issue of astrocyte heterogeneity is complicated, but can be approached with single cell expression profiling, which reveals and distinguishes cell subpopulations. With single cell resolution we can identify rare cells, an approach impossible in classical bulk measurements [37]. Furthermore, single cell profiling avoids the ambiguity of normalization [38].

Astrocyte Heterogeneity during Postnatal Development

We have shown that during postnatal development, the number of EGFP$^+$ cells expressing the astrocytic markers *Glul* and/or *Eaat1* increases towards adulthood, while the number of cells expressing *Cspg4* and/or *Pdgfra* is reduced. Similarly to previous findings, we show that in addition to *Glul*, the expression of *Eaat1*, *Aqp4* and *Grin2a* is induced during development [39]. This is an opposite tendency to that reported by Stanimirovic and colleagues [40], but their experiments were carried out *in vitro*, in a purely astrocytic culture, where glutamate uptake and glutamine synthesis might be compromised. We also found a substantial decrease in *Grik2, Grik3, Gria2, Gria3* and *Gria4* expression during development, which is in agreement with previous data demonstrating the expression of kainate receptors in glial precursor cells, while mature astrocytes show an NMDA-specific responses [41,42]. Similar decline in *Grik1-5* expression during development was described recently by Cahoy and colleagues (Cahoy et al., 2008). In agreement with the findings of Matthias and colleagues [43], we found that EGFP$^+$ cells that express *Cspg4* and/or *Pdgfra* also express *Gria2-4* at high levels, while the low expression of *Gria2-4* is observed in EGFP$^+$

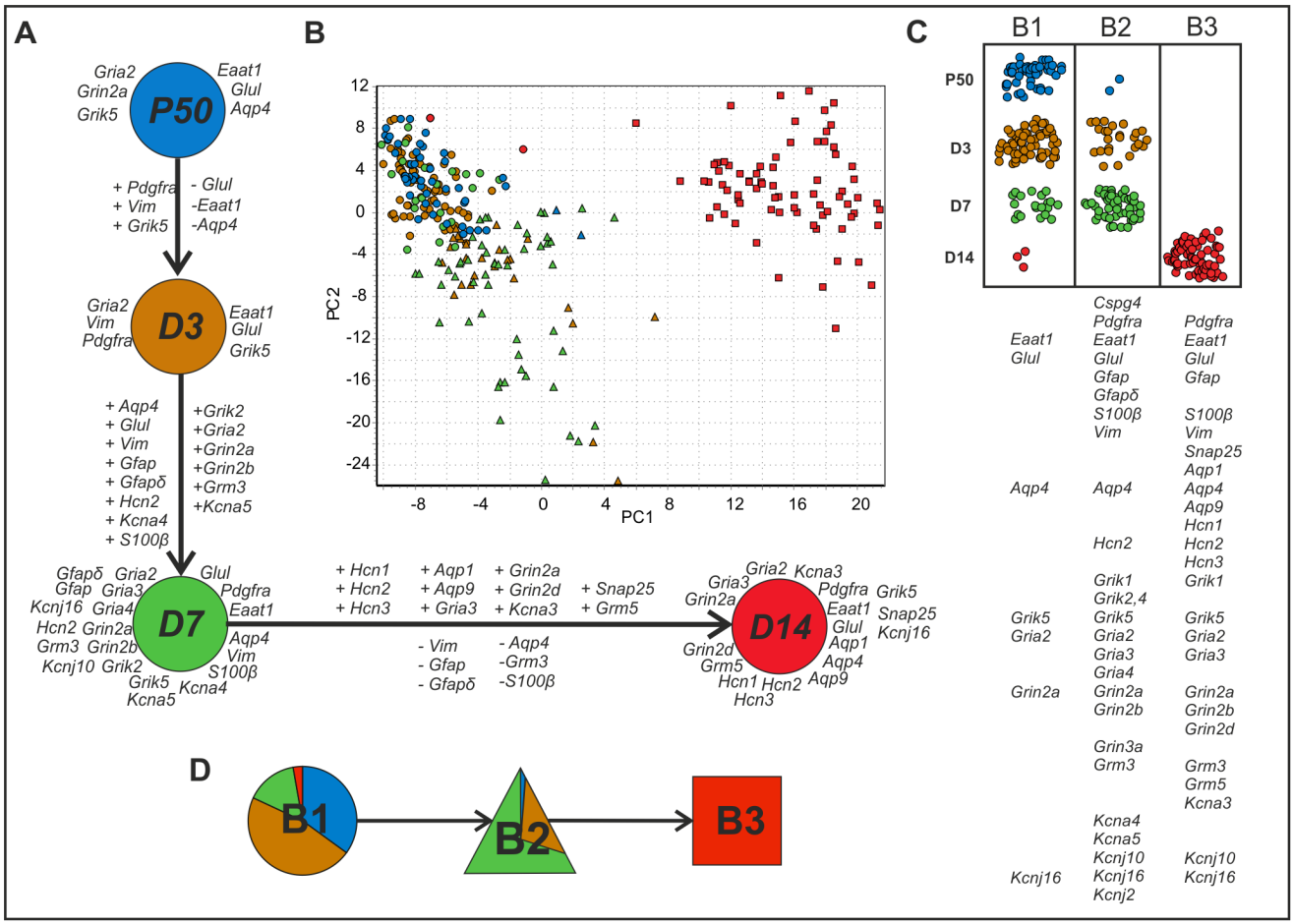


Figure 5. Change in the gene expression of EGFP$^+$ cells after MCAO. (**A**) Changes in the gene expression of highly expressed ($\log_2$ relative average expression above 2.3 from all data) astrocytic/NG2 glia markers and membrane proteins at P50 (blue), D3 (orange), D7 (green), and D14 (red). The listed genes show at least 2-fold up (+) or 2-fold downregulation (−) between sequential stages. (**B**) PCA clustering of cells from all post-ischemic stages and P50 (data mean-centered along genes). The stages are indicated in color (P50 blue, D3 orange, D7 green, and D14 red), and the three groups identified by SOM are indicated by symbols (squares for B3; circles for B1 and triangles for B2). (**C**) The incidence of cells from the three subpopulations at post-ischemic stages and P50. The genes under the table indicate highly expressed genes (log2 relative average expression above 1.8 and at least 40% positive cells) in particular subpopulations. (**D**) The distribution of control and post-ischemic stages in individual subpopulations.
doi:10.1371/journal.pone.0069734.g005

astrocytes that do not express markers of polydendrocytes. These authors also claimed that EGFP$^+$ cells co-express glutamate receptors and transporters, which is supported by our single cell data. As shown in Table 1, we found the co-expression of glutamate receptors and glutamate transporters in individual EGFP$^+$ cells. Among cells collected at the postnatal developmental stages P10-P50, we distinguish 3 subpopulations here referred to as A1, A2 and A3 (Figure 3). A3 cells exhibit features previously described in mature astrocytes with very high expression of *Eaat1*, *Glul* and *Aqp4* [23]. Cells in A1 also express *Eaat1*, but they also have high levels of *Cspg4* and *Pdgfra*, which are traditionally associated with NG2 glia [44]. Nevertheless, *Cspg4* expression in P1-P17 astrocytes was already described elsewhere (Cahoy et al., 2008). Subpopulation A2 is the most unique with high expression of *Glul*, *Hcn2*, *Gria3*, and *Grin2a*, while the transcriptional activity of the other studied genes is rather low. Based primarily on the elevated expression of *Glul* and the low *Gria3* levels, we hypothesize that A2 is an intermediate stage between A1 and A3 (Table S2). This hypothesis is also supported by the prevalence of A2 cells at P20. It is still a matter of debate whether astrocytes can be derived from CSPG4- and/or PDGFαR-positive cells; some recent evidence suggests this possibility following CNS injuries [9,12]. Interestingly, the A1 subpopulation, mostly comprising cells from P10–20, is characterized by the increased expression of subunits of ionotropic AMPA/kainate receptors, such as *Grik1-3*, *Grik5*, *or Gria2-4*, which makes these cells sensitive to AMPA/kainate receptor–mediated glutamate injury. The presence of *Gria2* encoding GluA2 subunits suggests that AMPA receptors in the A1 subpopulation might be impermeable for Ca^{2+}. The subpopulations A3 and B1, which mainly represent mature astrocytes at P30-P50, show besides the expression of classical markers such as *Eaat1*, *Glul* and *Aqp4*, also the dominant expression of *Gria2*, suggesting AMPA receptor impermeability to Ca^{2+}. Moreover, *Kcnj10* and *Kcnj16*, encoding inwardly rectifying Kir4.1 and Kir5.1 channels, are both highly expressed in immature cortical glia, while in mature astrocytes *Kcnj16* prevails. Since heteromeric Kir4.1/5.1 and homomeric Kir4.1 have distinct ion channel properties, such differences in the expression of K^+ channels that participate in K^+ uptake might result in the diverse ability of astrocytes to take up/distribute high extracellular K^+ during increased neuronal activity or in pathological states, such as ischemia or trauma. Notably, even though mature/immature

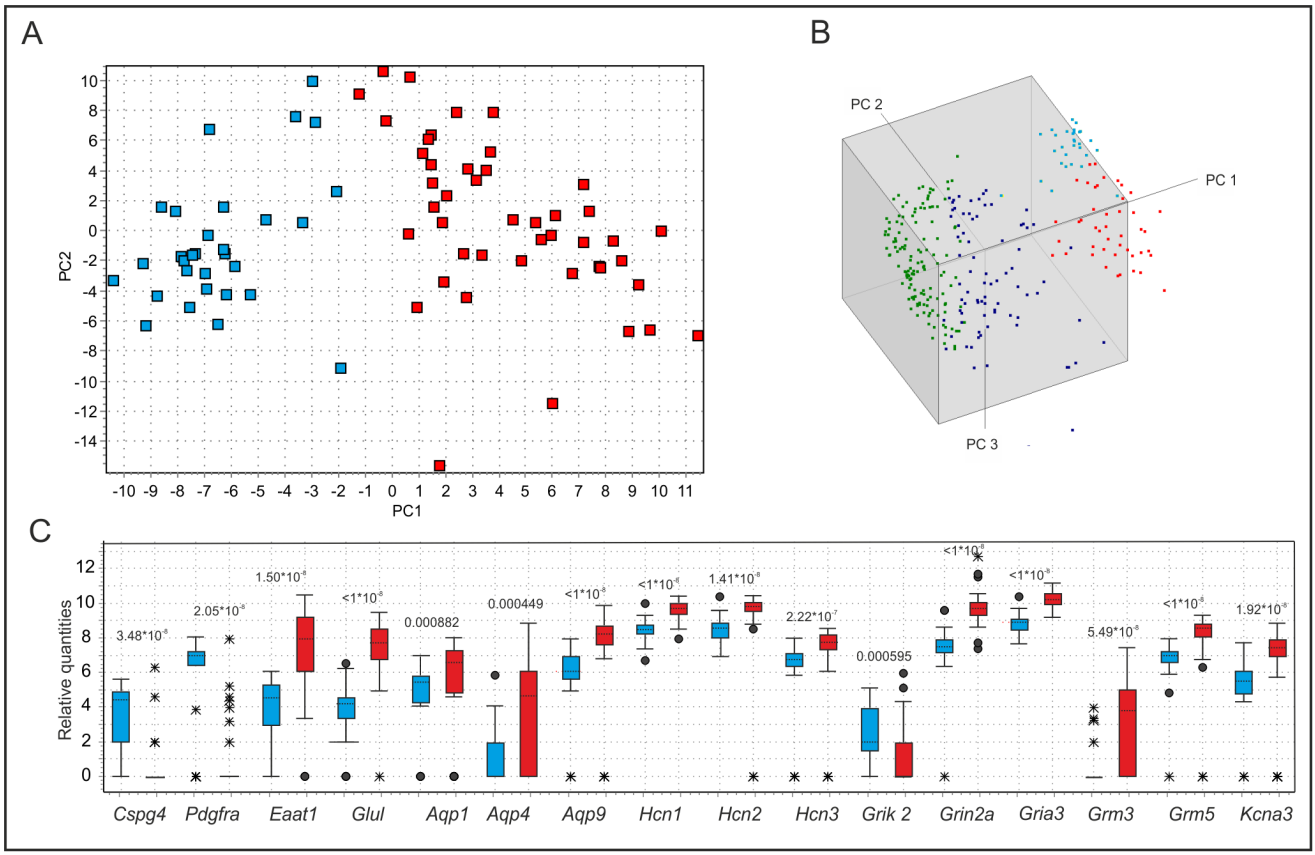


Figure 6. Classification of reactive glia (B3) into two subgroups. (A) PCA scatter plot of the cells in subpopulation B3 (reactive glia). Colors indicate the two groups (B3A red and B3B blue) obtained by decomposing the data by SOM analysis (data are mean-centered). (B) Three-dimensional PCA scatter plot of all post-ischemic cells and P50 reflecting the normal state for comparison - B1 (green), B2 (dark blue), B3A (red) and B3B (light blue). PC3 separates B3A from B3B. The first PC accounts for 32%, the second 14% and the third 8%, of the total variance in the data. (C) Box plots showing genes differentially expressed in B3A (red) and B3B (blue). The box indicates the median value and the 25th and 75th percentiles, the whiskers are 1.5× the distance of the 25th and 75th percentiles, the circles indicate outliers and the crosses extreme outliers. p-values (Mann-Whitney) are indicated for each gene.
doi:10.1371/journal.pone.0069734.g006

astrocytes have been shown to display different K^+ current profiles during development in the rat hippocampal CA1 region [45], such as outward rectifying, variably rectifying and passive current patterns, we found no significant differences in the transcription activities of inwardly and outwardly rectifying K^+ channels or K2P channels between the A1-A3 subpopulations. We found the expression of *Kcnj10* (encoding the Kir4.1 channel) in the $EGFP^+$ cells to be rather constant, while higher levels of *Kcnj16* (encoding Kir5.1) transcripts were found in cells from subpopulations A1 and A3. We did not see any correlation between *Aqp4* and *Kcnj10* expression on the cellular level in any of the subpopulations in agreement with previous data showing the lack of any direct interaction between Kir4.1 and AQP4 [46,47] and their different regulations of expression [48]. In agreement with recent findings [25,49] we showed that $EGFP^+$ mature cortical astrocytes from P30 and P50 (comprising the B3 subpopulation) express low levels of *Grm5*, as a result of a significant decrease in *Grm5* expression towards astrocytic maturation, and a high level of *Grm3*. Nedergaard and colleagues suggested that mGluR5 activity underlies glutamate–induced Ca^{2+} signalling only in immature postnatal astrocytes, while in mature astrocytes other transmitters, such as endocannabinoids, purines, norepinephrine, and acetylcholine, as well as changes in extracellular Ca^{2+}, may trigger astrocytic Ca^{2+} signalling. The activation of mGluR3, a Gi/Go receptor negatively coupled to adenylate cyclase, probably does not participate in glutamate-induced Ca^{2+} signalling as its activation did not trigger a Ca^{2+} increase in adult astrocytes [49]. Since the activation of mGluR3 inhibits cyclic adenosine monophosphate (cAMP) formation, it might participate in the regulation of processes such as astrocyte proliferation, the expression of glutamate receptor GLAST or GFAP expression [50,51].

Gene Expression in Post-ischemic Astrocytes

After CNS injury, such as trauma or ischemia, or in CNS neurodegenerative disorders, the properties of astrocytes change; the cells become reactive [52,53]. This is in line with our finding that the gene expression profile of astrocytes alters following focal ischemia. Particularly affected is the expression of *Gfap, Gfapδ*, *S100b* and *Vim*, which was also observed previously [13,53]. Fourteen days after ischemia, *Aqp1* and *Aqp9* were up-regulated as described earlier [14,15], and similarly to previous reports, we found upregulated *Grm5* [18,19]. Generally, *Aqp1* and/or *Aqp9* are elevated in hypertrophied, GFAP overexpressing astrocytes in a number of pathological states, such as ischemic or traumatic brain injury, Alzheimer's or Creutzfeldt-Jakob diseases [54–56]. In the present study, we detected their increased expression only in the B3 subpopulation, which comprises mostly $EGFP^+$ cells 14 days

after MCAO. Such a delayed increase in their expression suggests that they are probably not implicated in water movements during oedema formation/resolution, but they might play a role as metabolite channels facilitating the diffusion of glycerol and lactate, as suggested previously [57,58]. Moreover, the ischemic brain undergoes marked remodelling, which involves the migration of neighbouring cells to the injury site, thus the increased *Aqp1* expression may reflect a migratory phenotype of reactive astrocytes as AQP1 was shown to promote cell migration in epithelial cells [59] and glial tumors [60,61]. The B2 and B3 subpopulations also highly express AMPA receptor subunits, especially *Gria3*, which suggests that AMPA receptors may significantly contribute to Na^+/Ca^{2+} influx into the reactive astrocytes, and together with the strong expression of metabotropic glutamate receptors (*Grm1, Grm5*) these receptors possibly mediate Ca^{2+} oscillations and glutamate release, as mentioned previously [62]. Furthermore, an increase in *Grm5* expression in reactive astrocytes might lead to the increased activity of mGluR5 and thus contribute to astrocytic apoptosis, as described recently [63]. On the other hand, an anti-apoptotic effect mediated by mGluR3 activation that leads to reduced intracellular levels of cAMP was described in cultured astrocytes after their exposure to nitric oxide [64]. In addition, Aguado and colleagues [65] demonstrated that the activation of ionotropic glutamate receptors is required for the generation of correlated astrocytic network activity, essential for neuronal development and synaptic plasticity. In mature astrocytes under physiological conditions (P50), the Ca^{2+} permeability of AMPA receptors is diminished compared to immature stages (P10) due to the predominant expression of *Gria2*. Interestingly, mRNAs encoding kainate receptor subunits (*Grik1,2,3,5*) are also significantly increased in the B2 and B3 subpopulations; however, their function in reactive astrocytes and those from immature (P10) animals has not yet been elucidated.

Marked changes were also observed in the expression of different types of ion channels, such as outwardly and inwardly rectifying K^+ channels and chloride channels (ClC2), and moreover, Trpv4 expression almost doubled after ischemia, when comparing the B2 and B3 subpopulations to B1. Despite the fact that the expression of *Kcna3-5*, encoding the outwardly rectifying K^+ channels Kv1.3, Kv1.4 and Kv1.5, was comparable in the A1–3 subpopulations during development, it markedly increased in the post-ischemic B2 and B3 subpopulations. Such an increase might point to the fact that astrocytes enter the cell cycle and proliferate following ischemic injury, as shown previously [66]. In addition, an increase in *Clc2* expression could suggest the participation of astrocytes in delivering Cl^- to the site of intensive GABAergic transmission [67], or Cl^- efflux can play a role in astrocyte proliferation/migration as suggested for gliomas [68]. Furthermore, enhanced *Trpv4* expression following MCAO was detected in both the B2 and B3 subpopulations, which is in agreement with our recent data demonstrating an increased expression/function of TRPV4 following hypoxic/ischemic injury of the rat hippocampus [69]. TRPV4 upregulation might originate from its role as an osmosensor as shown in astrocytes [70] or from a possible role of this channel in Ca^{2+} signalling in post-ischemic astrocytes, which may result in astrocytic cell death [71]. A transient increase in *Nes* observed in cells 3 and 7 days after MCAO might support the hypothesis that these subpopulations comprise proliferative/newly derived cells. A striking finding is the high expression of *Hcn1-4*, which encodes hyperpolarization–activated non-specific cationic channels permeable for K^+/Na^+, so far described only in neurons. Despite the fact that their role in astrocytes is unknown, we hypothesize that they might have a role in determining the astrocyte resting membrane potential or they might interact with the glutamate release machinery as described recently for presynaptic terminals [72]. A question that still remains incompletely elucidated is the origin of reactive glia. Certain subpopulations of reactive astrocytes have been shown to arise from NG2 glia [73] or from proliferating astrocytes [74]. Based on our findings, we propose that the B2 subpopulation, which is characterized by an increase in the expression of several astrocytic markers including *Gfap, S100b, Gfapδ* and *Vim*, but also by a marked increase in *Nes, Pdgfra* and *Cspg4*, comprises astrocytes in an ''intermediate stage'' that increase in number as astrogliosis develops (Figure 5). We hypothesize that either NG2 glia give rise to the B2 subpopulation, which eventually develops into fully reactive astrocytes with a distinct expression profile as in subpopulation B3, or they might represent dedifferentiated mature astrocytes with increased proliferative activity. The latter possibility is supported by the fact that they display a relatively similar gene expression profile as $EGFP^+$ cells of the immature cortex (Figure 3). Interestingly, B1 and B2 show some similarity (e.g., the expression of *Pdgfra, Cspg4, Grik1-3, Grik5, Gria2-4, Grin2a* and *Kcnj16*) to the A1 subpopulation observed during early postnatal development (Table S2). Using partial Spearman correlation calculations, we did not identify any master gene in B3 that would account for all of the changes observed upon astrocyte reactivity that follows ischemic injury; however, it is clear that *Gria3* and *Hcn2* are of high importance. In subpopulation B3 we identified several, previously not recognized highly expressed genes: *Hcn1-3, Grin2a, Gria2, Gria3, Grm5* and *Kcna3*. We also found the high expression of *Snap25*, which is expressed only minimally in the other subpopulations and has been suggested to be a marker of cells with exocytotic capabilities under physiological conditions [25]. Similar observations were made in rats [75], where SNAP25 was found upregulated 3 and 12 days after injury. Despite the fact that synaptosomal-associated protein SNAP-25 has not been detected in astrocytes but SNAP-23 [76], our data revealed mRNA levels coding SNAP-25 were significantly increased in cortical astrocytes 14 days post-ischemia (B3 subpopulation). As astrocytes are known to release glutamate and aspartate in response to elevated intracellular calcium levels via a vesicular release mechanism in which SNARE proteins are implicated, high levels of *Snap25* might be a sign of a significant glutamate release from reactive astrocytes. We found a positive correlation between the expressions of *Snap25, Eaat1* and *Glul* and the absence of any correlation with *Cspg4* and *Pdgfra* in B3. We also found a strong correlation between *Eaat1* and *Aqp4* expression, which is in accordance with a recent report suggesting the close relation of excitatory amino acid transporters (*Eaat*) and *Aqp4* under pathological conditions with the massive release of glutamate [14]. Although an association between AQP4 and mGluR5 has been reported [77], we found no correlation on the gene expression level. On the other hand, we did find an extremely strong correlation between *Aqp1/Aqp9* and *Grm5* levels in B3.

Heterogeneity of reactive astrocytes in the vicinity of an ischemic lesion has been described previously [22,78,79]. Even within the B3 subpopulation of reactive astroglia, we found evidence for two subgroups using SOM and PCA: B3A and B3B. B3A is positive for traditional astrocytic markers, while B3B has a substantially higher expression of traditional NG2 glia markers (Figure 6). *Cspg4* has been proposed as a hallmark of reactive astrocytes [16]. Even though the entire B3 population has high overall transcriptional activity, much higher than B1 and B2, there is a difference in the expression levels of many genes between the B3A and B3B subgroups. Since we isolated cells from the vicinity of an ischemic lesion, it is possible that B3 comprises cells permanently converted to reactive glia, which are in different

states or at different distances from the site of the ischemic lesion. Employing Affymetrix GeneChip arrays, the gene expression profiling of reactive astrocytes by Zamanian and colleagues [53] provided transcriptome databases for two subtypes of reactive astrocytes that will be highly useful in generating new and testable hypotheses of their function, as well as for providing new markers to detect different types of reactive astrocytes.

Co-expression of PDGFαR and GFAP in EGFP$^+$ Cells

Our finding that at P10 almost all EGFP$^+$ cells express *Cspg4* and *Pdgfra* and that EGFP$^+$ cells co-express *Gfap* and *Cspg4*/*Pdgfra* was confirmed by immunohistochemistry. (Figure 4, Figure S3); [35]. Similarly, Cahoy and co-authors [25] also detected the high expression of *Cspg4* in immature astrocytes (P7, P17), which declined with astrocyte maturation; however, they never detected *Pdgfra* expression in astrocytes, but rather *Pdgfrb*, which is known to be expressed in pericytes [80]. Although GFAP is a traditional marker of astrocytes and we collected cells where the expression of EGFP is driven by a GFAP promoter, its mRNA level was very low, not at all comparable with the expression of *Cspg4* and *Pdgfra*. The GFAP protein must therefore be stable with slow turnover in the cortex. Nevertheless, *Gfap* and *Gfapδ* increased with astrocyte maturation similarly to the highly expressed *Glul, Eaat1* and *Aqp4*. Interestingly, in subpopulations A1, B2 and B3, *Cspg4* and *Pdgfra* are co-expressed on the mRNA level in 95% of cells, but the correlation between their expressions on the single cell level is not particularly strong ($r = 0.44$, $p = 0.001$ for A1, $r = 0.23$, $p = 0.151$ for B2, $r = 0.27$, $p = 0.159$ for B3). *Cspg4* and *Pdgfra* also show quite different correlations with other genes. This suggests *Cspg4* and *Pdgfra* are expressed independently of each other in individual cells, even in cells from the same subpopulation. The absence of correlation between highly expressed genes in individual cells of the same kind has been observed previously [33] and has been interpreted as the cells having independent transcription regulatory mechanisms, which leads to independent transcriptional bursts.

We do not think that the expression of *Cspg4* or *Pdgfra* in EGFP/GFAP cells isolated from the cortex of P10 animals was detected simply due to sensitivity in which low transcript levels are amplified. PDGFαR and NG2 are expressed in these cells also on the protein level as demonstrated by immunohistochemistry in Figure 4 for PDGFαR and in Figure S3 for NG2. These images show without any doubt that EGFP-positive cells (P10–20 mice) co-express GFAP and PDGFαR or NG2, the expression of which disappears at P50. More interestingly, in post-ischemic tissue the expression of both *Cspg4* and *Pdgfra* reappears; however, their expression on the protein level does not coincide with EGFP/GFAP-positive reactive astrocytes, which might suggest that newly generated reactive astrocytes lose both NG2 or PDGFαR when they reach the stage of fully developed reactive astroglia 14 days post ischemia, while those still expressing NG2 and/or PDGFαR might partially comprise cells in transition into reactive astrocytes or dedifferentiated astrocytes that display the gene expression profile of immature P10-P20 astrocytes (A1 subpopulation). This is also obvious from the division of the B3 subpopulation into two groups: B3A and B3B (Figure 6). Cells in the B3A group express *Cspg4* and *Pdgfra*, while the expression of *Eaat1, Glul* and *Aqp4* is significantly lower than in the B3B group. Therefore, NG2 or PDGFαR-positive cells may reflect astrocytes in a transitional stage similar to that described by Zhu and colleagues [81]. They showed that a subpopulation of GS$^+$ astrocytes is the progeny of NG2 cells, thus confirming the previous finding that NG2 cells give rise to protoplasmic astrocytes. They also showed the co-expression of aldehyde dehydrogenase (*Aldh1L*1, another marker of astrocytes) immunoreactivity in their somata and faint PDGFαR immunoreactivity in their processes, indicative of transitional cells that are losing PDGFαR and acquiring Aldh1L1. Similar data showing the co-expression of GFAP and NG2 in ischemic tissue were described in our recent publication [12].

The Basis of Astrocyte Heterogeneity

The heterogeneity of astrocytes even within an individual brain region, such as the cortex, might already arise during their development. Some astrocytes originate from cells in the ventricular zone via radial glia intermediates, while other astrocytes arise from immature cells that migrate in the perinatal period from the dorso-ventral subventricular zone into the brain [82]. Radial glia, which give rise to distinct subsets of forebrain neurons and later on to glial cells, must be highly heterogeneous themselves with respect to their progenitor function, which strongly depends on the expression of different sets of transcription factors such as Emx1 and Dach1. Progenitors expressing these transcription factors give rise, besides cortical and hippocampal CA1 neurons, to a subset of cortical and hippocampal astrocytes [83–85] and also to a subpopulation of astroglia in the dorsal roof of the subventricular zone [86]. How the developmental heterogeneity of astrocytes relates to their functional heterogeneity still remains unresolved. In addition, astrocytes might also display a spatial heterogeneity as they surround blood vessels and/or different synapses. Nonetheless, a diversity of astrocytic responses to pathological stimuli, such as oxygen-glucose deprivation or hypotonic stress, has been demonstrated in the cortex [5,87]. As reported earlier [88], there also exists a subpopulation of astrocytes that do not express GFAP and that were not considered in this study.

Conclusions

We have used single cell expression profiling and multivariate expression analysis to identify and characterize subpopulations of astrocytes present during postnatal development and after focal cerebral ischemia. We found that transcriptional activity decreases during development and that fully mature astrocytes express mainly *Eaat1, Glul, Aqp4* and *Kcnj10* and *Kcnj16*. After a brain injury the situation rapidly changes - the astrocytes become reactive and express *Eaat1, Glul, Aqp1, Aqp9, Snap25,* hyperpolarization-activated cation channels *Hcn1, Hcn2, Hcn3*, glutamate receptors *Grin2a, Gria2, Gria3, Grm5* and potassium channels *Kcna3* and *Vim*.

Supporting Information

Figure S1 Validation of pre-amplification. Three separate RNA samples were isolated from the cortex of three different mice, transcribed and preamplified. cDNA levels were measured with preamplification (P) and without preamplification (NP). The average difference (ΔCq) and the standard deviation of the difference between P and NP for each gene were calculated for each of the three RNA samples.
(TIF)

Figure S2 Schemas of all correlations higher than 0.6 for subpopulation A1 (A), subpopulation A2 (B), subpopulation A3 (C), subpopulation B1 (D), subpopulation B2 (E), and subpopulation B3 (F). Positive correlations are indicated by green lines, while red lines indicate negative correlations.
(TIF)

Figure S3 Immunohistochemical analysis of EGFP$^+$ cells. The expression of GFAP and NG2 was analyzed in the cortex of 10 days-old EGFP/GFAP mice. Note that at P10 there are EGFP-positive cells co-expressing GFAP and NG2.
(TIF)

Figure S4 Interactions between highly expressed "key" genes in subpopulation B3. (**A**) All significant correlations ($p<0.05$) between the expressions of gene pairs are indicated. (**B**) Partial Spearman correlation coefficients were calculated to separate direct and indirect interactions between genes. The lines indicate a direct correlation that remains significant after the removal of indirect (via a third gene) correlations. (**C**) Correlation that remains significant after removing the effect of Hcn2. (**D**) Correlation that remains significant after removing the effect of Gria3.
(TIF)

Table S1 PCR assay information and primer sequences.
(DOCX)

Table S2 Statistics describing the gene expression for each postnatal developmental subpopulation or post-ischemic subpopulations.
(DOCX)

Table S3 Correlation within development subpopulation A1.
(XLSX)

Table S4 Correlation within development subpopulation A2.
(XLSX)

Table S5 Correlation within development subpopulation A3.
(XLSX)

Table S6 Correlation within development subpopulation B1.
(XLSX)

Table S7 Correlation within development subpopulation B2.
(XLSX)

Table S8 Correlation within development subpopulation B3.
(XLSX)

Author Contributions

Conceived and designed the experiments: VR MK MA. Performed the experiments: VR PH DD. Analyzed the data: VR AS MK MA. Contributed reagents/materials/analysis tools: MK MA. Wrote the paper: VR MA.

References

1. Reichenbach WH (2005) Astrocytes and ependymal cells. In: Kettenmann H, Ransom BR, editor. Neuroglia. 2 ed. New York: Oxford University Press. 19–36.
2. Oberheim NA, Takano T, Han X, He W, Lin JH, et al. (2009) Uniquely hominid features of adult human astrocytes. The Journal of neuroscience : the official journal of the Society for Neuroscience 29: 3276–3287.
3. Matyash V, Kettenmann H (2010) Heterogeneity in astrocyte morphology and physiology. Brain research reviews 63: 2–10.
4. Seifert G, Huttmann K, Binder DK, Hartmann C, Wyczynski A, et al. (2009) Analysis of astroglial K+ channel expression in the developing hippocampus reveals a predominant role of the Kir4.1 subunit. The Journal of neuroscience : the official journal of the Society for Neuroscience 29: 7474–7488.
5. Benesova J, Rusnakova V, Honsa P, Pivonkova H, Dzamba D, et al. (2012) Distinct expression/function of potassium and chloride channels contributes to the diverse volume regulation in cortical astrocytes of GFAP/EGFP mice. PLoS One 7: e29725.
6. Ge WP, Miyawaki A, Gage FH, Jan YN, Jan LY (2012) Local generation of glia is a major astrocyte source in postnatal cortex. Nature 484: 376–380.
7. Freeman MR (2010) Specification and morphogenesis of astrocytes. Science 330: 774–778.
8. Zhang Y, Barres BA (2010) Astrocyte heterogeneity: an underappreciated topic in neurobiology. Current opinion in neurobiology 20: 588–594.
9. Trotter J, Karram K, Nishiyama A (2010) NG2 cells: Properties, progeny and origin. Brain research reviews 63: 72–82.
10. Stallcup WB, Beasley L (1987) Bipotential glial precursor cells of the optic nerve express the NG2 proteoglycan. The Journal of neuroscience : the official journal of the Society for Neuroscience 7: 2737–2744.
11. Alonso G (2005) NG2 proteoglycan-expressing cells of the adult rat brain: possible involvement in the formation of glial scar astrocytes following stab wound. Glia 49: 318–338.
12. Honsa P, Pivonkova H, Dzamba D, Filipova M, Anderova M (2012) Polydendrocytes display large lineage plasticity following focal cerebral ischemia. PLoS One 7: e36816.
13. Robel S, Berninger B, Gotz M (2011) The stem cell potential of glia: lessons from reactive gliosis. Nature reviews Neuroscience 12: 88–104.
14. Zelenina M (2010) Regulation of brain aquaporins. Neurochemistry international 57: 468–488.
15. Hwang IK, Yoo KY, Li H, Lee BH, Suh HW, et al. (2007) Aquaporin 9 changes in pyramidal cells before and is expressed in astrocytes after delayed neuronal death in the ischemic hippocampal CA1 region of the gerbil. Journal of neuroscience research 85: 2470–2479.
16. McKeon RJ, Jurynec MJ, Buck CR (1999) The chondroitin sulfate proteoglycans neurocan and phosphacan are expressed by reactive astrocytes in the chronic CNS glial scar. The Journal of neuroscience : the official journal of the Society for Neuroscience 19: 10778–10788.
17. Komitova M, Perfilieva E, Mattsson B, Eriksson PS, Johansson BB (2002) Effects of cortical ischemia and postischemic environmental enrichment on hippocampal cell genesis and differentiation in the adult rat. Journal of cerebral blood flow and metabolism : official journal of the International Society of Cerebral Blood Flow and Metabolism 22: 852–860.
18. Ferraguti F, Corti C, Valerio E, Mion S, Xuereb J (2001) Activated astrocytes in areas of kainate-induced neuronal injury upregulate the expression of the metabotropic glutamate receptors 2/3 and 5. Experimental brain research Experimentelle Hirnforschung Experimentation cerebrale 137: 1–11.
19. Ulas J, Satou T, Ivins KJ, Kesslak JP, Cotman CW, et al. (2000) Expression of metabotropic glutamate receptor 5 is increased in astrocytes after kainate-induced epileptic seizures. Glia 30: 352–361.
20. Jacque CM, Vinner C, Kujas M, Raoul M, Racadot J, et al. (1978) Determination of glial fibrillary acidic protein (GFAP) in human brain tumors. Journal of the neurological sciences 35: 147–155.
21. Sofroniew MV, Vinters HV (2010) Astrocytes: biology and pathology. Acta neuropathologica 119: 7–35.
22. Walz W (2000) Controversy surrounding the existence of discrete functional classes of astrocytes in adult gray matter. Glia 31: 95–103.
23. Regan MR, Huang YH, Kim YS, Dykes-Hoberg MI, Jin L, et al. (2007) Variations in promoter activity reveal a differential expression and physiology of glutamate transporters by glia in the developing and mature CNS. The Journal of neuroscience : the official journal of the Society for Neuroscience 27: 6607–6619.
24. Mearow KM, Mill JF, Vitkovic L (1989) The ontogeny and localization of glutamine synthetase gene expression in rat brain. Brain research Molecular brain research 6: 223–232.
25. Cahoy JD, Emery B, Kaushal A, Foo LC, Zamanian JL, et al. (2008) A transcriptome database for astrocytes, neurons, and oligodendrocytes: a new resource for understanding brain development and function. The Journal of neuroscience : the official journal of the Society for Neuroscience 28: 264–278.
26. Kimelberg HK (2004) The problem of astrocyte identity. Neurochemistry international 45: 191–202.
27. Klein CA, Zohlnhofer D, Petat-Dutter K, Wendler N (2005) Gene expression analysis of a single or few cells. Current protocols in human genetics/editorial board, Jonathan L Haines [et al] Chapter 11: Unit 11 18.
28. Ståhlberg A, Andersson D, Aurelius J, Faiz M, Pekna M, et al. (2011) Defining cell populations with single-cell gene expression profiling: correlations and identification of astrocyte subpopulations. Nucleic acids research 39: e24.
29. Raj A, Peskin CS, Tranchina D, Vargas DY, Tyagi S (2006) Stochastic mRNA synthesis in mammalian cells. PLoS biology 4: e309.
30. Raj A, van Oudenaarden A (2009) Single-molecule approaches to stochastic gene expression. Annual review of biophysics 38: 255–270.

31. Bengtsson M, Hemberg M, Rorsman P, Stahlberg A (2008) Quantification of mRNA in single cells and modelling of RT-qPCR induced noise. BMC molecular biology 9: 63.
32. Ståhlberg A, Rusnakova V, Forootan A, Anderova M, Kubista M (2013) RT-qPCR work-flow for single-cell data analysis. Methods 59: 80–88.
33. Ståhlberg A, Bengtsson M (2010) Single-cell gene expression profiling using reverse transcription quantitative real-time PCR. Methods 50: 282–288.
34. Nolte C, Matyash M, Pivneva T, Schipke CG, Ohlemeyer C, et al. (2001) GFAP promoter-controlled EGFP-expressing transgenic mice: a tool to visualize astrocytes and astrogliosis in living brain tissue. Glia 33: 72–86.
35. Benesova J, Hock M, Butenko O, Prajerova I, Anderova M, et al. (2009) Quantification of astrocyte volume changes during ischemia in situ reveals two populations of astrocytes in the cortex of GFAP/EGFP mice. Journal of neuroscience research 87: 96–111.
36. Wahl-Schott C, Biel M (2009) HCN channels: structure, cellular regulation and physiological function. Cell Mol Life Sci 66: 470–494.
37. Ståhlberg A, Rusnakova V, Kubista M (2013) The added value of single-cell gene expression profiling. Brief Funct Genomics.
38. Sindelka R, Ferjentsik Z, Jonak J (2006) Developmental expression profiles of Xenopus laevis reference genes. Dev Dyn 235: 754–758.
39. da Cunha A, Aloyo VJ, Vitkovic L (1991) Developmental regulation of GAP-43, glutamine synthetase and beta-actin mRNA in rat cortical astrocytes. Brain research Developmental brain research 64: 212–215.
40. Stanimirovic DB, Ball R, Small DL, Muruganandam A (1999) Developmental regulation of glutamate transporters and glutamine synthetase activity in astrocyte cultures differentiated in vitro. International journal of developmental neuroscience : the official journal of the International Society for Developmental Neuroscience 17: 173–184.
41. Palygin O, Lalo U, Pankratov Y (2011) Distinct pharmacological and functional properties of NMDA receptors in mouse cortical astrocytes. Br J Pharmacol 163: 1755–1766.
42. Ziak D, Chvatal A, Sykova E (1998) Glutamate-, kainate- and NMDA-evoked membrane currents in identified glial cells in rat spinal cord slice. Physiological research/Academia Scientiarum Bohemoslovaca 47: 365–375.
43. Matthias K, Kirchhoff F, Seifert G, Huttmann K, Matyash M, et al. (2003) Segregated expression of AMPA-type glutamate receptors and glutamate transporters defines distinct astrocyte populations in the mouse hippocampus. The Journal of neuroscience : the official journal of the Society for Neuroscience 23: 1750–1758.
44. Butt AM, Hamilton N, Hubbard P, Pugh M, Ibrahim M (2005) Synantocytes: the fifth element. Journal of anatomy 207: 695–706.
45. Zhou M, Schools GP, Kimelberg HK (2006) Development of GLAST(+) astrocytes and NG2(+) glia in rat hippocampus CA1: mature astrocytes are electrophysiologically passive. Journal of neurophysiology 95: 134–143.
46. Nagelhus EA, Horio Y, Inanobe A, Fujita A, Haug FM, et al. (1999) Immunogold evidence suggests that coupling of K+ siphoning and water transport in rat retinal Muller cells is mediated by a coenrichment of Kir4.1 and AQP4 in specific membrane domains. Glia 26: 47–54.
47. Connors NC, Adams ME, Froehner SC, Kofuji P (2004) The potassium channel Kir4.1 associates with the dystrophin-glycoprotein complex via alpha-syntrophin in glia. The Journal of biological chemistry 279: 28387–28392.
48. Liu H, Yang M, Qiu GP, Zhuo F, Yu WH, et al. (2012) Aquaporin 9 in rat brain after severe traumatic brain injury. Arquivos de neuro-psiquiatria 70: 214–220.
49. Sun W, McConnell E, Pare JF, Xu Q, Chen M, et al. (2013) Glutamate-dependent neuroglial calcium signaling differs between young and adult brain. Science 339: 197–200.
50. Lyon L, Kew JN, Corti C, Harrison PJ, Burnet PW (2008) Altered hippocampal expression of glutamate receptors and transporters in GRM2 and GRM3 knockout mice. Synapse 62: 842–850.
51. Masood K, Besnard F, Su Y, Brenner M (1993) Analysis of a segment of the human glial fibrillary acidic protein gene that directs astrocyte-specific transcription. J Neurochem 61: 160–166.
52. Pekny M, Nilsson M (2005) Astrocyte activation and reactive gliosis. Glia 50: 427–434.
53. Zamanian JL, Xu L, Foo LC, Nouri N, Zhou L, et al. (2012) Genomic analysis of reactive astrogliosis. The Journal of neuroscience : the official journal of the Society for Neuroscience 32: 6391–6410.
54. Hoshi A, Yamamoto T, Shimizu K, Ugawa Y, Nishizawa M, et al. (2012) Characteristics of aquaporin expression surrounding senile plaques and cerebral amyloid angiopathy in Alzheimer disease. J Neuropathol Exp Neurol 71: 750–759.
55. McCoy E, Sontheimer H (2010) MAPK induces AQP1 expression in astrocytes following injury. Glia 58: 209–217.
56. Rodriguez A, Perez-Gracia E, Espinosa JC, Pumarola M, Torres JM, et al. (2006) Increased expression of water channel aquaporin 1 and aquaporin 4 in Creutzfeldt-Jakob disease and in bovine spongiform encephalopathy-infected bovine-PrP transgenic mice. Acta Neuropathol 112: 573–585.
57. Badaut J, Petit JM, Brunet JF, Magistretti PJ, Charriaut-Marlangue C, et al. (2004) Distribution of Aquaporin 9 in the adult rat brain: preferential expression in catecholaminergic neurons and in glial cells. Neuroscience 128: 27–38.
58. Badaut J, Regli L (2004) Distribution and possible roles of aquaporin 9 in the brain. Neuroscience 129: 971–981.
59. Hara-Chikuma M, Verkman AS (2006) Aquaporin-1 facilitates epithelial cell migration in kidney proximal tubule. J Am Soc Nephrol 17: 39–45.
60. McCoy E, Sontheimer H (2007) Expression and function of water channels (aquaporins) in migrating malignant astrocytes. Glia 55: 1034–1043.
61. Papadopoulos MC, Verkman AS (2008) Potential utility of aquaporin modulators for therapy of brain disorders. Prog Brain Res 170: 589–601.
62. Bezzi P, Carmignoto G, Pasti L, Vesce S, Rossi D, et al. (1998) Prostaglandins stimulate calcium-dependent glutamate release in astrocytes. Nature 391: 281–285.
63. Paquet M, Ribeiro FM, Guadagno J, Esseltine JL, Ferguson SS, et al. (2013) Role of metabotropic glutamate receptor 5 signaling and homer in oxygen glucose deprivation-mediated astrocyte apoptosis. Mol Brain 6: 9.
64. Durand D, Carniglia L, Caruso C, Lasaga M (2011) Reduced cAMP, Akt activation and p65-c-Rel dimerization: mechanisms involved in the protective effects of mGluR3 agonists in cultured astrocytes. PLoS One 6: e22235.
65. Aguado F, Espinosa-Parrilla JF, Carmona MA, Soriano E (2002) Neuronal activity regulates correlated network properties of spontaneous calcium transients in astrocytes in situ. J Neurosci 22: 9430–9444.
66. Anderova M, Vorisek I, Pivonkova H, Benesova J, Vargova L, et al. (2011) Cell death/proliferation and alterations in glial morphology contribute to changes in diffusivity in the rat hippocampus after hypoxia-ischemia. J Cereb Blood Flow Metab 31: 894–907.
67. Sik A, Smith RL, Freund TF (2000) Distribution of chloride channel-2-immunoreactive neuronal and astrocytic processes in the hippocampus. Neuroscience 101: 51–65.
68. Ransom CB, O'Neal JT, Sontheimer H (2001) Volume-activated chloride currents contribute to the resting conductance and invasive migration of human glioma cells. J Neurosci 21: 7674–7683.
69. Butenko O, Dzamba D, Benesova J, Honsa P, Benfenati V, et al. (2012) The increased activity of TRPV4 channel in the astrocytes of the adult rat hippocampus after cerebral hypoxia/ischemia. PLoS One 7: e39959.
70. Benfenati V, Amiry-Moghaddam M, Caprini M, Mylonakou MN, Rapisarda C, et al. (2007) Expression and functional characterization of transient receptor potential vanilloid-related channel 4 (TRPV4) in rat cortical astrocytes. Neuroscience 148: 876–892.
71. Pamenter ME, Perkins GA, McGinness AK, Gu XQ, Ellisman MH, et al. (2012) Autophagy and apoptosis are differentially induced in neurons and astrocytes treated with an in vitro mimic of the ischemic penumbra. PLoS One 7: e51469.
72. Neitz A, Mergia E, Eysel UT, Koesling D, Mittmann T (2011) Presynaptic nitric oxide/cGMP facilitates glutamate release via hyperpolarization-activated cyclic nucleotide-gated channels in the hippocampus. Eur J Neurosci 33: 1611–1621.
73. Zhao JW, Raha-Chowdhury R, Fawcett JW, Watts C (2009) Astrocytes and oligodendrocytes can be generated from NG2+ progenitors after acute brain injury: intracellular localization of oligodendrocyte transcription factor 2 is associated with their fate choice. The European journal of neuroscience 29: 1853–1869.
74. Komitova M, Serwanski DR, Lu QR, Nishiyama A (2011) NG2 cells are not a major source of reactive astrocytes after neocortical stab wound injury. Glia 59: 800–809.
75. Patanow CM, Day JR, Billingsley ML (1997) Alterations in hippocampal expression of SNAP-25, GAP-43, stannin and glial fibrillary acidic protein following mechanical and trimethyltin-induced injury in the rat. Neuroscience 76: 187–202.
76. Hepp R, Perraut M, Chasserot-Golaz S, Galli T, Aunis D, et al. (1999) Cultured glial cells express the SNAP-25 analogue SNAP-23. Glia 27: 181–187.
77. Illarionova NB, Gunnarson E, Li Y, Brismar H, Bondar A, et al. (2010) Functional and molecular interactions between aquaporins and Na,K-ATPase. Neuroscience 168: 915–925.
78. Anderova M, Antonova T, Petrik D, Neprasova H, Chvatal A, et al. (2004) Voltage-dependent potassium currents in hypertrophied rat astrocytes after a cortical stab wound. Glia 48: 311–326.
79. Bordey A, Lyons SA, Hablitz JJ, Sontheimer H (2001) Electrophysiological characteristics of reactive astrocytes in experimental cortical dysplasia. Journal of neurophysiology 85: 1719–1731.
80. Arimura K, Ago T, Kamouchi M, Nakamura K, Ishitsuka K, et al. (2012) PDGF receptor beta signaling in pericytes following ischemic brain injury. Curr Neurovasc Res 9: 1–9.
81. Zhu X, Zuo H, Maher BJ, Serwanski DR, LoTurco JJ, et al. (2012) Olig2-dependent developmental fate switch of NG2 cells. Development 139: 2299–2307.
82. Marshall CA, Suzuki SO, Goldman JE (2003) Gliogenic and neurogenic progenitors of the subventricular zone: who are they, where did they come from, and where are they going? Glia 43: 52–61.
83. Gorski JA, Talley T, Qiu M, Puelles L, Rubenstein JL, et al. (2002) Cortical excitatory neurons and glia, but not GABAergic neurons, are produced in the Emx1-expressing lineage. J Neurosci 22: 6309–6314.
84. Machon O, van den Bout CJ, Backman M, Rosok O, Caubit X, et al. (2002) Forebrain-specific promoter/enhancer D6 derived from the mouse Dach1 gene controls expression in neural stem cells. Neuroscience 112: 951–966.
85. Prajerova I, Honsa P, Chvatal A, Anderova M (2010) Neural stem/progenitor cells derived from the embryonic dorsal telencephalon of D6/GFP mice differentiate primarily into neurons after transplantation into a cortical lesion. Cell Mol Neurobiol 30: 199–218.
86. Honsa P, Pivonkova H, Anderova M (2013) Focal cerebral ischemia induces the neurogenic potential of mouse Dach1-expressing cells in the dorsal part of the lateral ventricles. Neuroscience.

87. Benesova J, Hock M, Butenko O, Prajerova I, Anderova M, et al. (2009) Quantification of astrocyte volume changes during ischemia in situ reveals two populations of astrocytes in the cortex of GFAP/EGFP mice. J Neurosci Res 87: 96–111.

88. Walz W, Lang MK (1998) Immunocytochemical evidence for a distinct GFAP-negative subpopulation of astrocytes in the adult rat hippocampus. Neurosci Lett. 257(3): 127–30.